UNIVERSITAT POLITÈCNICA DE CATALUNYA

Programa de Doctorado en Ingeniería Ambiental

Ph.D. Thesis

Regional and urban evaluation of an air quality modelling system in the European and Spanish domains

María Teresa Pay Pérez

Directors:
Dr. Pedro Jiménez Guerrero
Dr. José María Baldasano Recio

Barcelona, October 2011

(To Martín)

Acknowledgements

La presente tesis doctoral es el resultado del esfuerzo, directo o indirecto, de un grupo importante de personas que merecen un especial reconocimiento. En primer lugar, quiero mostrar mi más sincero agradecimiento a los dos directores de este trabajo: Dr. Pedro Jiménez y Dr. José María Baldasano. Pedro me brindó la oportunidad de integrarme en este grupo de trabajo. Le agradezco sus buenos consejos, sus ánimos, su completa disponibilidad y el ser una fuente de buenas ideas. José María me ha enseñado a trabajar con rigor, exigencia y búsqueda de excelencia; aunque el aprendizaje haya sido duro, me alegra haberme ganado su confianza. A ambos les debo casi todo lo que soy profesionalmente.

M'agradaria donar les gràcies al Dr. Oriol Jorba per la seva suport en moments difícils i per ser-hi prop per parlar de ciència. También le agradezco al Dr. Matthias Piot su apoyo y buenos consejos. I'd like to acknowledge Prof. Donald Dabdub to his wise advises that let me grew up as a scientific and his help to write my first paper. Moreover, I am indebted with the CES-lab of the University of California (USA). Eu também gostaria de agradecer ao Prof. Carlos Borrego e seu grupo GMAC da Universidade de Aveiro (Portugal) para a oportunidade de colaborar em questões de previsão científica de melhorias da qualidade do ar.

Un especial reconocimiento se merecen todas aquellas personas que aportaron, o que continúan aportando día a día, su granito de arena en la construcción y mejora de este complejo sistema llamado CALIOPE, gestionado desde el inicio por José María Baldasano, y que es la base de esta tesis: grupo de emisiones (Santiago G., Eugeni L., Patricia G., Albert S., Mar M., Marc G., Regina I., Cristina C., Gina F.), grupo de meteorología (Oriol J., Angel R., Michele S., Alba B.); grupo de polvo (Carlos P., Karstein H., Sara B., Elies C.); grupo de calidad del aire (Pedro J., María G., Matthias P., Joana O., Valentina S., Gustavo A.) y grupo de informáticos (David C., Kim S., Luca T., Francecs M., Francesco B.). Igualmente, es de destacar la labor de los gestores de las redes de calidad del aire EMEP y de las Comunidades Autónomas españolas que han proporcionado una base de datos útil para el desarrollo de este trabajo de investigación, especialmente la grupo de IDAEA-CSIC, dirigido por Dr. Xavier Querol, que ha participado activamente proporcionando datos y contribuyendo científicamente a la discusión de los resultados.

En el mismo sentido, agradezco al Ministerio de Ciencia e Innovación de España y al Barcelona Supercomputing Center-Centro Nacional de Supercomputación (BSC-CNS) por el soporte económico y técnico para la realización tesis.

En cuanto a lo personal, me gustaría dar las gracias con todo mi cariño a mis compañeros y excompañeros del BSC-CNS, principalmente a aquellos que me han ofrecido su amistad y comprensión, y en especial a mi compañera en esta aventura, Sara Basart porque ha sido mi gran apoyo todo este tiempo. Mis padres (Manuel y Mª Teresa), mi familia y amigos se merecen un especial agradecimiento ya que desde Archena siempre han estado preocupados por mi. Gracias a ti Martín, que desde un principio hasta el día de hoy sigues ahí.

Summary

The impact of air pollution is a very important topic in environment and climate. Over recent decades, there has been a clear progress across Europe towards reducing anthropogenic emissions of the main air pollutants. However, poor air quality remains an important public health issue, especially in urban environments. Airborne particulate matter (PM), tropospheric ozone (O_3) and nitrogen dioxide (NO_2) are the main problematic pollutants in Europe and Spain. The European Commission has shown a great concern for developing actions that allow increasing the knowledge on transport and dynamics of atmospheric pollutants to assure the accomplishment of legislation and to inform the population about their levels. Indeed, the European directive 2008/50/EC establishes the possibility of using modelling techniques to assess air quality.

This Ph.D. thesis is developed in the framework of two projects: the CALIOPE project (CALIOPE 441/2006/3-12.1, A357/2007/2-12.1, 157/PC08/3-12.0) and the CICYT project (CICYT CGL2006-08903), both based on the necessity to develop an air quality modelling system that allows assessing and understanding the air pollution levels in Europe and Spain, with the aim of obtaining a precise forecast of air quality. For that purpose, the **CALIOPE air quality modelling system** has been developed with high spatial and temporal resolution over Europe (12 km x 12 km, 1 h), as a mother domain; and Spain (4 km x 4 km, 1 h), as the nested domain. The CALIOPE system consists in a set of models that take into account both anthropogenic and natural pollution. These models, highly supported and developed by the international scientific community, are the WRF-ARW meteorological model, the HERMES-EMEP emission model, the CMAQ chemical transport model and the BSC-DREAM8b natural dust model, which represent the state-of-the-science in air quality modelling at regional and urban scales. The availability of the MareNostrum supercomputer, held in Barcelona Supercomputing Center-Centro Nacional de Supercomputación (BSC-CNS), has allowed such configuration of the CALIOPE system.

The main objective of the present Ph.D. thesis is to increase the scientific confidence on the CALIOPE system, identifying skills and weakness with a degree of detail that contributes to establish necessities of improvements in the modelling process. Therefore, the present work has spatially and temporally evaluated CALIOPE air quality simulations over Europe and Spain in terms of O_3, NO_2, SO_2, PM2.5, PM10 concentrations over the full year 2004. In order to identify the origin of uncertainties in PM modelling, PM chemical composition has been also evaluated in both target domains. Evaluations have been performed across more than 150 air quality-monitoring stations and over more than 2 million of experimental data. Furthermore, this Ph.D. thesis has used the CALIOPE system to assess air quality pattern over the year 2004, identifying clearly the areas of air pollution.

First of all, CALIOPE system has been evaluated at regional scale over Europe (CALIOPE-EU) against rural background measurements from the EMEP monitoring network. Modelled O_3 concentrations achieve satisfactory performances for both daily mean and daily maximum concentrations, especially in summer. The general trends and daily variability of primary pollutants are accurately reproduced. NO_2 daily mean concentrations tend to be underestimated; meanwhile SO_2 peaks are generally overestimated. The annual temporal variability of PM2.5 and PM10

modelled concentrations is well reproduced, but mean concentrations remain systematically underestimated by a factor of 2. The CALIOPE-EU evaluation in terms of PM chemical composition indicates that the system performs well at estimating secondary inorganic aerosol (SIA) (SO_4^{2-}, NO_3^-, NH_4^+), but errors are larger for precursors species (SO_2, HNO_3 and NH_3). N-compounds present the highest uncertainties. The temporal treatment of NH_3 emissions is found to be source of uncertainty in the model representation of SIA.

Once evaluation results have assured the CALIOPE-EU system is able to provide accurate chemical boundary condition with high spatial and temporal resolution to nested domains, the CALIOPE system has been run at a higher resolution at the urban scale over Spain (CALIOPE-IP). In the evaluation process of the CALIOPE-IP, the HERMES model has been improved (e.g. inclusion of agriculture and livestock emissions, improvement of the distribution biogenic emissions and population density). In addition, the implementation of the new emission module considering resuspended PM from paved road by on-road traffic in HERMES has highly improved the modelled PM10 concentrations over the Spanish domain in 2004, especially near the largest urban zones, contributing up to 17 $\mu g\ m^{-3}$ as the annual average. However, that positive effect is limited since the deposition mechanism has been found to be a significant sink of resuspended PM in the CMAQ model.

Evaluation of CALIOPE-IP has been performed with measurements from the Spanish monitoring network for O_3, NO_2, SO_2 and PM10 on an hourly basis, and with PM chemical composition measurements from the IDAEA-CSIC monitoring network on a daily basis. The performance has shown a strong dependency on the type of environment (urban, suburban, and rural) and the dominant emissions sources (traffic, industrial, and background). Modelled O_3 shows high performance at urban stations, especially at those affected by on-traffic in large cities (i.e., high-NO_x environments), where modelled hourly O_3 concentracions agree with the pronounced daily variability measured. NO_x/O_3 chemistry is better represented under non-limited-NO_2 regimes. Modelled high SO_2 concentrations are of frequent episodic character, showing high dependency on meteorological pattern and distribution of emission sources.

Performances of CALIOPE system are in accordance with the recommendations of the European Commission and the U.S. Environmental Protection Agency. Even more, the CALIOPE system has been compared with other European evaluation studies at regional scale, since there is not any comparison done at urban scale over Spain up to this Ph.D. thesis. The results have shown that while O_3 statistics generally remain lower than those obtained by the other consider studies (but similar to those system using CMAQ), statistics for NO_2, SO_2, PM2.5 and PM10 present higher scores than most modelling systems. Comparisons performed on PM chemical compounds and gas-phase precursors have shown that CALIOPE-EU's skills for HNO_3, NH_3 and NH_4NO_3 are relatively poor, but it is a general feature affecting most models.

The CALIOPE modelled air quality spatial patterns have indicated that urban pollution is mainly due to the NO_2 emissions from on-road traffic, especially in largest European metropolitan areas, such as Madrid and Barcelona (~25-40 $\mu g\ NO_2\ m^{-3}$ annual mean). Nowadays, SO_2 concentrations are under control, although the power plants and refineries located in northern Spain and eastern Europe present high mean concentrations (~50 $\mu g\ m^{-3}$ annual mean). The Algeciras bay (southern Spain) is identified as highly polluted area due to the influence of shipping combining with the

diverse contributions from industrial processes. The highest O_3 concentrations are found over the Mediterranean Basin, especially downwind of main NO_x emission sources from the largest Spanish cities and industrial areas along the Spanish Mediterranean coast, where 8-h maximum O_3 concentrations exceeded the value of 120 μg m^{-3} by more than 30 days. The complex topography and the high isolation during summertime develop mesoscale phenomena such as sea-breezes and mountain-valley winds that contribute to the accumulation and recirculation of aged air masses and O_3 aloft.

There are three major thrusts of the present Ph.D. thesis. *First*, chemical boundary condition based on a global model such as LMDz-INCA2 becomes essential to model O_3 background concentrations in Europe and Spain. *Second*, to simulate PM concentration in southern Europe, both regional and urban scales, the contribution of dust from the Saharan desert should be taken into account, since that region is frequently affected by Saharan desert outbreaks due to its proximity to the African continent. The contribution of desert dust through the BSC-DREAM8b helps to satisfactory model the observed episodic PM10 concentration peaks (~2-10 μg PM10 desert m^{-3} annual mean). Even more, the contribution of sea-salt aerosol is especially important over coastal areas (~2-3 μg m^{-3} annual mean). *Third*, to be able to model the air quality in urban scale over Spain it is essential (1) a high spatial (4 km x 4 km and 15 layers) and temporal (1h) resolution that allows describing mesoscale phenomena in very complex terrains; (2) a high disaggregated emission model to describe the sources, such as HERMES; and (3) an state-of-the-science meteorological and chemical models.

This Ph.D. thesis has demonstrated that **CALIOPE air quality modelling system** applied over Europe and Spain is a useful tool which may contribute to (1) forecast air pollution in urban/suburban areas with a pervasive influence of anthropogenic emissions on a local scale and over very complex terrains and meteorology patterns; (2) assess about air pollution, discriminating between anthropogenic and natural episodes; and (3) manage air pollution, by means of modification of urban strategies or requirements of the legislation.

Resumen

El impacto de la contaminación atmosférica es un tema de vital importancia en el medio ambiente y el clima. En las últimas décadas Europa ha presentado una claro progreso en temas de reducción de emisiones antropogénicas de los principales contaminantes. Sin embargo, la mala calidad del aire continúa siendo una amenaza para la salud pública, especialmente en ambientes urbanos. El material particulado (PM), el ozono troposférico (O_3) y el dióxido de nitrógeno (NO_2) son los principales contaminantes con problemas en Europa y España. La Comisión Europea ha mostrado un gran interés por el desarrollo de acciones que incrementen el conocimiento sobre el transporte y la dinámica de contaminantes en la atmósfera para asegurar el cumplimiento de la legislación e informar a la población acerca de sus niveles. De hecho, la reciente directiva europea 2008/50/EC establece la posibilidad de usar técnicas de modelización para informar sobre la calidad del aire.

La presente tesis doctoral está desarrollada en el marco de dos proyectos: el proyecto CALIOPE (CALIOPE 441/2006/3-12.1, A357/2007/2-12.1, 157/PC08/3-12.0) y el proyecto CICYT (CICYT CGL2006-08903), ambos basados en la necesidad de desarrollar un sistema de modelización de la calidad del aire que permita entender los niveles de contaminación en Europa y España, con la intención de obtener una preciso pronóstico de la calidad del aire. Con este propósito, se ha desarrollado el sistema de modelización de la calidad del aire CALIOPE con alta resolución espacial y temporal sobre Europa (12 km x 12 km, 1 h), como dominio madre, y España (4 km x 4 km, 1 h), como dominio anidado. El sistema CALIOPE consiste en un conjunto de modelos que tienen en cuenta tanto la contribución antropogénica como natural. Estos modelos son el modelo meteorológico WRF-ARW, el modelo de emisiones HERMES-EMEP, el modelo de transporte químico CMAQ, y el modelo de transporte de polvo mineral BSC-DREAM8b, los cuales representan el estado actual del conocimiento en modelización de calidad del aire a escala regional y urbana.

El objetivo principal de esta tesis doctoral ha sido incrementar la confianza científica en el sistema CALIOPE, identificando sus habilidades y puntos débiles con un grado de detalle que ha contribuido a establecer las necesidades de mejora en el proceso de modelización. Por tanto, el presente trabajo ha evaluado espacial y temporalmente las simulaciones de calidad del aire calculadas con CALIOPE sobre Europa y España en términos de concentración de O_3, NO_2, SO_2, PM2.5, PM10 para el año completo 2004. Con la intención de identificar el origen de las incertidumbres en la modelización de PM, los componentes químicos del PM han sido también evaluados en ambos dominios objetivo. La evaluación se ha realizado sobre más de 150 estaciones de calidad del aire y sobre más de 2 millones de datos experimentales. Además, esta tesis doctoral ha utilizado el sistema CALIOPE para informar sobre los patrones de calidad del aire en 2004, identificando claramente las zonas de contaminación.

En primer lugar, el sistema CALIOPE se ha evaluado a escala regional sobre Europa (CALIOPE-EU) frente medidas de fondo regional de la red EMEP. La modelización de O_3 en superficie alcanza resultados satisfactorios tanto para concentraciones medias como para máximos diarios, especialmente en verano. La tendencia general y la variabilidad diaria de los contaminantes primarios son reproducidas con fidelidad. Las concentraciones medias diarias de NO_2 tienden a

estar subestimadas, mientras los picos de SO_2 están generalmente sobreestimados. La variabilidad temporal de las concentraciones de PM2.5 y PM10 modeladas concuerda con las observaciones, aunque la concentración media permanece sistemáticamente subestimada en un factor de 2. La evaluación de CALIOPE-EU en términos de componentes químicos de PM indica que el sistema presenta un buen rendimiento al simular aerosoles inorgánicos secundarios (SIA) (SO_4^{2-}, NO_3^-, NH_4^+), aunque los errores son mayores para las especies precursoras (SO_2, HNO_3 and NH_3). Los compuestos de Nitrógeno presentan las mayores incertidumbres. El tratamiento temporal de las emisiones de NH_3 es una fuente de incertidumbre en la representación de los SIA modelados.

Una vez los resultados de la evaluación han asegurado que CALIOPE-EU es capaz de proporcionar unas condiciones de contorno químicas fiables con alta resolución espacial y temporal al dominio anidado, el sistema CALIOPE se ha ejecutado a mayor resolución a escala urbana sobre España (CALIOPE-IP). En el proceso de evaluación de CALIOPE-IP, el modelo HERMES ha sido mejorado (ej. Implementación de emisiones de agricultura y ganadería, mejora de la distribución de las emisiones biogénicas y densidad de población). Además, la implementación de un nuevo módulo de emisión que considera la resuspension de PM de carreteras asfaltadas por tráfico rodado en HERMES ha mejorado sustancialmente la concentración de PM10 modelada sobre el dominio de España en 2004, especialmente cerca de grandes de zonas urbanas, contribuyendo en más de 17 μg m^{-3} como media anual. Sin embargo, ese efecto positivo es limitado ya que se ha encontrado que los mecanismos de deposición son importantes sumideros de PM resuspendido en el modelo CMAQ.

La evaluación de CALIOPE-IP se ha realizado sobre medidas de la red española de monitorización para O_3, NO_2, SO_2 and PM10 en base horaria, y sobre medidas de composición química de PM de la red IDAEA-CSIC en base diaria. Los resultados han mostrado una fuerte dependencia con el tipo de entorno (urbano, suburbano y rural) y el tipo de emisión dominante (tráfico, industrial y fondo). El O_3 modelado muestra buen comportamiento en estaciones urbanas, especialmente aquellas influenciadas directamente por tráfico en grandes ciudades (ej. Ambientes con altos niveles de NO_x), donde la concentración horaria de O_3 modelada concuerda con la pronunciada variabilidad medida. La química NO_x/O_3 está mejor representada bajo regímenes no limitados por NO_2. La modelización de altas concentraciones de SO_2 es de carácter episódico, mostrando una alta dependencia con el patrón meteorológico y la distribución de las fuentes de emisión.

Los resultados de evaluación del sistema CALIOPE siguen las recomendaciones de la Comisión Europea y de la Agencia de protección de medio ambiente americana. Además, el sistema CALIOPE se ha comparado con otros estudios de evaluación europeos a escala regional, ya que no hay ningún resultado a escala urbana sobre España hasta la presente tesis doctoral. Los resultados han mostrado que mientras que los estadísticos para O_3 son ligeramente inferiores a los obtenidos en otros estudios (pero los mismos que los sistemas que utilizan CMAQ), los estadísticos para NO_2, SO_2, PM2.5 and PM10 presentan mejores resultados que el resto de sistemas de modelización. Comparaciones realizadas sobre los componentes químicos del PM y sus gases precursores han mostrado que las cualidades de CALIOPE-EU para HNO_3, NH_3 y NH_4NO_3 son relativamente bajas, pero esto una característica generalizada en el resto de sistemas europeos.

Los patrones espaciales de calidad del aire modelizados por CALIOPE han indicado que la contaminación urbana es principalmente debida a las emisiones de NO_2 procedentes del tráfico

rodado, especialmente en las grandes áreas metropolitanas europeas, como Madrid y Barcelona (~25-40 μg NO_2 m^{-3} media anual). Hoy en día, las concentraciones de SO_2 están controladas, aunque las centrales térmicas y las refinerías localizadas en el norte de España y este de Europa presentan altas concentraciones medias (~50 μg SO_2 m^{-3} media anual). La bahía de Algeciras (sur de España) se ha identificado como una zona de alta contaminación debido a la influencia combinada del transporte marítimo y procesos industriales. Las mayores concentraciones de O_3 se encuentran sobre la cuenca mediterránea, especialmente a sotavento de las principales fuentes de emisión de NO_2 procedentes de grandes ciudades españolas y áreas industriales de la costa mediterránea, donde las concentraciones máximas octo-horarias excedieron los 120 μg m^{-3} en más de 30 días. La compleja orografía y la alta insolación durante el verano desarrollan fenómenos mesoescalares como brisas y vientos de montaña que contribuyen a la acumulación y recirculación de masas de aire envejecidas y por tanto de O_3 a capas superiores.

Hay tres ideas centrales que se desprenden de la presente tesis doctoral. *Primera*, las condiciones de contorno químicas basadas en un modelo global como el LMDz-INCA2 resultan esenciales para describir las concentraciones de O_3 de fondo, tanto a escala regional como urbana. *Segunda*, para reproducir la concentración de PM en el sur de Europa tanto a escala regional como urbana, la contribución del polvo del desierto procedente del Sahara debería ser tenida en cuenta, pues esa zona sufre la frecuente intrusión de tormentas de polvo debido a su proximidad al continente africano. La contribución de polvo de desierto a través del modelo BSC-DREAM8b ayuda modelizar satisfactoriamente los episódicos picos de concentración de PM10 observados (~2-10 μg m^{-3} media anual). Además, la contribución de aerosol marino es especialmente importante sobre zonas costeras (~2-3 μg m^{-3} media anual). *Tercera*, para ser capaz de reproducir la calidad del aire a escala urbana sobre España es esencial (1) una alta resolución espacial (4 km x 4 km and 15 layers) y temporal (1h) que permita describir fenómenos mesoescalares en topografías complejas; (2) un modelo de emisiones altamente desagregado para describir las fuentes, como HERMES; (3) modelos que representen el estado del conocimiento en meteorología y química atmosférica.

Esta tesis doctoral ha demostrado que el sistema de modelización de calidad del aire CALIOPE aplicado sobre Europa y España es una herramienta útil que contribuye a (1) predecir la contaminación en zonas urbanas/suburbanas con influencia dominante de fuentes antropogénicas a escala local y sobre complejas topografías y situaciones meteorológicas; (2) informar sobre la contaminación, discriminando entre episodios naturales y antropogénicos; (3) gestionar la contaminación, mediante modificación de estrategias urbanas o requerimientos de la legislación.

Publications

International Journals Included in the Science Citation Index (SCI)

1. <u>Pay, M.T.</u>, Piot, M., Jorba, O., Basart, S., Gassó, S., Jiménez-Guerrero, P., Gonçalves, M., Dabdub, D., Baldasano, J.M., 2010a. A full year evaluation of the CALIOPE-EU air quality system in Europe for 2004: a model study. *Atmos. Environ.*, **44**, 3322-3342. doi:10.1016/j.atmosenv.2010.050140.

2. <u>Pay, M.T.</u>, Jiménez-Guerrero, P., Baldasano, J.M., 2010b. Implementation of resuspension from paved roads for the improvement of CALIOPE air quality system in Spain. *Atmos. Environ.*, **45**, 802-807. doi:10.1016/j.atmosenv.2010.10.032.

3. Baldasano, J.M., <u>Pay, M.T.</u>, Jorba, O., Gassó, S., Jiménez-Guerrero, P., 2011. An annual assessment of air quality with the CALIOPE modeling system over Spain. *Sci. Total Environ.*, **409**, 2163-2178. doi:10.1016/j.scitotenv.2011.01.041.

4. Jiménez-Guerrero, P., Jorba, O., <u>Pay, M.T.</u>, Montávez, J.P., Jerez, S., Gomez-Navarro, J.J., Baldasano, J.M., 2011. Comparison of two different sea-salt aerosol schemes as implemented in air quality models applied to the Mediterranean basin. *Atmos. Chem. Phys.*, **11**, 4833-4850. doi:10.5194/acp-11-4833-2011.

5. Sicardi, V., Ortiz, J., Rincón, A., Jorba, O., <u>Pay, M.T.</u>, Gassó, S., Baldasano, J.M., 2011. Ground-level ozone concentration over Spain: an application of Kalman filter post-processing to reduce model uncertainties. *Geosci. Model Dev. Discuss.*, **4**, 343-384. doi: 10.5194/gmdd-4-343-2011.

6. Basart, S., <u>Pay, M.T.</u>, Jorba, O., Pérez, C., Jiménez-Guerrero, P., Schulz, M., Baldasano, J.M., 2011. Aerosol in the CALIOPE air quality modelling system: validation and analysis of PM levels, optical depths and chemical composition over Europe. *Atmos. Chem. Phys. Discuss.*, **11**, 20575-20629. doi: 10.5194/acpd-11-20575-2011.

7. <u>Pay, M.T.</u>, Jiménez-Guerrero, P., Jorba, O., Basart, S., Pandolfi, M., Querol, X., Baldasano, J.M., 2011. Spatio-temporal variability of levels and speciation of particulate matter across Spain in the CALIOPE modeling system. In Press, *Atmos. Environ., doi:* doi:10.1016/j.atmosenv.2011.09.049.

8. <u>Pay, M.T.</u>, Jiménez-Guerrero, P., Baldasano, J.M., 2011. Assessing sensitivity regimes of secondary inorganic aerosol formation in Europe with the CALIOPE-EU modeling system. Submitted in *Atmos. Environ.*

9. Borrego, C., Monteiro, A., <u>Pay, M.T.</u>, Ribeiro, I., Miranda, A.I., Basart, S., Baldasano, J.M., 2011. How bias-correction can improve air quality forecast over Portugal. *Atmos. Environ.*, **45**, 6629-6641.

Proceedings of International Congresses

1. Pay, M.T., Jiménez-Guerrero, P., Jorba, O., Pérez, Gassó, S., Baldasano, J.M., 2008. A long-term evaluation study of the atmospheric dynamics of aerosols and gaseous species over Europe using an integrated air quality modelling system with high resolution. European Geoscience Union (EGU) General Assembly. Vienna, Austria. April 13-18.

2. Jiménez-Guerrero, P., Pay, M.T., Jorba, O., Piot, M., Baldasano, J.M., 2008. Inclusion of Saharan dust in an integrated air quality forecasting system for Europe. European Geoscience Union (EGU) General Assembly. Vienna, Austria. April 13-18.

3. Jiménez-Guerrero, P., Pay, M.T., Jorba, O., Piot, M., Baldasano, J.M., 2008. Evaluating the annual performance of an air quality forecasting system (Caliope) with high resolution for Europe and Spain. In: ACCENT/GLOREAM workshop Antwerp, Belgium. October 29-31.

4. Jiménez-Guerrero, P., Pay, M.T., Baldasano, J.M., Jorba, O., Gómez-Navarro, J.J., Jerez, S., Montávez, J.P., 2008. Comparison of two different sea salt aerosol schemes as implemented in air quality models applied to the Mediterranean. In: ACCENT/GLOREAM workshop. Antwerp, Belgium. October 29-31.

5. Pay, M.T., Jiménez-Guerrero, P., Jorba, O., Pérez, C., Baldasano, J.M., Querol, X., Pandolfi, M., 2009. An assessment of the ability of an integrated air quality forecasting system to simulate chemically speciated PM2.5. In: 7th International Conference on Air Quality - Science and Application (Air Quality 2009). Istanbul, Turkey. March 24-27.

6. Pay, M.T., Piot, M., Jiménez-Guerrero, P., Jorba, O., Pérez, C., Baldasano, J.M., 2009. Evaluation of the chemically speciated particulate matter from a high-resolution air quality modelling system over the Iberian Peninsula. European Geoscience Union (EGU) General Assembly. Vienna, Austria. April 19-24.

7. Piot, M., Pay, M.T., Jorba, O., Baldasano, J.M., Jiménez-Guerrero, P., López, E., Pérez, E., Gassó, S. 2009. Evaluating the CALIOPE air quality modelling system: dynamics and chemistry over Europe and the Iberian Peninsula for 2004 at high horizontal resolution. European Geoscience Union (EGU) General Assembly. Vienna, Austria. April 19-24.

8. Piot, M., Pay, M.T., Jorba, O., Jiménez-Guerrero, P., López, E., Gassó, S., Baldasano, J.M., 2009. Annual dynamics and statistical evaluation of an air quality forecasting system (Caliope) with high resolution for Europe. In: 30th NATO/SPS International Technical Meeting on Air Pollution Modeling and Its Application. San Francisco, USA. May 18-22.

9. Gonçalves, M., Piot, M., Jorba, O., Pay, M.T., López, E., Gassó, S., Baldasano, J.M., 2009. Near real time of the Spanish air quality forecast system: CALIOPE. In: HARMO 13 Paris, France. June1-4.

10. Jorba, O., Piot, M., Pay, M.T., Jiménez-Guerrero, P., López, E., Pérez, C., Gassó, S., Baldasano, J.M., 2009. Air quality over Europe and Iberian Peninsula for 2004 at high horizontal

resolution: evaluation of the CALIOPE modelling system. In: 9th Annual Meeting of the European Meteorological Society (EMS). Toulouse, France. September 28- October 2.

11. Baldasano, J.M., Piot, M., Jorba, O., Gonçalves, M., Pay, M.T., Lopez, E., Pérez, C., Gassó, S., 2009. The CALIOPE high-resolution air quality forecasting system: development and evaluation for Spain and Europe. In: 8th Annual CMAS Conference. Chapel Hill, NC, USA. October 19-21.

12. Baldasano, J.M., López, E., Gonçalves, M., Pay, M.T., Güereca, P., Jiménez-Guerrero, P., Gassó, S., 2009. The HERMES high-resolution emission system: simulating anthropogenic and biogenic emissions for the Iberian Peninsula, Canary Islands and Europe. In: GEIA ACCENT 2009. Oslo, Norway. October 26-28.

13. Pay, M.T., Piot, M., Jiménez-Guerrero, P., Jorba, O., Pérez, C., Baldasasano, J.M., Querol, X., Pandolfi, M., Alastuey, A., Dabdub, D., 2009. In: American Association for Aerosol Research 28th Annual Conference. Minneapolis, Minnesota. October 26-30.

14. Gonçalves, M., Piot, M., Jorba, O., Pay, M.T., López, E., Gassó, S., Baldasano, J.M., 2009. Operational evaluation system of the Spanish air quality forecasting model CALIOPE. In: ACCENT/GLOREAM workshop. Brescia, Italy. November 27-29.

15. Piot, M., Pay, M.T., Jorba, O., Climent, N., Lopez, E., Pérez, C., Gassó, S., Baldasano, J.M., 2009. The evaluation of the Spanish air quality modeling system: CALIOPE. Dynamics and chemistry over Europe and Iberian Peninsula for 2004 at high horizontal resolution. American Geoscience Union (AGU) Fall meeting. San Francisco, USA. December 14-18.

16. Baldasano, J.M., Piot, M., Jorba, O., Gonçalves, M., Pay, M.T., Pérez, C., López, E., Gassó, S., Martín, F., García-Vivanco, M., Palomino, I., Querol, X., Pandolfi, M., Diéguez, J.J., Padilla, L., 2009. Operational air quality forecasting system for Spain: CALIOPE. American Geoscience Union (AGU) Fall meeting. San Francisco, USA. December 14-18.

17. Baldasano J.M., Piot, M., Jorba, O., Gonçalves, M., Pay, M.T., Basart, S., Jiménez, P., Gassó, S., 2010. CALIOPE: an Operational Air Quality Forecasting System for Europe and Spain. In: Mesoscale Modelling For Air Pollution Applications: Achievements And Challenges (COST 728 Final Workshop), Organisers: COST 728, WMO/GURME and MEGAPOLI. Geneva, Switzerland. February 25-26.

18. Piot, M., Pay, M.T., Jorba, O., Basart, S., Gassó, S., Querol, X., Pandolfi, M., Baldasano, J.M., et al., 2010. Preliminary modelling results of the chemical composition of particulate matter in NE Spain for the DAURE campaign. European Geoscience Union (EGU) General Assembly. Vienna, Austria. May 2-7.

19. Basart, S., Pay, M.T., Pérez, C., Cuevas, E., Jorba, O., Piot, M., Baldasano, J.M., 2010. Aerosol Optical Depth over Europe: evaluation of the CALIOPE air quality modelling system with direct-sun AERONET observations. European Geoscience Union (EGU) General Assembly. Vienna, Austria. May 2-7.

20. <u>Pay, M.T.</u>, Piot, M., Jorba, O., Basart, S., Gassó, S., Dabdub, D., Jiménez-Guerrero, P., Baldasano, J.M., 2010. Chemical composition of particulate matter in Spain: modelling evaluation of the CALIOPE system for 2004. European Geoscience Union (EGU) General Assembly. Vienna, Austria. May 2-7.

21. Gonçalves, M., Piot, M., Jorba, O., <u>Pay, M.T.</u>, Gassó, S., Baldasano, J.M., 2010. Near real time evaluation system of the Spanish air quality forecasting system CALIOPE. European Geoscience Union (EGU) General Assembly. Vienna, Austria. May 2-7.

22. Baldasano, J.M., <u>Pay, M.T.</u>, Jorba, O., Ortiz, J., Gonçalves, M., Basart, S., Gassó, S., Jiménez-Guerrero, P., 2010. Evaluation of the Spanish operational air quality forecasting system: diagnostic and near real time. In: International workshop on air quality forecasting research. Quebec, Canada. November 16-18.

23. Basart, S., <u>Pay, M.T.</u>, Jorba, O., Pérez, C., Baldasano, J.M., 2011. Aerosol in the CALIOPE air quality modeling system: validation and analysis of PM levels, optical depths and chemical composition over Europe. European Geoscience Union (EGU) General Assembly. Vienna, Austria. April 4-8.

24. Borrego, C., Monteiro, A., Ribeiro, I., Miranda, A.I., <u>Pay, M.T.</u>, Basart, S., Baldasano, J.M., 2011. How different air quality forecasting systems operate over Portugal. In: HARMO 14 Kos Island, Greece. October 2-6.

Chapter in Books

1. Piot, M., <u>Pay, M.T.</u>, Jorba, O., Jiménez-Guerrero, P., López, E., Gassó, S., Baldasano, J.M., 2010. Annual Dynamics and Statistical Evaluation of an Air Quality Forecasting System (CALIOPE) with High Resolution for Europe. Air Pollution Modeling and its Application XX. Ed. Down G. Steyn and S.T. Rao. Springer: 241-245. ISBN: 978-90-481-3810-4, January 2010, 737 pp.

Index

List of figures

List of tables

Acronyms

AQ	Air Quality
AQM	Air Quality Model
BSC-CNS	Barcelona Supercomputing Center-Centro Nacional de Supercomputación
BSC-DREAM8b	Dust REgional Atmospheric Model version 8 bins developed at the BSC-CNS
EEA	European Environmental Agency
bVOC	Biogenic Volatile Organic Compounds
CALIOPE system	WRF-ARW/EMEP-HERMES/CMAQ/BSC-DREAM8b system
CMAQ	Models-3 Community Multiscale Air Quality Modeling System
COST	European Cooperation in Science and Technology
CTM	Chemical Transport Model
DD	Desert Dust
CORINAIR	CORe INventory AIR Emission
EC	European Commission
EEA	European Environmental Agency
EMEP	European Monitoring and Evaluation Programme
EPER	European Pollutant Emission Register
E-PRTR	European Pollutant Release and Transfer Register
EU	European Union
FNL/NCEP	Final Analyses of the National Centers of Environmental Prediction
GEMS	Global Monitoring for Environment and Security
GIS	Geographical Information System
GLOREAM	Global and regional atmospheric modelling
HERMES	High-Elective Resolution Modelling Emission System
IP	Iberian Peninsula
ITL	Iberian Thermal Low
JRC	Joint Research Center
MACC	Monitoring Atmospheric Composition and Climate
MB	Mean Bias
MFB	Mean Fractional Bias
MFE	Mean Fractional Error
MNGE	Mean Normalized Gross Error
MNBE	Mean Normalized Bias Error
NMVOC	Non Methane Volatile Organic Compounds
MSC-W	Meteorological Synthesizing Center-West
NEC	National Emissions Ceiling
NEI	National Emission Inventory
TC	Total Carbon
PM	Particulate Matter

PM2.5-10	Coarse PM
PM2.5	Denotes fine PM, defined as the integrated mass of aerosol with diameter less than or equal to 2.5 µm. In the WRF-ARW/HERMES-EMEP/CMAQ/BSC-DREAM8b system, PM2.5 is calculated as the sum: PM2.5= SO_4^{-2}(fine)+NO_3^-(fine)+NH_4^+(fine)+ TC (fine) + DD (fine) + SS (fine) + PM undefined (fine)
PM10	Integrated mass of aerosol with diameter less than or equal to 10 µm. In the WRF-ARW/HERMES-EMEP/CMAQ/BSC-DREAM8b system, PM10 is calculated as: PM10= PM2.5 + DD (coarse) + SS (coarse) + PM undefined (coarse)
PROMOTE	Protocol Monitoring fo the GMES Sevice Element
QA	Quality Assurance
RPR	Resuspended Particulate Matter from Paved Roads
r	Correlation Coefficient
RMSE	Root Mean Squared Error
SIA	Secondary Inorganic Aerosols
SOA	Secondary Organic Aerosols
SP	Spain
SS	Sea Salt
UNECE	United Nations Economic Commission for Europe
US EPA	Environmental Protection Agency from United States
VOC	Volatile Organic Compounds excluding CO and CO_2
WHO	World Health Organization
WRF-ARW	Advanced Research Weather Research and Forecasting Model

1. Introduction

This section discusses the issue of air pollution as a health and environmental problem. It analyses the current state of air quality and the elements which force on air pollution, with special focus on the European and Spanish regions. Furthermore, the present section revises current initiatives to manage air quality in terms of environmental policy and science. In the context of the present Ph.D. thesis, such initiatives are focused in air quality modelling and how these numerical models have to be evaluated in order to assure the confidence on them. Precedents and previous results about air quality modelling in the Earth Science Department of the Barcelona Supercomputing Center-Centro Nacional de Supercomputación are revised. Such experiences have established the framework where the present Ph.D. thesis is carried out.

1.1   Air pollution in Europe and Spain: levels and origin

Air pollution can be defined as "a situation in which substances are present in the atmosphere at concentration sufficiently high above their normal levels to produce a measurable effect on humans, animals, vegetation, or materials" (Seinfeld and Pandis, 1998). The state of air pollution is often expressed as Air Quality (AQ). Therefore, AQ is a measure of the concentration of gaseous pollutants and size or number of solid or liquid pollutants (particulate matter).

Nowadays, the majority of large cities in the world have problems related to AQ, not only in developed countries (North America, Europe and Japan), but also in cities of developing areas such as Mexico City, Santiago de Chile, Cairo, Bangkok, etc. (Baldasano et al., 2003). SCIAMACHY satellite image of NO_2 in Figure 1-1 makes clear how human activity impacts on AQ. Industrial areas in North America, West Europe, North East China and South Africa are clearly visible.
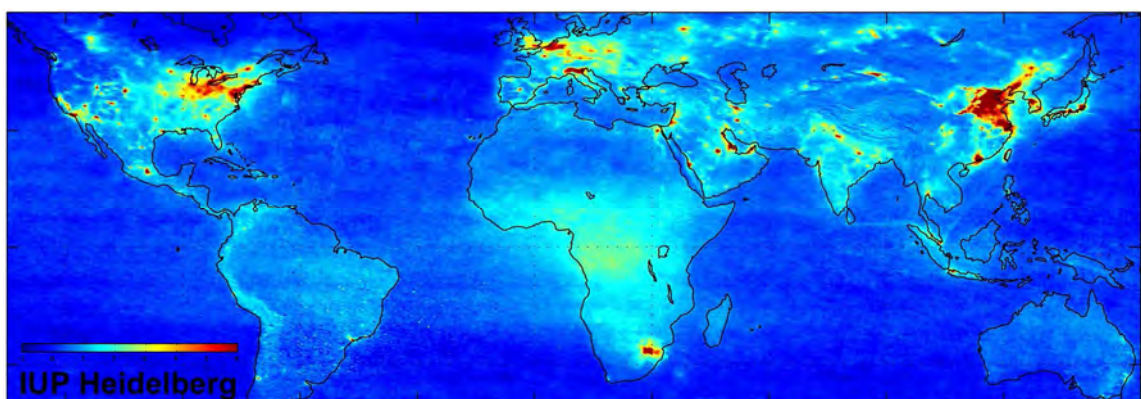
Figure 1-1. Global mean tropospheric NO_2 vertical column density between January 2003 and June 2004, as measured by the SCIAMACHY instrument on European Space Agency's Envisat. The scale is in 10^{15} molecules cm^{-2}. The present image is produced by S. Beirle, U. Platt and T. Wagner of the University of Heidelberg, Institute for Environmental Physics. Available at: http://www.esa.int/.

Air pollution is not a modern issue (Baldasano, 1999; Jacobson, 2002; Finlayson-Pitts, 2010). Urban growth and industrial development have caused serious problems of air pollution in the last decades. Dramatic incidents of excess deaths such as in London, England, on Thursday 4 December 1952 (Wilkins, 1954) (Figure 1-2) brought public and scientific attention to "smog" (smog = smoke + fog) and, in particular, to the problem of sulphur dioxide and sulphate particles that form in air, as well as to direct emissions of particles from combustion sources. Around 1950 a different kind of smog was identified in the Los Angeles area by Haagen-Smit (1952) from symptoms of damage to plants. Today, this condition is called photochemical smog because it contains an increase concentration of ozone formed by the interaction of volatile organic compounds, nitrogen oxides, and sunlight. Nowadays, it is known that air pollution is a multi-pollutant, multi-effect and trans-boundary environmental problem affecting both developed and developing countries around the world (Baldasano et al., 2003).
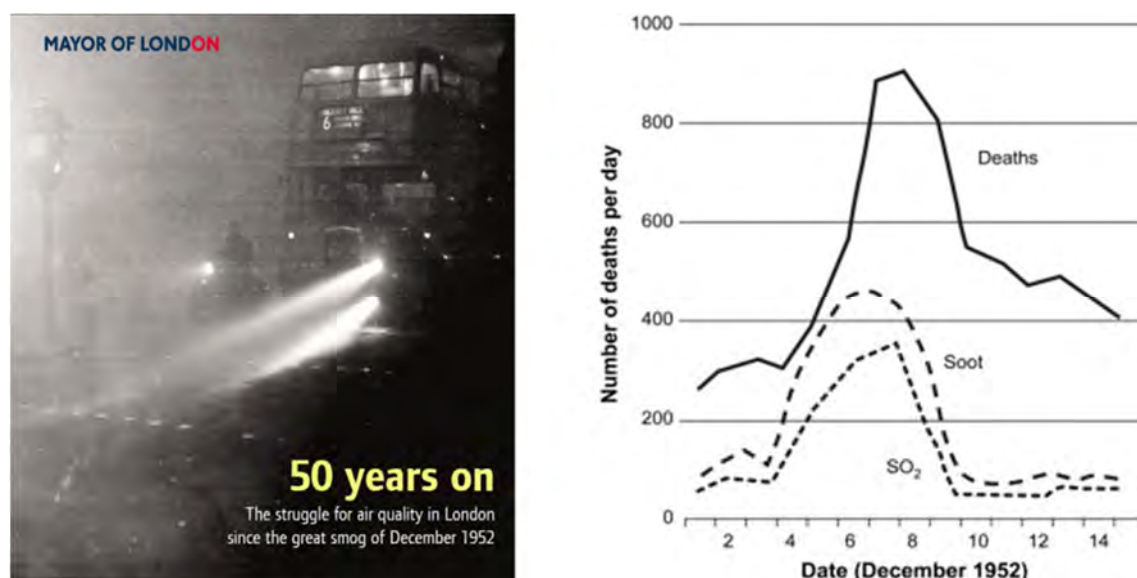
Figure 1-2. On Thursday 4 December 1952 started an episode of 4 days where pollution levels rose to unprecedented levels and more than 4,000 extra deaths occurred. The disastrous outcome was due to a combination of various factors. The anticyclone situation gave low winds and damp air. This required more heating in the cold winter climate and thus gave further pollution (source: Monks et al., 2009).

The most relevant atmospheric pollutants include **sulphur dioxide** (SO_2), **nitrogen oxides** ($NO_x \equiv NO + NO_2$), **tropospheric ozone** (O_3), **ammonia** (NH_3), a number of **volatile organic compounds** (VOC) and **particulate matter** (PM) (Figure 1-3). In AQ, carbon dioxide (CO_2) and methane () are treated separately from the other pollutants because their effects are significant at global scale through the greenhouse effect and global warming. In this sense, usually the VOC group is referred as non-methane volatile organic compounds (NMVOC) which excluds the particular case of CH_4.

The air pollutants of most concern for their multi-effects are O_3, PM and NO_2. On the one hand, O_3 is a secondary pollutant produced in the atmosphere from gaseous precursor pollutants such as

NO$_x$, NMVOC and the presence of solar radiation (Atkinson, 2000; Jacob, 2000). On the other hand, PM can be primary in the sense that they are emitted as particles from the source, or secondary produced from gaseous precursors, mainly SO$_2$, NO$_x$, NH$_3$ and NMVOC. PM includes PM10 (particulate matter with median aerodynamic diameter less than 10 μm), PM2.5 (particulate matter with median aerodynamic diameter less than 2.5 μm), fine and ultrafine particles which include many pollutants (metals, inorganic and organic compounds) in a complex multiphase system.
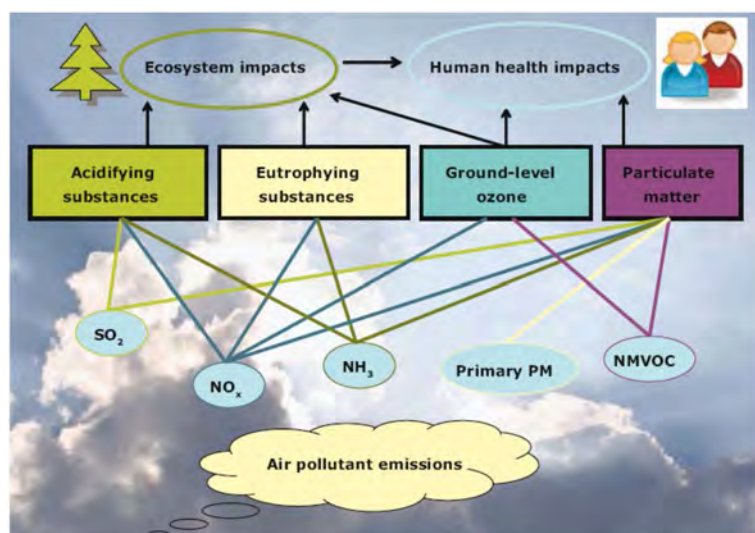
Figure 1-3. Major air pollutants and their interaction clustered according to their impact.

Air pollution has implications for a number of contemporary issues including human health (WHO, 2003; Gurjar et al., 2010), ecosystems (Lovett et al., 2000), visibility (Hyslop and White, 2008), Earth's climate (IPCC, 2007) and degradation of building materials (Cowell and Apsimon, 1996) (Figure 1-3). The World Health Organization (WHO) estimated that exposure to urban outdoor PM2.5 caused approximately 25,600 deaths and over 862,00 lost years of healthy life due to acute lower respiratory infections in 2000 (Cohen et al., 2004). Tropospheric O$_3$ and PM particularly affect human health. Fine particles (diameters less than 2.5 μm) are associated with increase mortality, especially from cardiovascular and cardio pulmonary diseases (Pope and Dockery, 2006). In the case of European, in 2005 more than 20,000 premature deaths were associated with O$_3$ and approximately 500,000 with PM2.5 (EEA, 2010a). About 5 million years of life lost were estimated in Europe due to PM2.5 pollution in 2005. The average loss of life expectancy owing to PM2.5 exposure is estimated to be nine months (EEA, 2007) (Figure 1-4). Exposure to air pollutants is largely beyond the control of individuals and requires action by public authorities at the national, regional and even international levels.

AQ transcends all scales within the atmosphere, from the local to the global with handovers and feedbacks at each scale interaction (Monks et al., 2009). In remote regions, the overall tropospheric O$_3$ concentrations results from a balance between chemistry and transport of precursors from polluted regions and from natural sources (biogenic VOC emissions, biomass burining, lighting) and deposition. Experimental O$_3$ studies carried out in Europe (Gerasopoulos et al., 2005;

Cristofanelli and Bonasoni, 2009), reported high background O_3 levels, especially during summer episodes with stagnant meteorological conditions, when high insolation and temperatures persist. These observations showed that while primary pollutant levels decrease downwind, O_3 is secondary photochemically produced during transport of precursors downwind from the large agglomeration centres and from the surrounding regions of Europe: Balkans, north of the Black Sea; and the Mediterranean Basin. Long-range transport of O_3 and precursors toward the Mediterranean is significantly affected by local meteorological parameters like land-sea breeze circulations and orographic flows (Lelieveld et al., 2002).

Estimated losses in life expectancy attributable to exposure to fine particulate matter ($PM_{2.5}$) from anthropogenic emissions for 2000 (left) and 2020 (right)

Months: 0 1 2 4 6 9 12 36   No data   Outside study area
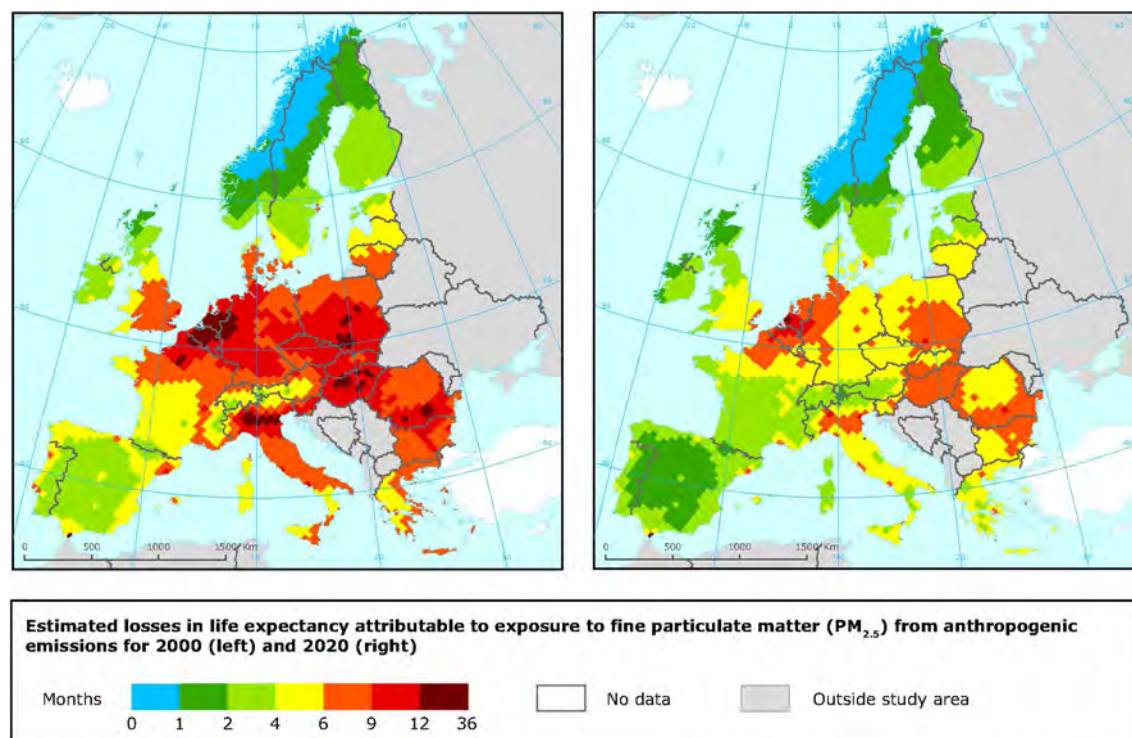
Figure 1-4. Health impact of PM2.5 concentration ($\mu g \ m^{-3}$). Loss in statistical life expectancy (months) that can be attributed to anthropogenic contribution to PM2.5 for the year 2000 (left) and 2020 (right) (EEA, 2007).

Concerning PM, experimental studies (Putaud et al., 2004; Querol et al., 2008a) illustrate that high PM10 levels in European cities is a common problem with different origin due to the AQ interactions in the different scales. As an example, Figure 1-5 shows PM10 in two high-populated cities in Europe, Barcelona (Spain) and Amsterdam (The Netherland). PM10 concentrations at hot spots in Barcelona (60 $\mu g \ m^{-3}$) mainly result from the urban background contribution (~20 $\mu g \ m^{-3}$). In contrast, PM10 concentrations in Amsterdam (45 $\mu g \ m^{-3}$) present high contribution of long-range transport from other European neighbours (~30 $\mu g \ m^{-3}$). PM is efficiently scavenged by precipitation resulting in having an atmospheric lifetime of a few days in the boundary layer and a few weeks in the free troposphere. The PM background in the free troposphere is thus generally unimportant for surface AQ (Heald et al., 2006; UNECE, 2007). Exceptions are plumes from large dust storms and forest fires which can be transported on intercontinental scales in the free troposphere (Prospero, 1999; Foster et al., 2001).
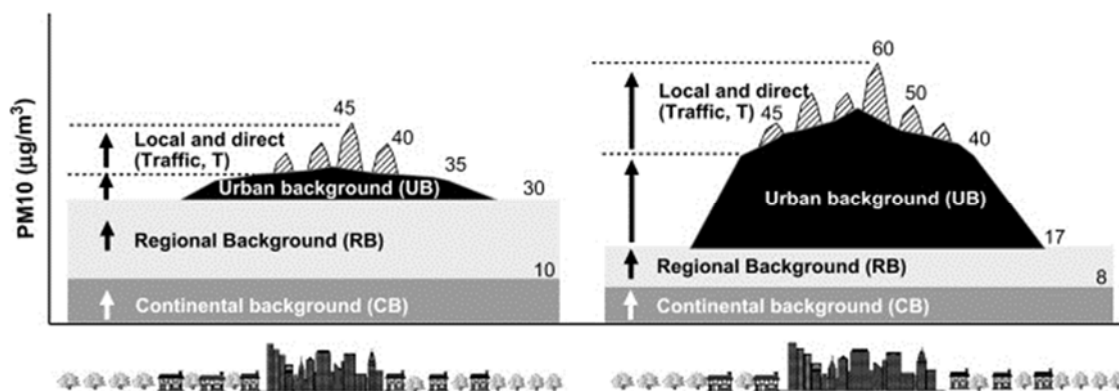
Figure 1-5. Schematic illustration of different PM10 concentrations in the European cities of Amsterdam (left, data from Visser et al., 2001) and Barcelona (right, Querol et al., 2004a) for continental, regional and urban background sites and traffic sites (source: Querol et al., 2008a).

Therefore, the contribution of air pollution at different scales (urban, regional, continental or global) depends on the lifetime and properties of pollutants, emission sources, meteorological variables, and transport patterns (Seinfeld and Pandis, 1998; Jacob and Winner, 2009; Monks et al., 2009; EEA, 2010a). Each of these issues are discussed in the following sections.

1.1.1 Emissions as source of air pollution

Knowledge of the levels of air pollutants emitted by different sources and activities is crucial for understanding the origin of air pollution. Anthropogenic emissions of main pollutants occur as a result of almost all economic and societal activities. Emissions from natural sources are also important for certain pollutants, for example PM from forest fires, sea spray, and dust episodes from Sahara and other arid regions; and NMVOC from forest and crops.

Anthropogenic emissions of the main air pollutants across Europe have deceased continuously between 1990 and 2008 in Europe (Figure 1-6, left). The largest relative reductions in Europe have been reported for SO_x (78%), NMVOC (51%), NO_x (39%) and NH_3 (24%). Emissions of primary PM2.5 and PM10 have both decreased by 13% and 7%, respectively, since 2000. As for Europe, the main Spanish emission reductions (Figure 1-6, right) have been reported for SO_2 (76%), NMVOC (21%), NO_x (8%), PM2.5 (1%) and PM10 (6%).

Figure 1-7 shows the main anthropogenic emission sources of the principal air pollutants across Europe and Spain in 2008. SO_x is mainly emitted by the combustion of fossil fuels containing sulphur, therefore power generation and industrial combustion are the most significant sources in Europe (61% and 16% of the total, respectively) and Spain (48% and 27%, respectively). High reductions in SO_x emissions result from the abatement policies through efficient measures like fuel gas desulphuration and switching to cleaner fuels.
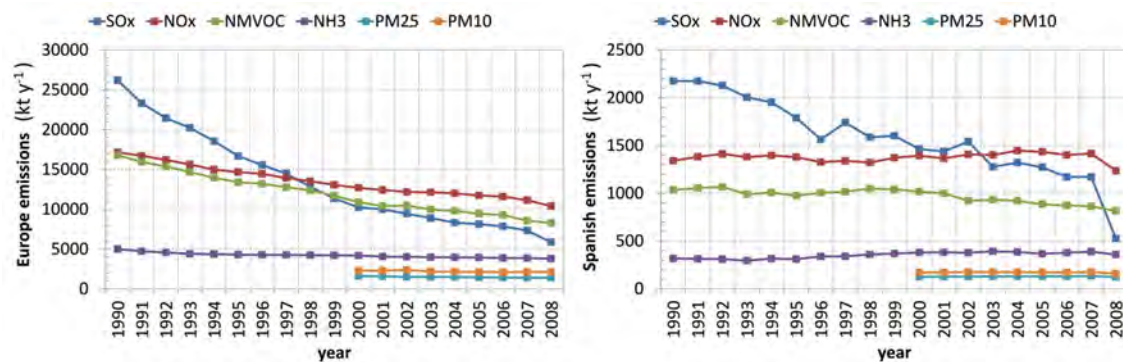
Figure 1-6. Air pollutant emission trends in Europe (left) and Spain (right) for the 1990-2008 period (Units are kilotons species per year, kt y^{-1}) (source: www.emep-emissions.at/emission-data-webdab).

The main source of anthropogenic NMVOC is the solvent industry both in Europe and Spain (41% and 48%, respectively), with contributions of industrial activities or domestic heating in urban areas. On-road transport is another important contributor (16% in Europe and 6% in Spain). Reduction of NMVOC emissions was due to the introduction of vehicle catalytic converters as well as the introduction of legislative measures limiting the use of solvents in non-combustion sector (EEA, 2010a). Although it is not shown in Figure 1-7, biogenic sources are also important contributor to NMVOC emissions (Monks et al., 2009); as an example, the Spanish National Emission Inventory (NEI, 2009) reported that in 2008 biogenic emission contributes by a 53 % to the total NMVOC emissions.
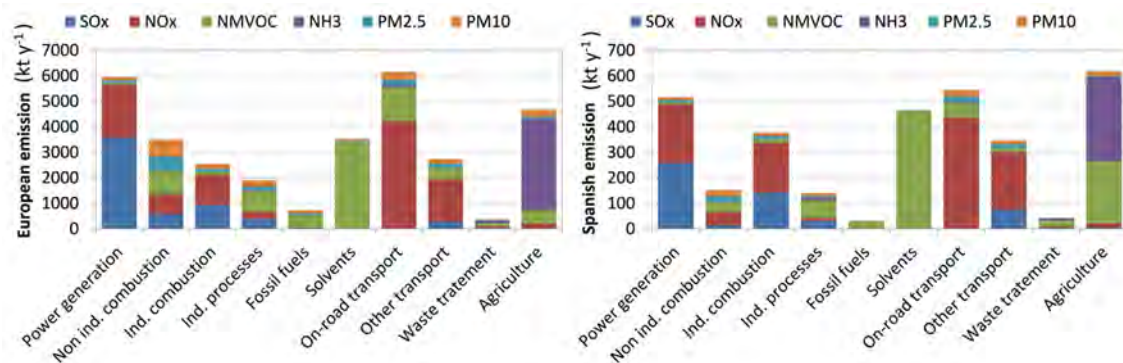
Figure 1-7. Pollutant mass emissions (kilotons per year, kt y^{-1}) by sector in 2008 for Europe (left, source: www.emep.int) and Spain (right, source: Spanish National Emission Inventory; NEI, 2009).

The NO$_x$ emissions are originated by combustion at high temperatures. The on-road traffic mainly emits NO (40% in EU and 37% in Spain) which oxidizes in the atmosphere to form NO$_x$ and other oxidized compounds. Power plants (20% both in EU and Spain) and combustion by industry (11% in EU and 17% in Spain) are also significant NO$_x$ contributors. Emission reductions from the on-

road transport sector have occurred despite the general increase in activity within the traffic sector, and they have been achieved mainly as a result of fitting catalysis to vehicles.

The NH_3 emissions, which contribute to acidification, eutrophication and fine PM formation, have as main source the agricultural activities (94% and 93% in Europe and Spain, respectively). NH_3 has decreased in EU in part because the number of livestock fell, but also because improvements in agricultural practices (EEA, 2010a) driven by EU Nitrates Directives (European Commission, 1991). However, NH_3 emissions in Spain have not decreased.

Non-industrial combustion and on-road traffic are the most important sources of PM2.5 in Europe and Spain, counting 37-16% and 27-25%, respectively in 2008. Emissions of primary PM2.5 and PM10 are expected to decrease as vehicles technologies are improving and fuel combustion emissions are controlled (low-S fuels such as natural gas) and also owing to improvements in the levels and performance of particulate abatement equipment at coal-fired power stations and industrial plants (EEA, 2010a).

As a conclusion, energy production and distribution sector remains a large source of air pollution, responsible of 70% of SO_x emissions and 21% of NO_x emissions. The on-road transport is an important contributor of emissions of different pollutants (mainly NO_x, but also PM2.5, NMVOC) in urban areas.

1.1.2   Meteorology and transport patterns forcing on air pollution

Several meteorological variables, including temperature, precipitation and atmospheric ventilation impact AQ (Jacob and Winner, 2009). As depicted in Table 1-1, among these variables, temperature is shown to have the largest effect on O_3. Temperature increases enhance biogenic emissions (isoprene and other VOC) as well as photochemical activity since most thermal atmospheric reactions show a positive temperature dependence. Regional stagnation affects both O_3 and PM (Table 1-1). The processes that control the pollutant transport are scale-dependent. In the case of Europe, and specifically of the Iberian Peninsula, the atmospheric transport is influenced by the complex topography.

Eastern Europe meteorology is controlled by the following factors (Querol et al., 2009a): (1) the development of Saharan depressions to the south of the Atlas Mountains during spring and early summer (Moulin et al., 1998); these cyclones move across the Mediterranean transporting large amount of desert dust; and (2) the influence of the Azores anticyclone during summer; additionally, a strong influence of the Indian Monsoon on the dry Mediterranean climate (Rodwell and Hoskins, 2001) combined with the complex orography result in persistent northerly winds, called "Etesians".

On the other hand, western Europe presents peculiar and complex atmospheric dynamics affected by mesoscale and local meteorological processes but also regional factors, such as (1) the considerable influence of the Azores high-pressure system in the meteorology of the Iberian Peninsula, (2) the coastal ranges surrounding the Mediterranean coast, (3) the influence of the Iberian and Saharan thermal lows causing weak pressure gradients over the Mediterranean, (4) the intense breeze action along the Mediterranean coast favoured by the prevailing low advective

conditions, (5) the scarce summer precipitation, and (6) the intense seasonal contrast concerning temperature, humidity and rainfall (Baldasano et al., 1994; Millán et al., 1997; Toll and Baldasano, 2000; Martin-Vide and Olcina, 2001; Soriano et al., 2001; Pérez et al., 2004).

Table 1-1. Dependence of surface AQ on meteorological variables[a]. (Source: Jacob and Winner, 2009)

Variable	O_3	PM
Temperature	++	-
Regional stagnation	++	++
Wind speed	-	-
Mixing depth	=	--
Humidity	=	+
Cloud cover	-	-
Precipitation	=	--

[a]Sensitivities of surface O_3 and PM concentrations in polluted regions as obtained from the model perturbation studies reviewed in Jacob and Winner (2009). Results are summarized as consistently positive (++), generally positive (+), weak or variable (=), generally negative (-), and consistently negative (--)

Jorba et al. (2004) used the trajectory and cluster analysis to climatologically study the movement of air masses which transport pollutants from sources located at a long distance and they indicated that the dominating situations in the Iberian Peninsula are the regional re-circulations of pollutants, especially in summer, including situations of low pressure gradient and anticyclonic situations that are related to episodes of O_3 and PM pollution (Jiménez et al., 2006a, Jiménez et al., 2006b). This low pressure gradient is formed in 78% of the summer days in the scenario of Catalan central coast.

The intense heating over the Iberian Peninsula during summer generates a thermal low (Figure 1-8) and favours the convergence of air flows towards the centre of the Iberian Peninsula and the injections of air pollutants (gaseous and PM) in high layers of the atmosphere, where they are transported towards the coast in return flows in 2-3 km in altitude (Millán et al., 1997). During the night, the layers formed during the previous days act as reservoirs of pollutants; the sea breeze of the following morning transports the low layers inland and close all the recirculation process (Millán et al., 1997; Gangoiti et al., 2001).

The main characteristics of the Iberian Peninsula, that reflect its complexity, can be summarized as (Millán et al., 1997; Martin-Vide and Olcina, 2001; Rodríguez et al., 2002; Querol et al., 2004a): (1) high index of insolation, which enhances the processes of photochemical pollution and the formation of secondary aerosols respect to northern Europe; (2) meteorological characteristics that allow the accumulation of air pollutants. Basically, these are translated into a low rain regime and a scarce renovation of air masses, associated to regional re-circulations that are consequence of the abrupt topography of the Mediterranean; and (3) important contributions of mineral dust, which can take place through local resuspension processes over grounds with scarce land cover; or long-distance transport from northern Africa.
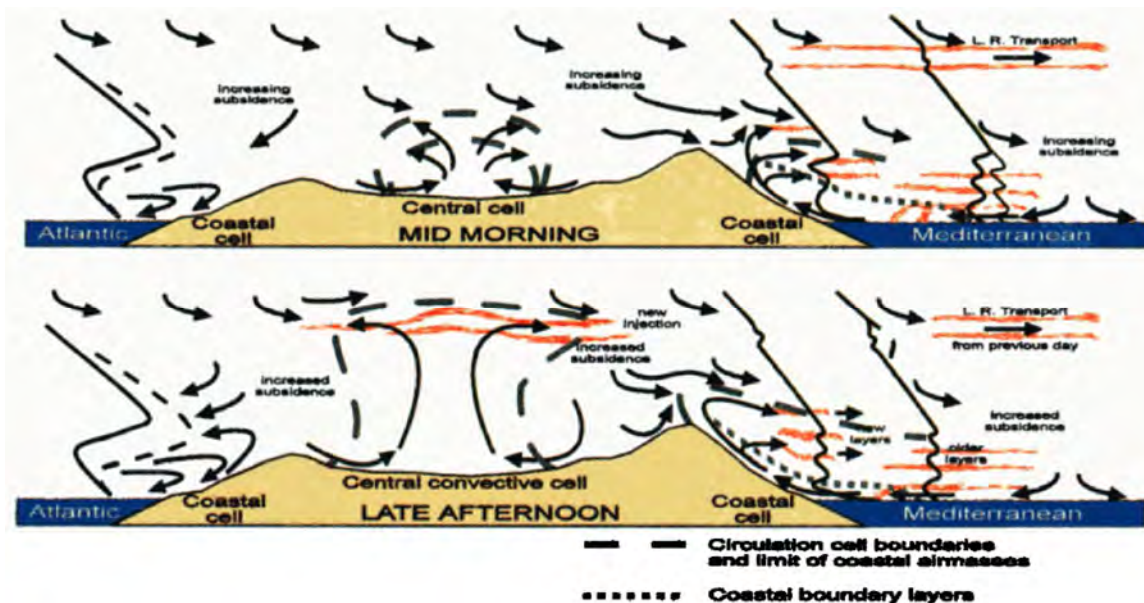
Figure 1-8. Schematic cross section of the Iberian Thermal Low (ITL) circulation in the morning (up) and late afternoon (down) during summer. During the day the sea breezes combine with upslope winds to transport coastal pollutant inland and inject part of these pollutants in their return flows aloft (2 to 3 km). Pollutants move back to the sea and create "stratified reservoir layers" of aged pollutants. Over the central plateau one or various deep convective cells develop and inject aged pollutants, from either the Madrid area and/or those transported previously from the coastal areas, directly into the middle troposphere (Source: Millán et al., 1997).

1.1.3   Atmospheric processing in air quality

Air pollutant concentrations depend not only on the primary emissions and the transport patterns due to meteorological condition, but also on the chemical transformation in the troposphere. The troposphere behaves as a chemical reactor where pollutants react by gas-phase and/or heterogeneous chemistry processes to generate a wide variety of products.

Detailed analysis of gas-phase chemical processes and PM physico-chemistry and dynamics can be found in Seinfeld and Pandis (1998), Atkinson (2000), Finlayson-Pitts and Pitts (2000), Wayne (2000), Pöschl (2005), and Atkinson (2007). Nevertheless, this section provides an overview of major findings and the main research lines nowadays in (1) O_3 and oxidized compounds, and (2) atmospheric PM. Note that, despite O_3 and its precursors and PM are treated separately, there is a chemical coupling between them which is important for understanding the processes controlling their levels (Meng et al., 1997; Jacob 2000).

1.1.3.1 Ozone and precursors

O_3 is considered as the main product of the gas-phase tropospheric chemistry. As shown in the diagram of Figure 1-9 right, O_3 is produced by photochemical oxidation of VOC by the hydroxyl radical (OH·) in the presence of reactive NO_x (Sander and Crutzen, 1996; Seinfeld and Pandis,

1998; Jacobson, 1999; Atkinson, 2000; Jacob 2000). O_3 pollution is in general a summer problem because of the photochemical nature of the source, especially in southern Europe (EEA, 2010b). O_3 production depends on the VOC/NO_x ratios (Jiménez and Baldasano, 2004). The principal sinks of tropospheric O_3 are photolysis in the presence of water vapour and uptake by vegetation (dry deposition) in the continental boundary layer (< 2km). Wet deposition is negligible as O_3 and its major precursors have low solubility in water.
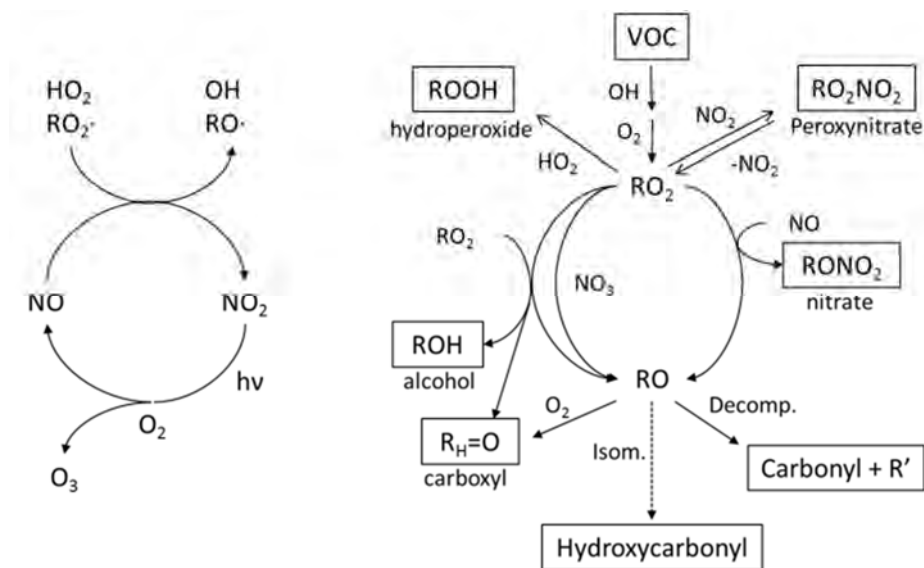
Figure 1-9. (Left) Schematics of the reactions involved in NO-to-NO_2 conversion and O_3 formation in the presence of VOC (adapted from Atkinson, 2000). (Right) Simplified schematic VOC degradation chemistry to first generation RO_2 and RO radicals (adapted from Monks et al., 2009).

During the 20th century the changing balance between O_3 production and loss has changed, owing in the main to human activity resulting in an increase in remote O_3 concentrations (Volz and Kley, 1998). For example, Marenco et al. (1994) and Vingarzan (2004) found out that tropospheric O_3 concentrations have increased in a factor of five since the final years of 19th century. A recent study of Marine Boundary Layer (MBL) concentrations in upwind European and American air found significant trends of about 0.5 ppbV yr^{-1} (Figure 1-10a), a rate comparable to the average rate over the 20th century (Parrish et al., 2009). At regional scale, weak positive background O_3 trends compete with the effects of decreasing precursor emissions over continental areas (Jenkin, 2008). High distribution percentiles decrease while low percentiles increase as shown in Figure 1-10b for the rural site of Lullington Heath in England (Jenkin, 2008). The decreasing trend of highest percentiles is compatible with the known emissions reductions since 1990 (Figure 1-6). In large cities the O_3 trends can have a different behaviour, as O_3 concentrations are largely limited by the presence of abundant NO_x. Mean O_3 concentrations often have a positive trend in city centres owing to NO_x emission reductions (Figure 1-10c).
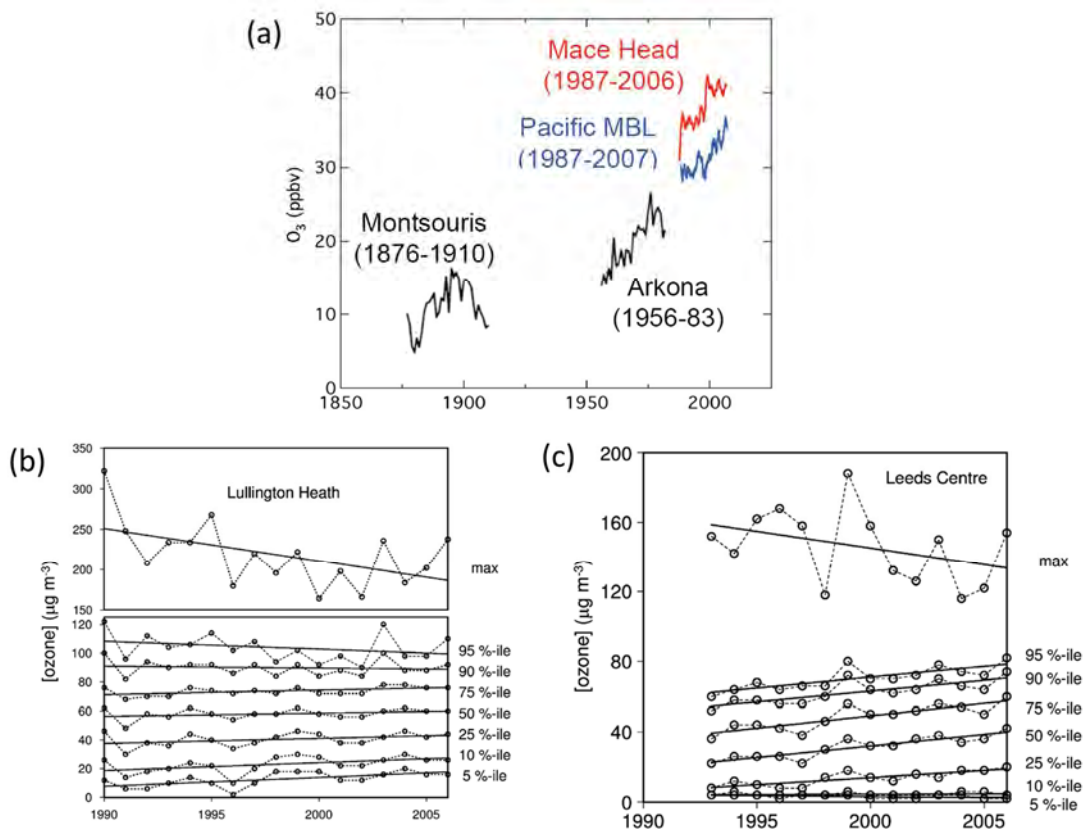
Figure 1-10. (a) Comparison of the 12-month running mean O_3 concentrations from the Pacific MBL sites and Mace Head station in Ireland with the annual averages of earlier measurements reported from two European sites (Montsouris and Arkona stations) by Volz and Kley (1988) (source: Parrish et al., 2009). (b) Trend in hourly mean ozone distribution percentiles at Lullington Heath and (c) Leeds Center, England (source: Jenkin, 2008).

O_3 formation is conditioned by the VOC degradation. This process starts with the attack of free radical initiating chain reactions over VOC and CO. Figure 1-9 left illustrates a simplified schematic of the OH-initiated chemistry. The chemistry initiated by reaction with O_3 and NO_3 radicals, and via direct photolysis, tends to feed into similar reaction mechanisms due to the formation of OH, RO_2 and RO radicals (Monks et al., 2009).

Free radicals OH_x ($OH_x \equiv OH + HO_2$) and RO_2 are of major importance at daytime, both in polluted and clean troposphere. OH is the most significant reactive species because of its high reactivity towards other molecules and its relatively high concentration. The major primary sources of OH_x were identified to be the photolysis of nitrous acid (HONO) and aldehydes (R-CHO), ozonolysis of alkenes (C_nH_{2n}), and to less than 50% by photolysis of O_3 (Atkinson 2000; Monks et al., 2009; Volkamer et al., 2010). Urban air pollution affects human health and plumes of large (mega)cities may influence air quality and climate on regional to global scales (Molina et al., 2007). For these reasons radical chemistry in urban environments has received growing attention in the last years.
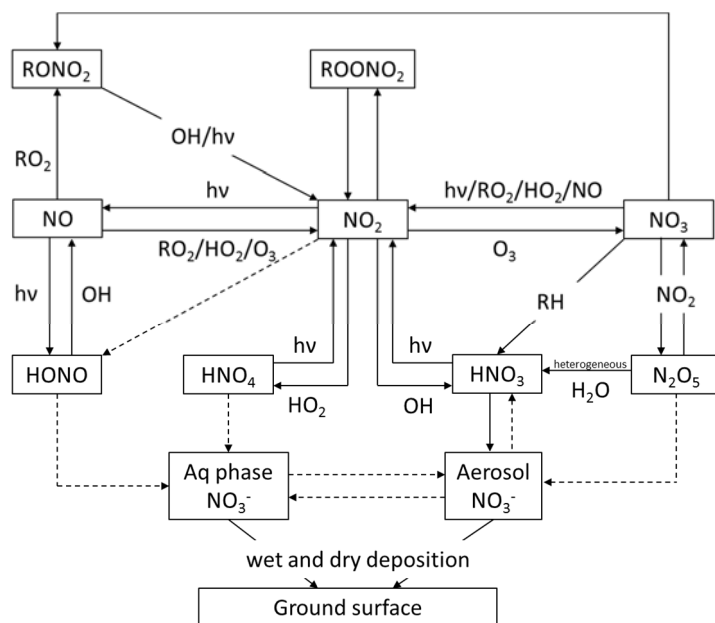
Figure 1-11. Schematic overview of the chemistry of nitrogen compounds in the lower troposphere. R represents hydrocarbon branches. Adapted from Seinfeld and Pandis (1998). Stable species are in squares. Dotted arrows indicate equilibrium gas-phase/aqueous-phase/aerosol.

Nitrogen oxides (NO_x) have also a key role in the atmospheric radical chemistry that leads to the oxidation of reactive trace gases and to the O_3 formation (Figure 1-11). The most important removal process of NO_x is the formation of HNO_3 which is formed via several chemical pathways. During the day, NO_2 may react with the OH radical and during the night another important formation pathway occurs via N_2O_5. Hydrolysis of N_2O_5 takes place on the surface of aerosols and it yields two equivalents of nitric acid. This process is not important during the day, since the NO_3 radical is readily photodissociated to NO and NO_2. Furthermore, N_2O_5 can photolytically and thermically dissociate to NO_2 and NO_3 radical. Uptake of N_2O_5 on aerosol surfaces has been found to be a major mechanism for production of HNO_3 and for removal of NO_x from the atmosphere. A modelling study by Liao and Seinfeld (2005) suggests that it accounts for approximately 30% for all HNO_3 formation in the atmosphere. Recent laboratory studies have addressed the uptake of N_2O_5 at different surfaces providing an improved basis for model simulations of this chemistry. The UV photolysis of HONO is an important source of OH radicals in the polluted urban atmosphere. A recent laboratory study by Li et al. (2008) suggests that the reaction of electronically excited NO_2 with water vapour may be a significant source of OH and HONO in the lower troposphere. Model calculations by Wennberg and Dabdub (2008) demonstrate that the new OH source could be relevant for the photochemical formation of O_3 and fine particles in urban environments and recommend further investigation of the kinetics of $NO_2^* + H_2O$ reaction. Wet and dry depositions are significant sinks for these species. Deposition of nitrogen compounds is of capital importance as an input of nutrients to vegetation.

Chemical reactions of VOC and anthropogenic NO_x emissions dominate over those of CH_4 and its degradation products. Tropospheric chemistry is significantly complicated because of the presence

of many NMVOC and complexity in their chemistry. Nowadays, there are still considerable gaps of knowledge in various aspects related to NMVOC degradation.

Alkanes, alkenes and alkynes constitute a major class of anthropogenic hydrocarbon emissions. Aromatic organic compounds are a major class of organics associated mainly with the urban environments.

Oxygenated volatile organic compounds (oVOC) are either emitted directly by anthropogenic and biogenic sources or are produced in the atmosphere in the course of the oxidation of hydrocarbons. The most abundant oVOC in the atmosphere are formaldehyde (HCHO), acetone (CH_3COCH_3) and methanol (CH_3OH).

Measured formaldehyde and acetone concentration from the Artic to the Mediterranean were 0.2-1.2 ppbV and 0.4-1.3 ppbV, respectively, with lowest values in the Arctic and highest concentrations in Southern Europe (Solberg, 2006). Formaldehyde plays a key role in atmospheric chemistry as it readily photolysis, being a source of the HO_2 and O_3. It is formed either as an intermediate during the oxidation of many VOC or is emitted directly by fossil fuel combustion or biomass burning. The European background level of less than 1 ppbV increases slightly in rural regions and over the Mediterranean. Higher values are measured in urban environments, as the primary emissions get more important. In Europe the highest values are measured at urban agglomerations in Southern Europe (30 ppbV in Athens (Bakeas et al., 2003)). Acetone is primarily emitted by fossil fuel combustion, biomass burning and industrial processes and is a secondary product in the atmosphere from the oxidation of anthropogenic isoalkanes (Jacob et al., 2002).

Methanol is the most abundant NMVOC in the atmosphere with concentrations in European background ranging from 0.6 ppbV at a high-Alpine site to nearly 4 ppbV in the Mediterranean (Kormann et al., 2003; Salisbury et al., 2003; Legreid et al., 2008). The atmospheric importance of alcohols will increase in the future as there is a rise in biofuel usage.

Atmospheric oVOCs have gained increasing attention over the last few years owing to a considerable progress in analytical methods and the realisation of their extensive involvement in atmospheric processes (Laj et al., 2009). There are still considerable gaps of knowledge in their influence on secondary organic aerosol (SOA). Halmilton et al. (2004) underlined the importance of oVOCs in SOA by means the detection of a multitude of oxygenated organic groups within SOA.

VOC with a biogenic origin (bVOC) are in general extremely reactive, and hence can exert a controlling influence over the oxidative chemistry near their emission source. For example, as the majore reaction partner for OH, these species can control OH levls, [OH]/[OH_2] ratios, and O_3 production (Monks et al., 2009). Isoprene, terpenes as sesquiterpenes are bVOC which represent an important source of SOA, thus providing an additional major impact of these species on both climate-related and air quality issues. Rate coefficient for reaction of OH, NO_3 and O_3 are well-established for most bVOC (Atkinson and Arey, 2003). However, the mechanisms involved in the oxidation of these bVOCs and the nature of the products formed are not so well-established (Atkinson and Arey, 2003).

1.1.3.2 Aerosols

Atmospheric PM, also namely aerosols, originates from a wide variety of natural and anthropogenic sources (Finlayson-Pitts and Pitts, 2000). Primary particles are directly emitted as liquids or solids from sources such as biomass burning, incomplete combustion of fossil fuels, volcanic eruptions, and wind-driven, industrial or traffic-related suspension of road, soil, and mineral dust, sea salt and biological materials (plant fragments, micro-organisms, pollen, etc.). On the other hand, secondary particles are formed by gas-to-particle conversion in the atmosphere and/or condensation of gaseous compounds on pre-existing aerosol particles. In particular, secondary aerosols dominate atmospheric PM in Europe at many monitoring sites (Putaud et al., 2004). Distinguishing between primary and secondary aerosols is critical for AQ management since primary sources can be controlled, in contrast to the secondary sources that are influenced by biogenic emissions and photochemistry and therefore are difficult to regulate.
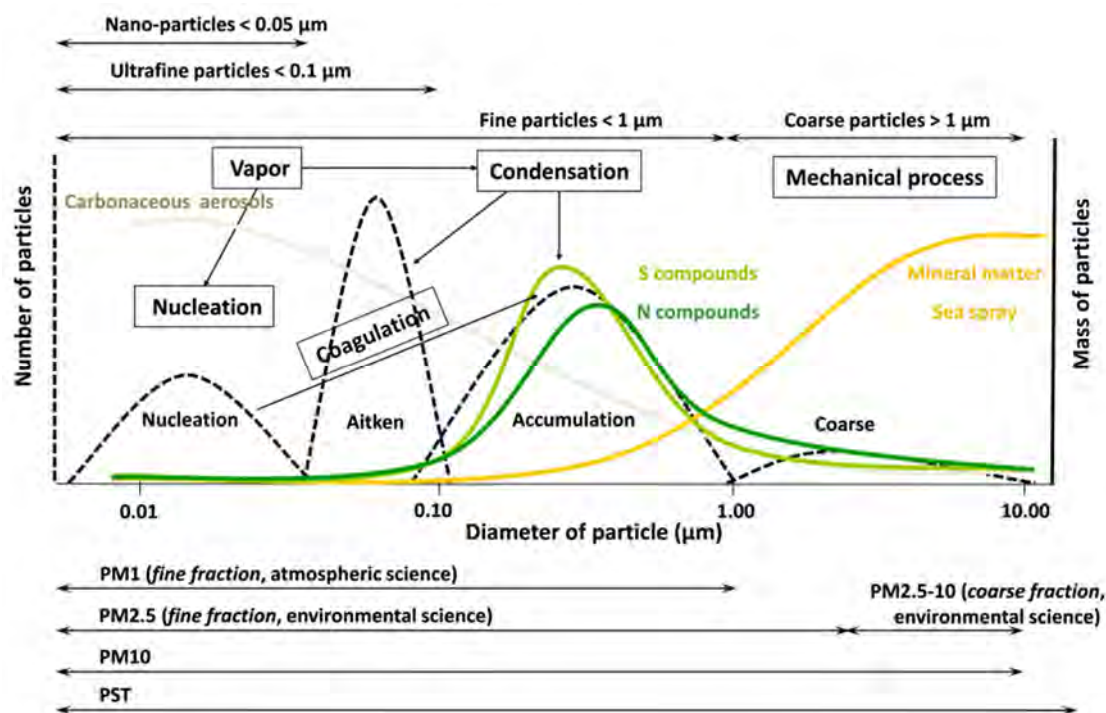
Figure 1-12. Relationship between particulate matter size, number of particles (discontinuous line), and chemical mass composition (solid line). Aerosol physical processes are represented in boxes. Adapted from Warneck (1988) and Harrison and van Grieken (1998).

Concerning the number of particle distribution (Figure 1-12), aerosol size is grouped into different modes: nucleation mode (<20 nm diameter), Aitken mode (20 – 100 nm diameter), accumulation mode (0.1 -1 μm diameter), and coarse particle mode (>1 μm diameter) (Finlayson-Pitts and Pitts, 2000). In environmental science, PM10 and PM2.5 (defined as the mass fraction of PM that pass through a selective inlet for an aerodynamic diameter of 10 and 2.5 μm, respectively, with a 50% efficiency) are usually selected as monitoring parameters in worldwide environmental standards. In

this field, coarse fraction is considered the fraction between 2.5 and 10 μm (PM2.5-PM10), whereas PM2.5 is considered the fine fraction.

As shown in Figure 1-12, aerosols undergo various physical and chemical interactions and transformations, such as changes of particles size, structure, and composition (Pöschl, 2005). Many chemical reactions also occur in clouds, which are formed by condensation of water vapour on pre-existing aerosol (cloud condensation or ice nuclei). Most clouds re-evaporate, and modified aerosol particles again released from the evaporating cloud droplets or ice crystals.

The concentration, composition, and size distribution of aerosol are temporally and spatially highly variable. In the troposphere, the total particulate number and mass concentrations typically vary in the range of about 10^2-10^5 cm^{-3} and 1-100 μg m^{-3}, respectively. PM includes as principal components sulphate, nitrate, ammonium, organic compounds, black or elemental carbon, mineral matter, and sea spray. The first five components are mostly present as fine particles less than 2.5 μm diameter (PM2.5), meanwhile mineral matter and sea spray are frequently in the coarse fraction (Figure 1-12). Sulphate, nitrate, and organic compounds are produced with in the atmosphere by oxidation of SO_2, NO_x, and NMVOC, respectively. Carbon particles are also emitted directly by combustion.

As an example, according to van Dingenen et al. (2004) and Putaud et al. (2004) the background annual average PM10 and PM2.5 concentrations for continental Europe have been 7.0±4.1 and 4.8±2.4 μg m^{-3}, respectively, over the past decade. In the observed aerosol composition at the surface, organic matter was found to be the major component of PM10 and PM2.5, except at natural and rural sites where sulphate and mineral matter prevailed. These results subscribe those present in Figure 1-13, extracted from Querol et al. (2009a). Figure 1-13 shows an European map of measured-speciated aerosol concentration at background stations, extracted from that study. The comparison of southern Europe and north and central Europe, in terms of composition, shows major gradients of mineral matter, nitrate, sulphate, organic matter and elemental carbon. At southern Europe, mineral matter is the major component of PM10 (22 to 38%), followed by sulphate, organic matter, nitrate and ammonium. A prominent north-south gradient in mineral matter is attributed to the proximity to dust sources and the higher frequency and intensity of African dust outbreaks. Sea spray shows a marked variation with a clear increasing trend towards the eastern Mediterranean Basin, especially in the coastal sites, where it may reach significant levels to become a major component of PM10. Sulphate levels measured in central, southern and eastern Europe and UK (2-4 μg m^{-3}) are higher than those measured at northern Europe (1-2 μg m^{-3}). SO_2 emissions from power generation, contribute to enhanced sulphate levels. Nitrate and ammonium levels in southern Europe (1.7 – 1.9 μg m^{-3}) are lower than in central Europe and UK (2-4 μg m^{-3}) and slightly higher than at rural background sites of northern Europe (0.5-1 μg m^{-3}). Higher ambient temperature favouring the gas phase prevalence of nitrate. Elemental carbon and organic matter are lower over southern Europe (0.2-0.4 and 5-6 μg m^{-3}, respectively) compared to central Europe (Putaud et al., 2004; Pio et al., 2007).
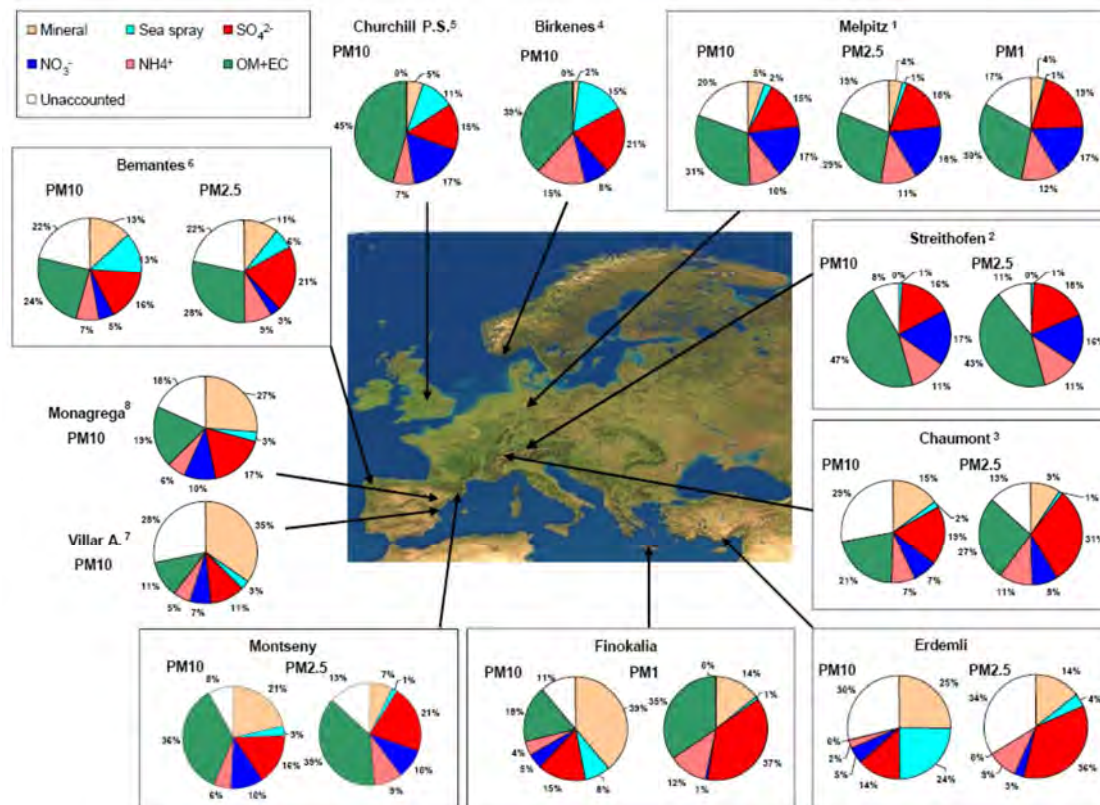
Figure 1-13. Annual mean levels of speciated PM10 and PM2.5 measured at rural background sites. OM+EC indicates the sum of organic matter + elemental carbon (Source: Querol et al., 2009a).

1.2 Air quality management

Exposure to air pollution is largely beyond the control of individuals and requires action by public authorities at the national, regional and even international levels. Air pollution can be basically regulated in various ways: by emissions standards, by AQ standards, by emission taxes and by cost benefit analyses. In the case of Europe, the European Union (EU) has developed a legal framework related to AQ that all the Member Countries have to accomplish. The European directives can be classified in two groups: (1) pollution emission control and (2) AQ standards.

In Europe, after major smog events in the 1950s in UK, air pollution became the focus of international negotiations as it appeared that polluting activities in a given country could have a significant impact on the air quality of its neighbours. Scientific collaborations and multilateral policy negotiation led to the 1979 Convention on Long-Range Transboundary Air Pollution (CLRTAP) and its Gothenburg Protocol accepted in 1999 (UNECE, 1999) as well as the EU National Emissions Ceiling (NEC) Directive (European Commission, 2001). In 2005, the European Commission published its Thematic Strategy on Air Pollution under the 6th Environmental Action Programme: the Clean Air For Europe (CAFE) programme (CAFE, 2005), which established a long-term policy strategy targeting the adverse effects on air pollution on human health and environment. It determined a set of objectives to be reached within the ongoing

revision of the Gothenburg Protocol and the NEC directive. It also sets the basis for the current standards on ambient air quality and cleaner air for Europe compiled in the Directive 2008/50/EC (European Commission, 2008).

Table 1-2. Current European/Spanish AQ standards and WHO guidelines for the protection of human health.

	Refr.[a]	Limit or target[b] value			Time extension[c]	Long-term objective		Information[d] and alert thresholds	
		Aver. period	Value ($\mu g \ m^{-3}$)	Date	New date applicable	Value ($\mu g \ m^{-3}$)	Date	Period	Value ($\mu g \ m^{-3}$)
SO_2	EU/ES	Hour	350 (< 25 h y^{-1})	2005				3 h	500
		Day	125 (< 3 d y^{-1})	2005					
	WHO	Day	20						
NO_2	EU/ES	Hour	200 (<18 h y^{-1})	2010	2015			3 h	400
		Year	40	2010					
	WHO	Hour	200						
		Year	40						
O_3	EU/ES	8-h[e]	120[b] (< 25 d 3y^{-1})	2010		120		1 h	180[d]
								3 h	240
	WHO	8-h[e]	100						
PM10	EU/ES	Day	50 (<35 d y^{-1})	2005	2011				
		Year	40	2005	2011				
	WHO	Day	50						
		Year	20						
PM2.5	EU/ES	Year	25[b]	2010		8.5 to 18	2020		
			20 (ECO*)	2015					
	WHO	Day	25						
		Year	10						
C_6H_6	EU/ES	Year	5	2010	2015				
CO	EU/ES	8-h	10	2005					
Pb	EU/ES	Year	0.5[b]	2005					

*ECO: The exposure concentration obligation for PM2.5 to be attained by 2015, is fixed on the basis of the average exposure indication, with the aim of reducing harmful effects on human health. The range for the long-term objective (between 8.5 and 18) indicates that the value is depending on the initial concentrations in the various Member States.
[a]References: EU, European Union, Directive 2008/50/EC (European Commission, 2008); ES, Spain, RD 102/2011 (BOE, 2011); WHO, World Health Organization (WHO, 2005).
[b]Indicates that this is a target value and not a legally binding limit value; see European Commission (2008) for definition of legal terms.
[c]For countries that sought and qualified for time extension.
[d]Indicates that this is an information threshold and not an alert threshold; see European Commission (2008) for definition of legal terms.
[e]Maximum daily eight-hour mean concentration shall be selected by examining eight-hour running averages, calculated from hourly data and updated each hour.

Table 1-3. European/Spanish AQ standards for the protection of vegetation.

	Refr.[a]	Critical level or target value			Long-term objective	
		Aver. period	Value	Date	Value	Date
SO₂	EU/ES	Calendar year and winter (1 October to 31 March)	$20\ \mu g\ m^{-3}$			
NOₓ	EU/ES	Calendar year	$30\ \mu g\ m^{-3}$			
O₃	EU/ES	May to July	AOT40* $18,000\ \mu g\ m^{-3} \cdot h$ averaged over five years	2010	AOT40* $6000\ \mu g\ m^{-3} \cdot h$	Not defined

*AOT40 (expressed in $\mu g\ m^{-3} \cdot h$) is the sum of the difference between hourly concentrations greater than $80\ \mu g\ m^{-3}$ (=40 parts per billion) and $80\ \mu g\ m^{-3}$ over a given period using only the one-hour values measured between 8:00 and 20:00 Central European Time (CET) each day from 1 May to 31 July each year, for vegetation protection and from 1 April to 30 September each year for forest protection.
[a]References: EU, European Union, Directive 2008/50/EC (European Commission, 2008); ES, Spain, RD 102/2011 (BOE, 2011).

The current AQ directive merges most of existing legislation into a single directive with no change to existing AQ objectives[1]. It includes for the first time an annual AQ objective for PM2.5 (25 µg m⁻³) including the limit value and exposure indicator for each State based on measurement at urban background stations. The Directive 2008/50/EC provides the possibility to discount natural sources of pollution when assessing compliance against limit values. This latter fact is relevant in southern European countries, frequently affected by Saharan dust events due to their proximity to the African continent. As a novelty, the recent European directive includes the possibility for time extensions of three years (PM10) or up to five years (e.g. NO₂, benzene) for complying with limit values, based on conditions and the assessment by the European Commission (EC). The Directive2008/50/EC has been recently transported to the Spanish legislation as a Real Decreto (RD) 102/2011 (BOE, 2011).

The World Health Organization (WHO) recommends AQ standards to the human health protection which are taken as a reference for the regulatory measures of large number of countries around the world, among then the European countries. Table 1-2 and Table 1-3 summaries the AQ standards of the main pollutants taken as reference in Europe and Spain for the protection of human health and vegetation, respectively.

1.3 State of the art in air quality modelling

Currently, the information sources on air quality are: (1) **air quality measurements** from monitoring stations, (2) **emission measurements** (emissions inventories), (3) **emission**

---

[1] Framework Directive 96/62/EC, 1-3 daughter Directives 1999/30/EC, 2000/69/EC, 2002/3/EC, and Decision on Exchange of Information 97/101/EC.

modelling, and (4) **air quality modelling** (AQM). AQ and emission measurements are efficient tools to directly assess AQ and pollution abatement policies. However, complex meteorology, land uses and lack of detailed chemistry may confer biased information. Emission modelling is essential to evaluate the effect of a management strategy introduced. Nevertheless, due to the non-linearity of the atmospheric chemistry and the transport processes that occur in the atmosphere it is not possible to establish a direct relationship between emissions reductions and local AQ improvements. Therefore, a proper use of observation and emission measurements and modelling can be assured complemented with AQ modelling.

Baldasano and Millán (2000) define AQM as computerized representations where the emissions of pollutants introduced into the atmosphere are related to the concentrations of these in the air, through the application of physical and chemical laws translated into basic thermodynamics, fluid mechanic equations and others which are typical for chemical reactions.

AQMs describe processes at a wide range of spatial and temporal scales, and they are used in widely differing applications ranging from research on atmospheric processes to AQ regulatory purposes. The recent European legislation framework on AQ (2008/50/EC, European Commission, 2008) explicitly recommends the use of modelling techniques for different AQ application classified as follows (Denby et al., 2010):

- **AQ management**. AQMs are important because they predict the impact of pollutants, identify source contribution to AQ problems and help in the design of effective strategies to reduce the effect of pollutants. AQMs are used extensively in AQ forecast, providing next day and near real time information to the public and for the implementation of short term action plans. AQMs are also useful to assist in the design and appraisal of monitoring networks, since they predict spatial patterns of pollutants, including the location of maximum and minimum concentrations as well as strong gradients.

- **AQ assessment**. AQMs can be used to supplement or even replace monitoring data for zones where the concentration of pollutants in ambient air does not exceed the upper limit and target values or where measurements do not give sufficient information to fulfil the requirements of an AQ assessment.

- **AQ source apportionment**. AQMs are useful to assess the causes of exceedances of AQ thresholds, the contribution from natural sources, neighbouring countries and the contribution from resuspended road sand and salt.

An integrated system for AQM should mainly include three modules, that take into account all the factors involved and closely related in the generation and dispersion of pollutants: (1) **meteorological model**, which describes the state and evolution of the atmosphere in which these emissions are introduced; (2) **emission model**, which describes the spatio-temporal distribution of both natural and anthropogenic emissions; and (3) **chemical transport model** (CTM), which describes the physical and chemical transformations that take place for emitted pollutant under specific meteorological situations. These components have been previously described in Seinfeld (1988), Russell and Dennis (2000) and more recently in Menut and Bessagnet (2010).

Nowadays, some relevant processes still remain missing in models (Menut and Bessagnet, 2010). As an example, PM derived from the erosion of rocks on land in Europe, which is important for PM budget and surface exceedances calculation are not well characterized. Fire emissions are another issue, with directly impact on radiation budget and surface PM load. Figure 1-14 shows the structure of an integrated AQM system and related modelling tools where main identified gaps are indicated.
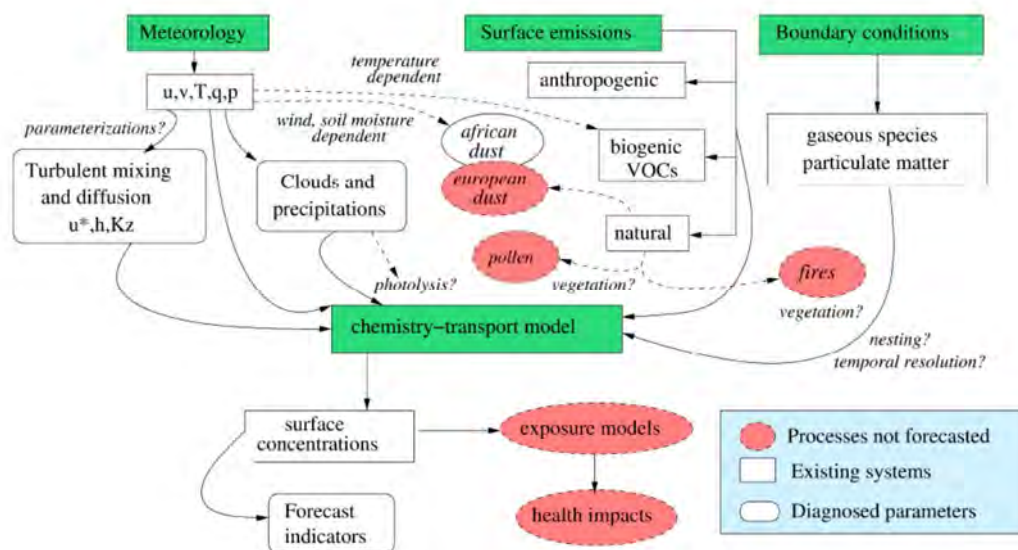
Figure 1-14. Flowchart of a AQM system, including all processes and interactions between them. Future direction in process modelling are highlighted in red. (Source: Menut and Bessagnet, 2010)

Emission models give information about quantity and kind of pollutants from different sources located in a determined geographical area (discretised in a grid cell) in a period of time (Baldasano, 1998). This information is essential to provide inputs to CTMs. Section 1.1.1 revised the main emission sources and trends in Europe and Spain. Emission estimates are collected together into inventories or databases which usually also contain supporting data about the source locations, emissions measurements (when available), emission factors, activity rates, operating conditions, methods of estimations emissions, etc. Fundamentally, there are two approaches in the development of emission inventories (Costa and Baldasano, 1996): (1) **top-down approach**, which estimates total emissions for the geographical under study and then prorates those emission in the cells of the grid of analysis by means different parameters (e.g. detailed information on activities, population, etc.); (2) **bottom-up approach**, which estimates emissions for all cells of the grid of analysis through establishing every parameter for each cell in particular, therefore total emission value is obtained by aggregation of estimation in every single cell. Information on emission modelling can be found in a variety of sources, e.g. the EMEP/EEA air pollutant emission inventory guidebook (EMEP, 2009).

According to the reference frame employed, CTMs can be **Eulerian** (or grid-based) and **Lagrangian** (or trajectory) models (Russell and Dennis, 2000). Nowadays, the use of Lagrangian models is limited in spite of being largely used in the past due to their simplicity and low computational requirements. The increasing computational capabilities and the larger database, together with advances in the knowledge and understanding of atmospheric processes lead to the extended used of Eulerian models. Currently the most advanced CTMs are the third generation systems, which are three-dimensional (3-D) non-hydrostatic Eulerian models.

An important component of AQMs is the gas-phase chemical mechanisms implemented in CTMs because secondary pollutants such as O_3 and PM are formed during the gas-phase degradation of anthropogenic and biogenic compounds (Seinfeld and Pandis, 1998; Finlayson-Pitts and Pitts, 2000). Different gas-phase chemical kinetic mechanisms have been developed to represent atmospheric chemistry, ranging from simple (< 10 species) to complex (> 1000 species). Hence, the chemical mechanisms used in 3-D AQMs must achieve a balance between the complexity of the mechanism and its computational efficiency (Dodge, 2000). Condensed mechanisms with 50 to 100 species (e.g., SAPRC, Carter (2010); RACM, Stockwell et al. (1997); Goliff and Stockwell, (2008)) and carbon-bond mechanisms (CBM-IV, Gery et al. (1989); CB05, Yarwood et al. (2005)) are typically used in 3-D AQMs. Several inter-comparison studies of different chemical mechanisms have been performed with trajectory models and 3-D AQMs over the last decade with the objective to simulating O_3 and its precursors (Kuhn et al., 1998; Gross and Sockwell, 2003; Jiménez et al., 2003; Luecken et al., 2008; Kim et al., 2009) and aerosols (Pan et al., 2008; Sarwar et al., 2008; Kim et al., 2011). A common conclusion in several of the documented inter-comparisons appears to be that most models are able to reproduce the O_3 concentrations, whereas they do not perform as well in simulating other compounds, such as NO_x and their reaction products.

The way in which meteorological models couple with CTMs can be realized in one of two principal ways (Grell et al. 2005; Baklanov et al., 2008). (1) **Off-line modelling systems**, also called one-way interactive models, contain a separate CTM driven by meteorological input data from meteorological pre-processors, measurements or diagnostic models at limited time intervals (e.g. 1, 3, 6 h). (2) **On-line modelling systems**, also called integrated or two-way interactive models, can be on-line access models, when meteorological data are available at each time-step, or on-line integration of a CTM into a meteorological model, where two-way feedbacks may be considered. Both offline and online modelling system are actively used in current regional models (Zhang, 2008). Off-line systems are frequently used in ensembles and operational forecasting, adjoint modelling and sensitivity studies, whereas on-line models are increasingly used for applications in which air-pollution feedbacks on meteorology processes and climate forcing become important and where higher computation cost is not a limiting factor.

The precise definition of the grid resolution is an important decision when applying an AQM (Russell and Dennis, 2000; Menut and Bessagnet, 2010). The average volume defined by the model's horizontal grid spacing must be sufficiently small to allow the AQ to be reproduced accurately. The large averaging volumes used by regional models are feared to lead to unacceptable errors for many species that are formed via nonlinear chemical reactions, particularly in areas with significant chemical gradients, such as cities. Recently, in the European model inter-comparison over cities, CityDelta, Vautard et al. (2007) compared the performance of different modelling

systems with fine (~5km) and large resolution (~50km) for simulating O_3 and PM10 over cities. They found that fine-scale models showed better performance for PM10 in cites, and treat the titration effect of O_3 better than large-scale models. But, even with the finest scale, the modelled concentrations are not necessary the better (Valari and Menut, 2008). This paradoxical result is mainly due to the fact that by increasing emissions and meteorology spatial resolution, uncertainties also increase with the risk of model error. Even more, computational cost increases markedly with the inverse of the grid spacing. McQueen et al. (1995) performed a sensitivity analysis on the influence of grid size when applying mesoscale numerical weather prediction models. The study showed the importance of using high-resolution grids when the model is applied to a complex terrain. Horizontal resolution up to 1 km should be considered when simulating vertical motion associated with sea breezes (Lyons et al., 1995).

Information of widely used AQM systems with sufficient availability of scientific literature and Web-based documentation in Europe are contained in the EIONET **Model Documentation System** (MDS[2]) of the European Environment Agency (EEA) and in the **Cost Model Inventory** (CMI[3]) of the European Cooperation in Science and Technology (COST) through the actions COST 728 and COST 732. Furthermore, AQ forecasting systems currently operating in Europe are compiled in the **European Open Access Chemical Weather Forecast Portal[4]**, in the frame of European Cooperation in Science and Technology (COST) Action ES0602 (Balk et al., 2010). This portal includes access to more than 20 AQ forecasting system and covers in total 31 areas in Europe. Also a critical review of 23 AQ forecasting system working routinely in Europe is presented in Menut and Bessagnet (2010).

The use of an AQM without comparison with observations is useless to an adequate AQ assessment. In this sense, some authors consider a fourth module corresponding to model evaluation which helps to the decision of the support system. To instil confidence in the model's prediction for the future or model assessment of the AQ, we must be assured that the model's process descriptions and interactions are as accurate and realistic as possible (Russell and Dennis, 2000). Therefore, model evaluation of the simulated results versus observations is strongly needed.

1.4 Model evaluation framework

1.4.1 Important concepts in model evaluation

AQM systems and their applications should be reliable and trustworthy on simulating the spatial and temporal features on the scales resolved by the model, and also to assess whether the physical and chemical processes are simulated correctly. In this sense, **model quality assurance** (AQ) and scientific **model evaluation** are crucial elements to get this purpose.

---

[2] Available at: http://acm.eionet.europa.eu/databases/MDS/index_html
[3] Available at: http://www.mi.uni-hamburg.de/index.php?id=539
[4] Available at: http://www.chemicalweather.eu/Domains

According to Denby et al. (2010), quality assurance is defined as an integrated system of management activities involving planning, documentation, implementation and assessment established to ensure that the process, item, or service is of quality needed and expected by the user. In AQM there are different concepts to determine the quality of a model. According to Russell and Dennis (2000) and Denby et al. (2010) model "evaluation" is different from model "validation" and "verification":

- **Verification** is an internal process that determines the consistency, completeness, and correctness of the fundamental equations, methods, hypotheses, computer codes and adequacy of the model design relative to the design criteria model. Verification does not assure that the model design criteria are necessarily sufficient to adequately represent the physico-chemical system for the modelling task at hand.

- **Validation** is an external process that determines the veracity and legitimacy of the model with respect to a user's needs and requirements or the correctness of the model's representation of reality. One works towards validation through a series of confirming observations. It is important to select a big group of observations including critical cases in order to assure that correct model results are not anomalies. These confirming observations, however, can only support the probability that a model is valid, not establish validity.

- **Evaluation** is the sum of processes that determine and quantify the model's performances capabilities, weaknesses and advantages for a specific application. As validation, model evaluation is done through comparison against experimental data. Evaluations can never demonstrate the veracity of a model, but can raise doubts about the science in a model.
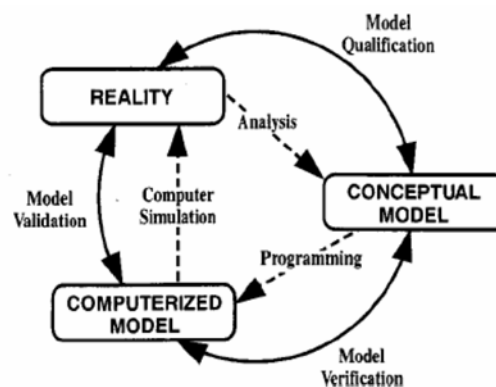
Figure 1-15. Phases of modelling and simulation and the role of verification, validation and evaluation. (Schlesinger et al., 1979)

The similarity between these three concepts is that they are tasks for QA of the modelling process. Differences between these concepts consist in the fact that they have different purposes and are

correlated in time (Figure 1-15). First, it is necessary to show that the model is built right (verification), then assure that the right model was built (validation), and finally determine the usefulness of the model for a specific application (evaluation or model qualification). According to Borrego et al. (2003), meanwhile model evaluation is related to measuring model quality, QA is a process to guarantee the expected quality for decision-making.

Model evaluation criteria are dependent of the AQM's applications (Section 1.3). For regulatory application, AQM must provide an adequate estimate of concentration response to forcing variables, such as emissions and meteorology, furthermore to adequate estimates of species concentrations. By contrast, a forecast model is judged solely by its ability to simulate the temporal evolution of chosen forecast variables. In this framework, there are three primary objectives in model evaluation (Dennis et al., 2010):

1. **Determining the suitability of an AQM for a specific application and configuration**. The main goal of the model evaluation exercise is to demonstrate that the AQ modelling system is making reasonable simulations, when compared with observations, taking into account the adequacy and correctness of the science represented in the model for the purposes, for which the model is applied.

2. **Distinguishing the performance among different AQMs or different versions of the same AQM**. It is necessary to compare the relative performance of different AQMs with observation to better understand AQM's strengths and weakness. Furthermore, inter-comparisons can identify areas requiring further model development.

3. **Guiding AQM improvement**. Evaluation results should lead to new directions in model development and improvement

Taking into account these objectives, Denby et al. (2010) and Dennis et al. (2010) define a framework for evaluating AQM systems classified in four modes (see Figure 1-16). **Operational evaluation** examines if the model estimates are in agreement with the observations in an overall sense. It utilizes routine observations of ambient pollutant concentrations, emissions, meteorology, and other relevant variables. **Diagnostic evaluation** focuses on process-oriented analyses to determine whether the individual processes and components of the model system are working correctly, both independently and in combination. This type of evaluation generally requires detailed atmospheric measurements that are not routinely available. **Dynamic evaluation** assesses the ability of the AQM systems to simulate changes in air quality stemming from changes in source emissions and/or meteorology; the principal forces driving the AQM, which required historical case studies that could be confidently estimated. Recognizing that there is an inherent uncertainty in both AQM systems and measurements, **probabilistic evaluation** attempts to assess statistical properties, including uncertainty or level of confidence in the model results for AQ management or forecast using techniques such as ensemble modelling and Bayesian model averaging.
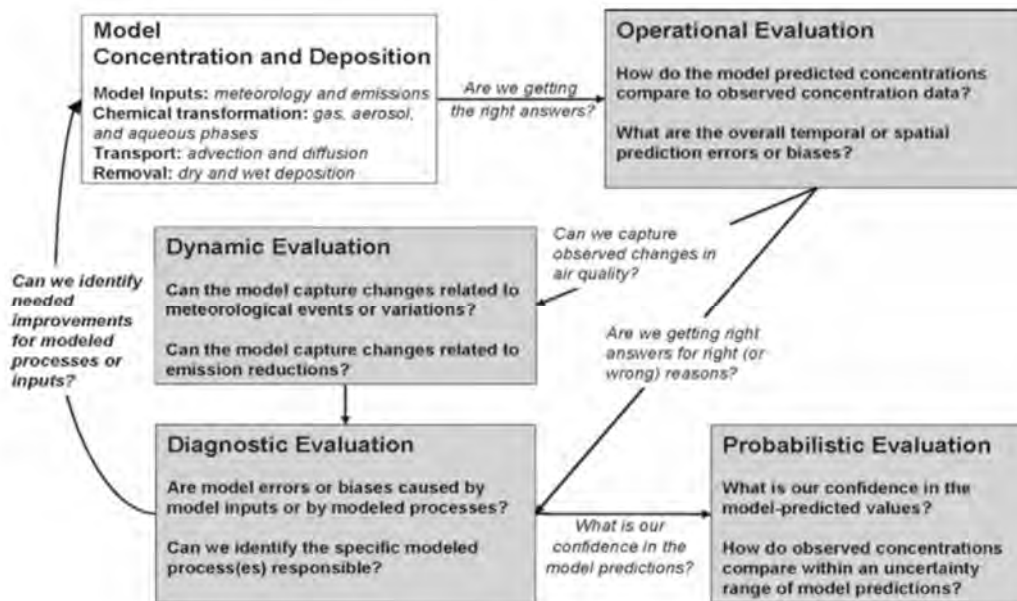
Figure 1-16. A framework for evaluating AQM systems (Source: Dennis et al., 2010).

Other aspects often mentioned as relevant or necessary for model evaluation are (Denby et al., 2010):

- **Uncertainty analysis**. The term uncertainty refers to lack of knowledge or information on the models, parameters, constants, input data and concepts (US EPA, 2009). The total model uncertainty may be defined by the sum of three components (Chang and Hanna, 2004; Borrego, 2008): (1) model uncertainty which is associated with model formulation; (2) input data uncertainty which is related to emissions, observational data, meteorology, chemistry or model resolution; and (3) inherent variability which refers to stochastic and anthropogenic processes that by nature are not known. Some methods for assessing model uncertainty are Monte Carlo analysis, sensitivity analysis, model ensemble, model inter-comparison and statistical analysis using observations.

- **Sensitivity analysis**, which is the process to understand how a given model depends upon the information, fed into it. Sensitivity testing can be performed with respect to models chemistry/physics parameters or with respect to input data (emissions, meteorology). Methods are explained in Saltelli et al. (2005).

- **Model inter-comparison,** which is the process to assess a model performance by simultaneous comparison of modelling results provided by different models for the chosen situations. The differences in model results can reveal the strengths and weaknesses of particular modules or parameterisations schemes and can help to characterize conceptual uncertainties arising from the choice and implementation of the physical models applied.

1.4.2 Review of initiatives in model evaluation

Nowadays, several studies have addressed the QA and evaluation of the modelling process. In Europe, different model evaluation initiatives have been supported by the EC through projects and networks of excellence as ACCENT. Table 1-4 summarizes the main initiatives developed in the last two decades in Europe. Single model evaluation studies offer the chance to see the weaknesses of the model and thereby lead to efficient improvements. Furthermore, multi-model evaluation projects can confront some of the problems more effectively, and in many cases more cost-effectively.

There are several reports available to support modelling systems and best practices. The EUROTRAC-2 subprojects SATURN (Studying Atmospheric Pollution in Urban areas) (Moussiopoulos, 2003) provided a review of AQ models for use in urban applications. Furthermore, within the EUROTRAC-2 subproject GLOREAM (GLObal and Regional Atmospheric Modelling) numerous activities were developed according to regional-scale model inter-comparison for O_3 (Roemer et al., 2003) and inorganic aerosol compounds (Hass et al., 2003). On the other hand, the Air4EU project[5] (Borrego et al., 2006; Borrego et al., 2008) provided a number of reports recommending best practises for the use of models in AQ assessment and estimations of model uncertainty.

Recently, in the context of the CAFE programme model inter-comparison studies have been performed to evaluate the impact of emission-reduction strategies on AQ at the European continental scale and in European cities in terms of O_3 and PM10. Meanwhile EuroDelta (van Loon et al., 2007) evaluated AQ improvements at the European scale in response to regional emissions reduction scenarios for 2010, CityDelta (Cuvelier et al., 2007; Vautard et al., 2007) evaluated AQ responses of emission abatement scenarios for 2010 in European cities (Berlin, Milan, Paris, and Prague). Furthermore, CityDelta evaluated the impact of horizontal resolution (50 km versus 5 km) in terms of O_3 and PM10.

Albeit a number of documents and projects have addressed the guidance on the use of AQM, the modelling community is so broad and the applications of AQM so varied that nowadays, there is not a clear and common understanding of the quality assurance requirements that should be applied in AQM. Indeed, there are still some aspects of the European AQ Directive itself that are ambiguous as required further clarification. In this context, the Forum for Air Quality Modelling in Europe (FAIRMODE), coordinated by the European Environmental Agency (EEA) and the European Commission Joint Research Center (JRC), aims to bring together AQ modellers and users in order to promote and support the harmonised used of models by EU Member countries, with emphasis on their application to the AQ Directive. In this sense, FAIRMODE provides a dynamic document (with regular updates base on internal or external activities) which represents a consensual guidance on AQ modelling (last version Denby et al., 2010).

In parallel, in North America, the United States Environmental Protection Agency (US EPA) has recently published a guide on environmental model which presents recommendations and provides an overview of best practises for ensuring and evaluating the quality of environmental models (US

---

[5]Available at http://www.air4eu.nl/reports_products.html

EPA, 2009). In recent times, a joint initiative between North America and EU has been established in terms of AQ model evaluation, namely AQMEII[6] (Air Quality Model Evaluation International Initiative) with the aim to bring together American and European regional scale modelling communities, for an effect and efficient exchanges of views and experiences through common activities.

Table 1-4. Current quality assurance and evaluation initiatives in AQM in Europe.

EU Initiative	Objective	References
ACCENT	Definition protocols and benchmark tests suitable for AQ assessment in regional and global scales.	http://www.accent-network.org/
Air4EU project	Evaluation strategy and uncertainty analysis for models from hotspot to regional scale	http://www.air4eu.nl, Borrego et al. (2006)
COST action 728	Standardised model evaluation protocol for mesoscale models	http://www.cost728.org/, Schlvenzen and Sokhi (2008)
COST action 732	QA for mesoscale models	http://www.mi.uni-hamburg.de/Home.484.0.html, Britter and Schatzmann (2007)
Cost Model Inventory	To compile a database with used European model	http://www.mi.uni-hamburg.de/index.php?id=539
ENSEMBLE platform	To on-line inter-compare and evaluate AQ models within the context of COST728	http://ensemble2.jrc.ec.europa.eu/, Galmarini et al. (2004a,b)
EuroDelta and CityDelta	Modelling inter-comparison exercises in support of the modelling activities within the CAFE programme	http://aqm.jrc.it/citydelta/, Cuvelier et al. (2007), van Loon et al. (2007), Vautard et al. (2007)
EUROTRAC2-SATURN	AQM inter-comparison and single evaluation of urban scale models	http://aix.meng.auth.gr/saturn/, Moussiopoulos (2003)
EUROTRAC2-GLOREAM	AQM performance and evaluation for global and regional scale model	http://www2.dmu.dk/AtmosphericEnvironment/gloream/, Hass et al (2003), Roemer et al., (2003)
FAIRMODE	To bring together air quality modellers and users in order to promote and support the harmonised use of modelling practices for the assessment of air quality by EU member countries.	http://fairmode.ew.eea.europa.eu/, Denby et al. (2010)
HARMO	Harmonization on model quality assurance	http://harmo.org/
Model Documentation System	To provide guidance to any model user in the selection of the most appropriate model for its application	http://acm.eionet.europa.eu/databases/MDS/index_html
The review of the Unified EMEP model	Modelling inter-comparison of regional scale models	van Loon et al. (2004)

---

[6] Available at http://aqmeii.jrc.ec.europa.eu/

1.4.3 Evaluation methods

Most AQ modelling evaluation methods usually rely on the comparison of paired data of modelled and observed concentrations that vary in time (fixed location), across the space (fixed time), or both. Comparisons do not take into consideration that simulated concentrations are volume-averaged means (representing average weather conditions, physical processes, and chemical reaction rates), whereas observations are point measurements reflecting individual events. This inconsistency is referred to as the incommensurability or change of support problem. One way to solve the problem is to use spatial smoothing (block-kriging) on the observed data to produce values that can be compared with the grid-averaged model estimates as suggested by Swall and Foley (2009). However, such techniques rely on statistical models to interpolate observations, and, thus, the evaluation is based on a comparison of the results of two different models. Even though, observations contain measurement errors while model outputs contain uncertainties in both the model inputs data and the model's representation of the relevant atmospheric processes. Thus, one should expect differences between model outputs and corresponding observations when they are compared.

According to Denby et al. (2010) the tools used to inform how well model fits the observations are namely **Model Quality Indicators** (MQI). MQI can be quantitative, such as statistical indicators, or qualitative, like representativeness and expert assessment. The selection of the most appropriate MQI depends on model application and purpose. MQI for concentration should be pollutant specific and scale specific, both temporal and spatial. Also representativeness of both model and observation must be considered when selecting MQI.

According to Dennis et al. (2010), the three statistical indicators most widely used in AQM evaluation are Mean Bias (MB), Root Mean Squared Error (RMSE) and correlation coefficient (r). However, the best selection of a statistic depends on available observation and range of magnitude of the evaluated pollutant. For example, for PM and their composition, Boylan and Russell (2006) suggested the Mean Fractional Error and Bias (MFE and MFB, respectively). The AQ directive 2008/50/EC establishes criteria for acceptable model uncertainty or quality objectives. It is understood that theses alone are not sufficient to build confidence in the use of models for air quality applications.

Despite statistical indicators provide quantifiable and comparable results, it is well known that they alone do not provide a conceptual understanding of how the model is performing (Denby et al. 2010). For this reason, qualitative analysis, also referred to as exploratory data analysis, is indispensable. Such an analysis may reveal shortcomings in input data, model setups or model descriptions. Some of the most widely used graphical depictions in AQ model evaluation include scatter plots, time series, Taylor diagram, concentration maps, among others. Visual inspection of the data (exploratory analysis, e.g. temporal series, concentration maps) should always be carried out prior to applying statistical software to identify obvious bias and outliers. Therefore, statistical analysis alone is a necessary, but not sufficient criterion, for model evaluation. It should be completed by evaluation studies on different modelling processes (diagnostic and dynamic evaluation).

1.5   History and previous results of the research group

The present investigation keeps within the line of research started in the Environmental Modelling Laboratory of the Technical University of Catalonia (UPC) and latter continued in the Earth Science Department of the Barcelona Supercomputing Center-Centro Nacional de Supercomputación (BSC-CNS) under the supervision of Dr. José María Baldasano.

The Earth Science Department of the BSC-CNS has the aim of modelling and understanding the behaviour of the Earth System, focusing its research activities on atmospheric processes and climate change modelling. Specifically, the air quality group focuses on understanding the physico-chemical processes in the atmosphere that contribute to a decrease of air pollution, and analyse a precise estimation of the air quality through high-resolution modelling, especially the relationship between emissions, atmospheric transport, chemistry and deposition. A review about relevant works in AQ modelling and its components developed in the research group are summarized in Table 1-5 and Table 1-6. Most of the studies have been applied over the northeastern Iberian Peninsula and have focused on meteorology modelling, emissions modelling, AQM and desert dust modelling. The objective of these studies has been to use models as assessment and management tools.

Table 1-5. Ph.D. thesis carried out in the Environmental Modelling Laboratory in the framework of AQM system over different Spanish domains.

Author	Year of publication	Topic	Studied domain
Calbó, J.	1993	Meteorological modelling	Barcelona
Costa, M.	1995	Gas-phase emission modelling	Barcelona
Soriano, C.	1997	Meteorological modelling	Barcelona
Gómez, O.	1998	bVOC emission modelling	Catalonia
Toll, I.	1999	AQ modelling	Barcelona
Parra, R.	2004	Emission modelling	Catalonia
Jorba, O.	2005	Meteorological modelling	Catalonia
Jiménez, P.	2005	AQ modelling	Catalonia
Arévalo, G.	2005	Emission modelling	Comunidad Valenciana
Pérez, C.	2005	Desert dust modelling	Mediterranean Basin
Gonçalves, M.	2009	AQ modelling as management	Madrid and Barcelona

The present Ph.D. thesis is performed in the framework of two recent projects developed at the BSC-CNS group: (1) the CALIOPE project (441/2006/3-12.1, A357/2007/2-12.1, 157/PC08/3-12.0), funded by the Spanish Ministry of the Environment and Rural and Marine Affairs and (2) the CICYT project (CICYT CGL2006-08903), funded by the Spanish Ministry of Science and Innovation. Specifically, CALIOPE project aims to develop an operational AQM system for Spain which provides a service of AQ forecast with high resolution over Iberian Peninsula, Balearic and Canary Islands with nesting in urban areas. On the other hand, the CICYT project, related to the CALIOPE project, has as main goal to model atmospheric pollution by anthropogenic and natural

PM with high-resolution over the Iberian Peninsula. Both projects are oriented to the development of a high-resolution modelling of atmospheric pollution in the Iberian Peninsula.

In this framework, a high-resolution AQM system, namely **CALIOPE system**, has been constructed and applied with high spatial and temporal resolution over the Iberian Peninsula (4 km x 4 km, 1 h) as well as to Europe (12 km x 12 km, 1 h). The CALIOPE system is formed by a set of models, **WRF-ARW/HERMES-EMEP/CMAQ/BSC-DREAM8b,** that will take into account both anthropogenic and natural pollution. These models are the WRF-ARW meteorological model, the HERMES-EMEP emission model, the CMAQ chemical transport model, and the BSC-DREAM8b desert dust model.

Each model has been used in a single way in different work developed in the BSC-CNS research group. The MM5, precursor of the WRF-ARW, has been used in Jorba et al. (2003) for describing circulation patterns in western Mediterranean coast. Jiménez and Baldasano (2004) and Jiménez et al. (2005a, b, 2006a, 2007) study the EMICAT2000 emission model developed over Cataluña (Parra et al., 2004, 2006; Parra and Baldasano, 2004) integrated in the MM5/EMICAT2000/CMAQ system.

The definition of the high-resolution selected in CALIOPE grids (both European and Spanish domains) is based on previous experiences and results (as discussed in Section 1.3). First, the results by Jiménez et al. (2005b) highlight the necessity for an integrated modelling system to include the interaction between different scales, through nested grids. The definition of the horizontal grid size should be able to reproduce the atmospheric circulations of the area of study. The complexity of the Iberian Peninsula forces to utilize resolutions ranging from 1 to 5 km. Second, the results of the CityDelta project (Vautard et al., 2007) showed that 5 km horizontal resolution was enough to reproduce O_3 and PM10 over cities. Finally, conditioned by the fact that the computational requirements increase markedly with the inverse of the grid size (for a given domain), the selected resolution for simulating the Iberian Peninsula (4 km) was determined by the scalability of the WRF-ARW model which also determined the resolution of the mother domain, European domain (12 km), through a one-way nesting with a rate of 1/3.

In addition, the definition of the vertical resolution should be able to simulate the layering of meteorology and pollutants. Jiménez et al. (2005b) indicated the need for a high vertical resolution to accurately simulate primary pollutants such as nitrogen oxides or particulate matter.

The previous results show that:

- There is a justified experience in the BSC-CNS group related to the use of AQMs, which demonstrates the accuracy of the set of models chosen to reproduce atmospheric dynamics processes involve in air pollution over small domains over the Iberian Peninsula under specific episodes.

- Until now, there are no studies dealing with the last version of the models covering the whole domain of the Iberian Peninsula and Europe with high spatial and temporal resolution (< 4-12 km, 1 h) on an annual cycle.

Table 1-6. List of relevant publications in international magazines related to AQM in Spain from the Environmental Modelling Laboratory of the Technical University of Catalonia and the Earth Science Department of the Barcelona Supercomputing Center-Centro Nacional de Supercomputación.

Reference	Objective	Domain
Meteorological modelling		
Calbó and Baldasano, 1995	Development of the hydrostatic mesoscale meteorological model **PROMETEO**	Barcelona
Soriano et al., 2001	Study of the atmospheric circulations for a typical summertime situation basing in lidar measurements and simulations with **MEMO** model. Establishment of circulatory pattern of atmospheric pollutants in a breeze situation.	Barcelona
Jorba et al., 2003	Description of circulatory patterns using the **MM5** model.	Western Mediterranean coast
Emission modelling		
Costa and Baldasano, 1996	**EIM-LEM** emission model based on the emission inventory for 1990	Barcelona
Delgado et al., 2000	Road traffic emission model with resolution of 1 km x 1 km	Catalonia
Toll and Baldasano, 2000	Extension of the domain of the **EIM-LEM** emission model	Barcelona
Parra et al., 2004 Parra and Baldasano, 2004; Parra et al., 2006	Develop high-resolution (1h, 1 km x 1km) **EMICAT2000** emission model	Catalonia
Baldasano et al., 2008a	Develop high-resolution (1h, 1 km x 1km) **HERMES** emission model	Spain
Desert dust modelling		
Pérez et al., 2006a, and b	Study the Saharan dust contribution with the Dust Regional Atmospheric Model (**DREAM**)	Mediterranean Basin
Jiménez et al. 2008	Off line coupling of the **DREAM** model within the **MM5/EMEP/CMAQ** modelling system to improve PM simulation	South Europe
Pérez et al., 2011	Develop a desert dust model from meso to global scales: the **NMMB/BSC-Dust model**	Global, North Africa, South Europe, the Middle East

Table 1-6. (continued)

Reference	Objective	Domain
	Air quality modelling	
Moussiopoulos, 1994	AQ simulation using the **MEMO/EIM-LEM/MARS** modelling system.	Barcelona
Baldasano et al., 1994	Description of the transport processes of air pollutant during summer days using the **MEMO/EIM-LEM/MARS** modelling system.	Barcelona
Baldasano et al., 1995	Study influence of atmospheric transport in urban air pollution using the **PROMETEO** and the **EIM-LEN** models.	Barcelona
Toll and Baldasano, 2000	Study O_3 pollution in summer using the **MEMO/EIM-LEM/MARS** modelling system.	Barcelona
Barros et al., 2003	Study diverse circulation pattern between two coastal cities in the Iberian Peninsula using the **MAR IV** and **MARS** chemical transport models.	Barcelona and Lisbon
Jiménez et al., 2003	Comparison of gas-phase chemical mechanism for CTMs	
Jiménez and Baldasano, 2004 Jiménez et al., 2005a, and b Jiménez et al., 2006a Jiménez et al., 2007	Study of (1) O_3 response to precursors controls, (2) O_3 weekend effect in very complex terrains, (3) influence of model grid resolution on O_3, (4) influence of initial and boundary conditions on O_3 using the **MM5/EMICAT2000/CMAQ** modelling system. (5) Model evaluation.	Catalonia
Jiménez et al. 2008	Off line coupling of the **DREAM** model within the **MM5/EMEP/CMAQ** modelling system to improve PM simulation	Southern Europe
Jiménez et al., 2008	Study AQ management with **WRF/EMICAT2000/DREAM/CMAQ** modelling system (1h, 2 km x 2 km). Model evaluation.	Catalonia
Gonçalves et al., 2008 Gonçalves et al., 2009a	Study AQ impact of emissions abatement in road-traffic: (1) natural gas vehicles, (2) biodiesel use, (3) electric hybrid vehicles, (4) reduction velocities, using the **WRF-ARW/HERMES/CMAQ** modelling system	Barcelona and Madrid
Gonçalves et al., 2009b	Study the contribution of atmospheric processes affecting air pollution using the **WRF-ARW/HERMES/CMAQ** modelling system	Barcelona and Madrid

In this sense, the present Ph.D. thesis, enshrined in the CALIOPE project and founded by the CICYT contract, means an advance in AQ modelling in Europe and Spain. This is possible thanks to the capacity of supercomputation of the MareNostrum supercomputer hold in the BSC-CNS

together with the advances in the parallelization of AQM codes for their implementation in these large infrastructures. MareNostrum is a supercomputer based in PowerPC processors, the BladeCenter architecture, Linux open operative system and Myrinet interconnection net. These four technologies configure the basis for an architecture that allocate MareNostrum as one of the most powerful supercomputer in Europe and the number 118 in the world, according to the last Top500 list (November 2010). The summary of the system is: 94.21 Teraflops of theoretical performance peak (94.21 billion (94.21 x10^{12}) operations per second); 10240 processors PowerPC 970MP at 2.3 GHz; 20 TB of memory; 390 TB of disk storage; 2 interconnection networks: Myrinet; Gigabit Ethernet.

Nowadays, the CALIOPE system provides end-users with an AQ forecasting and assessment service for both domains, Europe and Spain, with higher detail for some hot spot areas at http://www.bsc.es/caliope.

1.6 Objectives

The revision of the state-of-the-art of air pollution in Europe (Section 1.1), the AQM framework (Section 1.3 and 1.4); and previous AQM research at the Earth Science Department of the BSC-CNS group (Section 1.5) lead us to establish a series of working hypotheses and objectives that are presented in this section.

1.6.1 Justification

The justification of the present Ph.D. thesis stresses in the improvement of life quality, health; and protection of ecosystems through a more precise knowledge of the processes taking place in the atmosphere. Previous researches in the BSC-CNS group (Section 1.5) lead us to establish a series of working hypotheses:

1. Air pollution is the environmental factor with the greatest impact on health in Europe and is responsible for the largest burden of environment-related disease. Recent estimates indicate that 20 million Europeans suffer from respiratory problems every day.

2. Historically AQ assessment has been based on monitoring data as this has been seen to be as close as we come to the truth. Even though AQM is often seen as being more uncertain than monitoring there are three major reasons for using AQMs for air pollution assessment:

   - Meanwhile the spatial coverage of monitoring is usually limited, modelling can potentially provide complete spatial coverage of AQ.

   - Modelling can be applied to predict the AQ, e.g. as a result of changes in emissions or meteorological conditions.

   - Modelling provides an advanced understanding of the sources, causes and processes that determine AQ.

3. Atmospheric pollutants show strongly seasonal behaviour. A full year simulation on an annual cycle helps identifying important pollution episodes and discriminating those with an anthropogenic or natural origin. Since HERMES model is based on the emission inventory of 2004, this year could be a recommended choice for a reference year.

4. As Europe, especially Spain, presents a high spatial and temporal variability in the emission of pollutants, which interact in the atmosphere to potochemically produce secondary pollutants, it is demanding for the high-resolution AQM to consider a highly-disaggregated emission inventory of gaseous pollutants and anthropogenic PM and a chemical mechanism that explains the heterogeneous dynamics of air pollutants (such as HERMES emissions model specifically development for Spain).

5. Up to date, the AQMs applied over the whole Iberian Peninsula and Europe did not take into account the inclusion of atmospheric PM and allowed just to perform episodic simulations. The last-generation CTMs allow simulating the dynamics of pollutants (gaseous and PM) with very complex mechanisms (> 100 species). This is possible thanks to the increase of computational ability in supercomputers such as MareNostrum, hosted by BSC-CNS.

6. Due to the complex topography (important mountain ranges, plain zones and great depressions, and complicated system of smaller valleys linked to a dense hydrological net) and climatic particularities of Europe and the Iberian Peninsula (marked differences Atlantic-Mediterranean behaviour) it becomes necessary to make the simulation with high spatial and temporal resolution.

7. As southern Europe, especially the Iberian Peninsula, undergoes Saharan dust outbreaks, which can interact with the local dynamic in some summer episodes joining the typical cycles of recirculation, it is demanding for the high-resolution AQM to consider through initial and boundary conditions the contributions of a natural dust model (such as BSC-DREAM8b).

8. Since CALIOPE project aims to establish CALIOPE modelling system as an operational forecasting tool, a full year evaluation of the system is necessary to assure the confident on modelled output and to identify necessities of improvements, which can be implemented and testing during the evaluation cycle.

1.6.2 Objectives

Following the working hypothesis in Section 1.6.1, the main objective of the present Ph.D. thesis is **to explore the capabilities of an integrated modelling system, with high-spatial and temporal resolutions, to reproduce air quality across Europe and Spain for an annual cycle in order to assure its use as a forecast tool over Spain.**

According to the precedents and previous research in AQM, as described in Section 1.5, this Ph.D. thesis is based on the **CALIOPE modelling system**, which is potentially useful to accomplish the main goal. The CALIOPE system is used along the present Ph.D. thesis with two configurations according to the domain: Europe (namely CALIOPE-EU) and Spain (namely CALIOPE-IP). Table

1-7 summarizes the name codes and characteristics of the configurations investigated. Differences between both configurations are summarized as follows:

- **Domain and spatial resolution**. CALIOPE-EU is applied over Europe with 12 km x 12 km resolution, while CALIOPE-IP simulations are run over Spain with 4 km x 4 km resolution.

- **Emission inventory**. CALIOPE-EU uses a top-down approach for the emission inventory derived from the 2004 annual EMEP emission database (www.emep.int). On the other hand, CALIOPE-IP uses a bottom-up approach for the emission inventory specifically developed for Spain over the year 2004.

- **Boundary conditions**. CALIOPE-EU uses boundaries from global models (NCEP/FNL 1º x 1º, for meteorology, and LMDz-INCA2 3.75º x 2.5º for chemistry), meanwhile CALIOPE-IP uses boundary conditions from CALIOPE-EU (for meteorology and chemistry) in a one-way nesting.

Table 1-7. Simulation codes for the studied AQM system in the present Ph.D. thesis.

CALIOPE modelling system: WRF-ARW/HERMES-EMEP/CMAQ/BSC-DREAM8b		
Simulation code	CALIOPE-EU	CALIOPE-IP
Domain	Europe	Spain
Spatial resolution	12 km x 12 km	4 km x 4 km
Meteorology model (version)	WRF-ARW (v3.0.1.1)	WRF-ARW (v3.0.1.1)
Emissions model (reference year)	HERMES-EMEP (2004)	HERMES (2004)
Chemical transport model (version)	CMAQ (v4.5)	CMAQ (v4.5)
Natural dust transport model	BSC-DREAM8b	BSC-DREAM8b

Therefore, the main objective of the present Ph.D. thesis is increase the scientific confidence on the CALIOPE system over Europe (CALIOPE-EU configuration) and Spain (CALIOPE-IP configuration) to simulate spatio-temporal variability of AQ over the target domains for a full reference year (2004), identifying skills and weakness with a degree of detail that contributes to establish necessities of improvements in the modelling process.

With this milestone, the present Ph.D. thesis is structured as shown in Figure 1-17 in order to achieve the following objectives:

1. To develop an **evaluation methodology** for assessing the accuracy of the CALIOPE modelling system that includes:

- Bibliographical review on present air quality modelling evaluation studies for gas-phase, PM and PM chemical composition as a framework for comparing with the studied modelling system.

- Compilation and treatment of the measurements from monitoring networks available in Europe and Spain for gas-phase and PM pollutants

- Selection of model indicators and to establish model quality objectives.

- Identification of necessities of improvements and planning how to implement them.

2. To warrant the use of the **CALIOPE-EU** system to (1) accurately reproduce AQ background concentrations in terms of gas-phase (O_3, NO_2 and SO_2), PM (PM2.5 and PM10), and PM chemical composition (sulphate, nitrate, ammonium, organic carbon, elemental carbon, sea salt, and desert dust); and (2) to generate chemical boundary conditions for further nested calculation on the smaller domain of the Iberian Peninsula with **CALIOPE-IP**. To get these objectives the following tasks are developed:

- Improvement of the vertical resolution of the CALIOPE-EU system increasing the number of sigma layers to 15.

- Improvement of the quality of the information in the chemical boundary conditions using the global model LMDz-INCA2, in order to improve modelled ground-based O_3 concentrations from global contribution.

- Implementation of natural emissions: sea salt aerosol and desert dust through sea-salt emission implemented in CMAQv4.5 (AERO4) and the desert dust contribution form the BSC-DREAM8b model, respectively.

- Full year diagnostic evaluation (spatial and temporal) of CALIOPE-EU at remote rural background stations from the EMEP monitoring network.

- Comparative discussion with other European evaluation studies in terms of statistical indicators.

- Analysing AQ spatial pattern in Europe in terms of O_3, NO_2, SO_2 and PM10 ground-based concentrations modelled with CALIOPE-EU, identifying the main areas of pollution, discriminating between natural and anthropogenic.

- Discussing the annual pattern of each SIA and its gas precursor over Europe estimated with both the EMEP data and the CALIOPE-EU system, assessing about sensitivity regimes of SIA formation in Europe.

3. To warrant the use of the **CALIOPE-IP** over Spain to reproduce AQ on an hourly basis in urban/suburban areas influenced by local anthropogenic emission sources (industrial/traffic) by means of:

- Improving the HERMES emission model by implementing emissions of agricultural and livestock (SNAP 10), reviewing emission factors of biogenic emissions, methodologies of emission disaggregation. Furthermore, adding a new module for paved road resuspended PM emission by on-road traffic in the HERMES model that contributes to improve modelled PM10 in urban zones.

- Full year evaluation (spatial and temporal) of CALIOPE-IP system for gas-phase (O_3, NO_2, SO_2) and particulate matter (PM10) pollutants through comparisons with 82 ground-based stations from the Spanish network which comprises different kind of stations classified according to the type of zone (urban, suburban and rural) and the dominant emission sources (traffic, industrial, and background). Since measurements are on an hourly basis, evaluations are done in that way in order to evaluate the high temporal resolution of the model.

- Identifying source of uncertainty in modelling PM through an annual diagnostic evaluation of modelled PM chemical component (SO_4^{2-}, NO_3^-, NH_4^+, TC, sea salt and desert dust) comparing with measurements from the IDAEA-CSIC monitoring network. An important novel approach is the use of an experimental data set of African PM10-dust obtained with the methodology of IDAEA-CSIC to evaluate the BSC-DREAM8b model.

- Analysing AQ spatial pattern in Spain in terms of O_3, NO_2, SO_2 and PM10 ground-based concentrations modelled with CALIOPE-IP, identifying the main areas of pollution, discriminating between natural and anthropogenic.

- Assessing the spatial and seasonal distribution of PM over Spain modelled with CALIOPE-IP, for both size and chemical composition, comparing with those described in related studies based on experimental values.
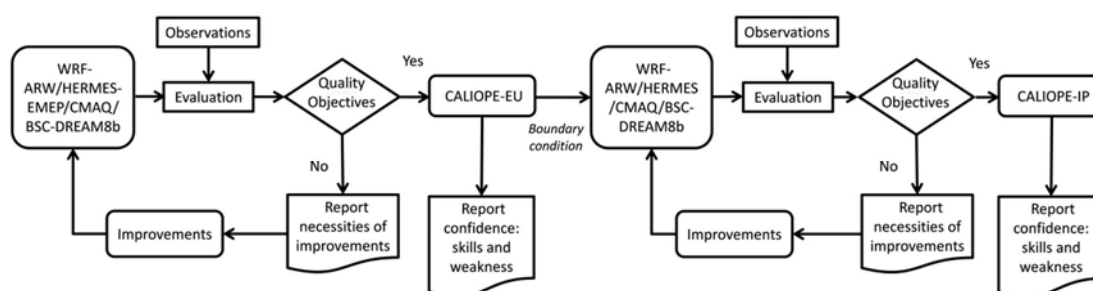
Figure 1-17. Flow diagram of the sequence of tasks in order to achieve the main goal of the present Ph.D. thesis.

1.7   Scope and structure

This document presents the discussion and the main results of the Ph.D. thesis entitled "Regional and urban evaluation of an air quality modelling system in the European and Spanish domains", and is structured as follows.

Chapter 1 has provided a short introduction to nowadays air pollution as a multi-pollutant, multi-effect and trans-boundary environmental problem, with special focus on the European and Spanish domains. Emission trends and meteorological dynamic affecting both target domains are treated as forces which determine air pollution at different scales. Furthermore, the interactions of the major pollutants in the low atmosphere have been indicated by reporting the most important chemical reactions occurring in the troposphere. In addition, this Chapter has provided a state-of-the-art in AQM and its evaluation framework, as well as the most important applications in Europe and Spain. Concerning all this information, the objectives to be achieved within this Ph.D. thesis have been stated.

Chapter 2 tests the performance of the CALIOPE-EU system in terms of AQ levels on an annual basis (2004) by means of a quantitative evaluation of gas-phase species (O_3, NO_2, and SO_2) and PM (PM2.5 and PM10) against ground-based measurements representative of the rural background levels. Modelled AQ spatial patterns across Europe are discussed and contrasted with other modelled and experimental studies. Statistical model performances are compared to model goals and criteria and to other published European studies.

In order to estimate the uncertainty of modelled PM is essential to evaluate their chemical components. In this sense, **Chapter 3** presents a diagnostic evaluation which assesses how well the CALIOPE-EU system reproduces the spatial and temporal variability of inorganic aerosol chemical components (SO_4^{2-}, NO_3^-, NH_4^+) and their gas precursor species (SO_2, HNO_3 and NH_3) at regional scale. Furthermore, Chapter 3 discusses the annual pattern of each SIA and its gas precursor over Europe estimated with both the EMEP data and the CALIOPE-EU system. Finally, Chapter 3 assesses about sensitivity regimes of SIA formation in Europe.

Model evaluations and assessments of AQ in Europe presented in Chapter 2 and Chapter 3 intend to warrant the use of CALIOPE-EU system as an accurate tool to reproduce AQ in Europe and to implement CALIOPE-EU outputs for further nested calculations on the smaller domains over Spain.

Ones CALIOPE-EU is able to provide accurate chemical boundary condition with high temporal and spatial resolution; the CALIOPE system was run and evaluated at urban scale over the Spanish domain. The first evaluation of the modelling system over Spain suggested some necessities of improvement in the HERMES emission model, such as inclusion of agriculture and livestock emissions (SNAP10 sector), improvements in the spatial distribution of biogenic emission and population density via the use of the CORINE Land Cover information at a 100-m resolution, and introduction of emissions from the road traffic sector in small cities (SNAP10 sector).

Emissions of resuspended particles from paved roads (RPR) have received an increasing attention in AQM, since chemistry transport models are generally unable to reproduce particulate levels near

road traffic. **Chapter 4** describes the inclusion of the resuspension of PM within the HERMES emission model, implemented in the CALIOPE-IP system, and the improvements obtained in the modelled PM10 concentration across Spain for a full year simulation (2004). The results are discussed in terms of emissions, concentration and deposition of PM.

After accurate boundaries conditions for the Iberian Peninsula have been obtained from the CALIOPE-EU simulations and some improvements have been implemented regarding this topic, **Chapter 5** provides an hourly evaluation and assessment of AQ across Spain within the CALIOPE-IP system over a full year (2004) in terms of gas-phase species (O_3, NO_2, and SO_2) and particulate matter (PM10) against ground-based measurements from the Spanish monitoring network. AQ spatial patterns across Spain modelled with the CALIOPE-IP system are discussed and contrasted with other modelled and experimental studies. This evaluation intends to warrant the use of the CALIOPE-IP system as an accurate tool to (1) reproduce AQ variability across Spain (urban/suburban areas and traffic/industrial environments); and (2) to forecast AQ over Spain.

Since evaluation of PM10 hourly concentration is not enough to identify uncertainties in modelling PM across Spain, **Chapter 6** presents a diagnostic evaluation of the CALIOPE-IP system in terms of aerosol size (PM2.5 and PM10) and chemical composition (SO_4^{2-}, NO_3^-, NH_4^+, TC, sea salt, desert dust) over 2004. A new data set of Saharan dust PM10 concentration is used to evaluate the PM10 contribution modelled by BSC-DREAM8b. In addition, this Chapter discusses the spatial and seasonal distribution of the different aerosols over Spain based on comparison of CALIOPE-IP outputs with experimental measurements.

Chapter 7 portrays a discussion of the main results achieved in the present Ph.D. thesis, analysing the advantages of the proposed methodology and its limitations attending to its state-of-the-science. In addition, this Chapter provides a summary of the main conclusions. Finally, suggestions of possible tasks and investigations derived from the continuation of the line of research developed within this work are depicted. Last, **Chapter 8** compiles all the references used in the present Ph.D. thesis.

2. A full year evaluation and assessment of air quality across Europe with the CALIOPE-EU system

2.1   Introduction

Atmospheric pollutants have significant impact on many main fields. One of the major areas impacted is human health. High correlations between long-term exposure to fine particles and human health issues have been detected in population-based studies for several decades (Lave and Seskin, 1970; Thibodeau et al., 1980; Lipfert, 1994; Pénard-Morand et al., 2005). The latest studies even quantify the effects of aerosols on human lifespan. It is suggested that a decrease of 10 μg m^{-3} in the concentration of fine particles may lead to an increase in life expectancy of 0.61 years (Pope et al., 2009). Another major area impacted by atmospheric pollutants is climate change. Particles scatter and absorb solar and infrared radiation in the atmosphere. In addition, they alter the formation and precipitation efficiency of liquid-water, ice and mixed-phase clouds (Ramanathan et al., 2001). Radiative forcing associated with these perturbations affects climate (Chylek and Wong, 1995; Jacobson, 2001). A third area impacted by air quality pollutants is atmospheric visibility. Since the size of atmospheric aerosols is similar to the wavelength of visible light, light is scattered and absorbed as it travels through the atmosphere (Japar et al., 1986; Adams et al., 1990). In brief, atmospheric pollutants are part of a highly complex system that affects the physics, chemistry, and life on the planet.

The EC and the US EPA, among others, have shown great interest in the transport and dynamics of pollutants in the atmosphere. According to the European directives (European Commission, 1996, 2008), air quality modelling is a useful tool to understand the dynamics of air pollutants, to analyse and forecast the air quality, and to develop plans reducing emissions and alert the population when health-related issues occur. Both have set ambient air quality standards for acceptable levels of O_3 (European Commission, 2002), NO_2 and SO_2 (European Commission, 1999, 2001), PM2.5 and PM10 in ambient air (European Commission, 1999, 2001, 2008).

The CALIOPE project, funded by the Spanish Ministry of the Environment and Rural and Marine Affairs (Ministerio de Medio Ambiente y Medio Rural y Marino), has the main objective to establish an air quality forecasting system for Spain (Baldasano et al., 2008b). In this framework, a high-resolution air quality forecasting system, namely WRF-ARW/HERMES-EMEP/CMAQ/BSCDREAM8b, has been developed and applied to Europe (12 km x 12 km, 1 h)

as well as to Spain (4 km x 4 km, 1 h). The simulation of such a high-resolution model system has been made possible by its implementation on the MareNostrum supercomputer hosted by the Barcelona Supercomputing Center-Centro Nacional de Supercomputación (BSC-CNS). In order to reduce uncertainties, the model system is evaluated with observational data to assess its capability of reproducing air quality levels and the related dynamics.

A partnership of four Spanish research institutes composes the CALIOPE project: the BSC-CNS, the "Centro de Investigaciones Energéticas, Medioambientales y Tecnológicas" (CIEMAT), the Institute of Earth Sciences Jaume Almera of the "Centro Superior de Investigaciones Científicas" (IJA-CSIC) and the "Centro de Estudios Ambientales del Mediterráneo" (CEAM). This consortium deals with both operational and scientific aspects related to air quality monitoring and forecasting. BSC-CNS and CIEMAT lead the model developments of the project while IJA-CSIC and CEAM are in charge of retrieving observational data for evaluation processes. Current experimental forecasts are available through http://www.bsc.es/caliope.

Several operational air quality forecasting systems already exist in Europe (see http://gems.ecmwf.int or http://www.chemicalweather.eu, Hewitt and Griggs, 2004; COST, 2009). CALIOPE advances our understanding of atmospheric dynamics in Europe as follows. First, CALIOPE includes a high-resolution computational grid. Most models use a horizontal cell resolution of at least 25 km x 25 km for domains covering continental Europe. CALIOPE uses a 12 km x 12 km cell resolution to simulate the European domain. Second, CALIOPE includes a complex description of the processes involved in the modelling of particulate matter. Both are important factors to obtain accurate results of air pollutant concentrations in a complex region such as southern Europe (Jiménez et al., 2006c). Moreover, to date, none of the existing European operational systems include the influence of Saharan dust on a non-climatic basis. Dust peaks cannot be represented by introducing boundary conditions derived from dust climatological data due to the highly episodic nature of the events in the region (1- to 4-day average duration) (Jiménez-Guerrero et al., 2008a). When considering only anthropogenic emissions, chemical transport model simulations underestimate the PM10 concentrations by 30-50%, using the current knowledge about aerosol physics and chemistry (Vautard et al., 2005a).

The purpose of the present paper is to provide a quantitative assessment of the capabilities of the WRF-ARW/HERMES-EMEP/CMAQ/BSC-DREAM8b air quality modelling system to simulate background concentrations of gas and particulate phase in the European domain. In the rest of the paper, this model system will be named "CALIOPE-EU". This evaluation intends to warrant the use of such simulation for further nested calculations on the smaller domain of the Iberian Peninsula (principal goal of the CALIOPE project). The results are evaluated statistically and dynamically, compared to performance goals and criteria, and to other model performances.

In this paper, Section 2.2 describes the models, the observational dataset and the statistical parameters calculated. Section 2.3 analyses the model results against available measurement data for the year 2004 and the modelled annual distribution of O_3, NO_2, SO_2, PM2.5 and PM10. A thorough comparison with other European studies is presented in Section 2.4. Conclusions are drawn in Section 2.5.

2.2 Methods

2.2.1 Model description

CALIOPE is a state-of-the-art modelling framework currently under further development. As shown in Figure 2-1, CALIOPE-EU is a complex system that integrates a meteorological model (WRF-ARW), an emission processing model (HERMES-EMEP), a mineral dust dynamic model (BSC-DREAM8b), and a chemical transport model (CMAQ) together in an air quality model system.
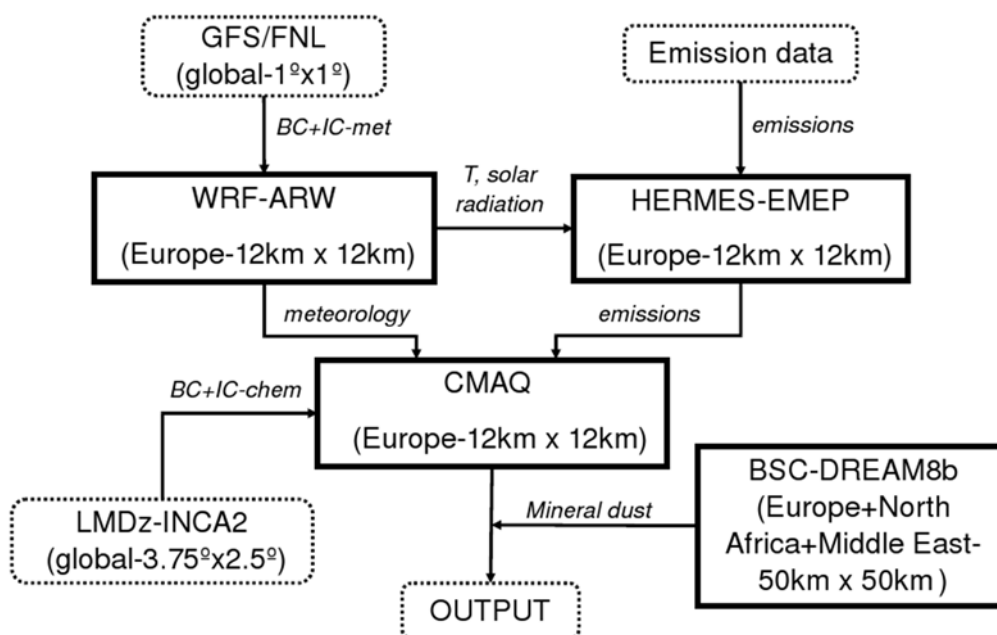
Figure 2-1. Modular structure of the CALIOPE-EU modelling system used to simulate air quality dynamics in Europe. Squared boxes with solid lines represent the main models of the framework. Boxes with dashed lines represent input/output dataset. Lines connecting boxes represent the information flow.

2.2.1.1 Meteorology

The Advanced Research Weather Research and Forecasting (WRF-ARW) Model v3.0.1.1 (Michalakes et al., 2004; Skamarock and Klemp, 2008) is used to provide the meteorology to the chemical transport model. WRF is a fully compressible, Eulerian non-hydrostatic model that solves the equations that govern the atmospheric motions. Microphysical processes are treated using the single-moment 3-class scheme as described in Hong et al. (2004). The sub-grid-scale effects of convective and shallow clouds are resolved by a modified version of the Kain-Fritsch scheme based on Kain and Fritsch (1990, 1993). The surface layer scheme uses stability functions from Paulson (1970), Dyer and Hicks (1970), and Webb (1970) to compute surface exchange coefficients for heat, moisture, and momentum. The Noah Land- Surface scheme is used to provide heat and moisture fluxes over land points and sea-ice points. It is a 4-layer soil temperature and moisture model with

canopy and snow cover prediction. The vertical sub-grid-scale fluxes caused by eddy transport in the atmospheric column are resolved by the Yonsei University planetary boundary layer (PBL) scheme (Noh et al., 2003). Finally, long-wave radiative processes are parameterized with the Rapid Radiative Transfer Model (Mlawer et al., 1997) while the shortwave radiative scheme is based on Dudhia (1989). Details about the performance of WRF-ARW over the European domain are provided as supplementary material (Annex I).

2.2.1.2 Emissions

The emission model is the High-Elective Resolution Modelling Emission System (HERMES, see Baldasano et al., 2008a). HERMES uses information and state-of-the-art methodologies for emission estimations. It calculates emissions by sector-specific sources or by individual installations and stacks. Raw emission data are processed by HERMES in order to provide a comprehensive description of the emissions to the air quality model. Emissions used for the European domain are derived from the 2004 annual EMEP emission database (EMEP, 2007). Disaggregation of EMEP (50 km resolution) data is performed in space (12 km x 12 km) and time (1 h). The spatial and temporal top-down disaggregation is sector-dependent. A Geographical Information System (GIS) is used to remap the data to the finer grid applying different criteria through three datasets: a high-resolution land use map (EEA, 2000), coordinates of industrial sites (European Pollutant Emission Register (EPER), Pulles et al., 2006), and vectorized road cartography of Europe (ESRI, 2003). In the vertical dimension, the sector-dependent emission distribution for gases is applied following the EMEP model (widely used for regional air quality studies in Europe, Simpson et al., 2003). Distinct distributions are used for aerosols, leading in most cases to lower average emission heights than for gas phase emissions (De Meij et al., 2006; Pregger and Friedrich, 2009). In the time dimension, data are mapped from annual resolution to an hourly basis using the temporal factors of EMEP/MSC-W (Meteorological Synthesizing Centre-West).

2.2.1.3 Chemistry

The selected chemical transport model is the Models-3 Community Multiscale Air Quality Modeling System (Models-3/CMAQ, Byun and Ching, 1999; Binkowski, 1999; Byun and Schere, 2006). CMAQ is used to study the behaviour of air pollutants from regional to local scales due to its generalized coordinate system and its advanced nesting grid capability. CMAQ version 4.5, used in this study, has been extensively evaluated under various conditions and locations (Appel et al., 2007, 2008; Roy et al., 2007). Following the criteria of Jiménez et al. (2003) the Carbon Bond IV chemical mechanism is applied (CBM-IV, Gery et al., 1989). It includes aerosol and heterogeneous chemistry. The production of sea salt aerosol (SS) is implemented as a function of wind speed and relative humidity (Gong, 2003; Zhang et al., 2005) through the AERO4 aerosol module. The AERO4 module distinguishes among different chemical aerosol components namely nitrate, sulphate, ammonium, elemental carbon, organic carbon with three subcomponents (primary, secondary anthropogenic and secondary biogenic), soil, sodium, and chlorine. Unspecified anthropogenic aerosols and aerosol water are additionally kept as separate components. Aerosols are represented by three size modes (Aitken, accumulation and coarse mode), each of them assumed to have a lognormal distribution (Binkowski and Roselle, 2003). Secondary inorganic aerosols (SIA) are generated by nucleation processes from their precursors to form nitrate

ammonium and sulphate aerosols. Secondary organic aerosol (SOA) can be formed from aromatics (anthropogenic organic aerosols) and terpenes (biogenic organic aerosols, Schell et al., 2001). The aerosol microphysical description is based on a modal aerosol model (Binkowski and Roselle, 2003) using the ISORROPIA thermodynamic equilibrium model (Nenes et al., 1998). For a more complete description of the processes implemented in CMAQ, the reader is referred to Byun and Schere (2006).

2.2.1.4 Mineral dust

The Dust REgional Atmospheric Model (BSC-DREAM8b) was designed to simulate and/or predict the atmospheric cycle of mineral dust (Nickovic et al., 2001; Pérez et al., 2006a,b). The simulations cover the Euro-Mediterranean and East-Asia areas. The aerosol description was improved from 4 to 8 bins to allow a finer description of dust aerosols. In this version dust-radiation interactions are included. The partial differential nonlinear equation for dust mass continuity is resolved in the Eulerian mode. BSCDREAM8b is forced by the NCEP/Eta meteorological driver (Janjic, 1977, 1979, 1984, 1990, 1994). BSC-DREAM8b simulates the long range transport of mineral dust at a 50 km x 50 km resolution using 24 vertical layers extending up to 15 km, every 1 h. In this version dust-radiation interactions are included. An offline coupling is applied to the calculated concentrations of particulate matter from CMAQ (Jiménez-Guerrero et al., 2008a)

2.2.2 Model setup

The model system is initially run on a regional scale (12 km x 12 km in space and 1 h in time) to model the European domain. WRF is configured with a grid of 479 x 399 points and 38σ vertical levels (11 characterizing the PBL). The model top is defined at 50 hPa to resolve properly the troposphere-stratosphere exchanges.

The simulation consists of 366 daily runs to simulate the entire year of 2004. The choice for this specific year is based on the direct availability of the HERMES-EMEP emission model for this year. The first 12 h of each meteorological run are treated as cold start, and the next 23 h are provided to the chemical transport model. The Final Analyses of the National Centers of Environmental Prediction (FNL/NCEP) at 12 h UTC are used as initial conditions. The boundary conditions are provided at intervals of 6 h. The FNL/NCEP data have a spatial resolution of 1º x 1º.

The CMAQ horizontal grid resolution corresponds to that of WRF. Its vertical structure was obtained by a collapse from the 38 WRF layers to a total of 15 layers steadily increasing from the surface up to 50 hPa with a stronger concentration within the PBL.

Due to uncertain external influence, the definition of adequate lateral boundary conditions for gas phase chemistry in a regional model is a complex issue and an important source of errors. Variable intercontinental transport of pollutants substantially influences the levels of pollution in Europe (see, e.g., Li et al., 2002; Guerova et al., 2006). This air quality issue has been extensively studied. Recent works addressed the use of global chemical models to investigate the impact of chemical

boundary conditions on regional scale O_3 concentrations. Various studies were performed over the U.S. (Tang et al., 2007, 2008; Song et al., 2008; Reidmiller et al., 2009), whereas investigations over Europe remain scarce (Szopa et al., 2009). In a previous assessment of the model performances of CALIOPE-EU (Jiménez-Guerrero et al., 2008a), static chemical boundary conditions, adapted from Byun and Ching (1999), were used. In the present work, boundary conditions are based on the global climate chemistry model LMDz-INCA2 (96 x 72 grid cells, namely 3.75° x 2.5° in longitude and latitude, with 19σ hybrid vertical levels, Szopa et al., 2009) developed by the Laboratoire des Sciences du Climat et l'Environnement (LSCE). Monthly mean data for the year 2004 are interpolated in the horizontal and vertical dimensions to force the major chemical concentrations at the boundaries of the domain (Piot et al., 2008; Annex II). A detailed description of the INteractive Chemistry and Aerosol (INCA) model is presented in Hauglustaine et al. (2004) and Folberth et al. (2006).

2.2.3 Air quality network

Model output for gas and particulate phase concentrations are compared with ground-based measurements from the EMEP monitoring network for the year 2004. According to the criteria proposed by the European Environment Agency (EEA, Larssen et al., 1999), EMEP stations are located at a minimum distance of approximately 10 km from large emission sources. Consequently, all EMEP stations are assumed to be representative of regional background concentrations (Torseth and Hov, 2003). Therefore, the authors wish to stress that the model performances presented in this paper are evaluated only for background concentrations. The measurements are well documented and freely available on the EMEP web page (http://www.emep.int).
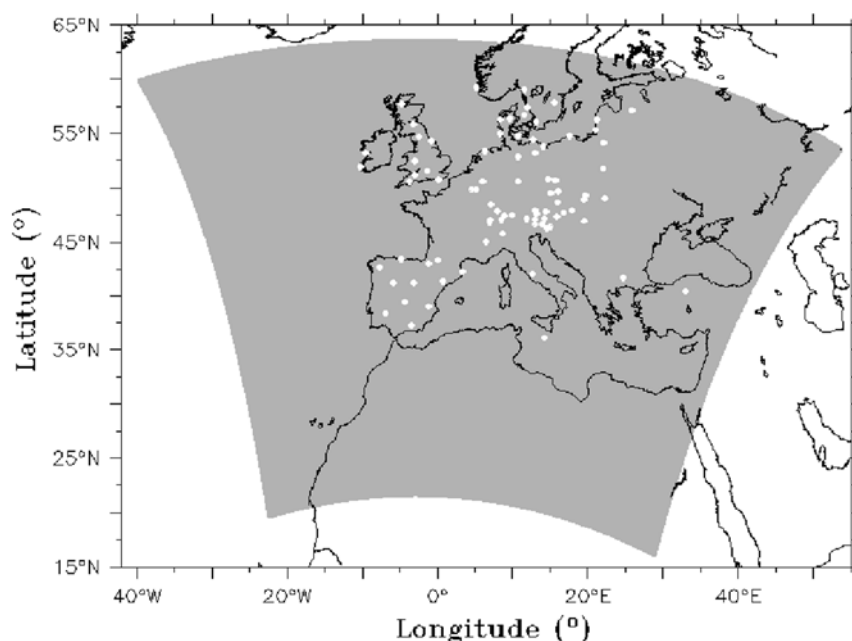
Figure 2-2. Grey shaded area: modelling domain used in this study. The white filled circles represent the selected subset of EMEP data collection sites. Characteristics of each station are listed in Table 2-1.

Before comparing the model results with EMEP data, the available measurements were filtered, and uncertain data (before and after a measurement interruption or a calibration of equipment) were removed. After this filtering, only observational sites with a temporal coverage greater than 85% were selected. Note that the final coverage of the dataset is rather disperse where France, Italy and southeastern Europe only include several stations. Measurement data used in this paper are given on a daily average. As a result, 60 stations were selected to evaluate O_3, 43 for NO_2, 31 for SO_2, 16 for PM2.5 and 25 for PM10, respectively. The selected EMEP stations and measured pollutants that are used for this comparison are briefly described in and their locations are Table 2-1 displayed in Figure 2-2.

As EMEP aerosol measurements supposedly remove all water content from samples to consider only dry aerosols, the simulated aerosol water was not taken into account in the model-to-data comparisons. However, as noted by Tsyro (2005), residual water persisting in sampled aerosols from EMEP may induce a substantial underprediction by the simulated dry aerosol concentrations. Moreover, although the aerodynamic diameter is used for PM10 and PM2.5 in measurement techniques, the model only considers the Stokes diameter to characterize the aerosol geometry. For more details on this issue, see Jiang et al. (2006).

2.2.4 Statistical indicators

There are a number of metrics that can be used to examine performances of air quality models (US EPA, 1984, 1991; Cox and Tikvart, 1990; Weil et al., 1992; Chang and Hanna, 2004; Boylan and Russell, 2006). In particular, mean normalized bias error (MNBE) and mean normalized gross error (MNGE) normalizing the bias and error for each model-observed pair by the observation are useful parameters. Correlation coefficient (r), root mean square errors (RMSE) and mean bias (MB) values are also commonly used by the modelling community. For the evaluation of particulate matter concentrations, Boylan and Russell (2006) indicated that MNBE and MNGE may not be appropriate and suggested the mean fractional bias (MFB) and the mean fractional error (MFE) parameters instead.

The US EPA suggested several performance criteria for simulated O3, such as MNBE $\leq \pm 15\%$ and MNGE $\leq 35\%$ (US EPA, 1991, 2007) whereas the EC proposes a maximum uncertainty between measured and modelled concentrations of 50% and 30% for $O_3/NO_2/SO_2$ daily mean and NO_2/SO_2 annual mean, respectively (European Commission, 2008). For particulate matter, Boylan and Russell (2006) proposed that the model performance goal be met when both the MFE and MFB are less than or equal to 50% and $\pm 30\%$, respectively, and the model performance criterion be met when both MFE $\leq 75\%$ and MFB $\leq \pm 60\%$. All these criteria and goals are selected to provide metrics for the CALIOPE-EU model performances.

The model-to-data statistics MB, RMSE, MNBE, MNGE, MFB and MFE are selected for the present study, together with the measured and modelled mean and the correlation coefficient. Annual and seasonal mean statistics are computed, with seasons corresponding to winter (January, February and December), spring (March, April and May), summer (June, July and August) and fall (September, October and November).

It is important to note that, unless explicitly stated otherwise, the statistical norms are calculated without any minimum threshold when considering the measurement data. However, in the present work, statistics of annual means using thresholds are also computed. In that case we chose $80\ \mu g\ m^{-3}$ for O_3 (according to recommendations of the US EPA, 1991; Russell and Dennis, 2000), $1.5\ \mu g\ m^{-3}$ for NO_2, $0.2\ \mu g\ m^{-3}$ for SO_2, $3.5\ \mu g\ m^{-3}$ for PM10 and $1.5\ \mu g\ m^{-3}$ for PM2.5, respectively.

Table 2-1. Location and characteristics of selected EMEP stations for 2004 on a daily basis.

	Station Code[a]	Latitude[b]	Longitude[b]	Altitude (m)	Station Name	O_3	NO_2	SO_2	Total PM2.5	Total PM10
1	AT02	+47.767	+16.767	117	Illmitz	x[c]	x	x[c]	x	x
2	AT04	+47.650	+13.200	851	St. Koloman			x		
3	AT05	+46.678	+12.972	1020	Vorhegg	x[c]				x
4	AT30	+48.721	+15.942	315	Pillersdorf bei Retz	x[c]				
5	AT32	+47.529	+9.927	1020	Sulzberg	x[c]				
6	AT33	+47.129	+14.204	1302	Stolzalpe bei Murau	x[c]				
7	AT34	+47.054	+12.958	3106	Sonnblick	x[c]				
8	AT37	+47.137	+11.870	1970	Zillertaler Alpen	x[c]				
9	AT38	+46.694	+13.915	1895	Gerlitzen	x[c]				
10	AT40	+47.348	+15.882	1170	Masenberg	x[c]				
11	AT41	+47.973	+13.016	730	Haunsberg	x[c]				
12	AT48	+47.833	+14.433	899	Zoebelboden	x[c]				
13	BG53	+41.700	+24.733	1750	Rojen peak	x[c]				
14	CH02	+46.817	+6.950	510	Payerne		x	x	x	x
15	CH03	+47.483	+8.900	540	Tänikon		x			x
16	CH04	+47.051	+6.981	1130	Chaumont	x[c]	x	x	x	x
17	CH05	+47.069	+8.466	1030	Rigi	x[c]	x	x		x
18	CZ01	+49.733	+16.033	737	Svratouch	x[c]	x	x		
19	CZ03	+49.583	+15.083	534	Kosetice	x[c]	x	x		
20	DE01	+54.926	+8.310	12	Westerland					x
21	DE02	+52.800	+10.750	74	Langenbrügge		x	x	x	x
22	DE03	+47.915	+7.909	1205	Schauinsland	x[c]			x	x
23	DE07	+53.167	+13.033	62	Neuglobsow					x
24	DE08	+50.650	+10.767	937	Schmücke					x
25	DE09	+54.433	+12.733	1	Zingst	x[c]				x
26	DE26	+53.750	+14.067	1	Ueckermünde	x[c]				
27	DE35	+50.833	+14.767	490	Lückendorf	x[c]				
28	DK03	+56.350	+9.600	13	Tange			x		
29	DK05	+54.733	+10.733	10	Keldsnor					x
30	DK08	+56.717	+11.517	40	Anholt		x	x		
31	DK31	+56.283	+8.433	10	Ulborg	x[c]				
32	ES07	+37.233	-3.533	1265	Víznar	x[c]	x[c]		x	x
33	ES08	+43.442	-4.850	134	Niembro	x[c]	x[c]	x[c]	x	x
34	ES09	+41.281	-3.143	1360	Campisábalos	x[c]	x[c]	x[c]	x	x
35	ES10	+42.319	+3.317	23	Cabo de Creus	x[c]	x[c]		x	x
36	ES11	+38.476	-6.923	393	Barcarrota		x[c]	x[c]	x	x
37	ES12	+39.086	-1.102	885	Zarra	x[c]	x[c]	x[c]	x	x
38	ES13	+41.283	-5.867	985	Penausende	x[c]	x[c]	x[c]	x	x
39	ES14	+41.400	+0.717	470	Els Torms	x[c]	x[c]	x[c]	x	x
40	ES15	+39.517	-4.350	1241	Risco Llano	x[c]	x[c]	x[c]	x	x
41	ES16	+42.653	-7.705	506	O Saviñao	x[c]	x[c]	x[c]	x	x
42	FR08	+48.500	+7.133	775	Donon	x[c]	x[c]	x		
43	FR09	+49.900	+4.633	390	Revin	x[c]		x		
44	FR12	+43.033	-1.083	1300	Iraty	x[c]		x		
45	FR13	+43.375	+0.104	236	Peyrusse Vieille	x[c]	x[c]	x		
46	FR16	+45.000	+6.467	746	Le Casset	x[c]				
47	GB13	+50.596	-3.713	119	Yarner Wood	x[c]				
48	GB14	+54.334	-0.808	267	High Muffles	x[c]				
49	GB15	+57.734	-4.774	270	Strath Vaich Dam	x[c]				
50	GB31	+52.504	-3.033	370	Aston Hill	x[c]				
51	GB33	+55.859	-3.205	180	Bush	x[c]				
52	GB35	+54.684	-2.435	847	Great Dun Fell	x[c]				
53	GB36	+51.573	-1.317	137	Harwell	x[c]	x[c]			
54	GB37	+53.399	-1.753	420	Ladybower Res.	x[c]	x[c]			

Table 2-1. (continued)

	Station Code[a]	Latitude[b]	Longitude[b]	Altitude (m)	Station Name	O$_3$	NO$_2$	SO$_2$	Total PM2.5	Total PM10
55	GB38	+50.793	+0.179	120	Lullington Heath	x[c]	x[c]			
56	GB44	+51.231	-3.048	55	Somerton	x[c]				
57	HU02	+46.967	19.583	125	K-puszta		x			
58	IE01	+51.940	-10.244	11	Valentina Observatory	x[c]	x			
59	IE31	+53.167	-9.500	15	Mace Head	x[c]				
60	IT01	+42.100	+12.633	48	Montelibretti		x	x		x
61	IT04	+45.800	+8.633	209	Ispra		x		x	x
62	LT15	+55.350	+21.067	5	Preilla	x[c]	x	x		
63	LV10	+56.217	+21.217	5	Rucava	x[c]	x	x		
64	LV16	+57.133	+25.917	183	Zoseni		x	x		
65	NL09	+53.334	+6.277	1	Kullumerwaard		x[c]			
66	MT01	+36.100	+14.200	160	Giordan lighthouse	x[c]				
67	NO43	+59.000	+11.533	160	Prestebakke	x[c]				
68	NO52	+59.200	+5.200	15	Sandve	x[c]				
69	PL02	+51.817	+21.983	180	Jarczew	x[c]	x	x		
70	PL03	+50.733	+15.733	1603	Sniezka	x[c]	x	x		
71	PL04	+54.750	+17.533	2	Leba	x[c]	x	x		
72	PL05	+54.150	+22.067	157	Diabla Gora		x			
73	SE11	+56.017	+13.150	175	Vavihill	x[c]	x	x		
74	SE14	+57.400	+11.917	5	Råö	x[c]	x			
75	SE32	+57.817	+15.567	261	Norra-Kvill	x[c]				
76	SI31	+46.429	+15.003	770	Zarodnje	x[c]				
77	SI32	+46.299	+14.539	1740	Krvavec	x[c]				
78	SK02	+48.933	+19.583	2008	Chopok		x			
79	SK05	+49.367	+19.683	892	Liesek		x			
80	SK06	+49.050	+22.267	345	Starina		x	x		
81	SK07	+47.960	+17.861	113	Topolniky		x			
82	TR01	+40.500	+33.000	1169	Cubuk II		x			

[a]2-letter country code plus 2-digit station code. [b]A positive value indicates northern latitudes or eastern longitudes. A negative value indicates southern latitudes or western longitudes. [c]Daily concentration calculated from hourly data.

2.3   Results and discussions

As CALIOPE-EU is a fundamental model system the authors wish to stress that, apart from the discussion of Figure 2-6 and its related statistics (Table 2-3), neither correction factors nor any adjusting model parameterization were applied to the model output or the original model codes. First, in Section 2.3.1, a thorough model evaluation is performed through statistical and dynamical performances. Later, in Section 2.3.2, a general description of the annual mean distribution of each pollutant is provided to determine each pattern throughout Europe.

2.3.1 Model evaluation

Figure 2-3 represents (left) the temporal series of the model (black lines) and daily measured EMEP data (grey lines) as an average of all the stations for each pollutant over the complete year 2004, together with (right) the scatter plot of the modelled-measured daily data. Table 2-2 shows annual and seasonal statistics calculated at the location of all EMEP stations. Statistics are calculated for daily averages of O$_3$, NO$_2$, SO$_2$, PM2.5 and PM10. In the case of O$_3$, the daily peak of hourly mean O$_3$ is also computed as it is one of the most important parameters to be considered.

2.3.1.1 Ozone

A total of 60 EMEP stations constitute the O_3 measurement dataset to be compared to the simulation (see Table 2-1). In Figure 2-3a, the time series of both simulated and observed O_3 concentrations are presented. The annual trend is well captured with an annual correlation of daily mean and daily peak concentrations of 0.66 and 0.69, respectively (see Table 2-2). Although the annual daily mean bias is null, the inter-annual variability leads to an annual RMSE of up to 20.6 μg m^{-3}. Annual and seasonal MNBE and MNGE values for daily mean and daily maximum concentrations show relatively good performances which are in accordance with the recommendations of the EC and the US EPA (see Section 2.2.4).

Table 2-2. Seasonal and annual statistics obtained with CALIOPE-EU over Europe for 2004 at the EMEP stations. Winter: January, February and December; Spring: March, April, May; Summer: June, July, August; Fall: September, October, November. The number of data points (n) indicates the number of pair measurement-model used to compute the statistics. The calculated statistics are: Observed Mean (OM) for available data (μg m^{-3}), Modelled Mean (MM) for the whole year (μg m^{-3}), correlation (r), Mean Bias (MB, μg m^{-3}), Root Mean Square Error (RMSE, μg m^{-3}), Mean Normalized Bias Error (MNBE, %), Mean Normalized Gross Error (MNGE, %), Mean Fractional Bias (MFB, %) and Mean Fractional Error (MFE, %). For the annual mean calculated with threshold, we used 80 μg m^{-3} for O_3, 1.5 μg m^{-3} for NO_2, 0.2 μg m^{-3} for SO_2, 1.5 μg m^{-3} for PM2.5 and 3.5 μg m^{-3} for PM10, respectively. Seasonal statistics are computed without threshold.

	Period	n	OM	MM	r	MB	RMSE	MNBE	MNGE	MFB	MFE
O_3 daily	Winter	5,257	60.8	54.8	0.54	-5.8	21.4	-1	34	-11	32
(60 stations)	Spring	5,466	84.5	82.6	0.55	-1.8	20.8	0	21	-4	22
	Summer	5,443	79.5	86.9	0.64	7.5	19.8	15	23	11	20
	Fall	5,197	60.7	60.1	0.58	-0.3	20.3	9	34	-1	30
	Annual (no threshold)	21,363	71.6	71.2	0.66	0.0	20.6	6	28	-1	26
	Annual (threshold)	7,299	96.9	91.1	0.44	-5.9	20.5	-6	17	-8	19
O_3 daily peak	Winter	5,257	73.7	67.3	0.50	-6.2	24.1	-5	28	-12	29
(60 stations)	Spring	5,466	101.9	97.3	0.55	-4.5	21.5	-4	18	-6	19
	Summer	5,443	101.1	100.5	0.65	-0.5	20.2	3	16	1	16
	Fall	5,197	77.2	70.2	0.65	-6.6	21.2	-6	25	-11	26
	Annual (no threshold)	21,363	88.7	83.9	0.69	-4.4	21.8	-3	22	-7	22
	Annual (threshold)	12,891	104.2	97.5	0.54	-6.7	22.4	-6	18	-9	19
NO_2 daily	Winter	3,600	12.1	8.0	0.67	-4.2	12.7	3	57	-21	55
(43 stations)	Spring	3,787	9.4	4.8	0.66	-4.5	10.6	-27	53	-51	67
	Summer	3,843	6.2	3.5	0.59	-2.7	5.7	-29	54	-53	69
	Fall	3,725	9.4	6.0	0.66	-3.4	10.1	-15	48	-34	56
	Annual (no threshold)	15,035	9.3	5.6	0.67	-3.7	10.1	-17	53	-40	62
	Annual (threshold)	14,138	9.8	5.8	0.66	-4.0	10.4	-20	51	-42	61
SO_2 daily	Winter	2,629	2.2	2.6	0.62	0.5	2.9	80	122	8	70
(31 stations)	Spring	2,749	1.6	2.0	0.63	0.4	1.9	62	96	13	62
	Summer	2,707	1.2	1.6	0.49	0.4	1.8	86	121	14	65
	Fall	2,604	1.4	2.0	0.56	0.7	2.3	105	134	25	68
	Annual (no threshold)	10,689	1.6	2.1	0.60	0.5	2.2	83	118	15	66
	Annual (threshold)	10,384	1.7	2.1	0.60	0.5	2.3	72	108	13	65
PM2.5 daily	Winter	1,171	13.7	4.8	0.63	-8.4	15.3	-47	59	-78	86
(16 stations)	Spring	1,264	12.2	5.2	0.50	-6.7	10.6	-50	59	-79	84
	Summer	1,396	12.2	6.8	0.49	-5.4	9.1	-45	56	-71	78
	Fall	1,287	11.5	6.2	0.52	-5.0	9.3	-39	53	-62	72
	Annual (no threshold)	5,118	12.3	5.7	0.47	-6.3	11.2	-45	56	-72	80
	Annual (threshold)	4,756	13.0	6.3	0.45	-6.7	11.6	-46	57	-74	81
PM10 daily	Winter	1,994	18.0	6.6	0.54	-11.2	18.2	-47	60	-78	86
(25 stations)	Spring	2,087	17.7	7.1	0.54	-10.5	15.0	-54	59	-84	87
	Summer	2,204	18.5	8.2	0.60	-10.5	16.1	-54	58	-83	86
	Fall	2,104	17.0	8.1	0.62	-9.0	13.5	-44	55	-70	77
	Annual (no threshold)	8,389	17.8	7.5	0.57	-10.3	15.8	-50	58	-79	84
	Annual (threshold)	7,918	18.7	7.8	0.55	-10.9	16.2	-53	57	-82	85

Results show distinct inter-seasonal behaviours between colder and warmer months. From January to March and from October to December, the model tends to underestimate the mean concentrations (in winter, MB = -5.8 μg m^{-3}), while it slightly overestimates concentrations in summer months (MB = 7.5 μg m^{-3}). Correlation values are lowest for both daily mean and daily peak correlations in the winter (r = 0.54 and 0.50, respectively). This inter-seasonal variability is attributed to the model sensitivity to boundary conditions near the surface in winter. During decreases of photochemical reactions in fall and winter the concentrations defined at the boundaries proportionally acquire an increasing role in the control of the concentration levels simulated within the domain. Also, the large concentrations of O$_3$ in the highest layers of the boundary profile (reaching the stratosphere) were found to be responsible for episodic inaccurate stratosphere-troposphere exchanges during colder months not shown here; also see (Eisele et al., 1999; Cristofanelli and Bonasoni, 2009). Such finding was highlighted very recently by Lam and Fu (2009) who pointed the inaccurate treatment of the tropopause in CMAQ as the issue causing such artifact. On the other hand, the mean biases for daily and daily peak concentrations are positive during warmer months with lowest RMSE values (19.8 and 20.2 μg m^{-3} in summer, respectively). Model-observations correlations, MNBE and MNGE values also reach the best values during this period. This performance demonstrates the greater ability of the model to accurately simulate ozone during its intense photochemical formation in warmer months. Daily variations are satisfactorily reproduced (see scatter plot in Figure 2-3b with nearly 95% of the data points falling within the 1:2 and 2:1 factor range). However, due to uncertainties in the modelled nocturnal NO$_x$ cycle, the O$_3$ chemistry at night tends to overpredict the observed concentrations. Such behaviour is partly reflected by the difference between the annual mean biases calculated with or without the minimum threshold of 80 μg m^{-3} on the measured data. By implementing this threshold a part of overestimated nocturnal measured values is not considered which induces a negative value of -5.9 μg m^{-3} compared to 0.0 using no threshold. For extreme values (above 150 μg m^{-3}) the observed concentrations are systematically underestimated by the model (see Figure 2-3b). This behaviour is most likely caused by high local pollution transported to rural sites but not captured with the current horizontal resolution of the model (see Ching et al., 2006).

Figure 2-4 and Figure 2-5 present the spatial distributions in winter (left) and summer (right) of the correlation and mean bias, respectively, without threshold on measurements. In the case of O$_3$ two different spatial regimes can be distinguished: seasonal correlations are highest in England, central and southern Europe, while Ireland and the countries along the North and Baltic Seas present lower performances. We attribute these lower performances of the model at these locations mostly to their relative proximity with the northern boundary of the domain. The most remote sites with low levels of O$_3$ display the lowest seasonal correlations (see Irish and northern stations; from -0.2 to 0.2 in winter, from 0 to 0.4 in summer). The model skills improve notably from winter to summer as a result of the increasing importance of the photochemical production of ozone. In summer most of the seasonal correlations are comprised between 0.4 and 0.9. Also, statistics are surprisingly satisfactory in complex regions such as the Alpine (stations CH02-CH05 and FR16) or the Pyrenean chains (FR12). As mentioned above in this section the model tends to underestimate the mean concentrations in winter and overestimate in summer (Figure 2-5). It is noted that mean biases in southern Europe have an inter-seasonal variability less pronounced than in the rest of Europe with values rather positive. In summer, the lowest MB values are found in regions of low mean O$_3$ levels such as the Alpine chain, Ireland and some Spanish stations.
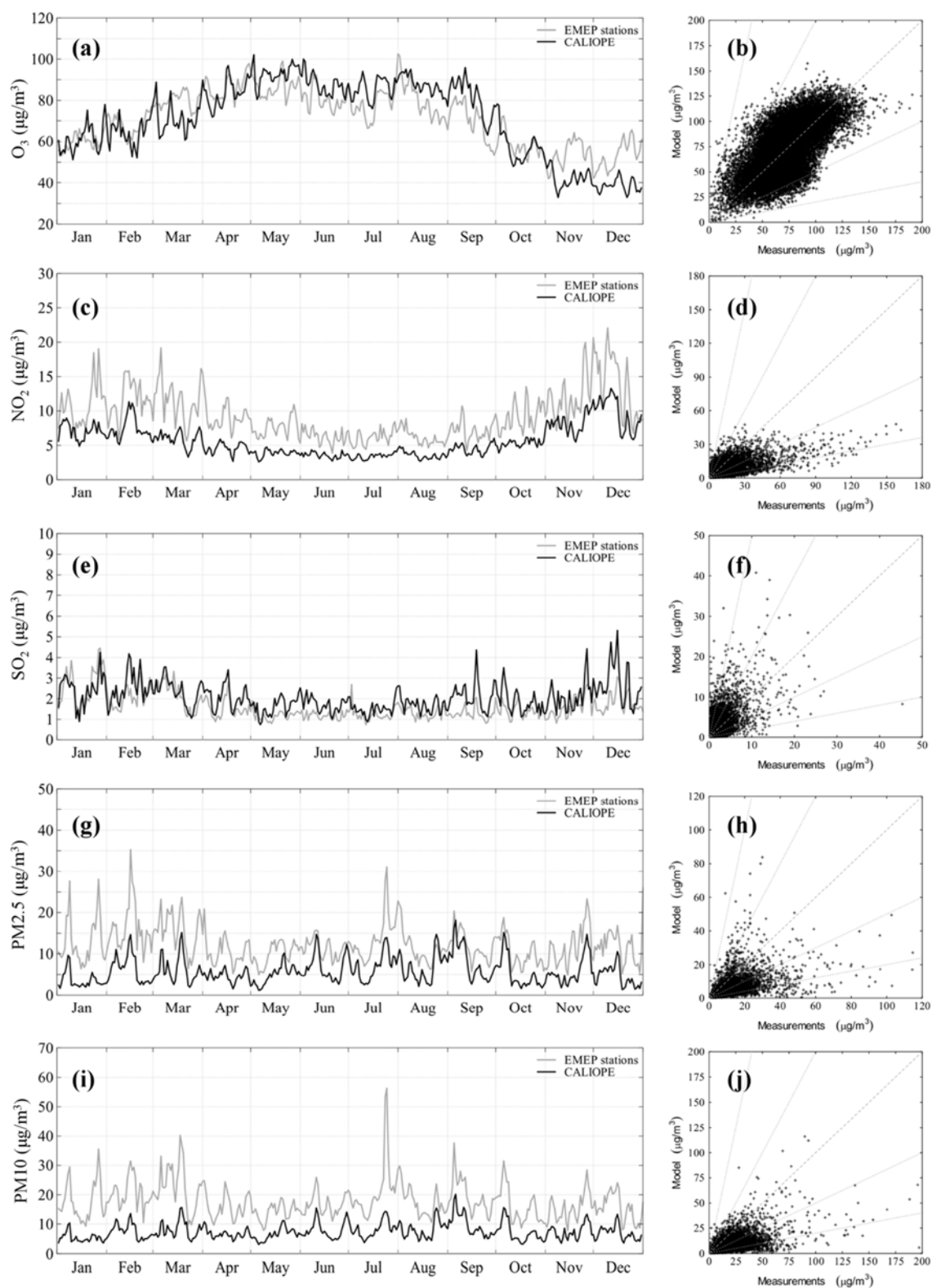
Figure 2-3. Modelled (black lines) and measured (grey lines) time series of daily mean concentrations (left) and scatter plots (right) for O_3, NO_2, SO_2, PM2.5 and PM10, respectively, at the EMEP stations. The scatter plots include the 1:1, 1:2, 2:1, 1:5 and 5:1 reference lines.

2.3.1.2 Nitrogen dioxide

As shown in Table 2-1, 43 stations were used to provide NO_2 measurements throughout Europe. The temporal and spatial variability of the simulated NO_2 in Europe is larger than for O_3, reflecting its higher sensitivity to meteorology and model resolution (Vautard et al., 2009). The model-observations comparison, presented in Figure 2-3c and d highlights a correct annual trend, but with a systematic negative bias throughout the year. The dynamics is often well captured but the amplitude of daily variations is underestimated. These low variations have a direct impact on the daily variations of ozone in the PBL. The annual average correlation is high (r = 0.67, see Table 2-2), with better performances in winter than in summer. Chemical processes, less dominant compared to transport in winter, could explain such differences (Bessagnet et al., 2004). Annual and seasonal mean biases are relatively high, ranging from -4.5 to -2.7 μg m^{-3}, leading to mean normalized error values rather near the maximum uncertainty proposed by the EC. High measured concentrations (above 70 μg m^{-3}) are particularly underestimated (see Figure 2-3d). When comparing modelled results versus measured data, 59.1% of the corresponding data pairs fall within a factor of 2 of each other, and 92.9% within a factor of 5.

The statistics of the model are spatially displayed in Figure 2-4 and Figure 2-5. NO_2 concentrations are mostly driven by local to regional emissions. Therefore, remote and clean boundary conditions are not significant contributors to the simulated concentrations of NO_2 in Europe. Correlations are highest in winter for the areas including UK, northern countries and some Spanish stations. In these regions emissions of NO_2 are generally either high or very low (also see Section 2.3.2.2). Low correlations are mainly concentrated in central Europe (coefficients between -0.2 and 0.4). Numerous stations located in low-NO_2 areas display satisfactory seasonal mean biases (see northern and central Europe and Spain with seasonal MB = ± 2 μg m^{-3}), while stations substantially affected by transport from source regions display the highest seasonal mean biases (Figure 2-5). The aforementioned large underestimations of high measured concentrations are mainly caused by the three stations from Great Britain (GB36, GB37 and GB38, see Table 2-1). These stations frequently undergo high pollution events caused by emissions from road traffic and combustion processes. To a lesser extent, these highly polluted plumes from the United Kingdom (UK) also affect the measuring station in The Netherlands (NL09) under westerly winds and contribute to the increase in mean bias values when the transport is not accurately simulated. At these locations, negative mean biases reaching up to 22 μg m^{-3} on annual average are noted with highest biases in winter. Such differences are most likely caused by the underestimation of emission sources in these areas. Altogether, the analysis of the spatial distribution of the model skills shows that the level NO_2 concentrations at very rural stations is well captured but with low correlation coefficients, while mean biases and correlation coefficients are greatest at polluted stations.

Apart from sources unaccounted for in the emission database, uncertainties may also arise in the spatial and temporal distribution of the sources (Stern et al., 2008). In the PBL NO_x concentrations are dominated by emissions near the surface, such as traffic and domestic heating, which are subject to strong spatial and temporal variations.
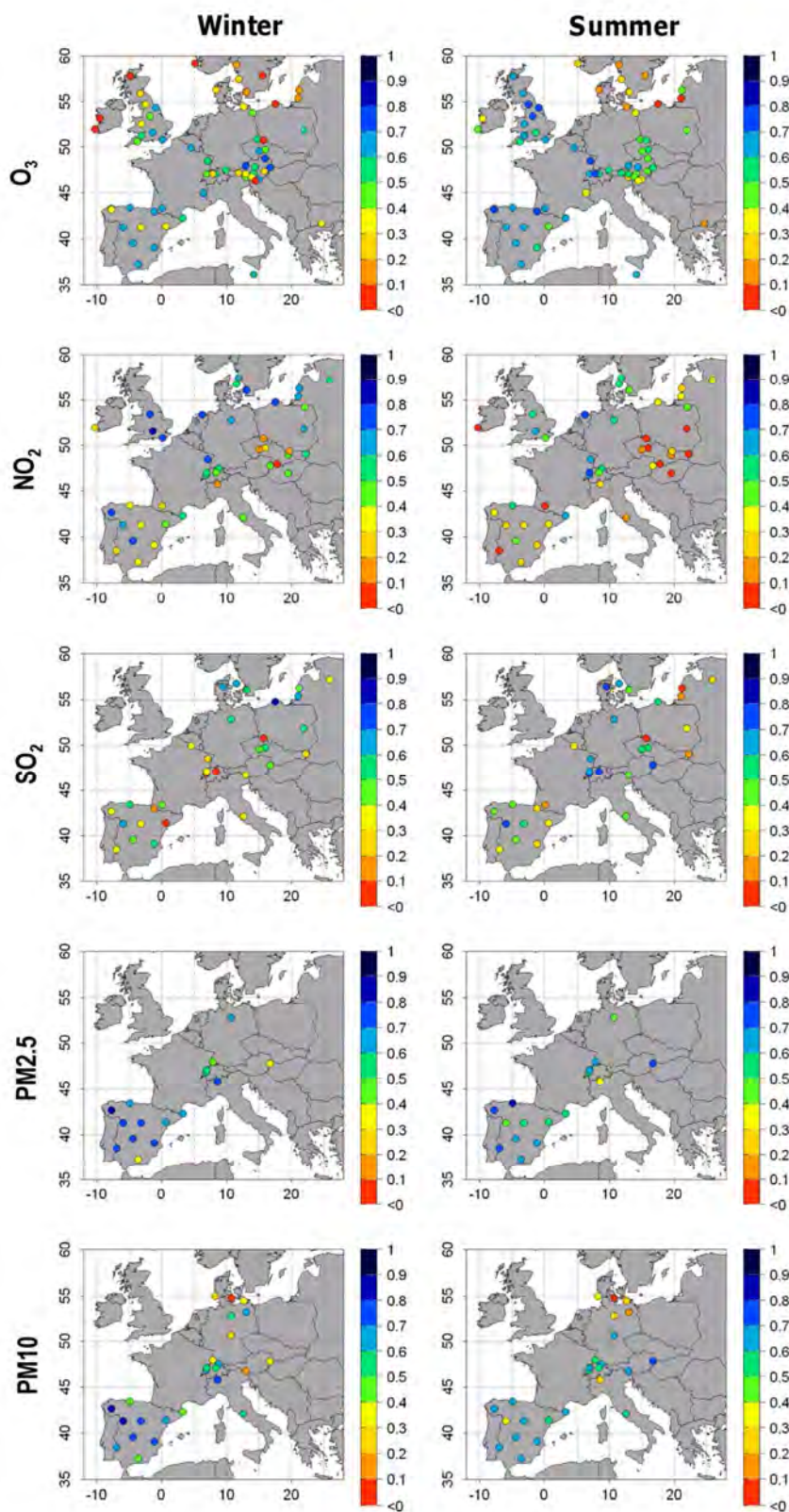
Figure 2-4. Spatial distribution of the correlation coefficient at all stations for O_3, NO_2, SO_2, PM2.5 and PM10. The two columns represent the winter and summer seasons for 2004, respectively.
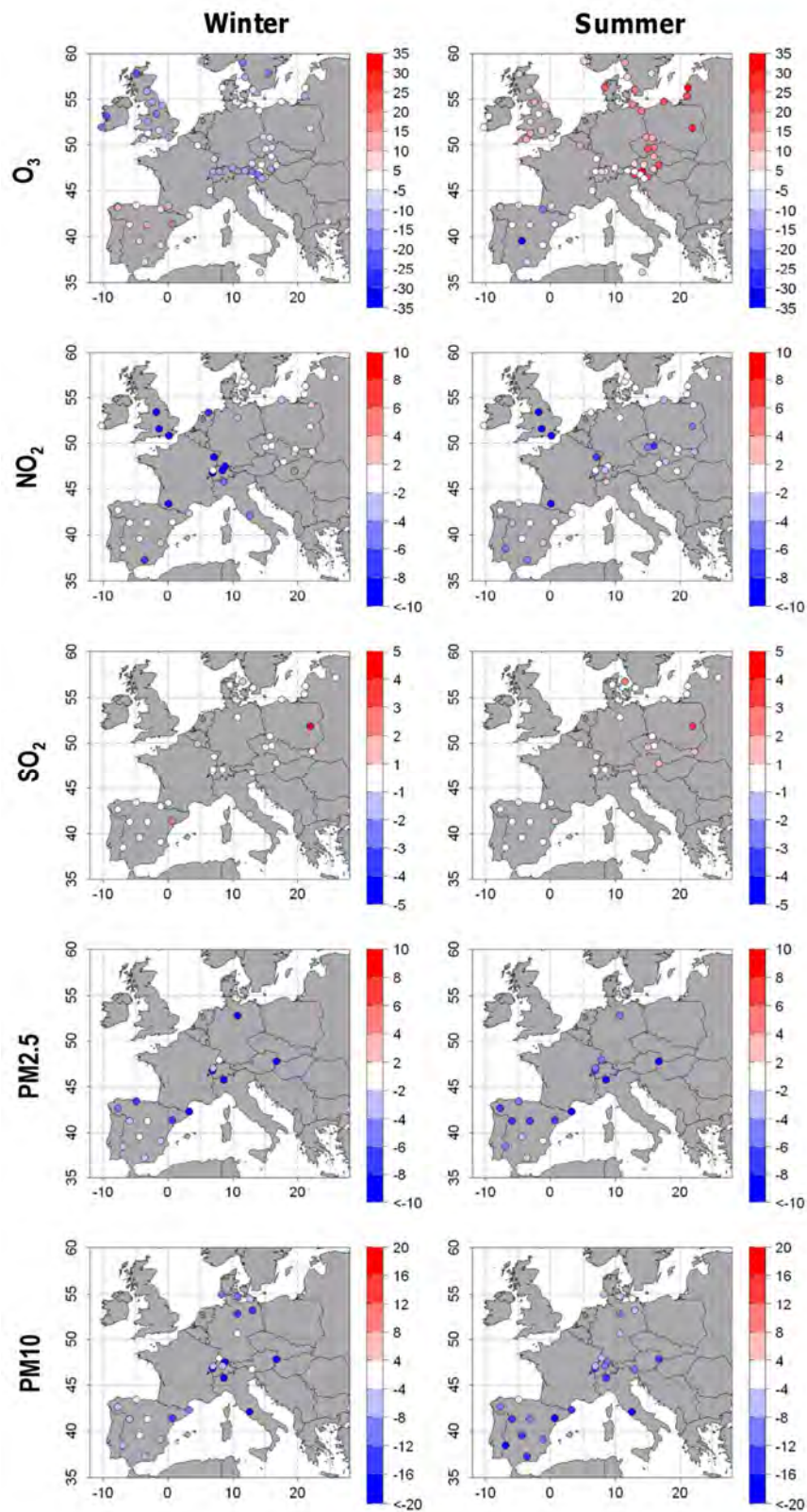
Figure 2-5. Spatial distribution of mean bias at all stations for O_3, NO_2, SO_2, PM2.5 and PM10 (in $\mu g\ m^{-3}$). The two columns represent the winter and summer seasons for 2004, respectively.

2.3.1.3 Sulphur dioxide

For SO_2, the model results were evaluated against 31 EMEP stations measuring daily mean concentrations of SO_2 at background sites. The stations are located across the Iberian Peninsula, central and north-eastern Europe. It is worth noting that the daily mean concentrations are low and provide information about the background levels of SO_2 across Europe only. Figure 2-3e shows the time series of the daily mean concentrations of SO_2 at the EMEP stations together with the model simulation at these stations. Results show that SO_2 concentrations are well captured by the model, although some observed peaks are overestimated. During the cold months (January, February, March, October, November) the model agrees well with observations, and monthly variations of SO_2 are well captured. On the other hand, during the warm period (April, May, June, July, August and September) results present an overall positive bias of 1 μg m^{-3}. September and December months are characterized by some episodes of large overestimations. Overall, the dynamical evolution of the model is in good agreement with the observations. For instance, January undergoes two major episodes of enhanced SO_2 that the model reproduces well. Although there is a clear overestimation during some periods, the model is able to reproduce the variations of the daily mean concentrations.

As regard to the scatter plot (Figure 2-3f), 54.3% of the model results match with observations within a factor of 2, and 90.1% within a factor of 5. The model results match the main tendency of the daily observations with an annual correlation factor r =0.60.

The annual mean MNGE and MNBE values reach up to 118% and 83% respectively (Table 2-2). Such rather high normalized errors are usual when evaluating background stations that measure very low values of SO_2. The annual RMSE is 2.2 μg m^{-3}, much lower than for the other pollutants analysed in the present work. The seasonal statistics show better results for spring, with mean MNGE value of 96%. The MNBE values increase for summer and fall as the daily mean observations remain below 2 μg m^{-3}.

The spatial distribution of the correlation coefficient r shows a large variability per station. For instance, during winter while some northern stations have high correlations (0.6 < r < 0.9), various low correlations are observed in central and southern Europe. During summertime the correlation improves in stations located over central Europe. In Spain, the model performs relatively homogeneously across the year, with a variation of the correlation between summer and winter less pronounced than in central Europe. However, the correlation per station in Spain is slightly lower than in the rest of Europe, especially during summer.

Considering the mean bias for winter and summer (Figure 2-5), results show a low bias across all stations. Only one station located in eastern Poland displays a high positive bias (> 5 μg m^{-3} in summer). This station may largely contribute to the seasonal and annual average positive bias mentioned in Table 2-2. The uncertainties of the emission inventory in eastern Europe may be associated to the higher bias observed in some stations of Poland and the Czech Republic, especially in winter. Also, the top-down disaggregation from 50 to 12 km is a source of uncertainties to be considered.

2.3.1.4 Particulate matter

A total of 16 and 25 stations are used to evaluate the simulated PM2.5 and PM10 concentrations, respectively. Although the model presents a clear systematic negative bias, it has noticeable capabilities to reproduce the dynamics of PM2.5 for the whole year (Figure 2-3g). The modelling system simulates the most important PM2.5 episodes across the whole year. The correlation coefficients for winter and fall seasons are 0.62 and 0.52, respectively, and 0.50 and 0.49 for spring and summer (Table 2-2). The MFE and MFB for PM2.5 do not fall within the performance criteria or performance goal proposed by Boylan and Russell (2006).

In order to evaluate the annual variability of PM in comparison to measurement data, Figure 2-6 displays the annual time series of PM2.5 and PM10 multiplied by a correction factor of 2. Such correction is not meant to modify the statistics but rather to evaluate the annual dynamics of the model and approximate the underestimation of PM mass. By multiplying the model results by such a factor, the results of the model system are in very good agreement with observations. The model is able to reproduce the daily evolution of PM2.5 across the year. Nevertheless, the model tends to underestimate the peaks during wintertime, while during summertime the model overestimates some episodes. By calculating the annual MFE and MFB with the adapted model output, the results now fall within the performance goal recommended by Boylan and Russell (2006) with an MFE = 49% and MFB = -12% (Table 2-3). It is important to note that the statistics are biased towards measurements obtained in Spain, since 10 out of 16 EMEP stations are located there (Figure 2-4 and Figure 2-5). Overall, the MFB and MFE are homogeneous at most stations (not shown).
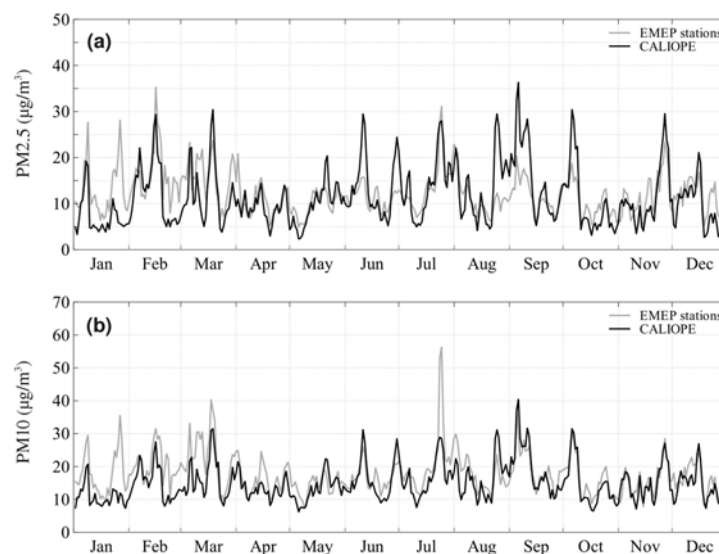
Figure 2-6. Modelled (black lines) and measured (grey lines) time series of daily mean concentrations for PM2.5 (top) and PM10 (bottom), multiplied by a correction factor of 2 at the EMEP stations.

For PM10, annual correlations are higher than for PM2.5 (annual mean correlation r = 0.57). The model is able to reproduce most of the particulate matter events, although the model hardly reproduces the amplitude of the events and presents a systematic underestimation. Concerning the variability of the results (Figure 2-3j), 69.4% of the data match with observations within a factor 2,

and 96.6% within a factor 5. As for PM2.5, PM10 results present a very good agreement with the observations if a factor of 2 is applied to the results (Figure 2-6b). The adapted results for PM10 match consistently with the observations except for the Saharan dust outbreak event on July 24-26th which affected southern, central and eastern Spain but was not captured by BSC-DREAM8b.

The annual mean MFB and MFE of the adapted results amount to -20% and 51%, respectively (Table 2-3). These results are in accordance with the recommendations for particulate matter mentioned in Section 2.2.4 and fall within the performance criteria of Boylan and Russell (2006). The spatial distribution of the correlation coefficient and the mean bias for winter and summer point out that the model performs better in southern than in northern Europe, for PM10 (Figure 2-4 and Figure 2-5). Stations located between the Baltic and the North Sea (DE01, DE09, DK05; see Table 2-1) display weak seasonal correlation coefficient (-0.1 < r < 0.3). However, continental stations of central Europe (Germany, Switzerland and Austria) mainly affected by anthropogenic emissions present good performances for PM10. Correlations are in the range of 0.3-0.7 during winter and improve in summer. From all coastal sites affected by SS, the stations in Spain display the highest correlations (Niembro and Cabo de Creus with 0.4 < r < 0.6). At the south European stations affected by Saharan dust outbreaks, namely Spain and Italy, correlations are high across the year (0.5 < r < 0.9, except ES13). The inclusion of BSC-DREAM8b model results largely contributes to the improvement of the model performances at such southern stations as previously noted by Jiménez-Guerrero et al. (2008a).

Many studies have recognized the difficulty of models to simulate the mass of particulate matter over Europe (van Loon et al., 2004; Matthias, 2008). The underestimation of total particulate mass is, among others, the result from the lack of fugitive dust emissions, resuspended matter (Vautard et al., 2005a), a possible underestimation of primary carbonaceous particles (Schaap et al., 2004a; Tsyro, 2005), the inaccuracy of SOA formation (Simpson et al., 2007), the difficulty of representing primary PM emission from wood burning and other sources (Tsyro et al., 2007) and a more general lack of process knowledge (Stern et al., 2008). While multiplying the model results of CALIOPE-EU by a factor of 2, it was shown that the dynamics of particulate matter (both PM2.5 and PM10) can be well captured. Using such methodology the levels generally simulated by CALIOPE-EU were quantified to be approximately half of the observed values.

Table 2-3. Seasonal and annual statistics obtained with CALIOPE-EU over Europe for 2004 (see Table 2-2). For quantification purposes, the simulated concentrations of PM are multiplied by a correction factor of 2 at the EMEP stations.

	Period	Data points	Measured mean	Modelled mean	r	MB	RMSE	MNBE	MNGE	MFB	MFE
PM2.5 daily	Winter	1,171	13.7	9.60	0.62	-3.3	12.4	6	60	-20	58
adapted (x 2)	Spring	1,264	12.2	10.4	0.50	-1.3	10.0	1	49	-19	47
(16 stations)	Summer	1,396	12.2	13.6	0.49	1.3	13.0	10	52	-10	45
	Fall	1,287	11.5	12.3	0.52	1.5	11.4	22	58	-1	47
	Annual (no threshold)	5,118	12.3	11.5	0.47	-0.3	11.8	10	54	-12	49
	Annual (threshold)	4,756	13.0	12.6	0.45	-0.4	12.2	7	53	-14	49
PM10 daily	Winter	1,994	18.0	13.3	0.54	-4.3	14.7	6	61	-21	57
adapted (x 2)	Spring	2,087	17.7	14.2	0.54	-3.4	12.4	-7	46	-25	48
(25 stations)	Summer	2,204	18.5	16.3	0.60	-2.4	14.8	-7	46	-23	49
	Fall	2,104	17.0	16.1	0.62	-0.9	12.1	13	56	-10	50
	Annual (no threshold)	8,389	17.8	15.0	0.57	-2.7	13.6	1	52	-20	51
	Annual (threshold)	7,918	18.7	15.6	0.55	-3.1	13.9	-5	48	-23	50

2.3.2 Pattern description

In the following section, it is important to note that the description of the simulated chemical patterns does not take into account the model-observations discrepancies highlighted in Section 2.3.1.

2.3.2.1 Ozone

Modelled O_3 average concentrations over Europe (Figure 2-7a) show an increasing gradient from the northern and western boundaries to the more continental and Mediterranean areas, resulting from large variations in climate patterns (Beck and Grennfeld, 1993; Lelieveld et al., 2002; EEA, 2005; Jiménez et al., 2006c). In the troposphere O_3 has a residence time of several days to a week which permits its transport on regional scales (Seinfeld and Pandis, 1998). The highest concentrations are found in the Mediterranean basin and southern Europe (nearly 90-105 μg m^{-3}), as this region is particularly affected by intense photochemical production of O_3 (EEA, 2005; Vautard et al., 2005b). Detailed descriptions of O_3 formation and transport over the Mediterranean area can be found in Gerasopoulos et al. (2005) or Cristofanelli and Bonasoni (2009). Other important factor for the land-sea difference is the slow dry deposition of O_3 on water and also the low photochemical formation due to the low precursor concentration (Wesely and Hicks, 2000). In central and eastern Europe, simulated annual O_3 concentrations range from 70 to 85 μg m^{-3}, with a slight west to- east gradual build-up caused by the association of precursor emissions and predominant westerly winds. Northwestern areas show rather low concentrations of O_3 (60-67 μg m^{-3}) due to reduced solar radiation and the influence of the clean marine air. Due to higher O_3 concentrations in elevated terrains, the major mountainous regions such as the Alpine and Pyrenean chains as well as the Carpathian Mountains (mainly in Rumania) display mean O_3 concentrations in the range of 85-95 μg m^{-3}. The minimum values of O_3 (50-55 μg m^{-3}) are found in regions of chemically-driven high-NO_x regime such as large polluted cities or within the shipping routes, Great Britain and The Netherlands, and in northernmost Europe due to the association of low precursor emissions and polar-like weather types. The O_3 distribution described in this section is in accordance with the EMEP model results for the year 2005 presented by Tarrasón et al. (2007). However, the rather coarse resolution used by the EMEP model (50 km x 50 km) led to a less accurate simulation of the chemical transition between urban and background areas.

2.3.2.2 Nitrogen dioxide

High concentrations of NO_2 within the PBL are directly related to anthropogenic emissions (EEA, 2007). The largest contributors to NO_2 atmospheric concentrations are the emissions from road transport (40% of NO_2 total emission) followed by power plants and other fuel converters 22% of NO_2 total emission (Tarrasón et al., 2006). High modelled NO_2 concentrations (20-30 μg m^{-3}) are reported in The Netherlands and Belgium, the industrial Po Valley (northern Italy), central and eastern England, and the Ruhr region (western Germany). Various important European cities even reach NO_2 levels up to 30-40 μg m^{-3} on annual average (e.g., Milan, London, Paris). Suburban areas surrounding the major cities often undergo advections of polluted air masses and display mean annual values near 10-25 μg m^{-3} while clean regions unaffected by emissions rather have

concentrations below 5 μg m^{-3}. Also note that the major shipping routes originating from the North Sea, passing by the English Channel, through Portugal, Spain and northern Africa towards the Suez Canal substantially affect the coastal NO$_2$ concentrations with a maximum of 18 μg m^{-3} for the annual mean concentrations. Qualitative comparisons between the simulated pattern of annual NO$_2$ and satellite-derived NO$_2$ tropospheric column densities from GOME (Beirle et al., 2004), SCIAMACHY and OMI (Boersma et al., 2007) revealed good agreement (not shown). Such finding demonstrates the relative accuracy in the spatial description of the source regions and various European hot-spots.
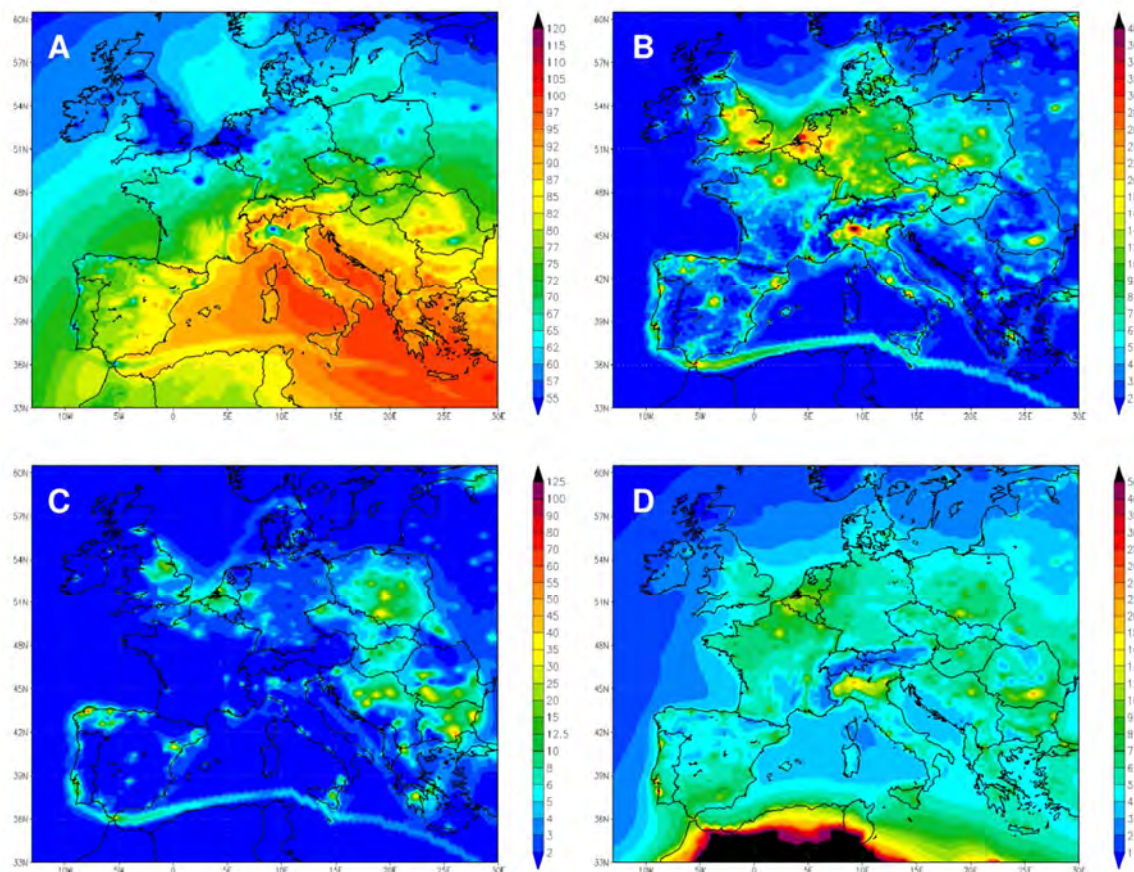
Figure 2-7. Simulated annual average concentrations (μg m^{-3}) of (a) O$_3$, (b) NO$_2$, (c) SO$_2$, (d) PM2.5 at ground level modelled with the CALIOPE-EU air quality modelling system for Europe with a 12 km x 12 km spatial resolution in 2004.

2.3.2.3 Sulphur dioxide

Simulated SO$_2$ annual average concentrations over Europe (Figure 2-7c) show highest levels over northwestern Spain, eastern Europe (Poland, Serbia, Rumania, Bulgaria and Greece), and over UK, Belgium and the southwestern part of The Netherlands. Combustion emissions from power plants and transformation industries are the main responsible for such high concentrations of SO$_2$ over Europe. 64% of SO$_2$ total emissions are attributed to these sectors (Tarrasón et al., 2006). The

highest annual concentrations (70-90 μg m^{-3}) are observed in northern Spain due to the presence of two large power plant installations. However, background regions in Spain remain below mean concentrations of 2 μg m^{-3}. On the other hand, east European countries are affected by higher background concentrations of SO$_2$ (8-20 μg m^{-3}) with various punctual emissions contributing to an increase of the regional concentrations (30-50 μg m^{-3}). Over sea, the highest concentrations are found along the main shipping routes, as emissions from ships largely contribute to the SO$_x$ concentrations due to combustion of fuels with high sulphur content (Corbett and Fischbeck, 1997; Corbett and Koehler, 2003). The distribution of mean annual SO$_2$ concentrations for 2004 shows the same pattern as that presented by Tarrasón et al. (2007) for 2005. However, note that the SO$_2$ levels have decreased according to the pattern shown in Schaap et al. (2004a) for the year 1995. Indeed, from the mid-1990s to 2004, SO$_2$ concentrations in air have strongly decreased due to reductions in SO$_x$ emissions. SO$_x$ emissions have reduced up to 50% mainly in the sectors of power and heat generation through a combination of using fuels with lower sulphur content (such as switching from coal and oil to natural gas) and implementing emission abatement strategies in the energy supply and industry sectors (EEA, 2007; International Maritime Organization and Marine Environment Protection Committee, 2001).

2.3.2.4 Particulate matter

The simulated spatial distribution of annual mean PM2.5 (Figure 2-7d) shows average background levels around 3-10 μg m^{-3} in northwestern, central and eastern Europe. Very low concentrations correspond to remote marine air and the major European mountain chains (e.g., the Alps, Massif Central, the Pyrenees and the Carpathians). The concentration levels are dominated by SIA, namely sulphate, nitrate and ammonium (not shown here). SSA does not substantially contribute to the PM2.5 fraction. The most polluted European region is the Po Valley with annual mean values near 14-22 μg m^{-3}. To a lesser extent, in the Benelux region (Belgium, The Netherlands, and Luxembourg) high concentrations of PM2.5 are found (8-12 μg m^{-3}). Such concentrations are mainly associated with primary anthropogenic emissions from road traffic and secondary aerosols. As mentioned in Section 2.3.2.3 Bulgaria, Rumania and Poland are important contributors of SO$_2$. At the hotspot locations, the large sulphate formation and primary PM emissions lead to annual mean concentrations of up to 20-22 μg m^{-3}. Interestingly, the large sources of SO$_2$ located in eastern UK and northwestern Spain do not contribute efficiently to the PM2.5 formation. Such low sulphate formation is most likely caused by high dispersion and strong removal by wet deposition in these regions. The north African continent constitutes a very large potential source of PM for the rest of the domain. During episodes of Saharan dust outbreaks, mineral dust largely contributes to the levels of PM2.5 in southern Europe.

Figure 2-8a and b presents the annual mean and 1-h maximum of PM10 concentrations in Europe, respectively. PM10 includes the PM2.5 fraction, the primary anthropogenic coarse fraction (PM10-2.5), as well as the contribution of coarse SSA and Saharan dust. Among other uncertainties, wind-blown or resuspended dust emissions (coarse fraction) are not taken into account yet. Such sources contribute to the underestimation of the total concentrations of PM10, especially in dry regions or in urban areas (see Amato et al., 2009a).
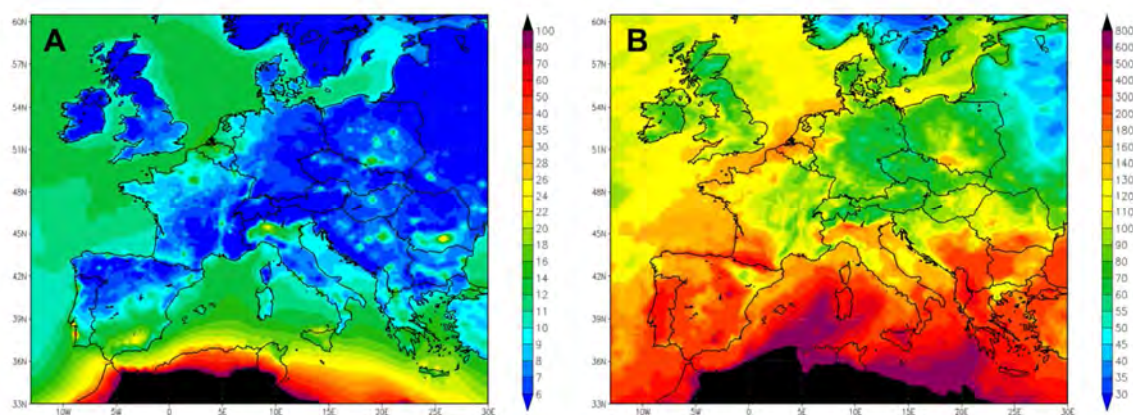
Figure 2-8. Simulated annual (a) average and (b) maximum concentrations for PM10 in μg m⁻³ in 2004.

High mean and maximum values of annual PM10 concentrations found in the North Sea and the nearshore Atlantic result from SS production. The mean contribution of SS in the Mediterranean Sea reaches around 10 μg m⁻³. The annual mean contribution of the anthropogenic coarse fraction remains low (5 μg m⁻³) and is located at or in the vicinity of important emission sources (not shown). Saharan dust is responsible for the very high levels of PM in northern Africa and also regularly affects the Mediterranean basin and southern Europe. Spain, southern France, Italy, and Greece are particularly affected by such episodes. Figure 2-8b reflects well the importance of including Saharan dust model data (on a non-climatic basis) since dust outbreaks lead to annual maximum concentrations of PM10 greater than 300 μg m⁻³ in most of the territories surrounding the Mediterranean Sea.

Qualitatively, the spatial distributions of PM2.5 and PM10 show similar patterns to distributions found in other European modelling studies including sea salt and Saharan dust emissions (see, e.g., POLYPHEMUS and the Unified EMEP model, Sartelet et al., 2007; Tarrasón et al., 2006). Substantial differences arise in concentrations over southern Europe when comparing spatial distributions with models not taking dust from the African continent into account (see Bessagnet et al., 2004).

2.4   Comparison with other evaluation studies

There are several air pollution modelling systems on the European scale operated routinely in Europe. Evaluations of these regional air quality models with ground-based measurements were carried out either individually or in comparison to other models. The following discussion presents a comparative analysis between various European model evaluations and CALIOPE-EU. This analysis does not attempt to be an inter-comparison study because the studies were performed under different conditions (simulated year, meteorological data, boundary conditions, emissions, etc.). However, it provides a good basis for assessing the reliability of the results obtained in the context of the European evaluation models. Table 2-4 shows a chronological list of published evaluation studies, which are presented along with CALIOPE-EU evaluation results. The presented

evaluation studies have several characteristics in common. First, they were carried out over Europe on a regional scale with horizontal resolutions in the range of 25-55 km x km. Second, the simulations were run over a long period, mainly a year. The given models were evaluated against ground-based observations at rural locations from EMEP or AIRBASE databases. Also note that these evaluation studies were performed using statistical methods.

Most of the studies presented here, evaluated independently in previous publications, focused on both gas and particulate phases. These studies comprise: LOTOS-EUROS (Schaap et al., 2008), POLYPHEMUS (Sartelet et al., 2007), Unified EMEP (Tarrasón et al., 2006; Yttri et al., 2006), and CHIMERE (Bessagnet et al., 2004; Schmidt et al., 2001). In the case of the Unified EMEP model, evaluation studies are being processed every year since 1980 (Tarrasón et al., 2005). For the purpose of this paper, we only exploited their evaluation of the year 2004, since it is the reference year modelled by CALIOPE-EU. The single evaluations of both CMAQ (Matthias, 2008) and LOTOS (Schaap et al., 2004a) only focused on particulate matter results.

Table 2-4. List of published European model evaluation studies and their main characteristics to be compared with CALIOPE-EU evaluation results (this study). A study code for each model is specified to ease the discussion in this paper.

Reference	Modelled year	Model name	Horizontal Resolution/layers	Study code
This study	2004	CALIOPE-EU	12 km x 12 km/15	CALIOPE-EU04
Matthias (2008)	2001	CMAQ	54 km x 54 km/20	CMAQ2
Schaap et al. (2008)	1999	LOTOS-EUROS	25 km x 25 km	LOTOS-EUROS3
Sartelet et al. (2007)	2001	POLYPHEMUS	0.5° x 0.5°/2	POLYPHEMUS4
van Loon et al. (2007)	1999	Unified EMEP	50 km x 50 km/20	EMEP5
van Loon et al. (2007)	1999	RCG	0.5° x 0.5°/5	RCG5
van Loon et al. (2007)	1999	LOTOS-EUROS	0.5° x 0.5°/4	LOTOS-EUROS5
van Loon et al. (2007)	1999	CHIMERE	0.5° x 0.5°/8	CHIMERE5
van Loon et al. (2007)	1999	MATCH	0.4° x 0.4°/14	MATCH5
Tarrasón et al. (2006)	2004	Unified EMEP	50 km x 50 km/20	EMEP6
Yttri et al. (2004)	2004	Unified EMEP	50 km x 50 km/20	EMEP7
Bessagnet et al. (2004)	1999	CHIMERE	0.5° x 0.5°/8	CHIMERE8
van Loon et al. (2004)	1999/2001	CHIMERE	0.5° x 0.5°/8	CHIMERE9
van Loon et al. (2004)	1999/2001	DEHM	50 km x 50 km/20	DEHM9
van Loon et al. (2004)	1999/2001	Unified EMEP	50 km x 50 km/20	EMEP9
van Loon et al. (2004)	1999/2001	MATCH	55 km x 55 km/10	MATCH9
van Loon et al. (2004)	1999/2001	LOTOS	0.25° x 0.5°	LOTOS9
van Loon et al. (2004)	1999/2001	CMAQ	36 km x 36 km/21	CMAQ9
van Loon et al. (2004)	1999/2001	REM-CALGRID	0.25° x 0.5°	REM-CALGRID9
Schaap et al. (2004)	1995	LOTOS	25 km x 25 km/3	LOTOS10
Hass et al. (2003)	1995	DEHM	50 km x 50 km/10	DEHM11
Hass et al. (2003)	1995	EURAD	27 km x 27 km/15	EURAD11
Hass et al. (2003)	1995	EUROS	0.55° x 0.55°/4	EUROS11
Hass et al. (2003)	1995	LOTOS	0.25° x 0.5°/3	LOTOS11
Hass et al. (2003)	1995	MATCH	55 km x 55 km/10	MATCH11
Hass et al. (2003)	1995	REM3	0.25° x 0.5°	REM11
Schmidt et al. (2001)	1998	CHIMERE	0.5° x 0.5°/5	CHIMERE12

In addition to the models evaluated independently and listed above, three model inter-comparisons were also carried out and are presented in Table 2-4. In the framework of EUROTRAC (Hass et al., 2003) the authors evaluated the ability of six models to simulate inorganic aerosol compounds. In the review of the Unified EMEP model (van Loon et al., 2004) the gas and particulate phases from seven models were compared. More recently, an inter-comparison was performed in order to study the response of five models to different emission scenarios in terms of O_3 levels EURODELTA project (van Loon et al., 2007).

Table 2-5 and Table 2-6 present the statistics of each reviewed study available for the gas (O_3, NO_2 and SO_2) and particulate (PM10 and PM2.5) phases, respectively. Three statistical parameters are considered, namely the annual daily means of MNBE, r, and RMSE. These parameters were calculated without threshold on the measurement data, except for the MNBE value of O_3 in POLYPHEMUS4 which is calculated using a threshold of 80 $\mu g\ m^{-3}$ as pointed out by Sartelet et al. (2007). The displayed results represent the annual means at all considered stations. Values in parentheses, when available, correspond to the minimum and maximum performances at individual stations.

For the O_3 daily mean CALIOPE-EU presents satisfactory annual MNBE values in comparison to the other studies (6 $\mu g\ m^{-3}$ versus 2-29 $\mu g\ m^{-3}$). The annual daily mean correlation is rather low (0.66 versus 0.53-0.83). Nevertheless, the RMSE obtained with CALIOPEEU is in the range of other models (20.6 $\mu g\ m^{-3}$ for CALIOPE-EU versus 18.4-28.1 $\mu g\ m^{-3}$). Values for the annual daily peak mean correlations for CALIOPE-EU are slightly below the range of the other studies. Note that the CMAQ9 model obtained the same annual daily peak mean correlation as CALIOPE-EU, namely 0.69 versus 0.71-0.84, which is lower than in the other studies. However, for individual stations, CALIOPE-EU remains within the same range of EMEP6 for the year 2004 (0.28-0.82 versus 0.10-0.84). This large range of values reflects the high variability of the model performances depending on the region of the domain (see Figure 2-4 and discussion in Section 2.3.1.1). RMSE and MNBE values for annual daily peak mean of O_3 lie within the range of the other models.

Overall, the CALIOPE-EU performances for NO_2 are superior to other models. The annual daily mean correlation obtained in this study is the highest from all considered models (0.67 versus 0.03-0.47). The annual daily mean RMSE value is among the lowest (10.0 $\mu g\ m^{-3}$ versus 8.5-13.9 $\mu g\ m^{-3}$). MNBE values for CALIOPE-EU are similar to CHIMERE8, the only study providing NO_2 annual daily mean values. Such a broad range of MNBE values is caused by the sensitivity to low observed concentrations, inducing problems of inflation and asymmetry (Yu et al., 2006). Therefore, we encourage future modelling studies to use threshold-filtered MNBE for NO_2 or else use fractional errors instead. The high performances of CALIOPE-EU with NO_2 are attributed mostly to the high resolution of the model system which enables a well-defined spatial and temporal description of NO_2 sources throughout Europe.

Table 2-5. Comparison of the statistics Mean Normalized Bias Error (MNBE, %), correlation (r), and Root Mean Squared Error (RMSE, μgm^{-3}) between CALIOPE-EU and other European models[a, b] for gas phase (O_3, NO_2 and SO_2 daily and O_3 daily peak). The statistics do not consider thresholds on measurement data except for the MNBE value (*) provided by the POLYPHEMUS study.

Study number	O_3 daily average			O_3 daily peak average			NO_2 daily average			SO_2 daily average		
	MNBE	r	RMSE	MNBE	r	RMSE	MNBE	r	RMSE	MNBE	r	RMSE
CALIOPE-EU04	-6	0.66	20.6	-3	0.69	21.8	-17	0.67	10.0	83	0.60	2.2
	(-22, 43)	(0.06, 0.81)	(15.8, 29.2)	(-23, 23)	(0.28, 0.82)	(17.5, 30.7)	(-74, 77)	(0.02, 0.84)	(1.4, 36.3)	(-28, 370)	(0.13, 0.80)	(0.8, 6.4)
LOTOS-EUROS3		0.65	25.2		0.75	20.4		0.40	11.4		0.40	3.4
POLYPHEMUS4				-14*	0.72	21.4		0.33	10.0		0.47	5.0
EMEP5	10	0.72		1	0.75							
RCG5	3	0.71		7	0.76							
LOTOS-EUROS5	2	0.70		7	0.76							
CHIMERE5	29	0.76		10	0.84							
MATCH5	6	0.80		2	0.81							
EMEP6	10	0.72		1	0.75 (0.10, 0.84)						0.67	
CHIMERE8							(-78, 349)	(-0.30, 0.70)	(1.0, 28.0)			
CHIMERE9		0.78/0.83	18.4/18.1		0.78/0.83	18.4/18.1		0.47/0.44	12.6/13.9		0.37/0.47	10.9/10.1
DEHM9		0.66/0.66	24.2/23.1		0.78/0.78	22.1/21.7		0.45/0.46	11.1/11.7		0.43/0.49	4.8/3.9
EMEP9		0.63/0.65	23.6/23.0		0.75/0.76	19.1/19.5		0.43/0.45	11.2/12.1		0.40/0.42	4.7/3.9
MATCH9		0.65/0.68	24.7/24.5		0.79/0.80	18.3/18.8		0.42/0.44	11.8/12.5		0.43/0.48	4.4/3.2
LOTOS9		0.53/0.54	27.7/28.1		0.74/0.73	21.7/22.0		0.25/0.30	12.9/13.6		0.24/0.45	5.9/4.6
CMAQ9		0.55/-	32.6/-		0.69/-	25.5/-		0.52/-	10.8/-		0.44/-	6.0/-
REM-CALGRID9		0.61/0.64	26.4/25.7		0.71/0.74	21.9/22.0		0.40/0.42	11.9/12.6		0.35/0.39	4.7/3.5
LOTOS10								0.48	4.1			
DEHM11								0.23	8.7		0.43	2.8
EURAD11								0.16	8.9		0.39	5.6
EUROS11								0.07	9.4		0.39	3.9
LOTOS11								0.03	9.2		0.39	3.1
MATCH11								0.23	8.5		0.45	2.7
REM311								0.13	9.3		0.35	3.3
CHIMERE12					(0.51, 0.88)	(13.4, 44.6)		(-0.05, 0.77)	(1.0, 10.0)			

[a] Value reported without parenthesis represents the annual average in the entire domain. The first and second values in parenthesis represent the minimum and maximum values obtained among all stations in the entire domain.

[b] Values reported before and after a slash correspond to the year 1999 and 2001, respectively.

Table 2-6. Comparison of the statistics MNBE (%), r and RMSE (μg m^{-3}) between CALIOPE-EU and other European models[a, b] for particulate matter PM2.5 and PM10. The statistics do not consider thresholds on measurement data.

Study number	PM2.5 daily average			PM10 daily average		
	MNBE	r	RMSE	MNBE	r	RMSE
CALIOPE-EU04	-45	0.47	11.2	-50	0.57	15.8
	(-68, -13)	(0.46, 0.79)	(5.5, 25.3)	(-72, 12)	(0.10, 0.77)	(5.7, 31.4)
CMAQ2					(0.35, 0.69)	
POLYPHEMUS4		0.54	8.6		0.54	12.6
EMEP7		0.44	10.6		0.48	14.1
		(0.28, 0.70)			(0.24, 0.66)	
CHIMERE8				(-80, 20)	(0.50, 0.70)	(0.8, 30.0)
CHIMERE9					0.55/ 0.55	14.4/13.8
DEHM9					0.50/0.49	16.0/14.5
EMEP9					0.52/0.48	15.7/14.9
MATCH9					0.44/0.49	14.9/12.9
LOTOS9					0.45/0.38	16.6/15.2
CMAQ9					0.54/-	15.0/-
REM-CALGRID9					0.57/0.49	13.2/12.4
LOTOS10					(0.35, 0.69)	

[a]Value reported without parenthesis represents the annual average in the entire domain. The first and second values in parenthesis represent the minimum and maximum values obtained among all stations in the entire domain.
[b]Values reported before and after a slash correspond to the year 1999 and 2001, respectively.

As with NO$_2$, the CALIOPE-EU evaluation results for SO$_2$ show very satisfactory performances in comparison to the other studies. The calculated RMSE is the lowest from all models (2.2 μg m^{-3} against 2.7-10.9 μg m^{-3}). Additionally the annual daily mean correlation obtained for CALIOPE-EU is the second highest value after the EMEP6 study with r = 0.60 against 0.67, respectively. The other studies calculated lower correlation coefficients between 0.24 and 0.49. No annual daily mean MNBE values were provided by the other evaluations. Also, the SO$_2$ model performances are mainly attributed to the high resolution of the CALIOPE-EU system enhancing the simulation accuracy. As mean background concentrations of observed SO$_2$ in Europe are low (2 μg m^{-3}, see Table 2-2), mean normalized errors may not adequately represent the performances of a model at rural sites. In that case, the use of thresholds on observational data or rather MFE and MFB should be considered.

Considering PM2.5, the model performance on the annual mean correlation coefficient is comparable with the two other studies POLYPHEMUS4 and EMEP7 (0.49 versus 0.44 and 0.54). Such correlation is rather low and reflects the high uncertainties in the sources of fine particles (see discussion in Section 2.3.1.4). The annual daily mean RMSE obtained by CALIOPE-EU is slightly higher than the values obtained by the two other studies (11.0 μg m^{-3} versus 8.6 and 10.6 μg m^{-3}).

Statistics for PM10 are in the same range as for the other studies. As with all other models, CALIOPE-EU tends to underestimate the PM10 concentrations, with the calculation of PM2.5 concentrations being a substantial source of underestimation. Per individual stations, the MNBE range for CALIOPE-EU is similar to that of CHIMERE8 (from -72% to 12% compared to -80%

to 20% for CHIMERE8). The calculated annual daily mean correlation coefficient of this work is the highest value from all other studies, together with the REM-CALGRID9 study for the year 1999. The annual daily mean RMSE remains in the range of other studies (15.7 $\mu g\ m^{-3}$ versus 12.4-16.6 $\mu g\ m^{-3}$).

Overall, the performances on the levels and variability of particulate matter are relatively poor, but this inter-comparison shows that the underestimated mean concentrations and the lack of understanding on the formation processes is a general feature affecting most models.

The results of this inter-comparison suggest that CALIOPE-EU performs relatively well for the simulation of O_3 concentrations while high scores were obtained for NO_2 and SO_2. In general, performances on particulate matter (PM2.5 and PM10) are satisfactory in comparison to the other studies. However, substantial efforts should be made in the chemical description of PM formation and the accuracy of PM sources.

From this model inter-comparison it was noticed that model systems based on the CMAQ chemical model (CALIOPE-EU and CMAQ9) perform better for daily mean NO_2 and SO_2 than for O_3 daily average and daily peak averages when compared to the other systems. While most European models obtain O_3 annual mean daily peak correlations between 0.7 and 0.8 for the year 2004, both CMAQ models reach a maximum of 0.69. However, note that this correlation obtained by CALIOPE-EU is higher than values reported by other studies using CMAQ and representing the US domain (see, e.g., Zhang et al., 2006; Yu et al., 2006; Eder and Yu, 2006). On the other hand, the correlations for NO_2 and SO_2 are notably higher for CMAQ models than for the other chemical models. All models are based on the same emissions from the EMEP database, but the disaggregation techniques or additional integrated modules may differ. These results indicate some potential limitations with the chemical mechanism used within this version of CMAQ (CBM-IV) when applied to the EMEP emissions over Europe (also see Emmerson and Evans, 2009). The Carbon Bond mechanism has recently been updated (Yarwood et al., 2005) and evaluated (Luecken et al., 2008). It is expected that the latest mechanism, namely CB05, could improve the behaviour of the CMAQ model over rural European areas considering the efforts done to improve the simulations under low NO_x conditions.

Another relevant issue that arises from the model comparison is the impact of horizontal resolution. As stated before in the text, all models are forced with EMEP emissions. These emissions have a spatial resolution of 50 km x 50 km. After different spatial disaggregation techniques most models perform similarly regardless of the target horizontal resolution. This result is not surprising if one considers that this evaluation focuses on rural environments limited by NO_x. The horizontal resolution may impact urban and industrial areas at a higher degree than rural areas. In this sense, the higher horizontal resolution of CALIOPE-EU system may be responsible for the better scores obtained in NO_2 and SO_2. It is reasonable to think that a detailed emission inventory at a finer horizontal resolution could further improve the air quality model performances.

Finally, the vertical resolution of the models presented in this evaluation ranges from 3 to 20 vertical layers. It is expected that models with higher vertical levels are able to simulate the vertical mixing better. However, the statistics do not show a direct relationship with the model vertical

resolution. That implies that various systems are strongly driven by surface emissions, and vertical exchange is not directly resolved though strongly parameterized.

2.5 Conclusions

This paper presented the evaluation results of the model system CALIOPE-EU (namely WRF-ARW/HERMES-EMEP/CMAQ/BSCDREAM8b) using a full year simulation for 2004 over a European domain. The evaluation focused on the capability of the model to reproduce the temporal and spatial distribution of pollutants, estimating their uncertainty and comparing them with other European evaluation studies. This article evaluated gas (O_3, NO_2 and SO_2) and particulate phase (PM10 and PM2.5) simulations with EMEP ground-based measurements. It is noteworthy mentioning that neither correction factors nor any adjusting model parameterization were applied to the model output or the original model codes. Only in the case of particulate matter, adjusted levels were discussed in order to quantify the missing source apportionment. CALIOPE-EU was able to reproduce the observed O_3 annual cycle. Moreover, CALIOPE-EU simulated the general features of O_3 fields over Europe, especially the differences between urban and background levels. In general, daily maxima were better simulated than daily averages, and summertime concentrations were better simulated than wintertime concentrations. The conditions at the lateral boundaries of the model domain were shown to strongly affect the evolution of O_3 throughout the year, especially at the stations near the boundaries and during wintertime. These conditions should be handled with care, as they occasionally lead to excessive O_3 concentrations near the surface. In CMAQ, the construction of boundary profiles from global chemistry models, in that case the LMDz-INCA2, should integrate the information of the tropopause in the downscaling process to avoid strong downdrafts of O_3-enriched air masses down to the surface.

Concerning NO_2, the annual trend was moderately well simulated with a systematic negative bias. High correlations were obtained over either very clean or highly polluted areas (stations around the Baltic Sea or UK). On average, the model underestimated both background levels and peaks, especially during winter and over high polluted areas where transport dominates compared to chemical processes. From the results of the annual pattern, CALIOPE- EU was able to simulate maximum concentrations over most important emission sources in Europe, since concentrations sharply decrease from urban-suburban to rural areas.

The model system was able to reproduce the annual variability of daily mean concentrations for background SO_2 throughout Europe. Monthly variations of SO_2 were well captured, especially from January to March, but false peaks were reported. Vertical mixing characteristics and the way emissions are distributed within the grid are potential key issues which may explain the overestimation detected in simulated SO_2. The spatial distribution of statistics showed low mean bias values with heterogeneous correlation coefficients. The spatial SO_2 pattern successfully represented the main European sources (in the vicinity of energy and transformation industries and shipping routes).

By comparing model results with measurements of PM2.5 and PM10 it was found that CALIOPE-EU reproduces most of the pollution events. However, the model underestimated the observed

values of PM2.5 and PM10. In order to identify the origin of such discrepancies and to determine the sources of uncertainty, the aerosol chemical composition should be evaluated. Among other sources not accounted for, particulate matter emissions from paved road re-suspension and wind-blown dust should be included in order to reduce the systematic biases. When a multiplying factor of 2 was applied to both simulated PM2.5 and PM10, MFE and MFB statistics lied within the performance goal defined by Boylan and Russell (2006). Moreover, the contribution of seasonal natural particulate matter, marine and Saharan mineral dust, was well characterized. Introducing dust aerosol outbreaks on a non-climatic basis with BSC-DREAM8bwas essential for the simulation of hourly peaks during dust outbreaks, especially in southern Europe.

When compared to other European models CALIOPE-EU performed reasonably well for ozone annual daily mean and daily peak concentrations. O_3 statistics lie within the US EPA guidelines although annual correlations are rather low compared to other European models. On the other hand, statistics for NO_2, SO_2, PM10 and PM2.5 present higher scores than most models. We noted a similar behaviour with the other CMAQ-based modelling system; both systems present lower annual correlations for O_3 while results of NO_2, SO_2, PM2.5 and PM10 are higher than other systems.

The horizontal resolution of CALIOPE-EU provided high details in the spatial distribution and temporal evolution of most relevant gas phase and particulate matter pollutants. Sharp and concentrated plumes and other sub-grid scale processes were represented correctly. Although emission data are based on the disaggregation from the EMEP inventory (emissions at 50 km x 50 km), the results are within the range of most European models.

This study warrants the use of the CALIOPE-EU system over Europe and results will be used as boundary conditions for the high-resolution air quality simulation over the Iberian Peninsula at a 4 km x 4 km resolution.

3. Assessing sensitivity regimes of secondary inorganic aerosol formation in Europe with the CALIOPE-EU system

3.1 Introduction

Atmospheric particulate matter (PM), or aerosols, play a central role in atmospheric processes (Fountoukis and Nenes, 2007). They have adverse effects on human health (Pope et al., 2009) and affect visibility (Altshüller, 1984), ecosystems (Niyogi et al., 2004; Bytnerowicz et al., 2007), air quality and climate change (IPCC, 2007). To alleviate some of these atmospheric problems, the control atmospheric PM concentration is demanding. European legislation has established regulations regarding PM10 (particles with $d_p < 10 \ \mu m$) and recently for PM2.5 ($d_p < 2.5 \ \mu m$) in order to reduce human exposure to high concentration of PM (European Commission, 2008).

PM is both emitted directly from a large variety of anthropogenic, biogenic and natural sources and formed in the atmosphere by chemical and physical processes from gas-phase precursors such as NMVOC, NO_x ($NO+NO_2$), SO_2 and NH_3 (Seinfeld and Pandis, 1998). Therefore, to fulfil the task of reducing human exposure to PM, policies must focus not only on the reduction of primary particulate emissions, but also on the reduction of precursor emissions for the formation of secondary particles (Wu et al., 2008; Renner and Wolke, 2010).

Several experimental studies have analysed levels, speciation and origin of PM over Europe (Querol et al., 2004a, 2009; van Dingenen et al. 2004; Putaud et al., 2004, 2010). They found that the European background levels, derived form 31 European air monitoring stations, have been 7.0 ± 4.1 $\mu gPM10 \ m^{-3}$ and $4.8\pm2.4 \ \mu gPM2.5 \ m^{-3}$, over the past decade. The observed aerosol composition revelled that organic matter is the major component in PM10 and PM2.5, except at rural background sites where secondary inorganic aerosol (SIA) contribution prevailed. The dominant SIA species are ammonium sulphates ((NH_4)$_2SO_4$) and ammonium nitrates (NH_4NO_3) salts.

The formation of SIA is a two-step process. First, the primary emissions of NO_x and SO_2 are oxidized to form aerosol precursor nitric acid (HNO_3) and sulphuric acid (H_2SO_4), respectively, precursors of secondary aerosols. Second, a fraction of the H_2SO_4, HNO_3 and NH_3 partition between the gas and particle phase according to thermodynamic equilibrium determined by temperature, relatively humidity and molar concentration of SO_4^{2-}, total nitrate ($TNO_3=HNO_3+NO_3^-$) and total ammonia ($TNH_3=NH_3+ NH_4^+$). SO_2 emissions in Europe have been reduced ~67% from 1980 to 2000 (EMEP, 2004; Fagerli and Aas, 2008; Hamed et al., 2010). Thus,

nowadays less NH_3 is converted to $(NH_4)_2SO_4$ and more NH_3 is available for the formation of NH_4NO_3. This situation leads to a higher residence time of TNO_3 in air (Fagerli and Aas, 2008).

Because of the complex relationship between SIA (Ansari and Pandis, 1998; Vayenas et al, 2005) the control of PM2.5 is still nowadays a difficult challenge. In this sense, air quality models (AQMs) are important tools for air quality management and the evaluation of emission control policies, but it becomes necessary to assess their ability not only in simulating air quality levels, but also to perform diagnostic evaluations. Single model evaluation studies (Schaap et al., 2004b, Sartelet et al., 2007; Stern et al., 2008; Matthias, 2008), model inter-comparison (Hass et al., 2003, van Loon et al., 2004); and model ensembles (Vautard et al., 2009) showed that models tend to underestimate observed PM. Furthermore, Renner and Wolke (2010) modelled the formation of atmospheric transport of SIA over high ammonia emissions areas in north Germany. The results of these studies point to large uncertainties in the estimation of the meteorological input data; uncertainties in the modelling of the anthropogenic PM sources, missing natural and anthropogenic sources and also with gaps in the knowledge of many of the physical and chemical processes which lead to the formation of SIA.

So, the main objective of this work is to investigate the formation regimes of SIA over Europe by means of the CALIOPE-EU air quality modelling system (Pay et al., 2010a; Baldasano et al., 2011) with a simulation covering the whole year 2004. For that purpose, this paper is structured as follows. Section 3.2 describes the modelling system, the observational database and the evaluation tools. Section 3.3 analyses the modelling results against available measured data for the year 2004 and discusses the modelled and observed annual patterns of SIA and their gas-precursors. Also a discussion about aerosol formation regimes over Europe is provided. Section 3.4 presents a thorough comparison with other European studies. Finally, conclusions are drawn in Section 3.5.

3.2 Methods

3.2.1 CALIOPE-EU modelling system

CALIOPE (Baldasano et al., 2008b) is a complex system that integrates a meteorological model (WRF-ARW), an emission processing model (HERMES-EMEP), a chemical transport model (CMAQ) and a mineral dust dynamic model (BSC-DREAM8b) together coupled in an air quality modelling system (Fig. 1 of Pay et al., 2010a). CALIOPE encompasses a high-resolution air quality modelling system which provides 48-h air quality forecasts in Europe (12 km x 12 km) and Spain (4 km x 4 km) (available at: www.bsc.es/caliope). The system has been widely evaluated during its development over northeastern Spain (Jiménez et al., 2005a,b, 2006a,c, 2007), the Iberian Peninsula (Jiménez-Guerrero et al., 2008a; Baldasano et al., 2008b, 2011; Pay et al., 2010b) and Europe (Pay et al., 2010a). Furthermore, it has been used for assessing air pollution dynamics (Gonçalves et al., 2009b) and as management tool to study air quality impact of urban management strategies (Jiménez-Guerrero et al., 2008b; Gonçalves et al., 2008; 2009a; Soret et al., 2011).

CALIOPE system applied over the European domain in 2004 is namely thereinafter as CALIOPE-EU. For a detailed description of the modelling system we refer to aforementioned studies. Here, we summary the main characteristics for this study.

Meteorological input data for the photochemical modelling runs are processed using the Advanced Research Weather and Forecasting model (WRF-ARW) version 3.6.1 (Michalakes et al., 2004; Skamarock and Klemp, 2008).

The Models-3 Community Multiscale Air Quality Modeling System (Models-3/CMAQ) version 4.5 is a three-dimensional Eulerian photochemical transport model that uses state-of-the-science routines to model gas and particulate matter formation and removal processes (Byun and Schere, 2006; Appel et al., 2008; Roy et al., 2007). The model is applied with the Carbon Bond IV chemical mechanism (CBM-IV, Gery et al., 1989) following the criteria of Jiménez et al. (2003). Photolysis rates are computed off-line, as done in the photolysis rate preprocessor JPROC. The aerosols are modelled using the AERO4 module (Binkowski and Roselle, 2003) which comprises the following aerosol components: SO_4^{2-}, NO_3^-, NH_4^+, elemental and organic carbon. SIA are generated by nucleation processes from their precursors. Then, the ISORROPIA thermodynamic module (Nenes et al., 1998) computes the equilibrium between gaseous HNO_3, NH_3 and fine-particle NO_3^-, SO_4^{2-}, NH_4^+, and aerosol water.

Emission data are processed using the High-Elective Resolution Modeling Emission System (HERMES, Baldasano et al., 2008a). In the European domain, the inventory of the anthropogenic emissions of SO_2, NO_x, NMVOC, CO, PM, and NH_3 is derived from the 2004 annual EMEP emission database (EMEP, 2007). The inventory uses the source categories following the Selected Nomenclature Air Pollution (SNAP). Disaggregation of EMEP (50 km x 50 km) data is performed in space (12 km x 12 km) and time (1h). The spatial and temporal top-down disaggregation is sector-dependent. In the horizontal dimension, emission data are remapping to finer grid applying different criteria through three datasets (1) high-resolution land use map (EEA, 2000), (2) coordinates of industrial sites (EPER), and (3) vectorized road cartography of Europe (ESRI). In the vertical dimension, the sector-dependent emission distribution for gases is applied following the EMEP model (Simpson et al., 2003). In the time dimension, data are mapping from annual to an hourly basis using the temporal factors of EMEP/MSC-W (Meteorological Synthesizing Centre-West). Biogenic emissions are estimated internally as a function of temperature, radiation and land-use (Baldasano et al., 2008a).

Figure 3-1 and Table 3-1 show the annual averaged emissions of the most contributed sectors of the emitted compounds SO_x, NO_x, NH_3 and NMVOC in Europe. In 2004, 56% of the total SO_x emissions were attributed to energy transformation. 64% of NO_x total emissions are attributed to transport (road and no-road, sector 7 and 8). 94% of NH_3 total emissions are attributed to agriculture and livestock. Domestic animals contribute most to total emissions, followed by fertilizers, crops and others. The fact that agricultural activities contribute most to ammonia emissions implies that densely populated regions tend to have the highest ammonia emissions. 33% of VOC total emissions are attributed to on-road transport and other 33% to the use of solvents. Last, 50% of CO total emissions are attributed to on-road transport.
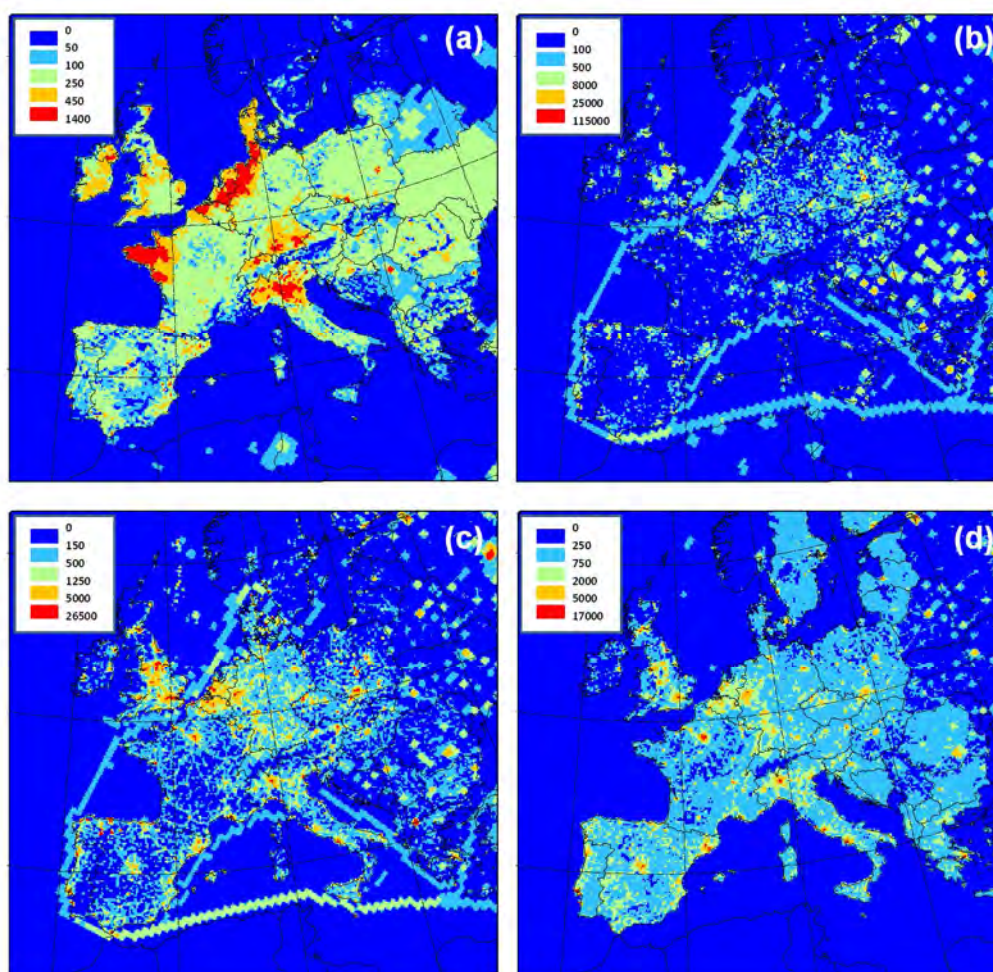
Figure 3-1. Distribution of the anthropogenic emission (Mg yr-1) of NH_3 (a), SO_2 (b), NO_x (c) and NMVOC (d) for the year 2004 in Europe.

Table 3-1. Total emission of SO_x, NO_x, NMVOC, PM2.5, PM coarse, CO and NH_3 for the year 2004 for anthropogenic activities in Europe sort by SNAP (Selected Nomenclature Air Pollution) category (in Mg yr-1).

SNAP	Description	SO_x	NO_x	NMVOC	PM2.5	PM coarse	CO	NH_3
1	Energy transformation	9,323	3,483	137	295	386	852	7
2	Small combustion sources	1,161	1,028	1,163	825	314	10,803	7
3	Industrial combustion	2,096	2,096	180	299	202	5,499	6
4	Industrial process	734	385	1,504	552	315	3,643	106
5	Extraction of fossil fuels	0	0	0	0	0	0	0
6	Solvent and product use	0	0	4,300	21	11	22	5
7	Road transport	314	6,491	4,355	361	95	26,001	82
8	Non road transport	2,868	6,166	754	487	57	3,115	2
9	Waste handling and disposal	25	41	159	97	15	1,832	143
10	Agriculture	2	246	508	176	332	535	5,823
	Total	**16,522**	**19,937**	**13,059**	**3,113**	**1,727**	**52,303**	**6,182**

The photochemical modelling domain consists of 479 cells in the X direction and 399 cells in the Y direction covering the European domain with 12 km x 12 km grid cells in a Lambert projection. The CMAQ horizontal grid resolution corresponds to that of WRF. Its vertical structure was obtained by a collapse from the 38σ-WRF layers to a total of 15 σ-layers steadily increasing from the surface up to 50 hPa with a stronger concentration within the PBL. The chemical boundary conditions are based on the global climate chemistry model LMDz-INCA2 (Piot et al., 2008; Szopa et al., 2009).

3.2.2 Air quality network for gas and aerosol phase

Model output for gas precursors and SIA particulate phase concentrations are compared with ground-based measurements of SO_2, SO_4^{2-}, HNO_3, NO_3^-, NH_3, NH_4^+, TNO_3, and TNH_3 from the EMEP monitoring network for the year 2004. EMEP stations are assumed to be representative of regional background concentrations (Torseth and Hov, 2003). Therefore, the authors wish to stress that the model performances presented in this paper are evaluated only for background concentrations. EMEP has an extensive quality control of the data that are included in the database, freely available on its web page (http://www.emep.int). However, accurate measurements of SIA aerosol remain a challenge. Inorganic species may be accurately measured with an uncertainty of about ±10% for major species (Putaud et al., 2004). Hence, measured NO_3^- and NH_4^+ are found to be uncertain under warm conditions (Schaap et al., 2004c).
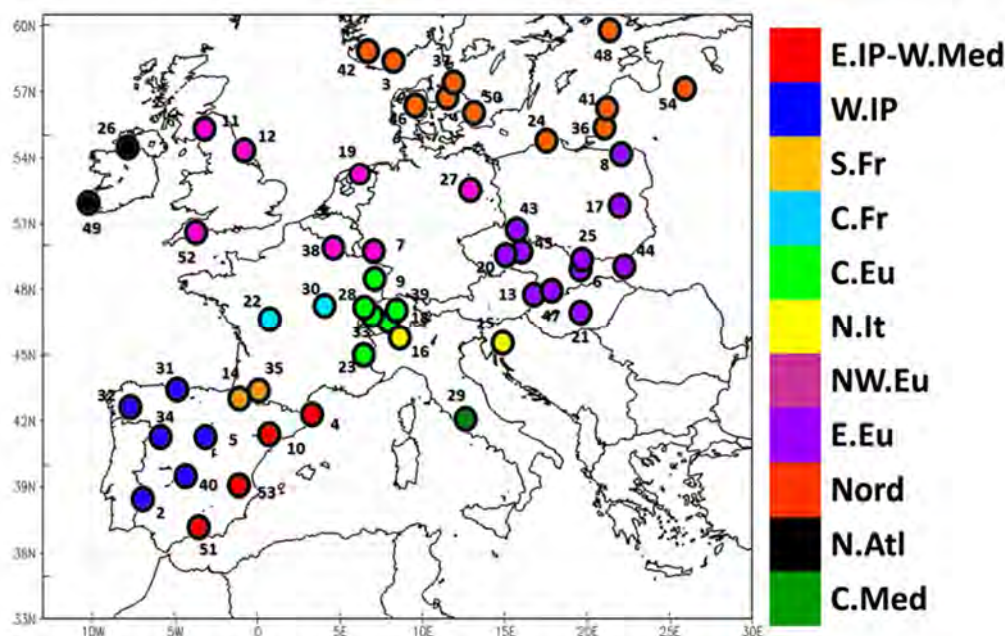
Figure 3-2. Spatial distribution of 54 selected EMEP stations over the study domain. The different colours indicate the different zones defined in Table 3-2. Number of each station is listed in Table 3-2.

Table 3-2. Coordinates, altitude and the chemical species measured of the 54 selected EMEP stations. The code is composed by 2-letter country code plus 2-digit station code. Zone is defined as follows: Western Iberian Peninsula (W.IP); Eastern Iberian Peninsula-Western Mediterranean (E.IP-W.Med), Central Mediterranean (C.Med), Eastern Mediterranean (E.Med), North of Italy (N. It.), Eastern Europe (E.Eu), Northwestern Europe (NW.Eu), Southern France (S.Fr.), Central Europe (C.Eu), Nordic (Nord), Central France (C.Fr) and North Atlantic (N.Atl).

	Station Name	Station Code[a]	Zone	Lat.[b]	Lon.[b]	Alt. (m)	SO_4^{2-}	NO_3^-	NH_4^+	NH_3	HNO_3	TNH_3	TNO_3	SO_2
1	Anholt	DK08	Nord	+56.717	+11.517	40	x					x	x	x
2	Barcarrota	ES11	W.IP	+38.476	-6.923	393	x	x				x	x	x
3	Birkenes	NO01	Nord	+58.383	+8.250	190	x	x	x	x	x	x	x	
4	Cabo de Creus	ES10	E.IP-W.Med	+42.319	+3.317	23	x	x				x	x	
5	Campisábalos	ES09	W.IP	+41.281	-3.143	1360	x	x		x		x	x	x
6	Chopok	SK02	E.Eu	+48.933	+19.583	2008	x							
7	Deuselbach	DE04	NW.Eu	+49.767	+7.050	480	x					x	x	
8	Diabla Gora	PL05	E.Eu	+54.150	+22.067	157	x					x	x	
9	Donon	FR08	C.Eu	+48.500	+7.133	775	x							x
10	Els Torms	ES14	E.IP-W.Med	+41.400	+0.717	470	x	x				x	x	x
11	Eskdalemuir	GB02	NW.Eu	+55.313	-3.204	243	x							
12	High Muffles	GB14	NW.Eu	+54.334	-0.808	267	x							
13	Illmitz	AT02	E.Eu	+47.767	+16.767	117	x	x	x	x	x			x
14	Iraty	FR12	S.Fr	+43.033	-1.083	1300	x							x
15	Iskrba	SI08	N.It	+45.567	+14.867	520	x					x	x	
16	Ispra	IT04	N.It	+45.800	+8.633	209	x	x	x					
17	Jarczew	PL02	E.Eu	+51.817	+21.983	180	x	x	x			x	x	x
18	Jungfraujoch	CH01	C.Eu	+46.550	+7.983	3573	x	x	x					
19	Kollumerwaard	NL09	NW.Eu	+53.334	+6.277	1		x	x					
20	Kosetice	CZ03	E.Eu	+49.583	+15.083	534	x					x	x	x
21	K-puszta	HU02	E.Eu	+46.967	+19.583	125	x	x	x	x	x			
22	La Tardière	FR15	C.Fr	+46.650	+0.750	746	x							
23	Le Casset	FR16	C.Eu	+45.000	+6.467	746	x							
24	Leba	PL04	Nord	+54.750	+17.533	2	x	x	x			x	x	x
25	Liesek	SK05	E.Eu	+49.367	+19.683	892	x	x			x			
26	Lough Navar	GB06	N.Atl	+54.443	-7.870	126	x							
27	Melpitz	DE44	NW.Eu	+52.530	+12.93	86	x	x	x					
28	Montandon	FR14	C.Eu	+47.183	+6.500	746	x							
29	Montelibretti	IT01	C.Med	+42.100	+12.633	48	x	x	x	x	x			x
30	Morvan	FR10	C.Fr	+47.267	+4.083	620	x							
31	Niembro	ES08	W.IP	+43.442	-4.85	134	x	x		x		x	x	x
32	O Savñao	ES16	W.IP	+42.653	-7.705	506	x	x				x	x	x
33	Payerne	CH02	C.Eu	+46.817	+6.950	510	x					x	x	
34	Penausende	ES13	W.IP	+41.283	-5.867	985	x	x				x	x	x
35	Peyrusse Vieille	FR13	S.Fr	+43.375	+0.104	236	x							x
36	Preila	LT15	Nord	+55.350	+21.067	5	x					x	x	x
37	Råö	SE14	Nord	+57.400	+11.917	5	x					x	x	
38	Revin	FR09	NW.Eu	+49.900	+4.633	390	x							x
39	Rigi	CH05	C.Eu	+47.069	+8.466	1030	x					x	x	x
40	Risco Llamo	ES15	W.IP	+39.517	-4.350	1241	x	x				x	x	x
41	Rucava	LV10	Nord	+56.217	+21.217	5	x	x	x			x	x	x
42	Skreådalen	NO08	Nord	+58.817	+6.717	475	x	x	x	x	x	x	x	
43	Sniezka	PL03	E.Eu	+50.733	+15.733	1603	x	x	x			x	x	x
44	Starina	SK06	E.Eu	+49.050	+22.267	345	x	x			x			x
45	Svratouch	CZ01	E.Eu	+49.733	+16.033	737	x					x	x	x
46	Tange	DK03	Nord	+56.350	+9.600	13	x					x	x	x
47	Topolniky	SK07	E.Eu	+47.960	+17.861	113	x	x			x			
48	Utö	FI09	Nord	+59.779	+21.377	7	x		x			x	x	
49	Valentina Observatory	IE01	N.Atl	+51.94	-10.244	11	x					x	x	
50	Vavihill	SE11	Nord	+56.017	+13.150	175	x					x	x	x
51	Víznar	ES07	E.IP-W.Med	+37.233	-3.533	1265	x	x				x	x	
52	Yarner Wood	GB13	NW.Eu	+50.596	-3.713	119	x							
53	Zarra	ES12	E.IP-W.Med	+39.086	-1.102	885	x	x				x	x	x
54	Zoseni	LV16	Nord	+57.133	+25.917	183	x	x	x			x	x	x

[a]2-letter country code plus 2-digit station code. [b]A positive value indicates northern latitudes or eastern longitudes. A negative value indicates southern latitudes or western longitudes.

All EMEP measurement data are given on a daily average. As a result, 31 stations were selected to evaluate SO_2, 53 for SO_4^{2-}, 8 for HNO_3, 31 for NO_3^-, 7 for NH_3, and 15 NH_4^+, for respectively. SIA and gas precursors are also indirectly evaluated with measurements of TNO_3 and TNH_3 available over 31 stations. The selected EMEP stations and measured pollutants that are used for this comparison are briefly described in Table 3-2 and presented in Figure 3-2. Note that the final coverage of the dataset is rather disperse since France, Italy and southeastern Europe only include several stations. Also, it is important to remark that the availability of stations measuring nitrogenous gas precursors (HNO_3 and NH_3) is scarce and not well distributed.

3.2.3 Evaluation and assessment tools

Modelled aerosol outputs are post-processed for the comparison with quantified measured. A list of CMAQ aerosol module variables can be found in Table 1 of Binkowski and Roselle (2003). From these variables, fine-particles SO_4^{2-}, NO_3^-, and NH_4^+ are approximated by summing the appropriate Aitken- and accumulation-mode concentrations. Although CALIOPE-EU system estimates sulphate from sea salt, fine-particle sulphate only takes into account that with anthropogenic origin, hereinafter referred to as SO_4^{2-}.

To pair observations and model results in space a bilinear interpolation is used, since EMEP are representative of regional background concentrations. Measurements are in daily basis, thus aerosols are compared in terms of daily averages from the modelling system.

Metrics used to describe the modelling system performance include classical statistics. Besides mean of modelled and measured values we show Mean Bias (MB), Root Mean Square Error (RMSE), correlation coefficient (r), Mean Fractional Bias (MFB), and Error (MFE) (Boylan and Russell, 2006; Dennis et al., 2010). The bias and error describe the performance in terms of the measured concentration units ($\mu g\ m^{-3}$) assuming that measurements are the truth. On the other hand, fractional metrics describe performance as a percent, taking into account that the measurements have their own uncertainty due to biases and artifacts related to sampling and laboratory analysis methods (Boylan and Russell, 2006; Putaud et al., 2010). The best model performance is when MFB and MFE approach 0. The fractional metrics are bounded by 200%, which is considered very poor performance. The fractional bias and error metrics normalize large and small concentrations, making seasonal trends in model performance more discernable.

The aerosol compounds are compared to the daily averages from the model, and daily statistics and graphics methods were computed to describe the model skills and weaknesses. The inorganic chemical species data were analysed from the PM2.5 fraction.

The bias metrics between SIA and gas-phase precursors are examined for relationships to determined how much of the error in precursor model performance translates into error for co-located ion model estimates. Besides, to assess the chemical behaviour of aerosol chemical composition, we introduce three indicators extracted from bibliography to examine the SIA formation regimens. S-ratio (Hass et al., 2003) indicates the ability of the model to form the sulphate aerosols. Concentrations are expressed as $\mu g\ m^{-3}$ in the S-ratio (Eq. 3-1).

$$S-ratio = \frac{SO_2}{SO_2 + SO_4^{2-}} \tag{3-1}$$

SO_4^{2-} is produced during the transport by heterogeneous processes in clouds. A ratio close to unity indicates that only a small fraction of the emitted SO_2 has been converted to the sulphate aerosol.

Free ammonia (F-NH$_x$) indicator quantifies the amount of ammonia available, after neutralizing SO_4^{2-}, for NH_4NO_3 formation. This indicator is based on the fact that $(NH_4)_2SO_4$ aerosol is the favoured form for sulphate. F-NH$_x$ is defined as the total ammonia minus twice the sulphate concentration on a molar basis (Eq. 3-2):

$$F-HN_x = TNH_3 - 2SO_4^{2-} \tag{3-2}$$

The gas-aerosol equilibrium in the $SO_4^{2-}/NO_3^-/NH_4^+$ system is analysed using the G-ratio (Ansari and Pandis, 1998; Pinder et al., 2008) which indicates whether fine-particle NO_3^- formation is limited by the availability of HNO_3 or NH_3 (Eq. 3-3). All the terms in the following equation are expressed molar basis (μmole m^{-3}).

$$G-ratio = \frac{F-NH_x}{TNO_3} \tag{3-3}$$

G-ratio > 1 indicates that nitric acid is limiting, while G-ratio < 0 indicates the ammonia is severely limiting. G-ratio between 0 and 1 indicates ammonia is available for reaction with nitric acid, but ammonia is the limiting species.

Pinder et al. (2008) suggested an adjust G-ratio which takes into account that sulphate is not always fully neutralized. That is true especially during winter, when nitrate is thermodynamically more stable than sulphate. However, we decided not to use this adjust G-ratio since only 5 stations are available to evaluate the modelled pattern.

3.3   Results and discussion

First, in Section 3.3.1, a model evaluation is performed through statistical performance. Figure 3-3 compares the CALIOPE-EU model outputs with measurements for inorganic aerosols (sulphate, nitrate and ammonium) and their precursors (sulphur dioxide, nitric acid and ammonia) computed on a daily basis using all the EMEP stations with available data. Also, Figure 3-4 shows the monthly MFB and MFE for each species (gas and precursor) compared to proposed performance goals and criteria by Boylan and Russell (2006). Second, in Section 3.3.2, a general description of the annual mean distribution of each pollutant is provided to determine each pattern across Europe (Figure 3-5). Latter, Section 3.3.3 the discussion is focused on the use of indicators that allow detecting SIA formation regimens over Europe (Figure 3-6).
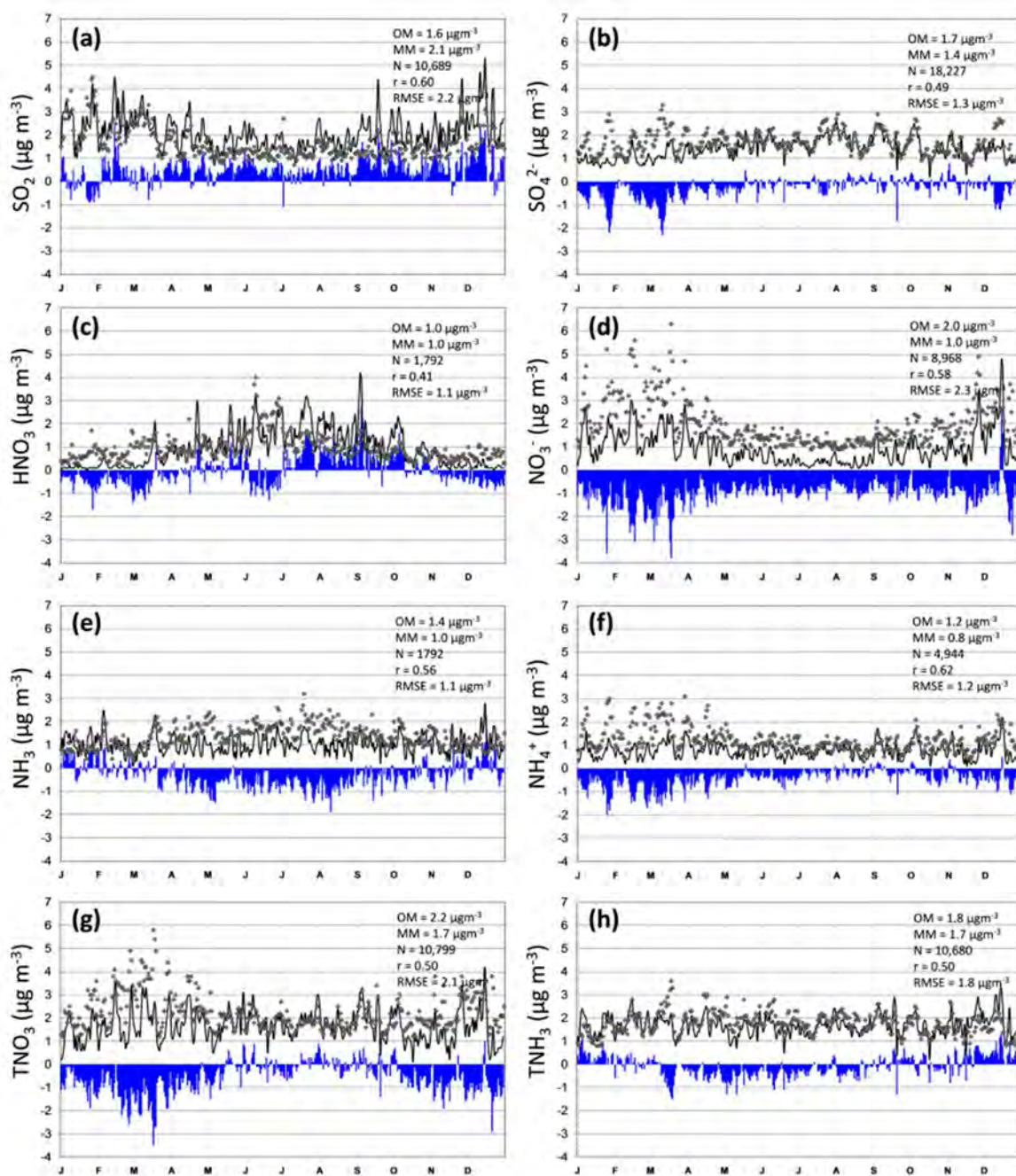
Figure 3-3. Annual temporal series for SO_2 (a), fine-particle SO_4^{2-} (b), HNO_3 (c), fine-particle NO_3^- (d), gas-phase NH_3 (e), fine-particle NH_4^+ (f), TNO_3 (g) and TNH_3 (h) in daily basis calculated as an average over all EMEP stations in 2004. Diamonds represent EMEP measurements (in $\mu g\ m^{-3}$) and black continuous lines represent CALIOPE-EU outputs (in $\mu g\ m^{-3}$). Blue columns indicate daily mean bias ($\mu g\ m^{-3}$). Annual statistics are shown top-right: Observed Mean (OM), Modelled Mean (MM), number of data points (N), correlation coefficient (r) and Root Mean Squared Error (RMSE).

3.3.1 Model evaluation

3.3.1.1 Sulphur dioxide and sulphate

For SO_2, the model results are evaluated against 31 stations located across the Iberian Peninsula, central and north-eastern Europe. Figure 3-3a for SO_2 shows the temporal evolution of CALIOPE-EU system which is able to reproduce the annual variation of daily measurements (r = 0.60) although it overestimates some observed peaks (MB = 0.5 μg m^{-3}). As shown in Figure 3-4a and b bias and errors for SO_2 do not present a significant seasonal variation. Monthly biases are relatively low (0 % < MFB < 30 %) and fall within the performance goal proposed by Bolan and Russell (2006). Nevertheless monthly fractional errors only accomplish the criteria (60 % < MFE < 75 %).
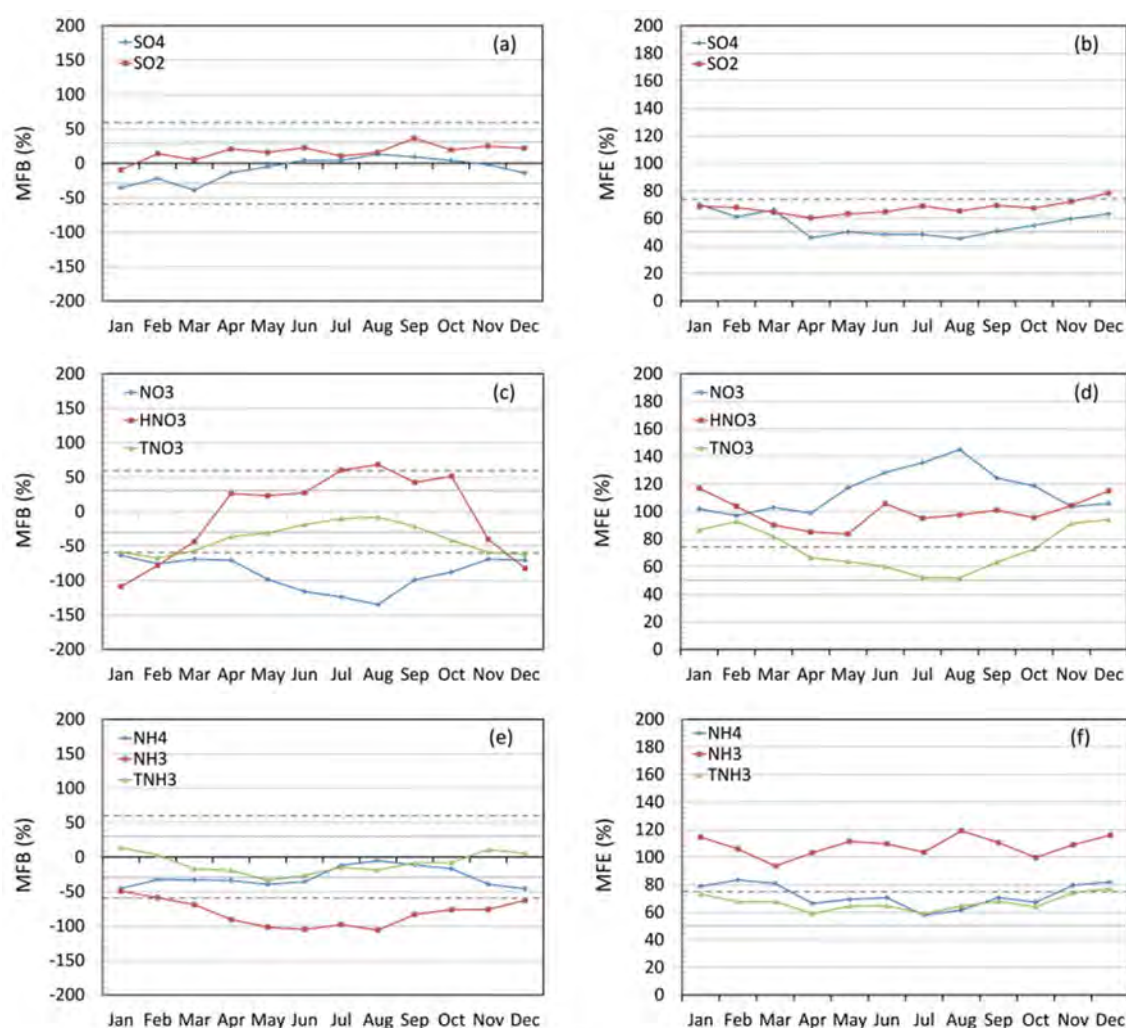
Figure 3-4. Monthly mean fractional bias (MFB, right column), and mean fractional error (MFE, left column) compared with goals and criteria proposed by Boyland and Rusell (2006). MFB and MFE are averaged over the sites within the EMEP network in 2004 for: SO_2 and SO_4^{2-} (a and b); HNO_3, NO_3^- and TNO_3 (c and d); and NH_3, NH_4^+ and TNH_3 (e and f). Dotted lines represent the goals (MFB ≤ ± 30 % and MFE ≤ 50%). Broken lines represent the criteria (MFB ≤ ± 60 % and MFE ≤ 75%).

SO_4^{2-} concentrations are compared with 53 stations which cover Spain, eastern and central Europe and Nordic countries. The annual variability of the modelled SO_4^{2-} concentrations agrees fairly well with measurements (r = 0.49, RMSE = 1.3 μgm^{-3}) and modelling results present a low negative bias along the year (MB < -0.3 μgm^{-3}) (Figure 3-3b). Best model performances are achieved during warm seasons (MFB ~ 0% and MFE ~50 %, Figure 3-4a and b) when ambient concentrations are highest due to enhanced photochemistry, low air mass renovation regional scale, and the increase of the summer mixing layer depth favouring the regional mixing of polluted air masses (Querol et al., 2009a). Only during cold seasons SO_4^{2-} from CALIOPE-EU does not accomplish the goal for MFB and MFE. This result is geographically biased by winter underestimations at eastern European stations (E. Eu region), where MB by station ranges from -0.5 $\mu g\ m^{-3}$ to -2.5 $\mu g\ m^{-3}$.

January and March undergo three major episodes of enhanced SO_2 and SO_4^{2-}. The model reproduces accurately the SO_2 variability meanwhile sulphate events are not reproduced. Overall, the positive mean bias only for SO_2 suggests that non-marine SO_4^{2-} formation in the modelling system is often limited by oxidant availability and not always by sulphur dioxide availability. Winter underestimation of SO_4^{2-} is a common issue in most models integrated in Europe which represent a direct couplet of sulphur chemistry with photochemistry, even detected with CMAQ over Europe (Matthias, 2008). This feature can be probably explained by a lack of model calculated oxidants or missing reactions (Kasibhatla et al., 1997). In this context, besides the gas phase reaction of SO_2 by OH, Tarrasón and Iversen (1998) and Schaap et al. (2004b) included additional oxidation pathways in clouds under cool and humid conditions that improve modelled SO_4^{2} performance.

3.3.1.2 Nitric acid, nitrate and total nitrate

HNO_3 is evaluated over 8 EMEP stations located in eastern Europe, Nordic countries and Italy. Overall, CALIOPE-EU system is able to reproduce annual variability for HNO_3 (Figure 3-3c), presenting the highest values during summer as measurements (r = 0.41, RMSE = 1.1 μgm^{-3}). However, as shown also in Figure 3-4c and d, CALIOPE-EU underestimates HNO_3 in coldest months (MFB > -30%), has a small bias during spring (MFB ≤ ±30%, within the goals) and overestimates in summer seasons (MFB > 30%). CALIOPE-EU NO_2 concentrations have already been evaluated over EMEP in Pay et al. (2010a). The MFB for NO_2 was examined by season and did not show a strong seasonal trend, but the lowest bias are found in summer and spring (MFB ~ -50%). This finding, together with an overestimation of HNO_3 in warm seasons indicates that either the chemical transport model (CMAQv4.5) may be generating too much nitric acid though photochemical reactions or summer deposition processes are not appropriately characterized (Baker and Scheff, 2007).

The NO_3^- concentrations are evaluated over 31 EMEP stations which cover mainly Spain and central Europe. Time series in Figure 3-3d show that the modelling system reproduces the NO_3^- daily variability throughout the year (r=0.58, RMSE= 2.3 $\mu g\ m^{-3}$), presenting higher levels during winter and lower levels during summer due to its thermal instability (Querol et al., 2009a). NO_3^- concentrations are on average underestimated, although large underestimations and errors are found in warm seasons (Figure 3-4c and d) with |MFE| ~ 130%. Note that summer underestimation occurs under low concentrations where relative model performance is not as important; indeed, both the model and observed NO_3^- are typically quite low during summertime

(Figure 3-3c). In any case, monthly fractional biases and errors for NO_3^- fall within the criteria. The NO_3^- errors are roughly 2 times higher than the corresponding SO_4^{-2} errors, reaching till 3 times in summer. Such finding is consistent with other modelling studies (Yu et al., 2005; Tesche et al., 2006). Diagnostic evaluations performed by Yu et al. (2005) indicate that a large source of error in simulating nitrate came from errors in the simulation of total ammonia, sulphate and, to lesser extent, total nitrate.

Measurements of TNO_3 are available over 31 stations covering Spain, north and central Europe. The TNO_3 in the modelling system reproduces the annual trend with high temporal correlation as shown the temporal series in Figure 3-3g ($r = 0.50$, $RMSE = 1.1$ μg m^{-3}). High modelled and measured levels of TNO_3 in winter can be explained by the higher stability of NH_4NO_3 in winter, which causes a higher portion of the NO_3^- to partition to aerosol, which has a longer lifetime than nitric acid against deposition (Schaap et al., 2004b). Monthly fractional biases and errors (Figure 3-4c and d) indicate that large deviations are presented in the coldest months, dominated by the calculated underestimation of HNO_3 and NO_3^- in these seasons (MFB < -50%). The low fractional bias in summer results from the compensation error between the overestimation of HNO_3 (MFB ~ 50%) and underestimation of NO_3^- (MFB ~ -130%). In warm months (from April to October) the model fractional biases and error are within the criteria: MFB $\leq$ ±60 and MFE $\leq$ 75.

The largest underestimations are located over the E.IP-W.Med and C.Med regions and the Eastern Europe (E.Eu regions, except Illmitz and Sniezka) with mean biases of -1.8 μg m^{-3} and -1.5 μg m^{-3}, respectively in both areas. The model presents the best skills in the western Iberian Peninsula, with high correlations ranging from 0.40 to 0.65 by stations, and with annual mean biases less than 1.0 μg m^{-3}, and RMSE less than 1.3 μg m^{-3}.

3.3.1.3 Ammonia, ammonium and total ammonia

NH_3 is measured in 7 stations located in western Iberian Peninsula (2), central Mediterranean (1), and northern (2) and eastern (2) Europe. Temporal series (Figure 3-3e) indicate that the CALIOPE-EU system reproduces the annual variability for NH_3 ($r = 0.56$) with a low mean bias (MB = -0.4 μg m^{-3}). However, during warm season, April to August, modelled NH_3 is systematically underestimated. NH_3 emissions predominantly come from agricultural sources, primarily from livestock animal waste (Table 3-1). Livestock sources vary during the year since volatilization of NH_3 from the animal waste is a function of temperature (Gilliland et al, 2003). Seasonality in NH_3 emission is expected since field application of fertilizers occurs during specific seasons (Asman, 2001).

A total of 15 EMEP stations provide measurements of NH_4^+ to evaluate ammonium in 2004, mainly covering eastern Europe. Modelled NH_4^+ comparisons to measured data (Figure 3-3f) revels that annual variability is correctly reproduced ($r = 0.62$, $RMSE = 1.2$ μg m^{-3}). However annual mean model is on average underestimated in 36%. Monthly fractional errors (Figure 3-4e and f) fall within the criteria (-60% < MFB < 0 and MFE < 75%) except in the coldest months. Despite the underestimations during winter, the temporal variability is correctly captured in these months ($r = 0.70$).

TNH_3 measurements are available over 31 stations covering Spain, north and central Europe. The temporal series (Figure 3-3f) indicates that the TNH_3 levels are on average in agreement with observation along the year (r $= 0.50$, $\mathrm{RMSE} = 2.1$ µg m^{-3}) with relatively low bias (MB $= - 0.5$ µg m^{-3}). The fractional bias distribution by months (Figure 3-4e and f) for TNH_3 shows that the modelling system does not provided enough TNH_3 in spring (MFB ~ -25%) and lightly too much in winter (MFB ~ 10%). TNH_3 falls within criteria for fractional bias and error, but partition between gas and aerosol is not totally well characterized. On one hand, TNH_3 underestimation in the warm season is biased by gas-phase NH_3 which presents its largest underestimation from May to August with MFF ~ -100% (Figure 3-3e). On the other hand, TNH_3 overestimations in winter are biased by the tendency of the model to overestimate gas-phase NH_3 at some stations (Figure 3-3e).

From May to October, SO_4^{2-} is overestimated (MFB ~10%) and NH_4^+ reaches its minimum bias (MFB ~ - 10%). In this case, the underestimation of ammonia during the same period indicates that the excessive SO_4^{2-} in the model keeps ammonium in the particulate phase when it should be in the gas phase or available to potentially neutralize NO_3^-. This fact also explains the maximum overestimation of HNO_3 (MFB ~ 50%), the large underestimation of NO_3^- (MFB ~ -120%) and the minimum bias in TNO_3 (MFB ~ -20%) during the same period, since too much NO_3^- is remaining in the gas phase because there is not enough NH_4^+ to neutralized NO_3^-. This fact demonstrates that temporal representation of NH_3 emission could have a large effect on the results. Significant uncertainty exists in the magnitude and temporal variability of NH_3 emissions in Europe (Gilliland et al., 2003, 2006; Schaap et al. 2004b).

Table 3-3. Bias correlation coefficients of the secondary inorganic aerosol and their gas precursors between each other for all the data points available for 2004. Mean and standard deviation (STD) of the bias are in µg m^{-3}.

	NH$_3$	NO$_3^-$	HNO$_3$	SO$_2$	SO$_4^{2-}$	NH$_4^+$
Mean	*-1.36*	*-1.01*	*-0.97*	*0.50*	*-0.29*	*-0.45*
STD	*1.09*	*2.10*	*1.64*	*2.14*	*1.31*	*1.08*
NH$_3$	1.00 (7/2562)	0.03 (7/2562)	0.55 (5/1830)	-0.03 (4/1464)	0.02 (7/2562)	0.07 (5/1830)
NO$_3^-$	-	1.00 (27/9882)	-0.16 (8/2928)	-0.06 (15/5490)	0.29 (26/9516)	0.75 (14/5124)
HNO$_3$	-	-	1.00 (8/2928)	-0.07 (3/1098)	0.04 (8/2928)	0.00 (5/1830)
SO$_2$	-	-	-	1.00 (31/11346)	0.01 (25/9150)	0.07 (7/2562)
SO$_4^{2-}$	-	-	-	-	1.00 (53/19398)	0.59 (14/5124)
NH$_4^+$	-	-	-	-	-	1.00 (15/5490)

3.3.1.4 Bias relationships between SIA and gas precursors

The relationship in model-observation bias for SIA species and precursors is examined using the correlation coefficient (Table 3-3) to determine whether biases in precursor species directly translate into biases for aerosol species. These correlation coefficients compare the bias metric distributions over all sites and days for a pair of species. A number close to 1 indicates a strong relationship in the bias metric between a pair of species. A strong relationship is seen between model-observation bias for SO_4^{2-} and NH_4^+ (bias correlation = 0.59) and also between NO_3^- and NH_4^+ (bias correlation = 0.75). This makes sense since these ions are chemically coupled in the atmosphere. SO_2 bias has a fairly weak relationship with SO_4^{2-} bias, which is interesting since a more direct relationship might be expected between them. HNO_3 and NH_3 bias is weakly associated with biases in the aerosol species (bias correlation < 0.1). These weak relationships between precursor gases and aerosol species indicate that model performance for precursor gases does not directly translate into model biases for particulate matter species in the same ambient sample. This likely reflects the different time scales of particulate formation and the influence of the regional transport.

3.3.2 Pattern description

Next section discusses the spatial distribution of annual concentrations modelled with CALIOPE-EU system (12 km x 12 km) for SIA and gas-phase precursors in 2004 taking into account annual mean concentrations measured with EMEP monitoring network.

3.3.2.1 Sulphur dioxide and sulphate

Figure 3-5a shows the SO_2 pattern over Europe which presents a significant relationship with the distribution of SO_2 emission sources in Figure 3-1c. They are mainly produced by power generated and transformation industries (Table 3-1) located in northwestern Spain, eastern Europe, UK, Belgium and the southwestern Netherlands. These localized industries generate large plumes of high-SO_2 affecting the air quality on a local to regional scale. Background concentrations in eastern countries (8-20 $\mu g\ m^{-3}$) are greater than in West (~2 $\mu g\ m^{-3}$). Various disperse punctual SO_2 emissions in the east contribute to an increase of the regional concentration (30-50 $\mu g\ m^{-3}$). Over sea, the highest concentrations are found along the main shipping routes, since fuels used have high-SO_2 content. Comparisons with 31 observed annual means show a high spatial correlation (r = 0.80), resulting from the detailed methodology of spatial (horizontal and vertical) disaggregation of EMEP (50 km x 50 km) data over the high-resolution CALIOPE-EU grid (12 km x 12 km).

In CALIOPE-EU system fine-particle SO_4^{2-} has an anthropogenic origin and is directed emitted, generated by nucleation and/or condensation from the gas phase oxidation of SO_2 and hydroxyl radical (OH) and by heterogeneous oxidation of SO_2 in clouds (aqueous-phase oxidation by H_2O_2, O_3, Fe^{3+} and Mn^{2+}, and peroxyacetic acid) (Binkoswki and Roselle, 2003). With respect to SO_2, SO_4^{2-} presents more dispersive pattern (lower spatial variability) since SO_4^{2-} is partly produced during the transport of the SO_2 air masses (Figure 3-5b). Regions with high levels of SO_4^{2-} correspond with important SO_2 emission point sources (Figure 3-1c and Figure 3-5a). The highest SO_4^{2-} levels are found in eastern and south-eastern Europe and Po Valley (2 to 5 $\mu g\ m^{-3}$), followed

by those obtained over the Benelux region and northeastern Spain (2-3 μg m^{-3}). The highest SO_4^{2-} levels over eastern Europe deplete the available gas-phase NH_3 so that little NH_4NO_3 can form due to the low NH_3 levels as can be seen latter in Figure 3-5c. These findings are consistent with the results presented in Querol et al. (2009a). In remote continental regions SO_4^{2-} mean levels range between 1-2 μg m^{-3}. However, over Scandinavia and elevated terrains (e.g. Alpine and Pyrenean chains) levels remain below 1.0 μg m^{-3}. Over the ocean, fine-particle SO_4^{2-} contributes < 1.5 μg m^{-3} in the Atlantic Ocean and between 1.0 - 2.7 μg m^{-3} over the Mediterranean Sea. The calculated spatial correlation over 53 EMEP stations indicates that there is a high agreement for background annual sulphate levels between CALIOPE-EU and EMEP stations over Europe, indicating that the modelling system is able to reproduce long-range transport, chemical processes and sinks of sulphate.

3.3.2.2 Nitric acid and nitrate

HNO_3 is produce by heterogeneous hydrolysis of N_2O_5 and by oxidation of NO_2 by hydroxyl radicals (Meng et al. 1997; Nguyen and Dabdub, 2002). According to NO_2 performance, a detail discussion is provided in a separate paper Pay et al. (2010a). However, additional information about NO_2 is provided in the supplementary material. CALIOPE-EU is able to reproduce NO_2 with high good agreement over Europe, with spatial correlation of 0.75 (Figure AIII - 1, Annex III). Nevertheless, NO_2 background levels are significantly underestimated, MB = -3.7 μg m^{-3} (Pay et al., 2010a).

The annual pattern of HNO_3 over Europe presents a high spatial variability (Figure 3-5c). At continental regions the annual concentrations remain mainly below 1.0 μg m^{-3}, meanwhile over the sea concentrations are larger than those over land. A long the shipping routes, where large amount of NO_x are emitted (Figure 3-1c), the largest concentrations of HNO_3 are also modelled. Mean values in the Mediterranean Sea are $\sim$ 3 μg m^{-3} reaching maximum levels over the Alboran Sea along the Strait of Gibraltar ($\sim$ 5 μg m^{-3}), meanwhile over North Sea and English Channel HNO_3 levels are lower ($\sim$ 3 μg m^{-3}). The calculated spatial correlation is 0.63 which is biased by the stations of Illmitz where measurements seem to have more variability during winter than modelled (without Illmitz, the spatial correlation increase to 0.77).

NO_3^- is modelled as NH_4NO_3 in the fine fraction and its formation is bound by NH_4^+ and HNO_3. NO_3^- spatial variability is high over Europe (Figure 3-5d) with no clear relationship either anthropogenic activities or gas precursor HNO_3 (Figure 3-5c) and NO_2 (Figure AIII - 1, Annex III). Both ammonium nitrate and nitric acid are water soluble and efficiently wet deposited. However, nitric acid is a volatile gas with a rapid dry deposition, meanwhile ammonium nitrate particles dry deposit slowly. NO_3^- levels are significant over land, since NO_3^- concentrations rapidly decrease from the coast to open ocean. NO_3^- presents the highest concentration in the Po valley (between 3 and 4 μg m^{-3}) where both large anthropogenic sources of NO_x and NH_3 from agriculture and industrial-related sources are located. Elevated concentrations are also identified over The Netherland, Belgium, eastern Germany and northern France ($\sim$ 2.4 μg m^{-3}) which are affected by high levels of NH_3. Overall, in southern Europe (latitude less than 44ºN) NO_3^- concentrations are lower, not exceeding 1.5 μg m^{-3} and remaining below 0.6 μg m^{-3} over the sea. Despite the high HNO_3 levels due to ship tracks over the Mediterranean Sea, NO_3^- concentrations

remain low because NH_3 availability is limiting. The annual spatial correlation shows a high agreement between CALIOPE-EU and EMEP observations (r=0.80). Despite such good spatial correlation, modelled background mean NO_3^- levels are somehow underestimated ~ 1 μg m^{-3} over most of the stations as shown in the evaluation section.

Modelled TNO_3 annual distribution (Figure 3-5h) shows the sum of contribution of NO_3^- and HNO_3. In continental region, as for NO_3^-, the highest levels are found over the Po valley (~ 5 μg m^{-3}). Over the sea, the highest values are found along the maritime traffic routes and the Strait of Gibraltar (~ 4 μg m^{-3}). The spatial correlation for TNO_3 is relatively high (r=0.76), indicating a good agreement between formation of secondary gas and aerosol.

3.3.2.3 Ammonia and ammonium

Figure 3-5e shows annual European pattern of gas-phase NH_3 in 2004. Agriculture and livestock are estimated to produce around 94% of NH_3 emission in Europe (Table 3-1). Due to the short atmospheric lifetime of ammonia, its concentration field strongly resembles its emission distribution, as shown in Figure 3-1a, and maximum concentrations occur in the areas with the highest emissions. Outside the source areas the ammonia concentration declines rapidly (< 1 μg m^{-3}). Maximum concentrations are located in The Netherlands and Po valley (~ 8 μg m^{-3}), followed by southern Germany and western France (~ 5 μg m^{-3}). Significant high levels (2-4 μg m^{-3}) are also found over southwestern France, northeastern Spain, central Poland and southeastern Europe. Comparisons with annual mean observations show high spatial correlation (r=0.93). Nevertheless this correlation is not representative since only seven stations are taking into account.

In air masses with a continental signature aerosol NO_3^- and SO_4^{-2} are associated with NH_4^+. Atmospheric NH_3 is first neutralized by H_2SO_4 to form $(NH_4)_2SO_4$. Remaining NH_3 may then combine with HNO_3 to form NH_4NO_3. In this sense, NH_4^+ presents a gradient distribution pattern more similar to SO_4^{2-} and NO_3^- than to NH_3 since NH_4^+ neutralizes those anions (Figure 3-5f). NH_4^+ concentrations are around 1 μg m^{-3} over most of Europe and decrease near the coast. Like for NO_3^-, the highest NH_4^+ concentrations are detected over the Po Valley (2-3 μg m^{-3}). High NH_4^+ concentrations are also found over the Benelux region and southwestern Europe with values ranging from 1 and 2 μg m^{-3}. Low concentrations are found in southern Europe (<1.2 μg m^{-3}). The low NH_4^+ availability in the southern part of Europe ($< 40°$ N) is mainly used in the neutralization of SO_4^{2-}, meanwhile HNO_3 remains in the gas phase. The lowest concentrations are found in Nordic counties and high mountains ranges (< 0.6 μg m^{-3}). Annual mean spatial correlation shows a high agreement between model and observations (r=0.80).

TNO_3 annual distribution is also shown in Figure 3-5g; the pattern is obviously dominated by gas-phase NH_3. Spatial correlation for total ammonia is 0.68, lower than for NH_3 and NH_4^+. More stations are used to compute the correlation coefficient for TNH_3, and this result is deviated by the stations of Payerne and Els Torms. Without these two stations spatial correlation increase to 0.71.
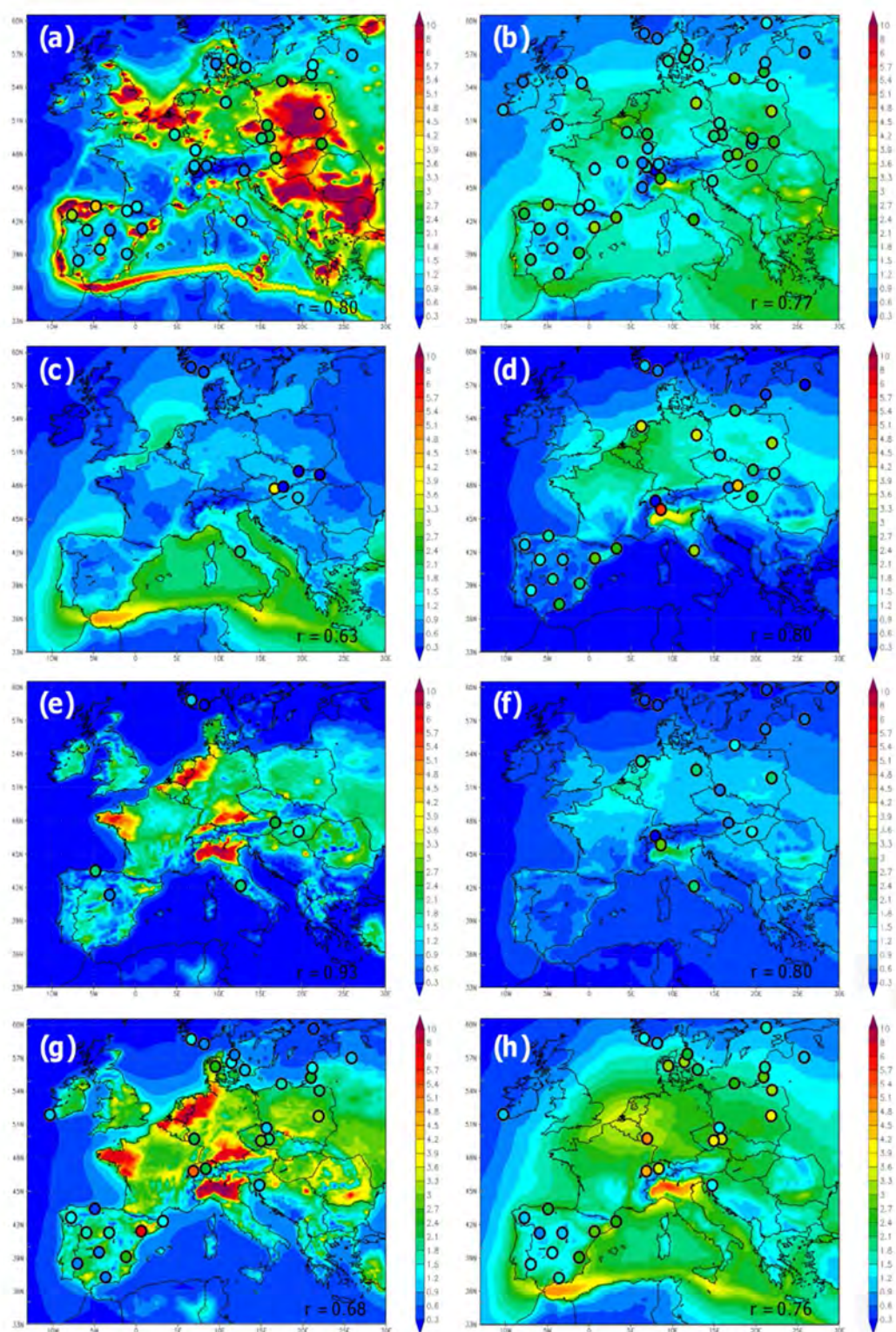
Figure 3-5. 2004 annual mean distributions over Europe for SO_2 (a), fine-particle SO_4^{2-} (b), HNO_3 (c), fine-particle NO_3^- (d), gas-phase NH_3 (e), fine-particle NH_4^+ (f), TNO_3 (g) and TNH_3 (h) at the lowest level. Points represent measured annual concentrations at the EMEP stations. Number at bottom-left in each figure is the spatial correlation between modelled and observed annual mean at each station.

3.3.3 Indicators for SIA formation regimes

3.3.3.1 S-ratio

The ability of the model to form fine-particle SO_4^{2-} is investigated by the use of the S-ratio indicator (Hass et al., 2003). Figure 3-6a presents the annual S-ratio distribution over Europe in 2004 modelled with CALIOPE-EU and measured at EMEP stations. Figure 3-7c shows the observed and calculated annual S-ratios at each EMEP station lumping by regions (described previously in Table 3-2 and Figure 3-2) and compared with the model performance for SO_2 (Figure 3-7a) and SO_4^{2-} (Figure 3-7b).
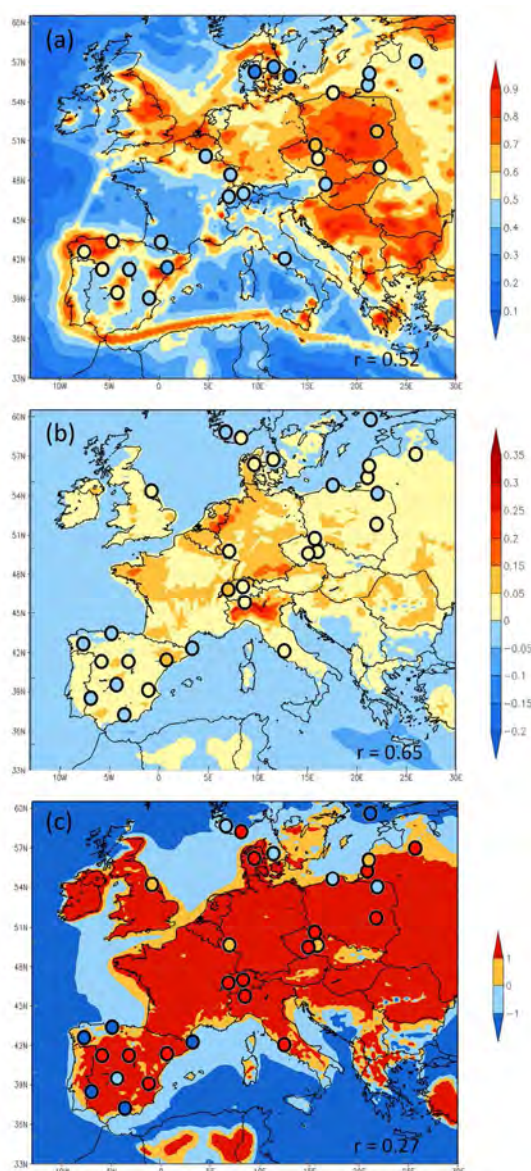
Figure 3-6. Annual spatial distribution of the indicators: S-ratio (a and b), Free ammonia (c and d, in molar basin), and G-ratio (e and f) calculated within the CALIOPE-EU system over Europe in 2004. Dots represent the estimated indicators based on EMEP measurements.
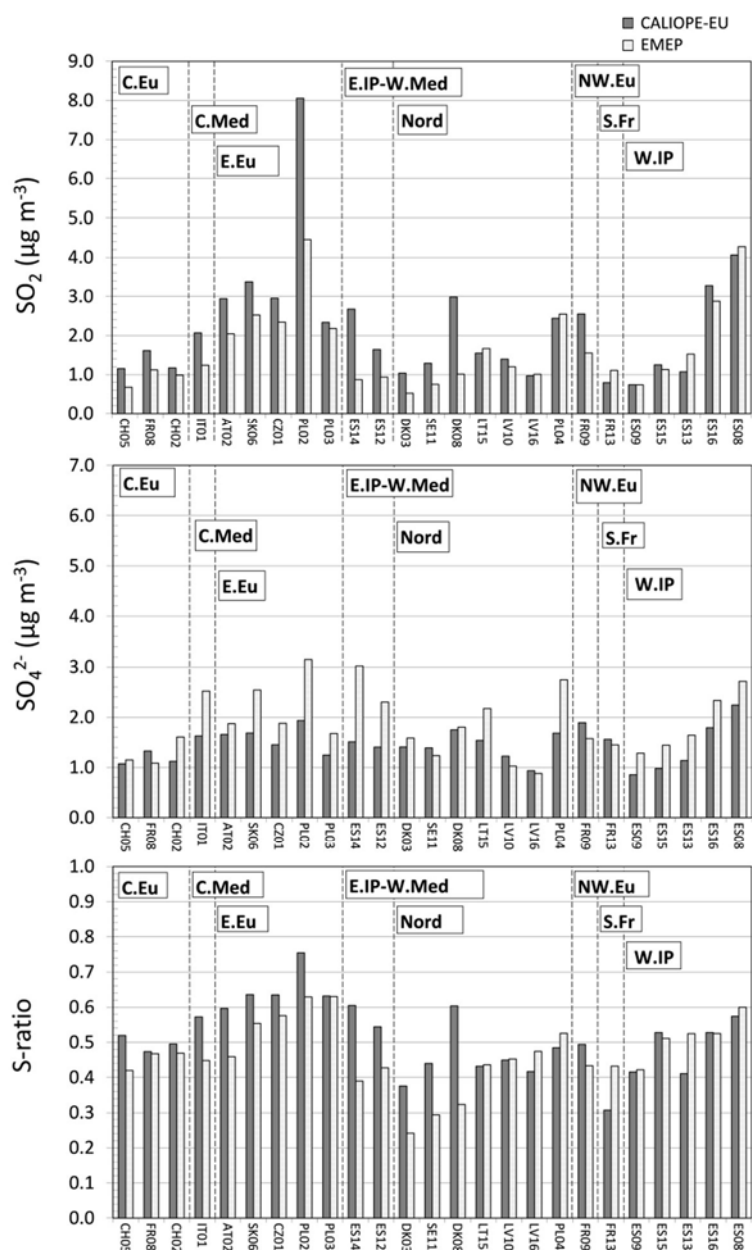
Figure 3-7. Modelled and observed annual (a) SO_2 concentrations ($\mu g\ m^{-3}$), (b) SO_4^{2-} concentrations, and (c) S-ratio defined as $SO_2/(SO_2+SO_4^{2-})$ for each EMEP stations. The observed values are the light grey columns and the modelled values are the dark grey column. EMEP stations are represented by a code defined in Table 2 and they are sorted according to zones described in Table 3-2.

The observed S-ratios range from 0.24 (Tange-DK03) to 0.63 (Sniezka-PL03), meanwhile the modelled S-ratios tend to basically overestimate the observed range due to different regimens dominated in diverse regions. The highest S-ratio (observed and modelled S-ratio > 0.5) are found in eastern Europe and western Iberian Peninsula which indicates that fresh sulphur dominates these regions (oxidation processes are limiting). In this case, CALIOPE-EU overestimates these ratios, which is consistent with the model overestimation of the highest SO_2 levels, especially in eastern Europe (Figure 3-7a and Section 3.3.1.1). S-ratios between 0.4 and 0.5 (modelled and observed) are

found over the Mediterranean Basin (C.Med and E.IP-W.Med), central, northwestern, and north Europe (C.Eu, NW.E. and Nor.) where sulphur is dominated by SO_4^{2-} generated during the long-range transport. In this regime, CALIOPE-EU tends to overestimate S-ratio, mainly dominated by the SO_4^{2-} underestimations, which depict deficiencies of the SO_4^{2-} parameterizations (e.g. limitation to the availability of aqueous phase oxidants such as H_2O_2 and ozone as shown in other European studies (Stern et al., 2008; Schaap et al., 2004b; Kim et al., 2011).

The lowest observed and modelled S-ratios (S-ratios < 0.35) are found in northern Europe, at the stations of DK03, DK08 and SE11. Thus, this region is affected by SO_4^{2-} from transport, since no large isolated point sources are located there (Figure 3-1a) and is only affected by ship emissions. Under this regime, CALIOPE-EU overestimates these ratios at these three stations, since modelled SO_2 levels are largely overestimated (Figure 3-7a). This could indicate that ship emission estimates in the EMEP inventory are too high over these areas as pointed out by Tarrasón et al. (2007).

The spatial correlation is relatively high (r = 0.52) since it is biased by the under- and overestimation of sulphur compounds in different regions. Nevertheless, the modelled S-ratio over Europe is consistent with the patterns discussed before for SO_2 and SO_4^{2-}. On the one hand, the major shipping routes (from the North Sea, passing by the English Channel, through Portugal, Spain and northern Africa towards the Suez Canal) and power plants in eastern Europe (Poland, Serbia, Rumania, Bulgaria and Greece), northwestern Spain and northwestern Europe (UK, Belgium, The Netherlands) are responsible for fresh sulphur. On the other hand, central Europe and over the Mediterranean Basin are regions affected by the secondary SO_4^{2-} transported from the aforementioned emitted areas which is secondary formed favoured by the meteorological pattern (Querol et al. 2009).

3.3.3.2 Free ammonia

The F-NH_x indicator is a useful tool to identify potential regions with high potential to generate NH_3NO_3, based on the fact that it will be formed if there is enough NH_3 available after the neutralization of the SO_4^2. Figure 3-6b presents the modelled annual F-NH_x distribution over Europe in 2004. Figure 3-8a shows the observed and calculated annual F-NH_x at each EMEP stations lumped by regions.

Observed F-NH_x is in a range of -0.05 to 0.13 μmol m^{-3} (Figure 3-6c and d). Calculated spatial correlation is relatively high (r=0.65). However, CALIOPE-EU system presents a tendency to overestimate F-NH_x. Under this condition, NH_4NO_3 could be enhanced in the model. Nevertheless, the dominant regimens depend on the region.

Modelled F-NH_x decreases from the coastal areas to the ocean. The lowest (modelled and observed) free ammonia (F-NH_x < 0 μmol m^{-3}) is mainly confined to coastal stations where acid displacements with sea-salt aerosol take place (Athanasopoulou et al., 2009).

Regions with low potentiality to form NH_4NO_3 (0 μmol m^{-3} < F-NH_x < 0.02 μmol m^{-3}) are found in northern Europe and western Iberian Peninsula. In the first case, it is due to the low emissions and gas-phase NH_3 (Figure 3-1a and Figure 3-6e, respectively). In the second case, despite there is

enough NH_3 emission, the elevated S-ratio regime indicates that available NH_3 is partitioned to aerosol phase to neutralized SO_4^{2-}.
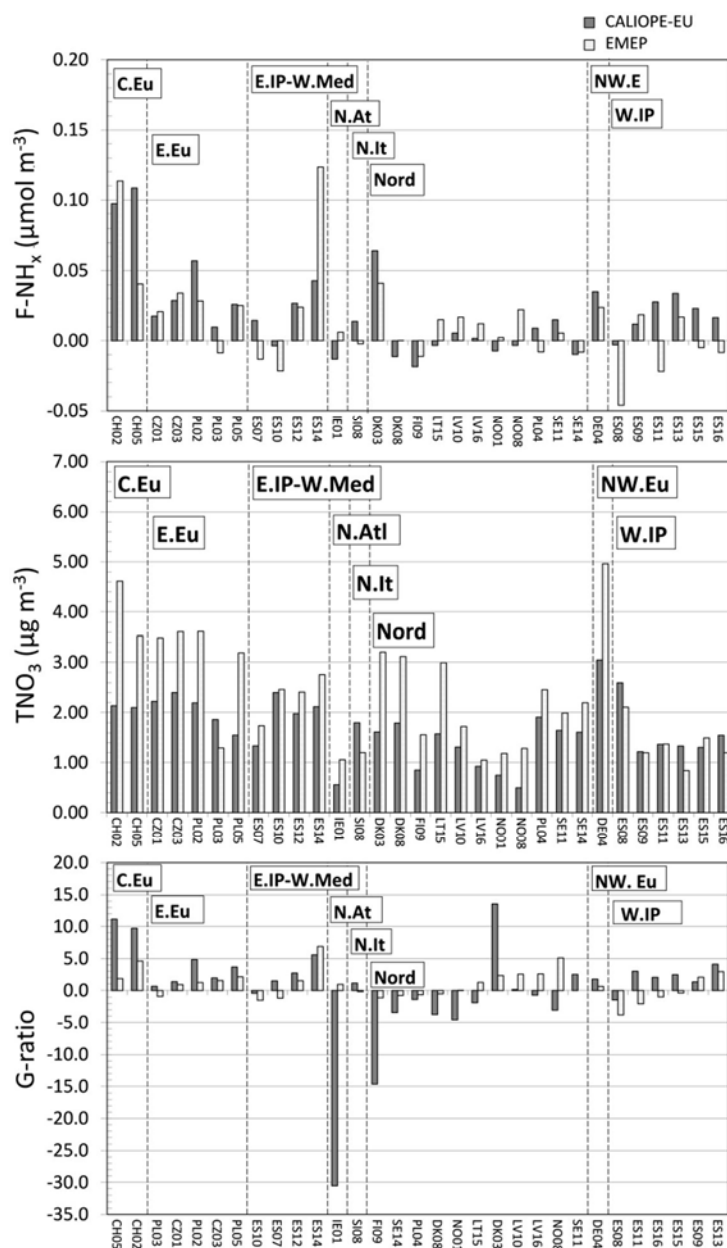
Figure 3-8. Modelled and observed annual (a) Free ammonia (F-NH_x, $\mu mol\ m^{-3}$), (b) Total nitrate (TNO$_3$, $\mu g\ m^{-3}$), and (c) G-ratio defined as F-NH_x over TNO$_3$ on molar basis. The observed values are the light grey columns and the modelled values are the dark grey column. EMEP stations are represented by a code defined in Table 2 and they are sorted according to zones described in Table 3-2.

Regions with relatively high potentiality to form NH_4NO_3 (0.02 $\mu mol\ m^{-3}$ < F-NH_x < 0.04 $\mu mol\ m^{-3}$) are eastern Iberian Peninsula and eastern Europe. In both cases, NH_3 emissions are high (100-250 Mg yr^{-1} and small areas 250-450 Mg yr^{-1}). CALIOPE-EU tends to underestimate F-NH_x over Iberian Peninsula since TNH$_3$ are underestimated.

The highest measured and observed F-NH$_x$ (F-NH$_x$ > 0.04 μmol m^{-3}) are found in central (south Germany and Po valley) and northwestern Europe (Benelux and eastern France) where the highest and extended NH$_3$ emissions (>1,400 Mg yr^{-1}) together with meteorological conditions (low temperature and high relatively humidity) favoured the partition of NO$_3^-$ to aerosol phase. In this case, CALIOPE-EU tends to overestimate the highest F-NH$_x$ since TNH$_3$ are overestimated in those areas.

3.3.3.3 G-ratio

Figure 3-6c shows the annual distribution pattern of observed and calculated G-ratios over 2004. G-ratio is useful to analyse which reactant, NH$_3$ or HNO$_3$, limits the formation of NH$_4$NO$_3$ (Ansari and Pandis, 1998). Figure 3-8c shows the observed and calculated annual G-ratio at each EMEP stations compared with the performance of F-NH$_x$ (Figure 3-8a) and TNO$_3$ (Figure 3-8b).

The modelled and observed spatial distribution of G-ratio indicates that, based on annual average concentration, over continental Europe the NH$_4$NO$_3$ formation is limited by the formation of HNO$_3$ (G-ratio > 1). Adams et al. (1999) showed the same tendency over the European continent using the global model GISS GCM II. Also Sartelet et al. (2007) and Kim et al. (2011) estimated the same pattern over continental areas with the POLYPHEMUS system using different chemical mechanisms (CB05 and RACM). Such findings indicate that NH$_4$NO$_3$ concentration in these areas could increase dramatically given an increase in HNO$_3$ concentration, or indirectly given an increase of NO$_x$ emissions. It is also consistent with results obtained by Renner and Wolke (2010) over northwestern Europe, who demonstrate that ammonium nitrate, but above all ammonium sulphate, is not sensitive to NH$_3$ emission changes when SO$_2$ and NO$_x$ are limiting.

Over ocean, NO$_3^-$ is produced over the English Channel, Atlantic coast of France, and the North Sea, although NH$_3$ limits its formation (0 < G-ratio < 1). An acidic sulphate aerosol dominates the Mediterranean Sea (G-ratio < 0) severely limited by NH$_3$, where intense maritime traffic generate high NO$_x$ (indirectly HNO$_3$) and SO$_2$ emissions.

The low spatial correlation (r = 0.27) are related with the fact that this equation may be too simplistic for location where NO$_3^-$ is often neutralized by sodium or calcium, such as coastal areas or western Mediterranean Basin (Querol et al., 2009a). Even though, CALIOPE-EU system estimates sea-salt emissions; however, replacement of chloride by nitrate in mixed marine/urban air masses is not implemented in AERO4 (Kelly et al., 2010).

3.4   Comparison with other AQM evaluation studies

Recent AQM studies have provided more insight in the SIA formation in Europe. This section discusses a comparative analysis between various European model evaluations and the results obtained here form the CALIOPE-EU system. Note that this is not an exhaustive inter-comparison study because of the different configuration of the diverse works. Nevertheless, it provides a good basis for assessing the reliability of the results obtained in the context of the European model evaluation which also complement that presented in Pay et al. (2010a). Table 3-4 shows a

chronological list of published AQM evaluation studies on SIA and precursors gases, which are presented along with CALIOPE-EU evaluation results. Following the criteria in Pay et al. (2010a) those evaluation studies have several characteristics in common: (1) European domain; (2) the regional scale (horizontal resolutions are between 12 km to 55 km); (3) the simulation period, mainly annual, except in the case of Kim et al. (2011) and Stern et al. (2008); and (4) the used of the EMEP monitoring network to evaluate the models. Table 3-5 presents the common statistics for the fine inorganic aerosols (SO_4^{2-}, NO_3^- and NH_4^+). Gas-phase aerosol precursors (nitric acid and ammonia) and total nitrate and ammonia are presented in Table 3-6. Results for sulphur dioxide are presented at Table 3-5 in Pay et al. (2010a). Three common statistics parameters are considered: the ratio between modelled mean and observed mean (Ratio), correlation coefficient (r), and RMSE.

For SO_4^{2-} concentration CALIOPE-EU presents satisfactory annual correlations in comparison to the other studies (0.49 versus 0.37-0.65 in annual basis). However, the RMSE obtained with CALIOPE-EU is the lowest form all the models (1.3 $\mu g\ m^{-3}$ for CALIOPE-EU versus 1.7-5.89 $\mu g\ m^{-3}$). As other European modelling system, CALIOPE-EU tends to underestimate SO_4^{2-} annual concentrations.

Considering NO_3^-, the annual correlation obtained for CALIOPE-EU (r = 0.58) is, with LOTOS8, the third highest value after EURAD9 (r=0.61) and the EMEP6 (r = 0.80). Note that EMEP6 presented also the highest correlation for NO_2 (Pay et al., 2010a). The other studies calculated lower correlations for nitrate ranging from 0.17 to 0.50. The RMSE for CALIOPE-EU are in the low range from the other studies (2.30 $\mu g\ m^{-3}$ against 1.59-6.39 $\mu g\ m^{-3}$). Differently from the other European modelling system, CALIOPE-EU tends to simulates slightly lower aerosol nitrate concentrations than those measured presenting the lowest Ratio (Ratio = 0.50), closely followed by CMAQ3 (Ratio = 0.63).

As for NO_3^-, the annual correlation for NH_4^+ obtained within CALIOPE-EU (r = 0.62) is the same as for LOTOS8, and the second highest value after EMEP6 (r = 0.82). The other studies present lower correlations but always higher than those obtained for NO_3^- (0.39-0.61). RMSE for CALIOPE-EU is in the same range as the other studies (1.20 $\mu g\ m^{-3}$ against 0.83-2.90 $\mu g\ m^{-3}$). Again, conversely from the other studies, CALIOPE-EU tends to underestimate NH_4^+, presenting the second lowest Ratio (Ratio = 0.67), after MATCH9 (Ratio = 0.55) and relatively closer to CMAQ3 (Ratio = 0.75).

As discussed in Pay et al. (2010a), the CALIOPE-EU evaluation results for SO_2 show very satisfactory performances in comparison with other studies, mainly attributed to the high resolution of the CALIOPE-EU system which enables a well-defined spatial and temporal description of SO_2 sources over Europe. As CALIOPE-EU most of the European models present the a tendency to overestimate SO_2, e.g. bias of 1.3 $\mu g\ m^{-3}$ for CALIOPE-EU versus biases between 1.0 and 2.3 $\mu g\ m^{-3}$ for EUROTRAC models (Hass et al., 2003). For HNO_3, not too much comparison can be done since there are only few stations that measured this compound. Annual correlation coefficient is higher than that presented in other studies (0.41 for CALIOPE-EU versus 0.26 (POLYPHEMUS5) - 0.38 (EMEP6)). RMSE is in the same range than that obtained POLYPHEMUS5.

Table 3-4. List of published European model evaluation studies for secondary inorganic aerosol and their main characteristics to be compared with CALIOPE-EU evaluation results (this study).

Reference	Modelled Year[1]	Modelling System	Horizontal Resolution/layers	Chemical Mechanism[2]	Thermodynamic Inorganic Equilibrium[3]	Study number
This study	2004	CALIOPE	12 km x 12 km/15	CBM-IV	ISORROPIA	CALIOPE-EU04
Kim et al. (2011)	2001	POLYPHEMUS	0.5° x 0.5°/5	RACM	ISORROPIA	POLYPHEMUS1
Kim et al. (2011)	2001	POLYPHEMUS	0.5° x 0.5°/5	CB05	ISORROPIA	POLYPHEMUS2
Matthias (2008)	2001	CMAQ	54 km x 54 km/20	CBM-IV	ISORROPIA	CMAQ3
Stern et al. (2008)	2003	CHIMERE	0.25 ° x 0.25 °/8	MELCHIOR	ISORROPIA	CHIMERE4
Stern et al. (2008)	2003	EURAD	125 km x 125 km/23	EuroRADM	RPMARES	EURAD4
Stern et al. (2008)	2003	LOTOS-EUROS	0.25° x 0.25°/4	CBM-IV	ISORROPIA	LOTOS-EUROS4
Stern et al. (2008)	2003	REM-CALGRID	0.25° x 0.25°/5	CBM-IV	ISORROPIA	REM-CALGRID4
Stern et al. (2008)	2003	LM-MUSCAT	0.25° x 0.25°/40	RACM	Hinneburg et al. (2007)	LM-MUSCAT4
Sartelet et al. (2007)	2001	POLYPHEMUS	0.5° x 0.5°/5	RACM	ISORROPIA	POLYPHEMUS5
Tarrasón et al. (2006)	2004	Unified EMEP	50 km x 50 km/20	EMEP	EQSAM	EMEP6
van Loon et al. (2004)	1999/2001	CHIMERE	0.5° x 0.5°/8	MELCHIOR	ISORROPIA	CHIMERE7
van Loon et al. (2004)	1999/2001	DEHM	50 km x 50 km/20	EMEP	EQSAM	DEHM7
van Loon et al. (2004)	1999/2001	Unified EMEP	50 km x 50 km/10	EMEP	EQSAM	EMEP7
van Loon et al. (2004)	1999/2001	MATCH	55 km x 55 km/10	EMEP	EQSAM	MATCH7
van Loon et al. (2004)	1999/2001	LOTOS	0.25° x 0.5°/3	CBM-IV	ISORROPIA	LOTOS7
van Loon et al. (2004)	1999/2001	CMAQ	36 km x 36 km/21	RADM2	ISORROPIA	CMAQ7
van Loon et al. (2004)	1999/2001	REM-CALGRID	0.25° x 0.5°	CBM-IV	ISORROPIA	REM-CALGRID7
Schaap et al. (2004)	1995	LOTOS	25 km x 25 km/3	CBM-IV	ISORROPIA	LOTOS8
Hass et al. (2003)	1995	DEHM	50 km x 50 km/10	CBM-IV	EQSAM	DEHM9
Hass et al. (2003)	1995	EURAD	27 km x 27 km/15	EuroRADM	RPMARES	EURAD9
Hass et al. (2003)	1995	EUROS	0.55° x 0.55°/4	CBM-IV	EQSAM	EUROS9
Hass et al. (2003)	1995	LOTOS	0.25° x 0.5°/3	CBM-IV	ISORROPIA	LOTOS9
Hass et al. (2003)	1995	MATCH	55 km x 55 km/10	EMEP	EQSAM	MATCH9
Hass et al. (2003)	1995	REM-CALGRID	0.25° x 0.5°	CBM-IV	ISORROPIA	REM-CALGRID9

[1]Evaluation studies are done over a full year. Evaluated period for Kim et al (2001) corresponds from 15 July to 15 August. Evaluated period for Stern et al. (2008) corresponds from 6 February to 30 March. [2]CBM-IV, see Gery et al. (1989); CB05, see Yarwood et al. (2005); EMEP, see Simpson et al. (2003); EuroRADM, see Stockwell and Kley (1994); MELCHIOR, see Schmidt et al. (2001); RACM, see Stockwell et al. (1997); RADM2, see Stockwell et al. (1990).[3]ISORROPIA, see Nenes et al. (1998); RPMARES, see Binkowski and Shankar (1995); EQSAM, see (Metzger et al., 2002).

Overall, CALIOPE-EU performances for NH_3 are superior to other European studies. The correlation obtained is this study is the highest from all considered models (0.56 against 0.05-0.33). The RMSE is in the lowest range from other European studies (1.1 μg m^{-3} for CALIOPE-EU versus 5.40 -7.50 μg m^{-3}). As other European studies, the CALIOPE-EU system tends to

underestimate NH_3 in the gas phase (0.77 against 0.18-0.85). Given the strong gradients in NH_3 levels, the high resolution of CALIOPE-EU, both vertical and horizontal, could justify its better skills to reproduce the large NH_3 gradients compared to other European models (Asman, 2001).

For TNO_3, correlations are in the same range of the other European studies (0.50 for CALIOPE-EU against 0.37-0.56). Only EMEP6 is out the mean (r = 0.87) consistently with its highest correlation for NO_3^-. RMSE for all the models is in the same range (2.1 for CALIOPE-EU versus $1.80 \ \mu g \ m^{-3}$ - $3.70 \ \mu g \ m^{-3}$). Similar results for TNO_3 are found in LOTOS8 for correlation (0.50 against 0.52), RMSE (2.1 $\mu g \ m^{-3}$ against 2.3 $\mu g \ m^{-3}$), and a similar tendency to underestimate TNO_3 (Ratio = 0.77 vs. Ratio = 0.81). As for TNO_3, statistics for TNH_3 modelled by CALIOPE-EU system is in the range of other studies.

The different performance of SIA and precursor gases seems to be related with the chemical mechanism and thermodynamic equilibrium. Most of European models in this comparison used the Carbon Bond IV chemical mechanism. The CB-IV has recently been updated, namely CB05 (Yarwood et al., 2005). Yu et al. (2010) found that CB05 has the relatively better performance for HNO_3 and SO_2 than for CB-IV. This update is interesting since, as showed before, nitrate formation tends to be HNO_3-limited over continental areas. Recently, Kim et al. (2011) tested the impact of RACM2 (updated version of RACM) and CB05 on the formation of SIA over Europe and showed that differences in SIA result from differences in oxidant concentration (OH, O_3 and NO_3).

According to the thermodynamic equilibrium, EQSAM module (Metzger et al., 2002) is widely used in EMEP model and global models (MATCH and DEHM). This module is very simplified and tends to partition too much NO_3^- and NH_4^+ to aerosol phase under lower temperatures (Tarrasón et al., 2006) causing the aforementioned overestimation of these species. ISORROPIA has proved to be the model of choice for many three-dimensional air quality models in Europe due to its computationally efficient and rigor. An important limitation of ISORROPIA is the lack of treatment of crustal species (Ca^{2+}, K^+, Mg^{2+}), important in simulating the partitioning of NO_3^- and NH_4^+, especially in areas like the southern Europe where dust (from deserts or resuspended form arid areas) comprise a significant portion of PM10 and PM2.5 (Querol et al., 2009a). Recently, an update version of ISORROPIA that includes crustal species has been published, namely ISORROPIA II (Fountoukis and Nenes, 2007).

3.5   Summary and conclusions

This paper presents an evaluation of the results of the CALIOPE-EU high-resolution modelling system (12 km x 12 km, 1h) in terms of secondary inorganic aerosols (SIA) (SO_4^{2-}, NO_3^- and NH_4^+) and its gas precursors (SO_2, HNO_3 and NH_3) using a full- year simulation for 2004 over Europe. Modelling results have been compared to long-term surface concentration from the EMEP monitoring network and to other European evaluation studies. The evaluation is focused on the capability of the model to reproduce (1) the temporal and spatial distribution of SIA and its precursors, in terms of statistics; and (2) the inorganic aerosol formation regimens, in terms of so-called indicators, over Europe.

CALIOPE-EU presents a high accuracy for reproducing SIA levels and (spatial and temporal) variability. Although the total amount of SIA is on average underestimated by 18-50% in most regions of Europe, the temporal variability and hence the transport patterns of these species are captured rather well, as indicated by the temporal correlation coefficients, which range between 0.49 and 0.62. Taking into account that natural sources of SIA precursors are not considered in the emissions this result is satisfying. Performance for N-compounds gas precursor species (nitric acid and ammonia) is not as accurate as for aerosol based on fractional biases and errors.

Results indicate that there is no significant relationship between SIA evaluation and performance for gas-phase precursors. SO_2 is systematically over-predicted by CALIOPE-EU system. Since SO_2 emissions are dominated by large electrical power plants and they are traditionally well understood, deposition mechanism and meteorological performances could be responsible from this underestimation. Overall, the positive mean bias for only SO_2 suggests that non-marine SO_4^{2-} formation in the modelling system is often limited by oxidant availability and not always by sulphur dioxide availability.

Overall NO_3^- concentrations are underestimated in -60% in winter and < -100% in summer. The uncertainty of NO_3^- and HNO_3 measurements hampers to discern if the model overestimation of HNO_3, especially in summer, results from deficiency in model-process description. The summer overestimation of HNO_3 and underestimation of NO_3^- should have minimal impact on regulatory applications since the warm temperatures do not favour the ammonium nitrate formation.

Simulated NH_4^+ concentrations were generally underestimated (~ 20%). Two factors that most strongly influence simulated NH_4^+ concentration in Europe are NH_3 emissions and SO_4^{2-} concentration. Modelled NH_3 does not compare as well with observation as NH_4^+ does. The modelled NH_3 concentrations are underestimated by ~100% during summer.

SIA and its gas precursors have been also analysed in terms of goals and criteria following Boylan and Russell (2006). SO_2/SO_4^{2-} and TNH_3/NH_4^+ monthly concentrations accomplish the criteria for bias and errors. TNO_3 falls within the criteria in warm seasons for biases and errors. The larger errors and fraction biases are found for HNO_3 and NO_3^-.

Fine-particle SO_4^{2-} shows a lower spatial variation which indicates that it is produced mainly from cloud processing over large scales rather than from direct gas phase oxidation of SO_2. SO_4^{2-} presents a clear west-east gradient over Mediterranean Basin, dominated by the large isolated sources located in eastern Europe. In contrast with SO_4^{2-}, NO_3^- presents a prominent east-west and south-north increasing gradient over Europe. Special features may account for these differences: (1) the high levels of SO_4^{2-} in eastern Europe depletes the available gas-phase NH_3 so that little NH_4NO_3 can form in this region due to the low NH_3 levels, and (2) the higher ambient temperature in the south favours the gas phase prevalence of NO_3^-. Concerning NH_4^+, concentrations patterns shows low variability and it follows NO_3^- and SO_4^{2-} concentrations.

Table 3-5. Comparison of the statistics modelled mean/observed mean (Ratio), correlation coefficient (r), and root mean squared error (RMSE, μg m^{-3}) between CALIOPE-EU and other European models[1,2] for secondary inorganic aerosol (SO_4^{2-}, NO_3^-, and NH_4^+) in daily basis.

Study Number	SO_4^{2-} daily average			NO_3^- daily average			NH_4^+ daily average		
	Ratio	r	RMSE	Ratio	r	RMSE	Ratio	r	RMSE
CALIOPE-EU04	0.82 (0.56,2.0)	0.49 (0.15,0.81)	1.30 (0.3,2.3)	0.50 (0.14,2.0)	0.58 (0.20,0.77)	2.30 (0.6,3.8)	0.67 (0.38,1.35)	0.62 (0.30,0.73)	1.20 (0.3,4.1)
POLYPHEMUS1	0.86			1.5			1.1		
POLYPHEMUS2	0.96			1.7			1.2		
CMAQ3	0.83 (0.54,1.36)	(0.21,0.72)		0.62 (0.39,1.0)	(0.30,0.80)		0.75 (0.53,0.94)	(0.30,0.75)	
CHIMERE4	0.69	0.48	3.4						
EURAD4	0.64	0.46	3.3						
LOTOS-EUROS4	0.57	0.47	3.7						
REM-CALGRID4	0.99	0.47	2.9						
LM-MUSCAT4	0.91	0.57	2.7						
POLYPHEMUS5	0.84	0.56	1.7	1.6	0.41	3.1	1.1	0.52	1.3
EMEP6	0.86	0.67		1.4	0.80		1.2	0.82	
CHIMERE7	0.67/0.72	0.49/0.53	2.5/2.07	0.94/0.80	0.44/0.46	2.74/2.73	1.11/1.01	0.41/0.56	1.27/1.38
DEHM7	0.93/0.85	0.57/0.55	2.36/1.77	1.80/1.63	0.34/0.25	3.02/2.53	1.10/0.79	0.51/0.49	0.98/0.83
EMEP7	0.91/0.88	0.57/0.58	2.1/1.84	1.63/1.04	0.50/0.34	3.51/2.08	1.26/1.00	0.51/0.47	1.22/0.86
MATCH7	1.0/1.17	0.56/0.62	2.1/1.86	0.88/0.83	0.47/0.40	1.74/1.59	1.01/1.62	0.53/0.55	0.94/2.09
LOTOS7	1.03/1.3	0.37/0.50	2.9/2.89	0.79/0.95	0.26/0.17	2.19/1.94	1.21/1.01	0.37/0.44	1.21/1.10
CMAQ7	1.22/-	0.46/-	2.67/-	2.65/-	0.47/-	1.74/-	-/-	-/-	-/-
REM-CALGRID7	0.91/0.93	0.51/0.53	2.36/2.03	1.15/0.74	0.42/0.35	2.43/1.92	1.33/1.23	0.45/0.45	1.24/0.99
LOTOS8	0.92	0.60	2.60	1.10	0.58	3.57	1.08	0.62	1.54
DEHM9	1.11	0.37	5.89	1.07	0.32	4.12	0.94	0.39	2.43
EURAD9	1.52	0.52	4.25	2.04	0.61	6.14	1.87	0.50	2.90
EUROS9	0.98	0.47	4.39	2.13	0.30	6.39	-	-	-
LOTOS9	0.91	0.54	2.76	1.59	0.49	4.07	1.23	0.51	1.57
MATCH9	0.84	0.65	2.49	0.78	0.50	2.55	0.55	0.61	1.46
REM-CALGRID9	0.81	0.50	2.78	1.07	0.53	3.10	1.07	0.43	1.63

[1]Value reported without parenthesis represents yearly averages in the entire domain. The first and second values in parenthesis represent the minimum and maximum value respectively obtained among all stations in the entire domain. [2]Values reported with a slash correspond to two different years studied: the number before the slash corresponds to the year 1999; the number after the slash correspond to the year 2001.

Table 3-6. Comparison of the statistics modelled mean/observed mean (Ratio), correlation coefficient (r), and root mean squared error (RMSE, μg m^{-3}) between CALIOPE-EU and other European models[1,2] for total nitrate (TNO$_3$ = HNO$_3$+NO$_3^-$), total ammonia (TNH$_3$=NH$_3$+NH$_4^+$) and gas-phase aerosol precursors (HNO$_3$ and NH$_3$) in daily basis. Note that the other gas-phase aerosol precursors, SO$_2$ and NO$_2$ have been compared with other European studies in Pay et al. (2010a).

Study Number	HNO$_3$ daily average			TNO$_3$ daily average			NH$_3$ daily average			TNH$_3$ daily average		
	Ratio	r	RMSE	Ratio	r	RMSE	Ratio	r	RMSE	Ratio	r	RMSE
CALIOPE-EU04	1.00 (0.35,4.0)	0.41 (-0.11,0.78)	1.1 (0.4,3.5)	0.77 (0.45,1.2)	0.50 (0.14,0.70)	2.1 (0.9,3.6)	0.71 (0.1,1.0)	0.56 (0.10,0.40)	1.1 (0.3,1.3)	0.94 (0.62,2)	0.50 (0.10,0.72)	1.8 (0.4,3.3)
CHIMERE4				0.70	0.47	4.4				1.1	0.49	1.9
EURAD4				2.90	0.46	19.4				3.0	0.45	8.3
LOTOS-EUROS4				0.94	0.67	3.1				1.0	0.58	1.6
REM-CALGRID4				0.87	0.56	3.5				1.4	0.57	2.1
LM-MUSCAT4				0.44	0.42	5.8				1.6	0.56	3.5
POLYPHEMUS5	1.85	0.26	1.4				0.85	0.29	5.4			
EMEP6	0.73	0.38		1.23	0.87					1.26	0.63	
CHIMERE7				0.90/0.83	0.39/0.37	3.02/2.82				1.18/1.05	0.35/0.43	2.98/1.74
DEHM7				1.68/1.73	0.42/0.31	3.03/3.02				0.86/0.79	0.46/0.45	1.85/1.14
EMEP7				1.40/1.16	0.51/0.36	2.62/2.42				1.05/1.00	0.42/0.40	1.95/1.28
MATCH7				0.85/0.95	0.52/0.41	1.88/1.91				0.71/1.62	0.48/0.42	1.82/2.17
LOTOS7				0.72/0.70	0.23/0.20	2.31/2.27				1.12/1.01	0.27/0.29	2.25/1.49
CMAQ7				1.82/-	0.52/-	1.88/-				-/-	-/-	-/-
REM-CALGRID7				1.10/0.86	0.39/0.31	2.26/3.02				1.35/1.23	0.27/0.30	2.39/1.49
LOTOS8				0.81	0.52	2.31				0.88	0.58	1.50
DEHM9				1.09	0.45	2.75	0.38	0.27	7.38	0.79	0.47	3.69
EURAD9				1.85	0.50	3.72	0.56	0.15	5.88	1.24	0.54	3.40
EUROS9				2.49	0.41	5.17	-	-	-	-	-	-
LOTOS9				1.67	0.44	2.82	0.18	0.05	7.50	0.58	0.46	2.77
MATCH9				0.94	0.52	1.94	0.64	0.33	5.59	0.84	0.57	2.54
REM-CALGRID9				1.20	0.38	2.13	0.58	0.09	6.10	0.91	0.26	3.09

[1]Value reported without parenthesis represents yearly averages in the entire domain. The first and second values in parenthesis represent the minimum and maximum value respectively obtained among all stations in the entire domain. [2]Values reported with a slash correspond to two different years studied: the number before the slash corresponds to the year 1999; the number after the slash correspond to the year 2001.

HNO_3 levels decrease over land and increase over the oceans. Despite the high HNO_3 levels due to ship tracks over the Mediterranean Sea, NO_3^- concentrations remain low because NH_3 availability is limiting. Gas-phase NH_3 concentrations are high in continental areas with high NH_3 emissions, particularly if little SO_4^- is present. NH_3 concentrations are found to be highest regionally in UK, The Netherlands, southwestern France, the Po valley, central Poland, southeastern Europe and southern Sweden.

Modelled and observed S-ratios indicates that fresh sulphur dominate eastern Europe, western Iberian Peninsula, and the major shipping routes, where oxidants are limiting the formation of sulphate. On the other hand, central Europe and the Mediterranean Basin are regions affected by the secondary SO_4^{2-} transported form the aforementioned emissions. The free ammonia indicator estimated with CALIOPE-EU system tends to agree with the observed estimations and improves the confidence on the fact that modelled nitrate will respond appropriately to change in precursor emissions.

Fine-particle NO_3^- formation is mostly limited by the availability of HNO_3 over continental region in Europe. Based on the analysis of the three studied indicators (S-ratio, $F-NH_x$ and G-ratio) formation of SIA in Europe tends to be limited by precursors SO_2 and HNO_3 due to the relatively high NH_3 emission, mainly from agriculture, especially in northwestern Europe. Regulatory strategies in this part of Europe should focus on the reduction of NO_x and SO_2 rather than in NH_3 to control ammonium nitrate and ammonium sulphate, respectively.

The comparison with previous modelling studies suggests that CALIOPE-EU performs relatively well for NH_4NO_3 concentrations while higher scores are obtained for SO_4^{2-}, and gas-phase aerosol precursors (SO_2, HNO_3 and NH_3). However, substantial efforts should be made in the temporal description of NH_3 emissions, which determinates the formation of $(NH_4)_2SO_4$ and gas-aerosol partitions. The correlations of primary gases (SO_2 and NH_3, and also NO_2) are notably higher for CALIOPE-EU than for other European system. Most models are based on EMEP emission inventory, but the disaggregation methodologies are different in each case. The higher horizontal resolution and the detailed emission disaggregation techniques implemented in CALIOPE-EU system may be responsible for the better scores obtained in SO_2.

The horizontal resolution may impact urban and industrial areas at a higher degree than rural areas. In this sense, the higher horizontal resolution of CALIOPE-EU system may be responsible for the better scores obtained for NO_2 and SO_2. It is reasonable to think that a detailed emission inventory at a finer horizontal resolution could further improve the air quality model performances.

Another relevant issue that arises from the model comparison is the impact of vertical resolution. Models presented in this evaluation ranges from 3 to 20 vertical layers. It is expected that models with higher vertical levels are able to simulate the vertical mixing better, especially for NH_3 which is shown to have a high vertical gradient (Schaap et al., 2004b).

Overall, the performances on the gas-phase precursor gases (HNO_3 and NH_3) and fine-particle NH_4NO_3 are relatively poor, but the inter-comparison detailed in this work shows that the uncertainties and the lack of understanding around nitrate compounds is a general feature affecting most models. On the other hand, the model performance for SO_4^{2-} is better. The emissions of SO_2

are rather well known and the formation of SO_4^{2-} is not as complex as for NH_4NO_3; also a long history of research has been devoted to this component.

Furthermore, modelling evaluation of in terms of indicators suggests that CALIOPE-EU system is appropriate for regulatory modelling applications. Nevertheless, it is important to continue to examine CALIOPE-EU performance for these chemical species and their precursors to continue to improve model estimates of these species. The results of this study suggest several points for future research devoted to this topic, which are presently being implemented:

- A better characterization of NH_3 emission factors according to inter-annual variability.

- An increase of the spatial coverage and reliability of data sets on NO_3^-, HNO_3 , NH_3 and NH_4^+, which allow a full evaluation of photochemical model results.

- Implement ISORROPIA II thermodynamic equilibrium, allowing an accurate representation of nitrate since it includes interaction with crustal material.

- Implement the update version of the chemical mechanism CB05.

- Implement biomass burning and natural NO_x emissions (e.g. lightnings, soils) which could contribute to the underestimation of N-compounds

4. Implementation of resuspension from paved roads for the improvement of the CALIOPE-IP system

4.1   Introduction

Field measurements in urban areas or megacities showed elevated levels of PM10 in the vicinity of roads coming from the contribution from resuspended particles from paved roads (Lenschow et al., 2001; Querol et al., 2004a; Ketzel et al., 2007; Querol et al., 2008b). However, it is widely known that chemistry transport models are generally unable to reproduce particulate levels near road traffic. For instance, Vautard et al. (2005a) and Pay et al. (2010a) showed that simulated aerosol loadings, using the current knowledge on aerosol mechanisms, show a pervasive trend towards an underestimation by up to 30-50%.

Hence, since a decade, emissions of resuspended particles from paved roads (later referred to as RPR) have received an increasing attention in air quality modelling and forecasting. The first model attempts to quantify particle emissions resulting from abrasion of vehicle components and road surface were presented by Rauterberg-Wulff (2000), LUA (2000), Venkatram (2000) following a preliminary formulation by US EPA (1997), later improved by US EPA (2006). Empirical emission factors are presently retrieved from various field campaigns at different locations and road types of central and western Europe (Düring et al., 2002, 2004; Thorpe et al., 2007; Ketzel et al., 2007; Gehrig et al., 2004). More recently, the resuspendable amount of particles was experimentally evaluated in Barcelona (Spain) by Amato et al. (2009a,b, 2010), demonstrating that the contribution from road dust resuspension in the coarse fraction is comparable or even higher than the exhaust emissions in this urban environment. In this sense, Spain represents a paradigmatic case of study, since regions with low precipitation climates favour the accumulation of paved road dust and the resuspension of loose material on the road surface (Abu-Allaban et al., 2003; Thorpe and Harrison, 2008).

Nowadays, a total of 23 model systems routinely simulate the air quality over Europe, with seven systems also operated in the forecasting mode (Menut and Bessagnet, 2010). Because of the complexity of the physical processes leading to resuspension and the difficulties in measuring and/or modelling their effects on ambient PM levels, CALIOPE (Baldasano et al., 2008b) is the unique system including the contribution of resuspension of particulate matter on an hourly basis, to the authors' knowledge. Emission inventories of non-exhaust emissions are scarce despite their

suitability for researchers and regulating agencies for managing air quality and PM reduction measures (Oxley et al., 2009). Therefore, this contribution intends to describe the inclusion of RPR within HERMES (the emission model in CALIOPE) and the improvements obtained in the simulations of the PM10 mass over a domain covering Spain for a whole year of simulation (2004).

4.2 Methods

4.2.1 The CALIOPE modelling and forecasting system

The CALIOPE project, funded by the Spanish Ministry of the Environment and Rural and Marine Affairs, aims at establishing an air quality forecasting system for Spain (Baldasano et al., 2008a). CALIOPE encompasses a high-resolution air quality forecasting system being applied to Europe as a mother domain (12 km x 12 km,1 h) (Pay et al., 2010a) as well as to Spain as the nested domain (4km x 4 km, 1 h) (Baldasano et al., 2009). Such high resolution of the model system is made possible by its implementation on the MareNostrum supercomputer hosted by the Barcelona Supercomputing Center-Centro Nacional de Supercomputación (BSC-CNS). CALIOPE is a complex ensemble of models that integrates a meteorological model (WRFARWv3.0.1.1), an emission processing model (HERMES), a mineral dust dynamic model (BSC-DREAM8b), and a chemical transport model (CMAQv4.5) together in an air quality modelling and forecasting system. Current forecasts are available through http://www.bsc.es/caliope.

The HERMES model uses information and state-of-the-art methodologies for emission estimations. It calculates emissions by sector-specific sources or by individual installations and stacks following a bottom-up approach. Raw emission data are processed by HERMES in order to provide a comprehensive description of the emissions to the air quality model. Emissions used for the Iberian Peninsula are derived from the aggregation in space from 1 km x 1 km dataset to 4 km x 4 km. A more detailed description can be found in Baldasano et al. (2008a).

Specifically, the on-road traffic emissions module takes into account 72 diesel and gasoline vehicles categories according to COPERT III-CORINAIR methodology (Ntziachristos and Samaras, 2000; EEA, 2006); divided by fuel type, vehicle weight, age of the vehicle and cubic capacity; each of them with its specific emissions factors, defined as a function of the circulation speed. The model includes the definition of the road network, dividing it in stretches with specific temporary disaggregating profiles (distinguishing day-type: weekday-holiday, and month), specific average speed, daily average traffic (number of vehicles per day), stretch length, route type (highway, road or urban) and circulation zones. The emissions account in the on-road traffic module considers hot exhaust, cold exhaust and evaporative emissions. It also estimates particulate matter produced by brakes abrasion, tire wear and pavement erosion. The methodology described below presents a new approach to the inclusion of non-exhaust particulate matter originated by the resuspension from paved roads within the onroad traffic emission module of HERMES. The calculation of the emissions of RPR is proportional to the daily average traffic (DAT) measured in 20,934 observation points throughout Spain. Hourly emissions are based on coefficients calculated with the hourly

distribution of the DAT (Baldasano et al., 2008a). The RPR emissions in the road section r of k-cell per hour are calculated with Eq. (4-1):

$$E_r^{ires}(k, hourly) = Crh \sum_{j=1}^{n} Clf\ Crd\ DAT_{rf}(k) L_r(k) F^{ires} \qquad (4-1)$$

where Crh is the proportion of DAT at h-hour; Clf, the coefficient for daily traffic (labor day or weekend); Crd is the ratio between daily traffic for a specific month and DAT; $DAT_{rj}(k)$ is the daily average traffic for r-road section and j-vehicle category in k-cell (number of vehicles); $L_r(k)$ represents the length of the road section r in k-cell (km); n is the number of vehicle categories considered in HERMES emission model (72 in the present version); and Fires is the road dust emission factor.

As a first approach, the estimated PM10 emission factor measured in Düring et al. (2002) for Berlin has been selected. Taking into account the car type, the applied Fires is 88 milligrams per vehicle kilometer travelled (mg vkt[-1]) for light duty vehicle (LDV) and 217 mg vkt[-1] for high duty vehicles (HDV), respectively. In urban environments resuspension by road traffic tends to be significantly higher than on highways (Gehrig et al., 2004). However, due to its complex dependency on vehicle speed, traffic intensity and behavior (Kupiainen et al., 2005) the road type is not taken into account in the selection of the PM10 emission factor used in this study. The selected Fires resulted higher than those obtained for LDV in UK (14-23 mg vkt[-1], Thorpe et al., 2007), Germany (57-67 mg vkt[-1], Ketzel et al., 2007), Switzerland (17-92 mg vkt[-1], Gehrig et al., 2004) but lower than those in Scandinavian countries (121-198 mg vkt[-1], Ketzel et al., 2007) and those estimated in the United States (63-780 mg vkt[-1], Abu- Allaban et al., 2003). The selected Fires for LDV can be compared to the estimates for Spain by Schaap et al. (2009). In Spain mineral ambient PM10 concentrations in city backgrounds and near busy roads are larger than at central Europe (Pataud et al., 2004; Querol et al., 2004a). Due to climatic conditions, resuspension flux is higher in Spain than in central Europe.

Under precipitation conditions, emissions decrease proportionally to the frequency of measurable precipitation. The precipitation effect is included by the application of a correction factor (f_{prep}) on an hourly basis following the equation proposed by US EPA (2006). This factor is calculated with Eq. (4-2):

$$f_{prep} = (1 - 1.2 \frac{P}{N}) \qquad (4-2)$$

where P is the number of hours with at least 0.254 mm of precipitation during the averaging period, and N is the number of hours in the averaging period. For a precipitation situation occurring continuously for over 48 h, the emissions of RPR are switched off in HERMES. The accumulated precipitation is hourly provided by the WRF-ARW model.

Despite the diameter of RPR spans several orders of magnitude, the peak in the mass distribution is usually in the coarse size range (aerodynamic diameter greater than 2.5 μm) and therefore the emissions of resuspended particles are speciated into this fraction in the HERMES emission model.

In the CMAQ chemistry transport model, coarse particles are described with a unimodal lognormal distribution (Byun and Schere, 2006). The coarse particle mode is treated as dry and chemically inert with a fixed geometric standard deviation of 2.2 (Kelly et al., 2010).

For the present contribution two air quality simulations were performed over a domain covering Spain for a whole year of simulation (2004): (1) taking into account the RPR module within HERMES and (2) without the aforementioned module, here in after referred to as CALIOPE-IP-RPR and CALIOPE-IP, respectively.

4.3   Results

In order to evaluate the implementation of resuspended particles within HERMES emission model, the discussion focuses on a whole year of simulations (year 2004) over the Iberian Peninsula. Figure 4-1a and d displays the impact of the inclusion of RPR for PM10 emissions in Spain. This contribution is calculated by averaging the emitted loadings from the RPR module for each grid cell on the 24 h and is expressed in kg h^{-1} km^{-2}. The impact of this module is highest in cities of dense population such as Madrid, Barcelona or Valencia, with maximum average values increasing up to 10-18 kg h^{-1} km^{-2} downtown the largest conurbations, doubling the emissions when no resuspension is included in HERMES. The radial highways with the largest daily average traffic undergo a mean increase of 1 kg h^{-1} km^{-2} while the rest of the territory is mostly not affected by the RPR module.
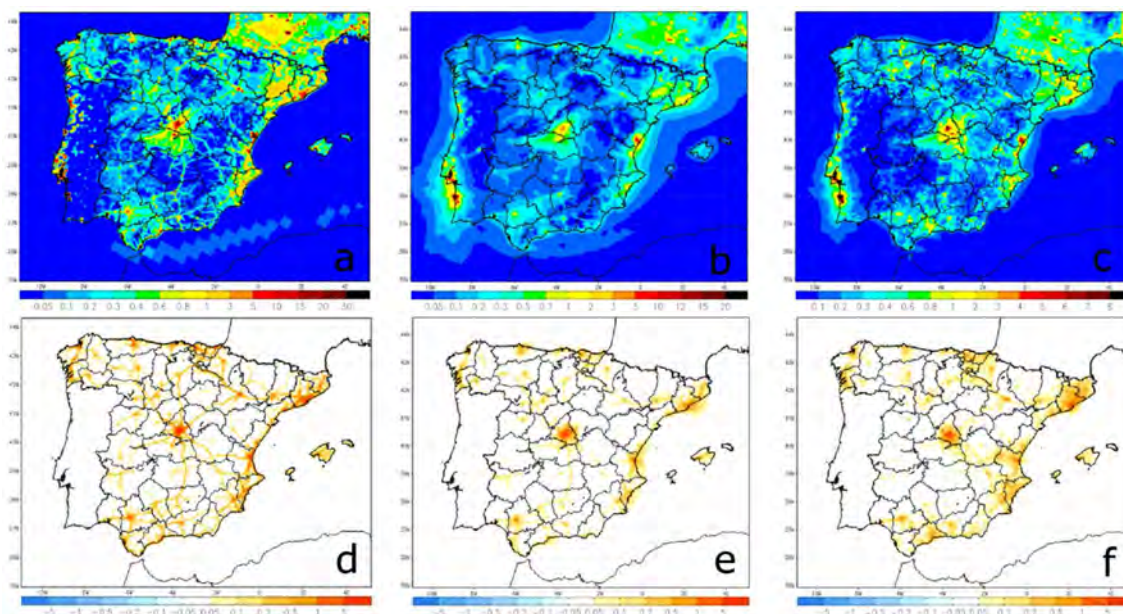
Figure 4-1. (a) Emission loading (kg day^{-1} km^{-2}), (b) air quality contribution (μg m^{-3}) and (c) total deposition (kg day^{-1} km^{-2}) of the coarse particulate matter fraction modelled with CALIOPE modelling system over 2004 including RPR (CALIOPE-IP-RPR) with a resolution of 4 km x 4 km. Annual coarse particulate matter differences with simulation not including RPR (CALIOPE-IP) in (d) emission loading (kg day^{-1} km^{-2}), (e) air quality concentration (μg m^{-3}); and (f) total deposition (kg day^{-1} km^{-2}).

Figure 4-1b and e represents the average contribution of the RPR module in terms of PM10 air concentrations at the surface layer for the same period. Both emission and air concentration patterns display similar behaviors. The RPR module mainly affects PM10 concentrations in Madrid with an average annual increase of around 4 to 10 μg m^{-3} depending on the area of the city observed (with hourly maxima of 26 μg m^{-3} at rush hours, Figure 4-2, up). This increase is similar in the city of Barcelona, with average increases ranging from 3 to 7 μg m^{-3} as the annual average. In other major Spanish cities particulate levels rather increase by 2 to 5 μg m^{-3}. PM10 concentrations in more remote areas are not substantially impacted upon by the inclusion of the resuspension module. Figure 4-1b and f shows that such a module may have strong local effects on the modelled particle concentrations in or in the vicinity of the largest urban zones, but not in the downwind areas from the local emitting sources.

In the domain of Spain, RPR emissions were included in the coarse fraction of the HERMES emission model. In urban areas of large cities coarse particulate matter by resuspension contributes by 40% to the total PM10 emitted, meanwhile PM coarse by road vehicle tyre and surface wear contributes by 6%. In this case, the main contributor to the PM coarse is resuspension (87 %) followed by road vehicle tyre and surface wear (13%). The deposition mechanism was found to be an important sink for resuspended particles from paved roads (Figure 4-1 c and f). Dry and wet depositions largely contribute to the air cleaning. Dry and wet depositions amounted 6-15 kg h^{-1} km^{-2} depending of the urban area, that is, from 60% to 90% of the total coarse particles emitted in large cities and on the main roads. The high local contribution and the lack of transport of coarse particulate matter is associated to the short lifetime of this kind of particles in the atmosphere as a consequence of the deposition implemented in CMAQ chemistry transport model. In this sense, Zhang et al. (2006) and Jiang et al. (2006) report an over-prediction of geometric mean diameter by CMAQ and Elleman and Covert (2009) also reported that CMAQ aerosol size distributions are shifted to a larger size compared with observations. Therefore, the deposition of coarse-mode particles is too rapid in CMAQ (Kelly et al., 2010). This fact may importantly affect to PM10 predictions that will increase if over-predictions of the geometric mean diameter were corrected, because a large fraction of the coarse mode would fail to the accumulation mode and hence deposition velocities would become much smaller.

Figure 4-2 represents the time series of observed and modelled concentrations of PM10 at the urban traffic station of Madrid- Recoletos (as a paradigmatic study case since at this station as the measuring instrument is mainly affected by road activities from the intense traffic nearby) and the average behaviour of all the urban traffic stations considered in the domain of study for which the PM10 increases are over 1 μg m^{-3}. All of these stations are located in the large metropolitan areas of Madrid (Recoletos and Alcobendas), Castellón (Castellón) and Malaga (Ps. Martiricos) with over 500,000 inhabitants where urban streets are specifically described in the HERMES model. Madrid-Recoletos is located in a wide avenue in central Madrid. The RPR module induces a mean annual increase of 2.8 μg m^{-3} in PM10 air concentrations in the coarse fraction compared to the annual simulation including no RPR module, which can achieve 4.2 μg m^{-3} in several stations and areas (Figure 4-1).

Table 4-1 summarizes the performance of the modelling system in the scenarios with or without resuspension, evaluated by means of comparisons with ground-based observations from four urban

traffic stations belonging to the Spanish monitoring network. The selected urban-traffic stations are characterized based on the proposition by Garber et al. (2002) and are representative of pollution levels determined by emission from nearby traffic (roads, motorways, highways) over fully urbanized areas. When the RPR module is implemented the temporal evolution of modelled PM concentration does not change significantly, since resuspension emissions follow the same diurnal profile as exhaust PM emissions.
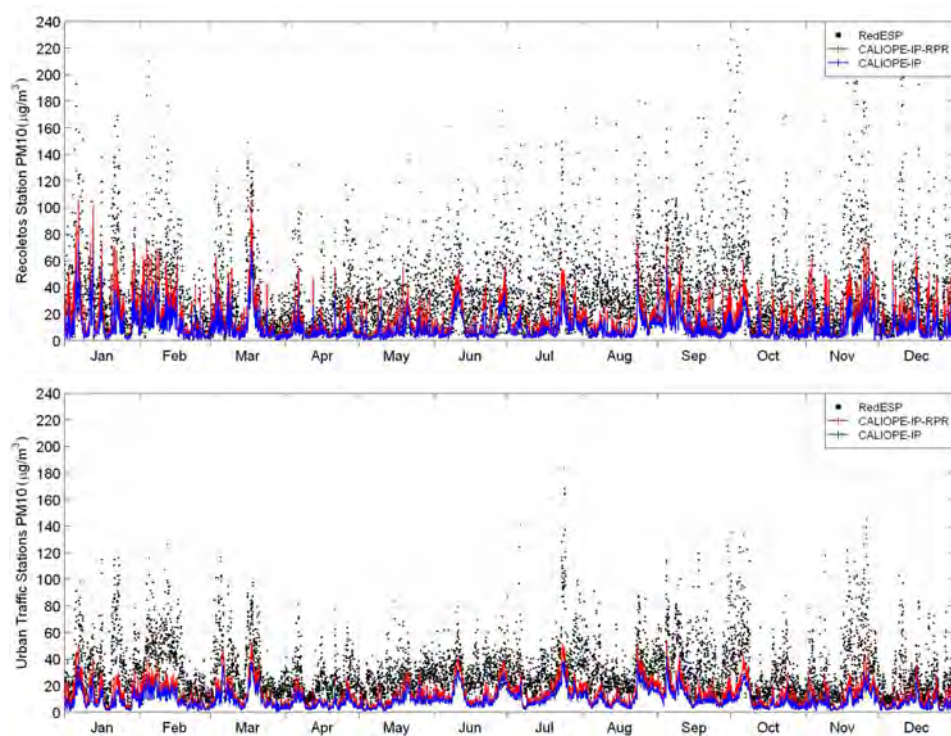
Figure 4-2. Annual hourly series of PM10 in the station of Madrid-Recoletos (up) and the average of urban traffic stations in Spain (bottom) over 2004: observations from the Spanish monitoring network, namely RedESP (black dots); model including RPR, namely CALIOPE-IP (red); and without the inclusion of the RPR module, namely CALIOPE-IP (blue).

Table 4-1. PM10 annual statistics obtained with the CALIOPE system with and without the inclusion of RPR emissions at several urban traffic stations and global average from the air quality Spanish monitoring network. Statistics parameters are: number of data (N), observed mean (OM), modelled mean (MM), correlation coefficient (r), root mean square error (RMSE), mean bias (MB), mean fractional bias (MFB) and mean fractional error (MFE).

Stations[a]	N	OM	CALIOPE-IP						CALIOPE-IP-RPR					
			MM	r	RMSE	MB	MFB	MFE	MM	r	RMSE	MB	MFB	MFE
MR	8740	36.3	10.2	0.49	38.1	-26.2	-104	109	14.4	0.50	35.1	-22.3	-80	**90**
MP	8416	16.2	12.2	0.42	13.0	-3.9	-46	70	13.3	0.43	12.7	-2.8	-34	**62**
CC	4420	36.3	10.9	0.46	34.3	-26.8	-113	115	15.1	0.46	31.4	-23.0	-91	**95**
MA	8598	36.0	7.1	0.55	40.6	-28.9	-133	135	8.8	0.55	39.1	-27.2	-118	**120**
Global	30171	30.6	9.3	0.38	33.7	-21.6	-101	108	12.8	0.41	31.4	-18.4	-80	92

[a]MR: Madrid-Recoletos; MP: Málaga-Ps.Martiricos; CC: Castellón-Castellón and MA: Madrid-Alcobendas

In this sense, correlation coefficients present a tiny variation from 0.41 to 0.48 globally. However PM concentrations are better reproduced with the inclusion of the RPR module, and the bias is reduced from -21.5 μg m^{-3} to -18.8 μg m^{-3}. The root mean squared error also decreases when RPR is included, with improvements in the predictions ranging from 0.3 μg m^{-3} in Malaga-Ps. Martiricos to 3.0 μg m^{-3} in Madrid-Recoletos. The global improvement of the bias and root mean squared error is 2.6 μg m^{-3} and 1.9 μg m^{-3}. The mean fraction scores are higher for all the stations when RPR emissions are included; the mean fractional bias and error improves by 18.3% and 15.5%, respectively. Hence, the inclusion of RPR importantly contributes to the achievement in several stations of the criteria established by Boylan and Russell (2006) for model performance regarding particulate matter (mean fractional error $\leq 75\%$ and mean fractional bias $\leq \pm 60\%$).

During winter days without rain and weak dispersion (see January and mid-March in Figure 4-2) PM10 concentrations are increased by up to 30 μg m^{-3}. These events are associated with meteorological conditions favouring the accumulation of pollutants. For instance, on the 22 January 2004, low wind velocities were monitored and modelled (approx. 1-2 μg m^{-3}), enhancing the increase of PM10 concentrations up to 26 μg m^{-3}. Melios et al. (2006) and Flaounas et al. (2009) evaluated PM emission factors in urban areas from the observation of PM10 to NO$_2$ ratios at urban stations. Following their methodology we observed a linear dependency between the two species for the stations in Table 1 during winter stagnant situations with negligible wind. Observed PM10/NO$_2$ ratios range about 0.7-0.9 while those calculated with HERMES vary between 0.4-0.6. This indicates that despite RPR module reduces the PM10 concentration bias, PM10 emissions from road traffic continue being underestimated in a factor between 3 and 5 during these episodes. This underestimation of urban PM may be related to the underestimation of real PM exhaust emission factors and the underestimation of urban PM sources like the local natural erosion emissions resulting from saltation processes, especially for the conditions in the Iberian Peninsula.

4.4   Conclusions

In this study, an emission module including resuspended particles from paved roads has been implemented in the CALIOPE air quality modelling and forecasting system (http://www.bsc.es/caliope) and assessed against observations for period covering the whole year 2004. The impact of the newly developed emission module considering RPR inclusion in the CALIOPE air quality modelling system highly improves the PM10 predictions in those areas of dense population in Spain, around 15-18% for the mean fractional scores and 2.6 μg m^{-3} for the average bias in all Spain. The RPR emission may have strong local effects on the modelled particle concentration in or near the largest urban zones (up to 7 μg m^{-3} as the annual average and a contribution of 30 μg m^{-3} to the rush hour peaks). Those positive effects are, however, more limited in background areas, since the deposition mechanism was found to be a significant sink for resuspended particulate matter from paved roads in the chemistry transport model.

However, there are still some development tasks for a better reproduction of particulate matter in the CALIOPE system. Presently, further research is devoted to the inclusion of specific emission factors for the area of Spain (from Amato et al., 2010 instead of those of Düring et al., 2002 which represent the conditions of more northern latitudes). Moreover, the large uncertainties in local

natural erosion emissions resulting from saltation processes need further development in emission estimates and modelling, especially for the conditions in the Iberian Peninsula. Despite the aforementioned limitations, the results demonstrate that this first approach is accurate and effective in order to improve the prediction of the PM10 mass and becomes essential to achieve the standards set in the regulations for modelling applications.

5. A full year evaluation and assessment of air quality across Spain with the CALIOPE-IP system

5.1   Introduction

In Europe, human health issues caused by degraded air quality have been extensively studied (Brunekreef and Holgate, 2002; Gryparis et al., 2004; Pénard-Morand et al., 2005) and have motivated the increase of monitoring infrastructures and modelling capabilities. In this sense, the EC and the US EPA, among others, have shown a great interest in air pollution transport and dynamics. Both entities have set ambient air quality standards for acceptable levels of O_3 (US EPA, 1991; European Commission, 2008), NO_2, SO_2, PM2.5 and PM10 in ambient air. According to the European regulations (European Commission, 2008), local to regional air quality models are useful tools to assess and understand the dynamics of air pollutants, to forecast the air quality, and to develop emission abatement plans and alert the population when health-related issues occur.

Air pollution limit values and allowed numbers of exceedances established by the European Commission (2008) are still exceeded in the atmospheric boundary layer in Europe and, particularly, in Spain (de Leeuw and Vixseboxse, 2010). Despite improvements due to European legislations, particulate matter and ground-level ozone remain important pollutants affecting human health (EEA, 2009a, b, 2010b). The impact of these European policies on the pollutant levels was assessed by the CAFE programme (Amann et al., 2004; Cuvelier et al., 2007).

The CALIOPE project, funded by the Spanish Ministry of the Environment (Ministerio de Medio Ambiente y Medio Rural y Marino), aims at establishing an air quality forecasting system for Spain (Baldasano et al., 2008b). CALIOPE (Figure 5-1) encompasses a high resolution air quality forecasting system, namely WRF-ARW/HERMES-EMEP/CMAQ/BSC-DREAM8b, being applied to Europe as a mother domain: 12 km x 12 km, 1 h (Pay et al., 2010a) as well as to Spain as the nested domain: 4 km x 4 km, 1 h. Such high resolution of the modelling system is made possible by its implementation on the MareNostrum supercomputer hosted by the Barcelona Supercomputing Center-Centro Nacional de Supercomputación (BSC-CNS). Four Spanish research institutes compose the CALIOPE project: the BSC-CNS, the "Centro de Investigaciones Energéticas, Medioambientales y Tecnológicas" (CIEMAT), the Institute of Earth Sciences Jaume Almera of the "Centro Superior de Investigaciones Cientificas" (IJA-CSIC) and the "Centro de Estudios Ambientales del Mediterráneo" (CEAM). In this project both experimental and

operational modelling aspects are conducted by the BSC-CNS and CIEMAT while IJA-CSIC and CEAM lead the data monitoring part for the evaluation processes. Current forecasts are available through http://www.bsc.es/caliope.

To date, a total of 23 model systems routinely simulate the air quality over Europe, with seven systems also operated in the forecasting mode (Menut and Bessagnet, 2010). Due to the episodic nature of dust outbreaks, the representation of these events cannot be well simulated with solely the information of aerosol boundary conditions (Jiménez-Guerrero et al., 2008a; Menut and Bessagnet, 2010). Vautard et al. (2005a) showed that simulated aerosol loadings, using the current knowledge on aerosol mechanisms, may be underestimated by up to 30-50% if only anthropogenic sources are taken into account. Among the seven operational systems CALIOPE is the unique system including the contribution of Saharan dust on an hourly basis. In addition, CALIOPE includes the High-elective Resolution Modelling Emission System (HERMES, see Baldasano et al., 2008a) specifically applied with high resolution over Spain.

Several studies investigated air quality concerns over selected areas in Spain (San José et al., 1999; Jiménez-Guerrero et al., 2008b; Vivanco et al., 2008) or over the entire Peninsula (Baldasano et al., 2008b; Jiménez-Guerrero et al., 2008a; Vivanco et al., 2009). Most models ran with horizontal cell resolution of 18 km x 18 km or coarser for domains covering the Spanish territory. CALIOPE now uses a 4 km x 4 km cell resolution to simulate the Iberian Peninsula domain. Such high resolution is a key factor to accurately simulate air pollution issues, especially over complex topography (Jiménez et al., 2006c) and meteorology patterns (Baldasano et al., 1994; Millán et al., 2002) in southern Europe.

The present paper provides a quantitative performance assessment of the CALIOPE modelling system to simulate the air quality in Spain (gas phase and particulate matter). As the HERMES emission database was compiled for the year 2004 the evaluation was carried out over this year. The performance of the modelling system is evaluated by means of comparisons with ground-based observations from the Spanish network hereinafter referred to as "RedESP" (source: CEAM, see Figure 5-2). The model dynamics are evaluated together with the corresponding statistics. The results are then compared to model performance goals and criteria. This study intends to warrant the suitability of CALIOPE over Spain for air quality concerns and forecast.

Section 5.2 describes the different models used in the CALIOPE system, the observational dataset and the statistical parameters calculated. Section 5.3 analyses the results against available observations for the year 2004 and the modelled annual distribution of NO_2, O_3, SO_2 and PM10. A discussion about the exceedances of O_3 during summertime is shown in Section 5.4. The conclusions are drawn in Section 5.5.

5.2 Methods

5.2.1 System description

The CALIOPE air quality system is a state-of-the-art modelling framework. As shown in Figure 5-1, CALIOPE is a complex system that integrates the meteorological model: WRF-ARW, the emission model: HERMES, the chemical transport model: CMAQ and the mineral dust atmospheric model: BSC-DREAM8b offline coupled in an air quality forecasting system (Baldasano et al., 2008b).
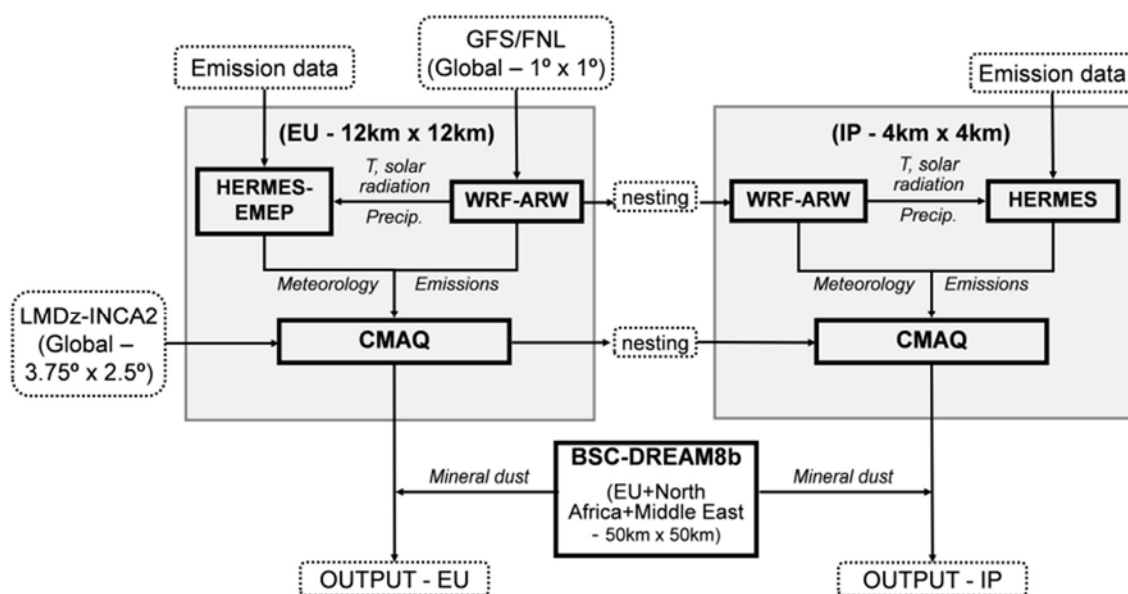
Figure 5-1. Modular structure of the CALIOPE modelling system used to simulate air quality dynamics in Spain. Squared boxes with solid lines represent the main models of the framework. Boxes with dashed lines represent input/output dataset. Lines connecting boxes represent the information flow.

The Advanced Research Weather Research and Forecasting (WRFARW) model v3.0.1.1 (Michalakes et al., 2004; Skamarock and Klemp, 2008) provides the meteorology fields required by the chemical transport model. For the Spanish domain WRF-ARW is configured with a grid of 397 x 397 points corresponding to a 4 km x 4 km horizontal resolution and 38 σ vertical levels with 11 characterizing the planetary boundary layer (PBL). The model top is defined at 50 hPa to resolve the troposphere-stratosphere exchanges properly. Details about the performance of WRF-ARW over the Spanish domain are provided as supplementary material (Annex III).

The Models-3 Community Multiscale Air Quality Modeling System (Models-3/CMAQ, Byun and Ching, 1999; Binkowski, 1999; Byun and Schere, 2006), v4.5 is used to study the behaviour of air pollutants from regional to local scales, due to its generalized coordinate system and its advanced nesting grid capability. It includes gas, aerosol and heterogeneous chemistry. According to the work by Jiménez et al. (2003) the gas-phase chemistry mechanism used in this study is the Carbon Bond

IV (CBM-IV, Gery et al., 1989). The version of CBM-IV mechanism is that presented in CMAQv4.5 original code (Appel et al., 2007, 2008) which introduces some changes and updates in the original CBM-IV mechanism such as an update isoprene chemistry to Carter's one product form (Carter, 2000) and an inclusion of gaseous species that are necessary to link gas-phase chemistry to aerosol formation.

The aerosols are modelled using the AERO4 module (Binkowski and Roselle, 2003). This module comprises the following aerosol components: nitrate, sulphate, ammonium, elemental and organic carbon (with three subcomponents: primary, secondary anthropogenic and secondary biogenic), soil, sodium, and chlorine. Unspecified anthropogenic aerosols and aerosol water are additionally kept as separate components. Aerosols are represented by a three size modes (Aitken, accumulation and coarse mode) each of them assumed to have a lognormal distribution. The coarse particles mode is treated as dry and chemically inert with a fixed geometric standard deviation of 2.2 (Kelly et al., 2010), thus there is no dynamic interaction between the fine and coarse mode. The production of sea salt aerosol (SS) is implemented as a function of wind speed and relative humidity (Gong, 2003; Zhang et al., 2005) through the AERO4 aerosol module.

Secondary inorganic aerosols (SIA) are generated by nucleation processes from their precursors to form nitrate ammonium and sulphate aerosols. The thermodynamic equilibrium between gas and inorganic fine aerosols is determined by the ISORROPIA model (Nenes et al., 1998). Secondary Organic Aerosols (SOA) are simulated following a traditional 2-product SOA model (Binkowski and Roselle, 2003) where SOA concentrations are yield from the oxidation of six primary organic gases: alkanes, alkenes, cresol, high-yield aromatics, low yield aromatics, and monoterpenes. Ten semi-volatile organic compounds are produced via these reactions-two each for olefins, monoterpenes, and aromatics, and one each for alkanes and cresol. The oxidants include the hydroxyl radical, the nitrate radicals, and O_3. The saturation vapour pressures and mass-based stoichiometric yield coefficients of semi-volatile organic compounds are obtained from either smog chamber experiments or from published estimates in cases where smog chamber data are unavailable. The SOA is calculated using the method developed by Schell et al. (2001) and gas and aerosol-phase concentrations of each semi-volatile organic compounds are calculated iteratively using a globally convergent variation of Newton's method. The formation rates of aerosol mass (in terms of the reaction rates of the precursors) are taken from Pandis et al. (1992).

Aerosol deposition is treated by a second-generation deposition velocity scheme (Binkowski and Shankar, 1995; Venkatram and Pleim, 1999). For a more complete description of the processes implemented in CMAQ see Byun and Schere (2006).

The CMAQ horizontal grid resolution corresponds to that of WRF. Its vertical structure was obtained by a collapse from the 38 WRF layers to a total of 15 layers steadily increasing from the surface up to 50 hPa with a stronger density within the PBL.

In order to provide adequate boundary and initial conditions to the IP domain the CALIOPE modelling system was initially run on a regional scale (12 km x 12 km in space and 1 h in time) to model the European domain (mother domain). Chemical boundary conditions for this domain were provided by the global climate chemistry model LMDz-INCA2 (Hauglustaine et al., 2004; Folberth et al., 2006). A detailed evaluation of the European simulation was recently presented in

the companion paper by Pay et al. (2010a). A one-way nesting was then performed to retrieve the meteorological and chemical conditions for the IP domain (see Figure 5-1).

As highlighted by Lam and Fu (2009) stratospheric amounts of O_3 interpolated from global chemical models and provided to the chemical lateral profiles may cause problems since CMAQ does not include a cross-tropopause exchange mechanism. Following their suggestion the stratospheric contribution of O_3 from the mother domain was suppressed from the chemical boundary conditions to avoid inconsistent intrusions of stratospheric O_3 down to the surface.

The HERMES model (Baldasano et al., 2008a) uses information and state-of-the-art methodologies for emission estimations. It calculates emissions by sector-specific sources or by individual installations and stacks. Emissions used for Spain are derived from the aggregation in space from 1 km x 1 km dataset to 4 km x 4 km. Raw emission data are processed by HERMES in order to provide a comprehensive description of the emissions to the air quality model. In this study estimated emissions are expressed in CBM-IV speciation.

According to natural emissions, HERMES calculates the biogenic volatile organic compounds (bVOC) from vegetation (Baldasano et al., 2008a). Three categories of bVOC are estimated according to their reactivity: isoprene, monoterpenes and other volatile organic compounds (OVOC). The model considers the influence of temperature and photosynthetically active radiation (PAR) by Guenther et al. (1995) algorithms, according to Parra et al. (2004, 2006). Emission factors for each individual vegetal species associated with emitter land-use categories are presented in Parra et al. (2004). The land-use categories for each grid cell are obtained from CORINE Land Cover 2000 map starting with a resolution of 100 m, and adapting to 22 the land-use categories according to Arévalo et al. (2004). In the updated version of HERMES model used in the present work, the influence of seasonality in the emission of bVOC is introduced through an environmental correction factor following Staudt et al. (2000) y Steinbrecher et al. (2009). In the specific case of bVOC, estimated emissions with the HERMES model are expressed in terms of CBM-IV variables based on profiles in SPECIATE 3.2 (http://www.epa.gov/ttn/chief/emch/speciation/cbiv-profiles_ mar_4_2002.xls). Wildfire emissions and NO_x production from soils and lightning are not currently calculated by HERMES model. Wildfires are an important source of atmospheric pollutants (NO_x, volatile organic carbon, particulate matter) on the Iberian Peninsula during the dry season, especially in summertime (European Commission, 2005). The inclusion of aforementioned natural emissions could be an important point to improve in order to better reproduce air quality in Spain during summer.

HERMES was recently updated with the following: inclusion of agriculture and livestock emissions (SNAP10 sector, see Baldasano et al., 2008a), improvement in the spatial distribution of biogenic emission and population density via the use of the CORINE Land Cover information at a 100-m resolution, and introduction of emissions from the road traffic sector in small cities (SNAP07 sector). In addition, the current version of HERMES model quantifies particulate emissions resulting from paved road resuspension following the parameterization described in Pay et al. (2010b). The inclusion of resuspended particles from paved road is an important feature for PM10 studies in urban air pollution (Querol et al., 2004a; Amato et al., 2009a,b, 2010).

The Dust REgional Atmospheric Model (BSC-DREAM8b) was designed to simulate and predict the atmospheric cycle of mineral dust (Nickovic et al., 2001; Pérez et al., 2006a,b). The domain considered in this study comprises northern Africa, the Mediterranean basin and Europe. BSC-DREAM8b is fully embedded within the NCEP/Eta meteorological driver (Janjic, 1994). It simulates the long range transport of mineral dust at a 0.3º x 0.3° resolution using 24 vertical layers extending up to 15 km in altitude on an hourly basis. The aerosol description contains 8 bins to allow a fine description of dust aerosols. Dust-radiation interactions are calculated online.

The BSC-DREAM8b is offline coupling and its outputs are then simply added to the CMAQ-calculated particulate matter (Jiménez-Guerrero et al., 2008a). Since BSC-DREAM8b used a 50 km x 50 km horizontal resolution, its outputs are interpolated to the CMAQ's Lambert conformal conic grid with a 4 km x 4 km horizontal resolution. After the interpolation, total modelled PM10 is the sum of the Aitken, accumulation and coarse species from CMAQ and the corresponding bins with diameter less than and equal to 10 μm. CMAQ internally distributes primary coarse particulate matter emissions into the model species ASOIL and ACORS using a 90%/10% split based on the fact that the US emissions inventory estimates that 90% of PM10 is fugitive dust (Binkowski and Roselle, 2003). In the CALIOPE modelling system the only primary natural dust emissions that are taken into account are those from the Sahara desert included offline through the BSCDREAM8b model. In this sense, we changed the internal distribution of primary coarse PM emission into the model species ASOIL and ACORS, where all the primary coarse PM emissions are included in ACORS and ASOIL remain near to zero. In this way, only anthropogenic coarse PM emissions (including resuspension from paved-road) are represented in the ACORS variable.

The simulation consists of 366 daily runs constituting the year 2004. The first 12 h of each daily meteorological runs is treated as cold start, and the next 23 h is provided to the chemical transport model via the Meteorology-Chemistry Interface Process from CMAQ (MCIP).

5.2.2 Air quality network

In order to evaluate the performances of the CALIOPE system at ground level over Spain, the hourly data from RedESP Spanish network of air quality monitoring stations were selected. The RedESP network comprises a relatively dense geographical coverage of the Spanish territory. The RedESP observational data provided by CEAM were subject to a preliminary quality control to exclude erroneous values. Then, all stations with a temporal coverage below 85% of the entire year 2004 were filtered out. The RedESP stations are characterized by the type of environment (urban, suburban and rural) and the dominant emission source (traffic, industrial, and background) based on the proposition by Garber et al. (2002). Characteristics, location and measured pollutants of the RedESP stations are presented in Table 5-1 and Figure 5-2. In summary, a total of 68 measuring stations were used for NO_2, 45 for SO_2, 82 for O_3, and 44 for PM10, respectively.
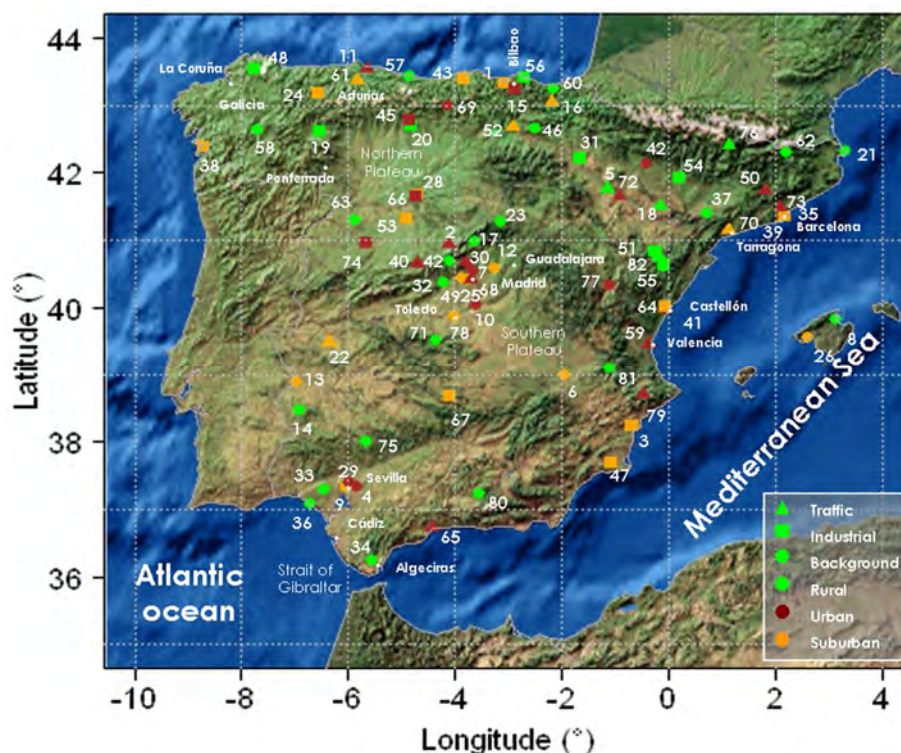
<Figure 5-2.> RedESP stations measuring air pollutants in Spain on an hourly basis in 2004. Different types of stations (U: Urban; S: Suburban; R: Rural; B: Background; I: Industrial; and T: Traffic) according to Garber *et al.* (2002) are represented by symbols and colour codes. The various symbols represent the major emission types affecting each station (Traffic: triangle; Industrial: square; and Background: circle) while the colours reflect the environment of each station (Urban: red; Suburban: green; and Rural: orange). Characteristics and number of each station are listed in Table 5-1.

5.2.3 Statistical indicators

A variety of statistical parameters may be used to quantify how well CALIOPE system reproduces the observations (Denby et al., 2010). In particular, specific metrics were proposed depending on the pollutants (US EPA, 1984, 1991; Cox and Tikvart, 1990; Weil et al., 1992; Chang and Hanna, 2004; Boylan and Russell, 2006).

Common statistical metrics used by the modelling community include the measured and modelled mean, the correlation coefficient (r), the root mean square error (RMSE) and the mean bias (MB). Additionally, the mean normalized bias and gross errors, MNBE and MNGE respectively, considering all modelled/observed pairs of values are also useful parameters. For particulate matter, Boylan and Russell (2006) rather suggested the consideration of the mean fractional bias (MFB) and the mean fractional error (MFE) parameters since they are symmetric metrics, bounding the maximum bias and error.

Table 5-1. Location and characteristics of selected RedESP stations (source: CEAM) for 2004 on an hourly basis. 68 Stations were used to monitor NO$_2$, 45 for SO$_2$, 82 for O$_3$, and 44 for PM10, respectively

	Station name	Latitude[b]	Longitude[b]	Altitude (m)	Type[b]	Hourly concentration			
						NO$_2$	SO$_2$	O$_3$	PM10
1	Abanto	+43.322	-3.073	75	SI	X	X	X	X
2	Acueducto	+40.950	-4.116	1002	UT	X		X	X
3	Agro	+38.242	-0.683	44	SI	X	X	X	
4	Al.Guadaira	+37.342	-5.833	68	UB	X		X	X
5	Alagón	+41.763	-1.143	235	RT	X	X	X	
6	Albacete	+38.981	-1.957	686	SB	X	X	X	X
7	Alcobendas(R.)	+40.541	-3.646	688	UB	X	X	X	X
8	Alcudial-Alc	+39.838	+3.147	15	RB	X		X	
9	Aljarafe	+37.340	-6.043	68	SB	X	X	X	X
10	Aranjuez	+40.034	-3.592	501	UB	X		X	X
11	Av.Castilla	+43.538	-5.646	7	UT	X	X	X	X
12	Azuqueca	+40.574	-3.263	662	SB	X	X	X	X
13	Badajoz	+38.892	-6.970	390	SB	X		X	X
14	Barcarrota	+38.476	-6.923	393	RB	X	X	X	
15	Basauri	+43.240	-2.881	125	UI	X	X	X	X
16	Beasain	+43.048	-2.191	153	ST	X		X	X
17	Buitrago	+40.979	-3.622	1024	RB			X	
18	Bujaralo	+41.505	-0.152	327	RT	X		X	
19	C.T. Compos1	+42.626	-6.521	720	RI	X		X	X
20	C.T. Guardo2	+42.704	-4.827	1065	RI			X	
21	Cabo de Creus	+42.319	+3.316	23	RB	X	X	X	
22	Cáceres	+39.482	-6.357	389	ST	X		X	X
23	Campisábalos	+41.281	-3.143	1360	RB	X	X	X	
24	Cangas	+43.181	-6.550	330	SI	X	X	X	X
25	Casa Campo	+40.420	-3.750	645	SB	X		X	X
26	Cast. Bellver	+39.564	+2.623	117	SB	X	X	X	X
27	Castellón	+39.983	-0.045	28	UT	X	X	X	X
28	Cementerio	+41.674	-4.697	695	SI	X		X	
29	Centro	+37.389	-5.992	19	UB			X	
30	Colmenar	+40.665	-3.774	905	UB	X		X	X
31	CTCC-Arguedas	+42.225	-1.667	490	RI	X	X	X	X
32	Chapinería	+40.378	-4.205	675	RB	X		X	X
33	Doñana	+37.285	-6.440	20	RB	X		X	X
34	E2 Alcornocales	+36.234	-5.540	189	RB			X	
35	Eixample	+41.386	+2.154	12	UT	X	X	X	
36	El Arenosillo	+37.088	-6.705	37	RB			X	
37	Els Torm	+41.395	+0.721	470	RB	X	X	X	
38	Esc. Naval	+42.395	-8.708	20	SI		X	X	
39	Escullera	+41.353	+2.177	16	SI			X	
40	Estación	+40.657	-4.690	1150	UT	X		X	X
41	Grao	+39.984	+0.009	10	SI	X	X	X	
42	Guadarra	+40.679	-4.105	1025	RB			X	
43	Guarnizo	+43.404	-3.842	16	SI	X	X	X	X
44	Huesca	+42.136	-0.404	488	UB			X	
45	Instituto	+42.792	-4.847	1120	UI	X	X	X	X
46	Izkiz	+42.653	-2.501	810	RB	X	X	X	X
47	La Aljorra	+37.694	-1.068	80	SI	X		X	X
48	Louseiras	+43.536	-7.740	540	RI	X	X	X	X
49	Majadahonda	+40.446	-3.868	730	SB	X		X	X
50	Manresa	+41.731	+1.826	238	UT	X		X	
51	Mas Matas	+40.841	-0.249	510	RI	X	X	X	X
52	Mda. de Ebro1	+42.682	-2.918	471	ST			X	
53	Medina	+41.316	-4.909	721	SI	X		X	X
54	Monzón	+41.918	+0.197	279	RI			X	
55	Morella	+40.636	-0.093	1150	RI	X	X	X	X
56	Mundaka	+43.406	-2.704	116	RI	X	X	X	X
57	Niembro	+43.439	-4.850	134	RB	X	X	X	
58	O Saviñao	+42.635	-7.705	506	RB	X	X	X	
59	P. Silla	+39.458	-0.377	11	UT	X	X	X	
60	Pagoeta	+43.251	-2.155	215	RB	X		X	X
61	Pal. Deportes	+43.367	-5.831	206	ST	X	X	X	X
62	Pardines	+42.312	+2.214	1224	RB		X	X	

Table 5-1. (continued)

	Station name	Latitude[b]	Longitude[b]	Altitude (m)	Type[b]	Hourly concentration NO₂	SO₂	O₃	PM10
63	Penausende	+41.289	-5.867	985	RB	X	X	X	
64	Peneta	+40.013	-0.058	106	SI	X	X	X	
65	Ps. Martiricos	+36.729	-4.427	4	UT	X		X	X
66	Pte. Regeral	+41.654	-4.735	691	UI	X	X	X	X
67	Puertollano	+38.683	-4.089	670	SI	X	X	X	X
68	Recoletos	+40.423	-3.692	648	UT	X	X	X	X
69	Reinosa	+43.001	-4.136	851	UB	X	X	X	X
70	Reus	+41.151	+1.120	103	ST	X	X	X	
71	Risco Llano	+39.523	-4.353	1241	RB	X	X	X	
72	Roger Flor	+41.651	-0.917	212	UT	X		X	X
73	S. Cugat	+41.481	+2.090	113	UT	X	X	X	
74	Salamanca2	+40.965	-5.656	797	UI	X	X	X	
75	Sierra Norte	+37.996	-5.666	569	RB	X		X	X
76	Sort	+42.407	+1.130	692	RT		X	X	
77	Teruel	+40.336	-1.107	915	UB			X	
78	Toledo	+39.867	-4.021	500	SB	X		X	X
79	Verge	+38.707	-0.467	534	UT	X	X	X	
80	Víznar	+37.237	-3.534	1230	RB	X	X	X	
81	Zarra	+39.086	-1.102	885	RB	X	X	X	
82	Zorita	+40.734	-0.169	619	RB	X	X	X	X

[a]positive value indicates northern latitudes or eastern longitudes. A negative value indicates southern latitudes or western longitudes.
[b]U: Urban; S: Suburban; R: Rural; B: Background; I: Industrial; T: Traffic (see Garber et al., 2002)

The US EPA suggested several performance criteria for simulated O_3, such as MNBE $\leq \pm 15\%$ and MNGE $\leq 35\%$ (US EPA, 1991, 2007) whereas the EC proposes a modelling quality objective given as a relative uncertainty (%): 50% and 30% for PM10/PM25/O_3 annual average and NO_2/SO_2 annual average, respectively (European Commission, 2008). However, the interpretation of the term model uncertainty remains unclear (Denby et al., 2010). Therefore, the latter criteria will not be further commented in this study. For particulate matter, Boylan and Russell (2006) proposed that the model performance criterion would be met when both MFE $\leq 75\%$ and MFB $\leq \pm 60\%$, respectively, and the model performance goal would be met when MFE and MFB are less than or equal to 50% and ± 30%, respectively.

The annual mean model-to-data statistics RMSE, correlation coefficient, MNBE, MNGE, MFB and MFE in hourly basis are calculated for the present study. According to the recommendations of the US EPA a cut-off value of 80 μg m^{-3} was applied to O_3 statistics before compilation (US EPA, 1991; Russell and Dennis, 2000). However, correlation coefficients for O_3 are calculated without cut-off value in order to test the capability of the model to reproduce the variation of O_3 concentrations.

5.3 Results and discussions

First, this section shows a model evaluation through statistical and dynamical performances. Statistics are calculated in hourly basis for NO_2, O_3, SO_2, and PM10. In the case of O_3, the daily peak of hourly O_3 is also computed as it is one of the most important parameters to be considered. Statistics are expressed in annual terms according to different categories: over all stations ("All"), over rural stations ("Rural"), over suburban stations ("Suburban") and over urban stations

("Urban"). Furthermore, a general description of the annual mean distribution of each pollutant is provided to determine each pattern throughout Spain. Note that model outputs are used without any correction factor and the coupling modelling system is used with original codes.
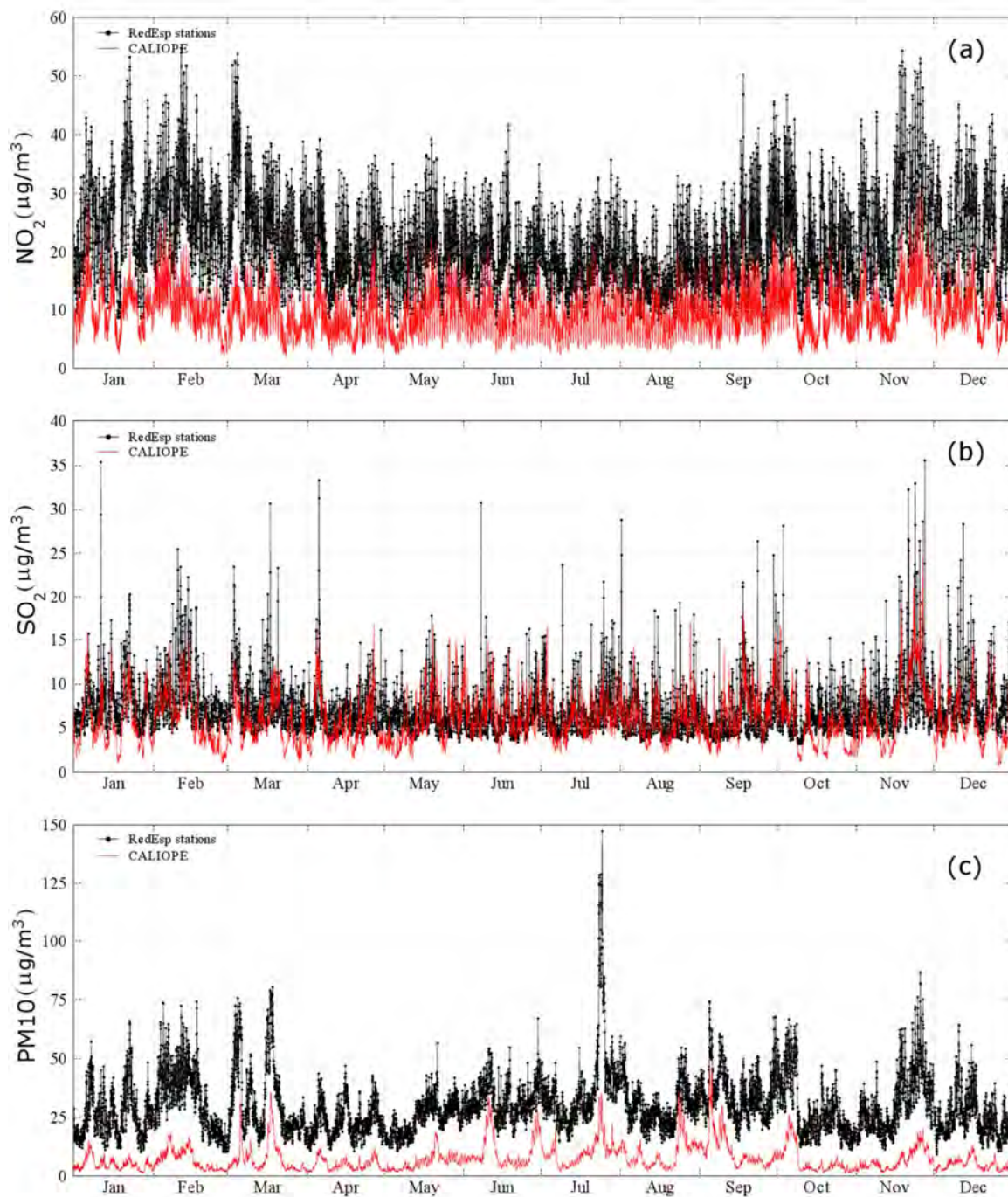
Figure 5-3. Modelled (red lines) and measured (marked black lines) time series of hourly mean concentrations (in µg m^{-3}) for NO$_2$ (a), SO$_2$ (b) and PM10 (c), respectively, averaged over all the RedESP stations available.

5.3.1 Nitrogen dioxide

The NO_2 measurement dataset comprises a relatively equal distribution of station types with 21 urban, 22 suburban and 25 rural stations, respectively. Figure 5-3a represents the measured (marked black line) and modelled (red line) time series of the hourly mean NO_2 at the 68 measuring stations. The general modelled dynamics is well captured with a clear signal of the main winter pollution events. However, mean levels of NO_2 are persistently underestimated (MB = -12.3 $\mu g\ m^{-3}$, see Table 5-2).

Table 5-2. Annual statistics obtained with CALIOPE over Spain for 2004 at the RedESP stations in hourly basis. Statistics are calculated according to four categories: over all stations ("All"), rural stations ("Rural"), suburban stations ("Suburban") and urban stations ("Urban"). Stations/data points column indicates the number of stations (values before slash) and the number of pair measurement-model (values after slash), respectively, used to compute the statistics. The calculated statistics are Observed Mean (OM, $\mu g\ m^{-3}$), Modelled Mean (MM, $\mu g\ m^{-3}$), correlation coefficient (r), mean bias (MB, $\mu g\ m^{-3}$), root mean square error (RMSE, $\mu g\ m^{-3}$), mean fractional bias (MFB, %) and error (MFE, %). All metrics are calculated without cut-off value.

	Category	Stations/data points	OM	MM	r	MB	RMSE	MFB	MFE
NO_2 hourly	All	68/552,941	21.6	9.6	0.53	12.3	23.3	-81.1	98.8
	Rural	25/203,606	7.6	3.3	0.51	3.7	7.6	-79.7	95.6
	Suburban	22/178,416	23.2	11.7	0.39	11.5	23.1	-66.7	93.6
	Urban	21/170,919	36.5	14.8	0.47	23.2	33.6	-97.7	107.9
SO_2 hourly	All	45/368,795	7.2	6.1	0.19	0.9	18.7	-33.1	97.8
	Rural	18/150,647	4.4	3.3	0.28	-0.5	14.0	-29.9	94.1
	Suburban	14/110,584	9.1	9.9	0.14	0.6	26.0	-23.8	95.5
	Urban	13/107,564	9.3	6.0	0.14	-3.1	15.1	-47.1	105.4
PM10 hourly	All	44/355,219	29.6	7.5	0.38	-21.8	33.4	-111.8	119.8
	Rural	12/94,873	19.6	5.9	0.43	-11.7	20.4	-96.0	110.4
	Suburban	17/139,479	35.0	8.0	0.36	-27.0	39.7	-118.6	123.6
	Urban	15/120,867	31.8	8.1	0.36	-23.7	33.8	-116.3	122.9

The statistics compiled in Table 5-2 show highest mean RMSE values at urban stations (33.6 $\mu g\ m^{-3}$) and lowest values for rural stations (7.6 $\mu g\ m^{-3}$). This characteristic is not surprising, since urban stations are more likely to be influenced by high, very local emission sources from urban activities which remain difficult to be captured by models. Both MFB and MFE metrics show relatively constant values among the station types, suggesting that the model error for NO_2 is proportional to the normalized observed value. Overall, however, the modelled daily and monthly variations of NO_2 are in good agreement with observations, although a reduced magnitude of the variability is noted. Among the best model behaviours reported, the majority corresponds to either rural stations influenced by background emissions (mean RMSE = 6.3 $\mu g\ m^{-3}$ compared to 7.6 $\mu g\ m^{-3}$ for all rural stations) or urban stations located in very large (and well characterized) cities such as Madrid or Barcelona (MFB = -46.4% compared to -97.7% for all urban stations). In general, measurements at suburban or urban stations from small- to medium-sized cities were simulated with less accuracy.

From the 68 stations measuring NO_2, 13 (19%) were not represented correctly by the model. Most of these stations are placed in small cities and are often located in the vicinity of isolated roads or highways (e.g., Acueducto, Estación, Roger Flor, Verge, Table 5-1). We attribute such behaviour to the incomplete characterization of emissions from small cities and to the influence of the model resolution on sub-grid emission sources. The latter, also known as sub-grid variability, is a well-known issue affecting the results of model-observation comparisons (e.g., Ching et al., 2006). Also, NO_2 concentrations in background areas were found to be systematically underestimated. This trend is supported by the lack of biomass burning (Ortiz de Zárate et al., 2005) and natural NO_x production such as lightnings which are currently not treated in the CALIOPE modelling system (Smith and Mueller, 2010). In addition, biogenic emissions from vegetated and agricultural areas (SNAP10 sector) in HERMES may need further revision.

Figure 5-4a displays the annual average modelled levels of NO_2 at lowermost levels over Spain. High concentrations of NO_2 within the PBL are directly related to anthropogenic NO_x emission. Baldasano et al. (2008a) estimated that the largest NO_x emission sources come from combustion in energy and transformation industries (41% of NO_x total emission) followed by road transport (37% of NO_x total emission).
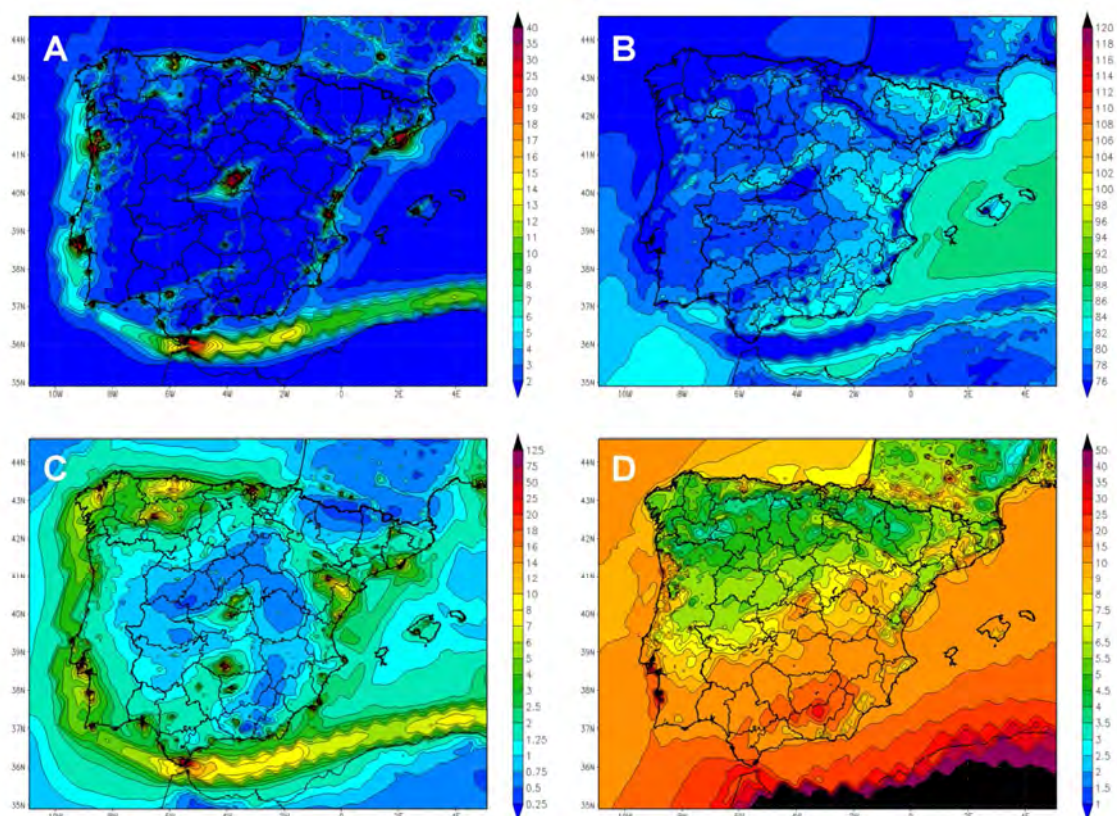
Figure 5-4. 2004 Annual average concentrations (μg m^{-3}) of (a) NO_2, (b) O_3, (c) SO_2, and (d) PM10 at lowermost level simulated by CALIOPE over Spain at a 4 km x 4 km spatial resolution.

The urban plumes from Madrid and Barcelona metropolitan areas reach the highest NO_2 concentrations (~25-40 $\mu g\ m^{-3}$). In both regions, on-road traffic constitutes the main source of primary pollutants in the region (Gonçalves et al., 2009b). In Madrid the NO_2 dispersion follows a south-western direction conditioned by the barrier of Central System (located in the north-western area, 2500 m height) and the canalization of Tajo valley (located in the southern part). The urban plume reaches the highest concentration at the urban nuclei (~40 $\mu g\ m^{-3}$), moving towards Toledo (south) and reaching Guadalajara (east) to a lesser extent. A different NO_2 pattern is observed in Barcelona area. The NO_2 dispersion shows a perpendicular flow to the coast dominated by the north-western winds. The very complex coastal terrain induces mesoscale phenomena which control the superficial wind flows. Sea-breezes and mountain valley winds contribute to the accumulation and recirculation of air masses. The littoral mountain chain (1000-1500 m height) acts as a barrier, recirculating NO_2 flow towards the Mediterranean Sea channelled by the river valleys.

The densely industrialized area of Tarragona and Castellón and the urban area of Valencia, all located along the Mediterranean coast, present significant levels of NO_2 also affected by mesoscale phenomena dominated by sea-breezes which determinate NO_2 flow perpendicular to the coast. In the northern Spain, the urban and industrial areas of Bilbao show significant NO_2 levels (~25 $\mu g\ m^{-3}$) dispersed along an estuary that runs almost 16 km from the centre of the city to the sea and is aligned in an SE-NW direction.

In the north-eastern Spain the NO_2 contribution from power plants emission is bigger than the urban contribution, where NO_2 annual mean concentration reaches ~7-15 $\mu g\ m^{-3}$ at the ground level. Due to the high disaggregation and the specifically detailed emissions implemented in the HERMES model, the impact of principal highways is noticeable, (e.g., Madrid-Sevilla, Barcelona-Bilbao, the A-7 Mediterranean highway) where annual mean values range from 3 to 7 $\mu g\ m^{-3}$. Background regions, unaffected by emissions rather have concentrations below 3 $\mu g\ m^{-3}$.

The major shipping route originating from the northern Atlantic and the British Channel, passing along Portugal coast, through the Strait of Gibraltar heading toward northern Africa and the Suez Canal is shown to have a notable impact on NO_2 levels. Concentrations of NO_2 range from ~5 $\mu g\ m^{-3}$, near the coastlines of Portugal and Gulf of Cadiz, to ~12 $\mu g\ m^{-3}$, over the Alboran Sea. This difference is accentuated by the distinct Atlantic-Mediterranean regimes of Spain. While in the Mediterranean dynamics in summer are characterized by re-circulation and accumulation of pollutant, a strong dynamically compensated anticyclonic inversion dominates the Spanish Atlantic coast and the west of Portugal (Millán et al., 1997). In the Strait of Gibraltar high NO_2 concentrations are estimated (~30 $\mu g\ m^{-3}$) where three contributions are combined: the maritime traffic and the industrial processes and electric generation developed in the Algeciras area. The complex topography of the Strait induces the NO_2 dispersion aligned in a west to east direction, with generalized strong east wind (Millán et al., 2002).

5.3.2 Ozone

This study comprises a total of 82 RedESP stations measuring O_3 throughout Spain for the year 2004. 24 Stations are located in urban areas, 25 in suburban zones and 33 in rural areas, respectively. Modelled and measured time series and scatter plot are shown in Figure 5-5 with the

corresponding statistics in Table 5-3. Time series for O_3 daily peak (Figure 5-5a) show that the O_3 chemistry is best represented in summer. In the high photolytical season, the mean variability and high peaks are generally well reproduced. The modelled variability in winter months is characterized by difficulties to capture the mean trend due to inaccurate description of cross-tropopause exchanges in CMAQ (Pay et al., 2010a). However, the discussion of the evaluation will mainly focus on the high O_3 season (from April to September).
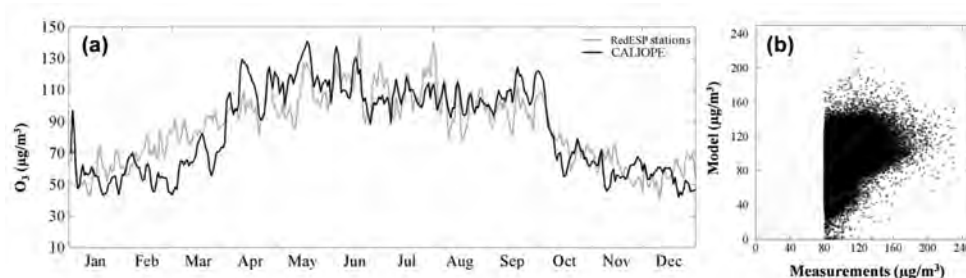
Figure 5-5. Modelled (black lines) and measured (grey lines) time series of O_3 daily peak concentrations averaged over the 82 RedESP stations (a) and scatter plots of the O_3 pair measurement model in hourly basis at the 82 RedESP stations (b). The scatter plot includes the 1:1, 1:2, 1:5, and 5:1 reference lines. A cut-off value of 80 $\mu g\ m^{-3}$ is applied to the observation in the scatter plot.
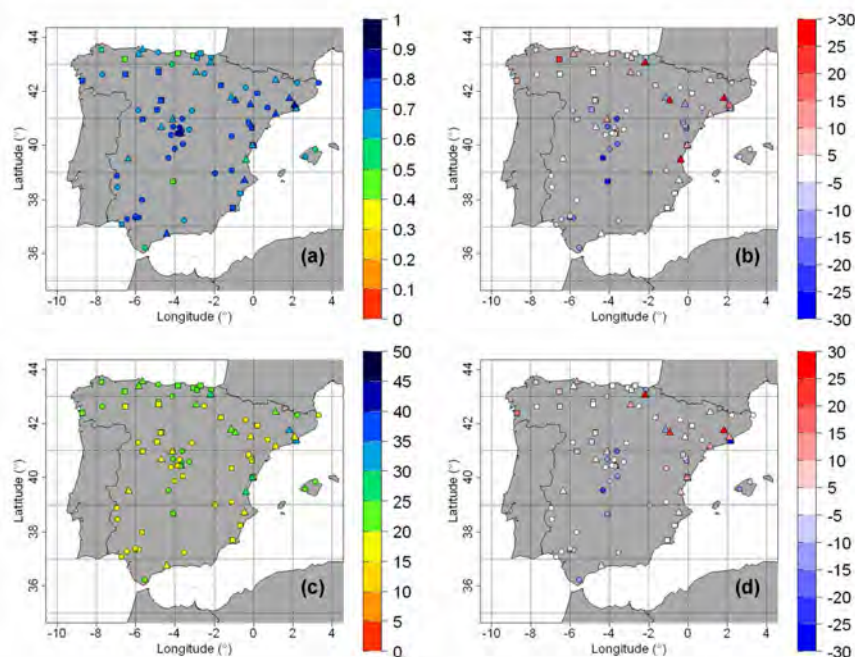
Figure 5-6. Spatial distribution of the statistics for O_3 over 2004 at the RedESP stations: daily peak correlation coefficient (r) (a), annual mean bias (MB, in $\mu g\ m^{-3}$) for daily peak (b), mean normalized gross error (MNGE, in %) in hourly basis (c), and mean normalized bias error (MNBE, in %) in hourly basis (d). Note that MB, MNGE and MNBE are calculated with 80 $\mu g\ m^{-3}$ cut-off according to US EPA (1991) and Russell and Dennis (2000). The various symbols represent the major emission types affecting each station (see Figure 5-2).

Statistical parameters in hourly basis (Table 5-3) consistently show similar results for stations located in urban areas, suburban and rural areas. The correlation coefficient at all urban stations reached a maximum of 0.60 with values per station ranging from 0.35 to 0.75. Most of stations display values of MNGE and MNBE lying within the acceptable range defined by the US EPA (Figure 5-6c and d, respectively) with low values for MFB and MFE metrics. Table 5-3 and Figure 5-6a also display the statistics for O_3 daily peaks. Rural areas are characterized by a general underestimation of O_3 daily peaks (~7 μg m^{-3}) while peak concentrations at urban stations are rather overestimated (8.4 μg m^{-3}) (Figure 5-6b). High correlations are noted for each type of station. In summary the modelling system used in this study performs well with respect to the simulation of high O_3 concentrations over Spain. However, an overestimation of nocturnal values is depicted with recurrent low daily variations due to uncertainties in the modelled nocturnal NO_x cycle, which is a common feature in chemical transport models.

Table 5-3. Annual statistics for O_3 (hourly and daily peaks) obtained with CALIOPE over Spain for 2004 at the RedESP stations in hourly basis. Statistics are calculated according to four categories: over all stations ("All"), rural stations ("Rural"), suburban stations ("Suburban") and urban stations ("Urban"). Stations/data points column indicates the number of stations (values before slash) and the number of pair measurement-model (values after slash), respectively, used to compute the statistics. The calculated statistics are Observed Mean (OM, μg m^{-3}), Modelled Mean (MM, μg m^{-3}), correlation coefficient (r), root mean square error (RMSE, μg m^{-3}), mean fractional bias (MFB, %) and error (MFE; %), mean normalized bias error (MNBE, %) and gross error (MNGE; %). All metrics, except for measured mean, modelled mean and r, are calculated with an 80 μg m^{-3} cut-off value (see US EPA, 1991; Russell and Dennis, 2000).

	Category	Stations/ Data points	OM	MM	r	RMSE	MFB	MFE	MNBE	MNGE
O_3 hourly	All	82/673,608	57.4	71.0	0.57	24.1	-9.3	21.2	-6.0	19.2
	Rural	33/272,923	70.1	76.2	0.51	24.1	-11.2	21.8	-7.7	19.5
	Suburban	25/204,225	51.7	67.5	0.56	24.7	-8.7	20.7	-5.4	18.9
	Urban	24/196,460	45.4	67.4	0.60	23.4	-4.2	19.8	-1.2	18.9
O_3 peaks	All	82/673,608	86.1	85.5	0.64	25.9	-9.8	21.2	-6.6	19.5
	Rural	33/272,923	93.8	86.9	0.67	24.8	-12.9	21.3	-9.7	19.0
	Suburban	25/204,225	84.7	84.1	0.65	27.9	-9.0	21.5	-5.7	19.9
	Urban	24/196,460	76.6	85.0	0.63	25.8	-4.2	20.7	-1.0	20.0

Stations influenced by traffic emissions (i.e., high-NO_x environments) are correctly characterized with a pronounced daily O_3 variability due to the O_3 destruction leaded by high NO_x. To complement such finding, Figure 5-7, representing the O_3 model-to-observation bias as a function of the modelled NO_2 concentrations for all the 68 stations measuring both NO_2 and O_3, is proposed in order to evaluate the performances of the model with respect to the NO_x/O_3 chemistry. While a deviation from the O_3 bias is mainly constrained by the lateral chemical boundary conditions, the width of the plotted dataset is controlled by the chemical mechanism implemented in the model. This figure clearly shows that the highest uncertainties in the reproduction of O_3 levels are related to NO_2-limited regime. Under this regime, corresponding to background conditions, the O_3 bias is slightly shifted to the right, meaning that the modelled O_3 tends to overestimate observed values, specifically during night-time (also see mean observed and

modelled values for rural stations in Table 5-3). As a contrary, the width of O_3 model-to-observation biases decreases with increasing modelled NO_2. Such behaviour reflects the better representation of the NO_x/O_3 chemistry under non-limited- NO_2 regimes, but it also shows that the chemistry under higher NO_2 regime has a reduced dependency to the lateral chemical conditions of the model (no shift on the X-axis). As an example, data from Víznar (Rural Background, light grey triangles) and Recoletos (Urban Traffic, dark grey squares) are overlaid on the figure. The O_3 bias at Víznar displays a wide variability related to low modelled NO_2 whereas the bias for Recoletos markedly diminishes with increasing modelled NO_2. Such description confirms high sensitivity of the model to NO_2 regimes. This behaviour highlights the need to better characterize the emission inventory in either rural (see discussion in Section 5.3.1) or urban areas. The curve interpolating the average O_3 bias in vertical also confirms the higher bias values under low NO_2 regime (maximum bias O_3 ~22 μg m^{-3} for $[NO_2]_{modelled}$=15 μg m^{-3}), while it remains significantly lower for NO_2 modelled concentration above 60 μg m^{-3}.
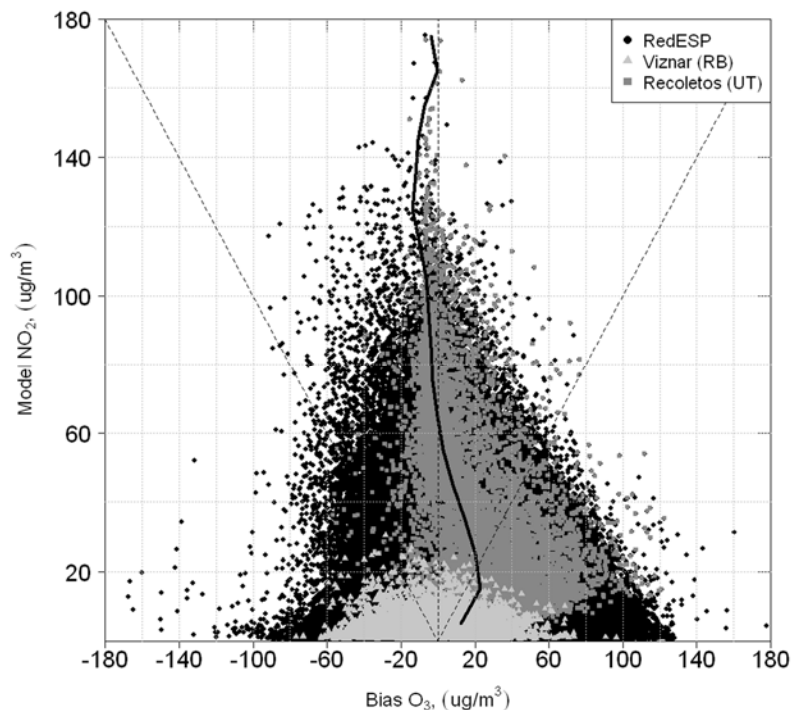
Figure 5-7. Modelled NO_2 levels versus model-observation O_3 bias. The 68 stations measuring both NO_2 and O_3 are represented on an hourly basis (black dots). Data from Víznar, a rural background station (light grey triangles) and Recoletos, urban traffic (dark grey squares) are also displayed. The vertical black curve represents the average concentration on the X-axis every 10 μg m^{-3} from the vertical axis.

Figure 5-8 shows the temporal series of the Recoletos (UT) and Víznar (RB) stations for O_3 and NO_2. There is a high correlation between O_3 and NO_2 in the two different environments.

The annual mean distribution of O_3 over the IP is shown in Figure 5-4b. Highest mean concentrations are located in the open Mediterranean Sea (up to 90 μg m^{-3}) and the Spanish Mediterranean coast (~80 μg m^{-3}). Such concentrations are favoured by the prevailing intense

photochemistry in the region (EEA, 2005; Vautard et al., 2005b), the local formation and transport (Lelieveld et al., 2002; Gerasopoulos et al., 2005; Cristofanelli and Bonasoni, 2009), the persistent subsidence over the region (Millán, 2002) and the low O_3 dry deposition over sea. The Spanish oceanic region in the north and north-western Spain, characterized by high frequency of precipitation presents lower O_3 levels than the Spanish arid and Mediterranean regions. The wet deposition of O_3 is an important sink in the oceanic regions, meanwhile local generation and transport are the processes which contribute to O_3 levels in arid and Mediterranean regions.
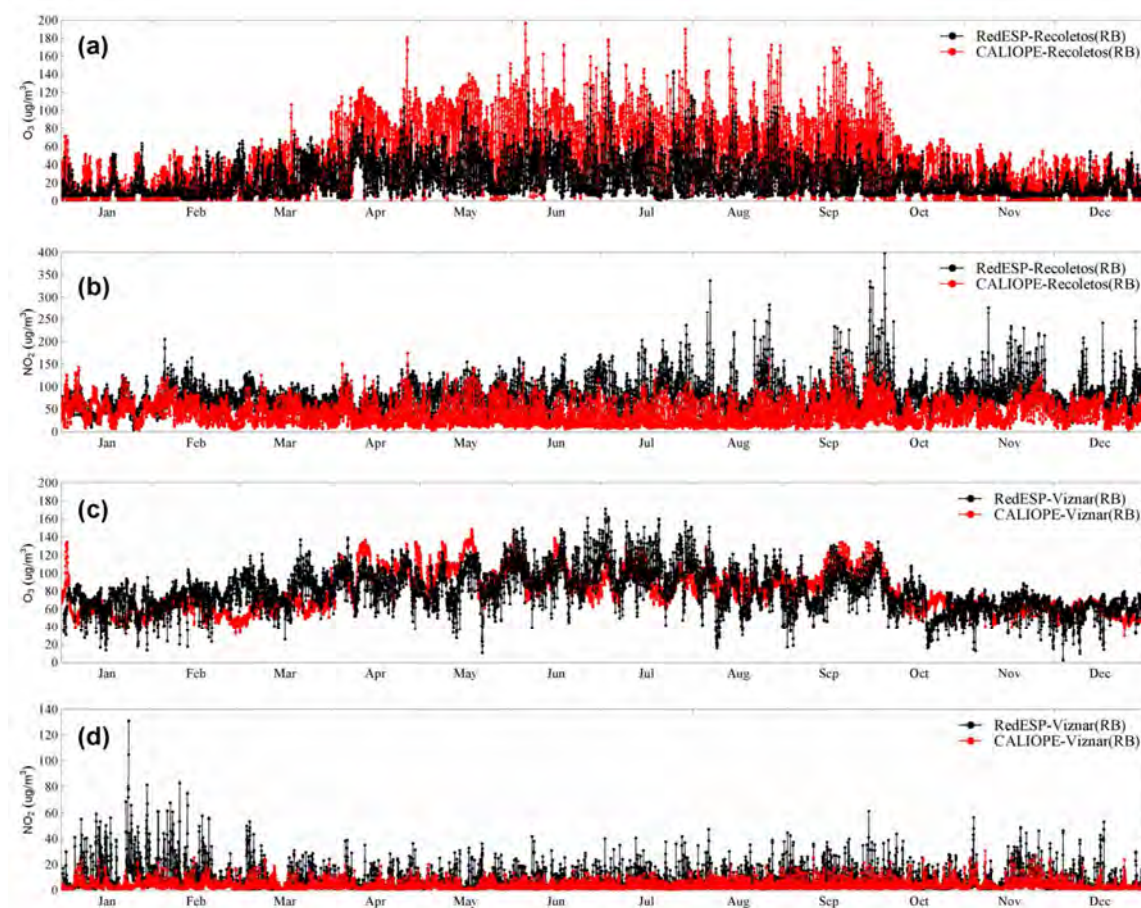
Figure 5-8. Modelled (marked red lines) and measured (marked black lines) time series of hourly mean concentrations (in $\mu g\ m^{-3}$) for O_3 and NO_2 at the urban traffic station (UT) of Recoletos (a and b, respectively) and at the rural background (RB) station of Víznar (c and d, respectively) over the year 2004.

Figure 5-4b also highlights significant levels over the major Spanish mountain ranges such as the Pyrenean chain, the Baetic Cordillera (southeastern Spain) or the Sierra Norte (laying north of Madrid in a west-to-northeast direction), reflecting the O_3 vertical gradient in the atmosphere.

O_3 is found lowest ($\sim50\ \mu g\ m^{-3}$) in either regions of low precursor emissions (northern and southern plateaus) or in areas affected by large NO-to-NO_2 concentration ratios (e.g., zones of intense on-road and ship traffic). Reactions involving nitrogen oxides are well-known key reactions controlling the amount of O_3 in the troposphere (Fishman and Crutzen, 1978). In this chemical

regime reactions between NO_2 and O_3 prevail, leading to low levels of O_3. These areas comprise the major Spanish metropolitan cities (i.e., Madrid, Barcelona, Valencia, Seville), highways of high traffic flow (like NO_2, see Section 5.3.1) and the major shipping routes in the Mediterranean Sea.

5.3.3 Sulphur dioxide

From a total of 45 stations measuring SO_2, 13 are located in urban areas, 14 are in suburban and 18 are in rural areas, respectively. In Spain, SO_2 is mainly produced by power generating and transformation industries. Indeed, Linares and Romero (2000) reported that electricity generation contributes 66% to the total SO_2 emitted in Spain. These very localized industries generate large plumes of high-SO_2 content affecting the air quality on a local to national scale. Modelling SO_2 for air quality purposes is a complex issue, since the accuracy in the meteorological patterns is crucial for the determination of plume dynamics. Also, the variability on the sub-grid scale must be considered when comparing model results with measured data.

The hourly SO_2 variability and levels, averaged over all available stations, are very well captured by the modelling system (Figure 5-3b). Episodic extreme values are underestimated in general, although the model is capable of reproducing the trend. Annual MB are low, from -3.1 for urban to 0.6 μg m^{-3} for suburban stations (Table 5-2). Due to the frequently episodic character of high SO_2 events and their dependency to meteorology correlation coefficients are rather low (r = 0.14 for urban/suburban stations; 0.28 for rural stations). Highest correlations were obtained for background stations (r = 0.34). MFB values show good performance comparing with the other primary pollutants (-47.1% < MFB < -23.8%) but MFE values highlight the need to further improve the modelled SO_2 physico-chemistry. Among the 45 stations measuring SO_2 in the Peninsula, the model-to-data comparison was distinctly unsatisfactory for three locations (7% of the total). Two of these locations were found in the same grid cell as large power plants (Abanto and Grao). A third station ("Salamanca2" in the city of Salamanca) displays high SO_2 measured concentrations which are strongly underestimated by the model. Such behaviour may be explained by emission sources unaccounted by the model system or by the erroneous coordinates of the instrument.

In Spain, Baldasano et al. (2008a) reported that combustion in energy and transformation industries contributes 83% to the total SO_2 emitted in Spain. In this framework, the SO_2 is emitted mainly from large isolated point sources, instantaneously mixed into high layers in the atmosphere and transported and dispersed following the plume dynamic. The mean chemical distribution of SO_2 over the IP, shown in Figure 5-4c, is characterized by two major patterns. First, the Spanish territory is marked by various emission hot-spots often reaching air concentrations above 15 μg m^{-3}. These localized sources originate mainly from power plants and refineries.

Northern Spain suffers substantial SO_2 mean annual levels of up to ~10 μg m^{-3} due to the presence of geographically close power plants and refineries in the area of Galicia, Ponferrada, Asturias and Bilbao. SO_2 reaches maximum levels (~50 μg m^{-3}) near the two refineries in Bilbao and La Coruña. The SO_2 dispersion pattern in north-western Spain is significantly dominated by the northern and north-western winds that transport SO_2 inland. Eastern Spain is mostly affected by a thermo-electrical power plant from Teruel (Aragón region), the pattern is dominated by the canalization of

the Ebro valley towards the Mediterranean sea. The southern Spanish plateau displays high SO_2 levels around Puertollano (Castilla-La Mancha region) due to the presence of a refinery and two power plants.

In the urban areas the SO_2 dispersive pattern remains ~6 μg m^{-3}; in Madrid and Barcelona cities the levels of SO_2 are the sum of two contributions, the on-road traffic and the cogeneration plants. Minimum concentrations from unpolluted areas display mean values near 0.5-2 μg m^{-3}.

The second pattern dissociated from this figure is the shipping route from the Atlantic, through the Strait of Gibraltar, toward the major Mediterranean harbours. Ship emissions are large contributors to the total SO_x concentrations along the main ship tracks due to fuel combustion of high sulphur content (Corbett and Fischbeck, 1997; Corbett and Koehler, 2003), although ship emission abatement strategies are under current application (Internacional Maritime Organization and Marine Environment Protection Committee, 2001). These emissions from maritime zones lead to coastal mean SO_2 concentrations from 2 to 8 μg m^{-3} on annual average, with a maximum of 12-18 μg m^{-3} in the narrow Gibraltar regions with a dispersion pattern dominated by western winds. The SO_2 contribution of shipping route in this area is combined with the contribution from one large refinery, industrial processes, and electric generation carried out in the Gibraltar bay.

5.3.4 Particulate matter

A total of 44 RedESP stations measured particulate matter concentrations over the IP and the Balearic Islands for the year 2004. 12 Stations were located in rural areas, 17 are in suburban and 15 are in urban areas, respectively. Among these 44 stations, the model represented the PM concentrations fairly well at 17 locations (nearly 40% of the total). These locations were mostly background rural. In these areas mean concentrations are often low with episodic high concentration peaks. The implementation of the Sahara desert dust contribution from the BSC-DREAM8b model is responsible for the satisfactory representation of such concentration peaks. The evaluation of the modelling system highlighted less accurate modelled levels at suburban and urban locations mostly influenced by background emissions. Model-to-data comparisons in urbanized areas of industrial or traffic emissions showed lowest accuracy. We attribute such behaviour to the inadequate characterization of emission sources in areas of intense human activity.

Figure 5-3c clearly highlights two distinct aspects of the model in the representation of hourly averaged PM10 concentrations at all available stations. Modelled concentrations were persistently underestimated throughout the year 2004. This underestimation is a common feature of most of the current regional models (Pay et al., 2010a). The annual MB amounts to -21.8 μg m^{-3} with an annual RMSE value of 33.4 μg m^{-3} (Table 5-2). On the other hand, the general PM10 dynamics are well captured, with the major events correctly modelled and synchronized with measured amounts. The mean correlation for all stations amounts to 0.38 with higher correlations at rural stations (r = 0.43, ranging from 0.28 to 0.58 per station). Due to the important underestimation of the model concentrations, MFB and MFE values are undoubtedly ranging above the criteria for acceptable model performances proposed by Boylan and Russell (2006).

Figure 5-4d shows the annual average pattern of natural and anthropogenic PM10 over the IP for 2004. Concentrations show a large variability across Spain depending on emission sources, climate and reactivity/stability of particulate species (see Querol et al., 2001, 2003, 2004b, 2008b; Rodríguez et al., 2002; Viana et al., 2005). The modelled spatial distribution of annual PM10 levels shows that particle concentrations reach high values (~15 μg m^{-3}) in large cities like Madrid, Barcelona, Valencia, and Bilbao. There is an important contribution of exhaust and non-exhaust emissions from road transport in urban areas.

Marine aerosols contribute nearly 3 and 5 μg m^{-3} to the annual mean PM10 concentration over the Mediterranean and Atlantic coasts, respectively (not shown). This difference in concentration reflects the higher wind speeds and fetch distances in the Atlantic than in the Mediterranean basin leading to more transport of sea salt aerosols from the Atlantic open ocean to the coasts. The contribution of marine aerosols to PM10 annual concentrations over the open ocean ranges from 6 (Mediterranean basin) to 9 μg m^{-3} (Atlantic) which is consistent with model data from Manders et al. (2010).

In the north, the industrial areas in Castellón dominated by ceramic industry, present high levels of PM10, dispersed along a perpendicular axis to the coast. Mediterranean coast shows PM10 dispersion pattern influenced by sea-breezes combined with upslope winds to create recirculations along the coast and within the western Mediterranean basin. In summer the higher temperatures and solar radiation lead to the formation of secondary aerosols contributing to the levels of particulate matter. The Ebro valley acts by channelling particulate matter flow inland. Meanwhile in the northern coastal Spain the Atlantic winds dominate the transport of particulate matter inland.

Large sources of SO$_2$ located in wet Spain region, in the north, (Figure 5-4c) do not contribute efficiently to the secondary inorganic aerosol since high dispersion and removal by wet deposition are important processes in this region (not shown). In the southern part of Spain, African dust outbreaks contribute significantly to the aerosol loadings, ranging from to 10 to 20 μg m^{-3}. The largest annual mean contribution of desert dust coincides with the Sierra Nevada mountain range with values reaching up to 30 μg m^{-3}. Such concentrations are the consequences of (1) the mountain range location within the main zone of dust deposition (70% of dust export is deposited within the first 2000 km, Jaenicke and Schütz, 1978) and (2) the existence of several peaks within the mountain range 3000 m above sea level (asl) which corresponds to the altitude range for Saharan dust transport (between 1500 and 4000 m asl, Talbot et al., 1986; Olmo et al., 2008).

5.4   Exceedances of ozone during summertime

This section analyses the O$_3$ exceedances during the high O$_3$ season (from April to September) when O$_3$ concentrations present peaks which frequently exceeded 120 μg m^{-3}, reaching 200 μg m^{-3}. The target value set in the European regulation is 120 μg m^{-3}, not to be exceeded on more than 25 days per calendar year averaged over 3 years (averaging as the maximum daily 8-h mean, European Commission, 2008). Figure 5-9 shows the number of days exceeding the concentration value of 120 μg m^{-3} for the 8-h maximum O$_3$ concentration and the VOC/NO$_x$ mass ratio over the land domain (Figure 5-9a) and over the entire domain, including the ocean (Figure 5-9b). The VOC/NO$_x$ ratio is

calculated as hourly average and is represented in logarithmic scale, since the ratio ranges from 1 to 10^6.
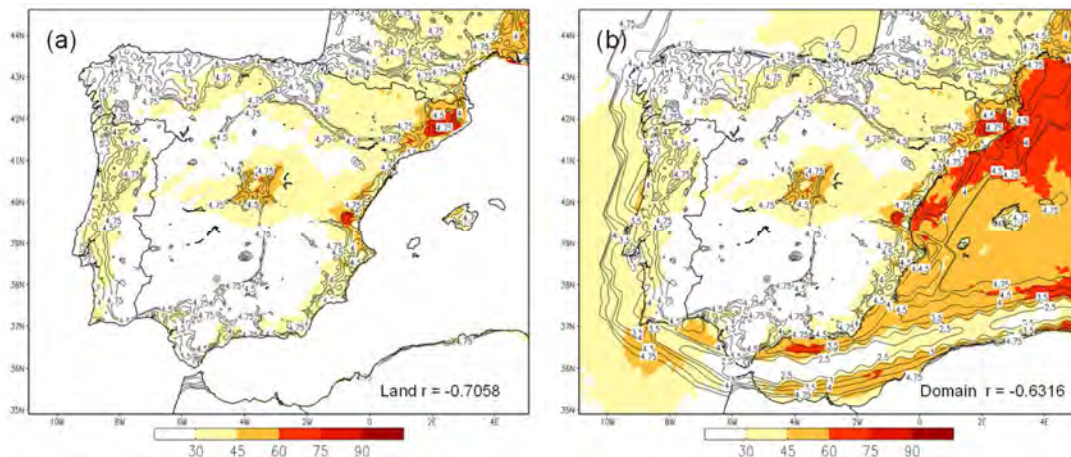
Figure 5-9. Days exceeding the concentration value of 120 μg m^{-3} for the 8-h maximum O_3 concentration (colour scale) and the logarithm of the VOC/NO_x concentration ratio (contour lines) during the high O_3 season (from April to September) in 2004 simulated by CALIOPE at a 4 km x 4 over the land domain (a) and the entire domain (b). In both cases, correlation between days exceeding the concentration value of 120 μg m^{-3} and the logarithm of the VOC/NO_x concentration ratio is showed at the bottom-right.

There is an overlap among ratios and number of days with exceedances. The number of exceedances is higher than 45 days where log(VOC/NO_x) ratio is between 3 and 4.5, approximately. Such situation corresponds to zones downwind of main NO_x emission sources (see annual mean concentration of NO_2 in Figure 5-4a) from the two largest Spanish cities (Madrid and Barcelona, see locations in Figure 5-9) and industrial areas along the eastern Spanish Mediterranean coast (Tarragona, Valencia and Castellón; see locations in Figure 5-9). Dynamics of pollutant during summer and primary emission sources along the eastern coast and the central plateau of the IP determinate the location of the calculated exceedances. Several studies performed over the western Mediterranean basin (e.g., Gangoiti et al., 2001; Jiménez and Baldasano, 2004; Stein et al., 2005; Jiménez et al., 2006c; Jiménez-Guerrero et al., 2008b; Gonçalves et al., 2009b) are in agreement with our findings. Along the coast the sea-breezes and mountain-valley winds contribute to the accumulation and recirculation of aged air masses and O_3 aloft. Besides, over the central plateau flows are dominated by the development of the IP Thermal Low (ITL). Several deep convective cells coupled with the ITL inject aged pollutant for the Madrid area and those transported previously from coastal area. On the other hand, the number of exceedances is less than 30 days for log(VOC/NO_x) ratio higher than 4.75, that regime, represented in white colour in Figure 5-9, covers the northern and southern Spanish plateaus, where there is no high density of anthropogenic emissions. Note that a quarter of the IP presents more than 30 days exceeding the value of 120 μg m^{-3} for the 8-h maximum O_3 concentration.

In general, there is a significant anti-correlation (r=-0.71) between O_3 exceedances and the $log(VOC/NO_x)$ ratio for the entire domain when only the inland O_3 formation is considered (Figure 5-9a). For high ratios, there is a NO_x limitation regime, and no O_3 exceedances are detected once there is not enough NO_x available. However, when we calculate the aforementioned correlation over the entire domain, including the ocean (Figure 5-9b), the anti-correlation slightly decreases (r=-0.63) as a result of two different behaviours. First, the Strait of Gibraltar region presents the lowest $log(VOC/NO_x)$ ratio (equal to 3) and no exceedances are detected (see Section 5.3.2). The frequent shipping traffic and the high density of industry in the area generate important NO_x emissions, VOC concentrations are not high enough to produce O_3; moreover the O_3 loss is high due to NO_x emissions act as O_3 sinks (Marmer et al., 2009). The opposite happens over the western Mediterranean basin which shows the highest $log(VOC/NO_x)$ ratio (over 5) and many exceeding days (more than 45). As we mentioned before, the complex layout of the coasts and surrounding mountain favours that the Mediterranean Sea acts as a reservoir of aged pollutants. Furthermore in summer the meteorological condition (high pressure, stability, clear sky and high solar radiation intensity) enhances photochemical processes and emissions of biogenic volatile organic compounds to the atmosphere (NO_x limited regime). Not only O_3 formation due to local and regional sources but also long-range transport of European air toward the Mediterranean basin (Lelieveld et al., 2002) could be important causes of the O_3 exceedances of the limit value. Furthermore, dry deposition over open oceans remains near zero (not shown here). All together contribute to increase levels of O_3 (lifetime typically of few weeks in summer, Seinfeld and Pandis, 1998).

5.5   Summary and conclusions

This work presents the evaluation and the assessment of the CALIOPE air quality forecasting system (namely WRF-ARW/HERMES/ CMAQ/BSC-DREAM8b) for a full-year simulation for 2004 over Spain. CALIOPE was applied with high resolution (4 km x 4 km, 1 h) using the HERMES emission model specifically developed for Spain. The evaluation of the modelling results for gas-phase pollutants (O_3, NO_2 and SO_2) and particulate matter (PM10) on an hourly basis showed a strong dependency of the performance of the model on the type of environment (urban, suburban and rural) and the dominant emission sources (traffic, industrial, and background). For NO_2, the best model behaviour corresponds to both background rural stations and urban stations located in very large cities such as Madrid or Barcelona. With respect to O_3, stations influenced by traffic emissions (NO_x-dominated) are better characterized with a more pronounced daily variability. NO_x/O_3 chemistry is better represented under non-limited-NO_2 regimes. For each station category, annual O_3 (hourly and peaks) statistics meet the range defined by the US EPA and European regulation for an acceptable performance of the model. Results show that a quarter of the Iberian Peninsula is affected by more than 30 days exceeding the value of 120 $\mu g\ m^{-3}$ for the 8-h maximum O_3 concentration.

The general spatial patterns and temporal characteristics simulated by CALIOPE for gas-phase pollutants and particulate matter are consistent with other studies and surveys. SO_2 is mainly produced from isolated point sources (power generation and transformation industries) which generate large plumes of high SO_2 concentration affecting the air quality on a local to national scale

where the meteorological pattern is crucial, whereas NO_2 concentration at ground level is dominated mainly by traffic emissions, which are subjected to a much stronger temporal variation than the SO_2 emissions.

PM10 and NO_2 mean levels are persistently underestimated. Highest PM10 mean bias corresponds to suburban and urban location mostly influenced by background emission. On the other hand, highest NO_2 errors are found in urban stations which are likely influenced by high local emission sources from urban activities. Such behaviour is attributed to the incomplete characterization of emissions from small cities and to the influence of the model resolution on sub-grid emission sources.

Despite the accurate performance of the modelling system, several aspects are now under further research in the framework of the CALIOPE project. Wind-blown dust should be taken into account since such source contributes to the underestimation of the total concentration of PM10, especially in dry and arid regions such Spain. Biomass burning and natural NO_x are currently not treated in the CALIOPE modelling system and could contribute to the NO_2 underestimation. In addition, ammonia emission and particulate matter from vegetated and agricultural areas in HERMES are under a continuous improvement. Last, a new version of CMAQ is being implemented in the MareNostrum supercomputing (CMAQv4.7) featuring a new aerosol module, AERO5, which contains substantial scientific improvements over the AERO4 released in version 4.5, especially devoted to improve secondary organic aerosol formation and dynamic interactions of fine and coarse aerosol.

The present analysis demonstrates that the high spatial resolution (4 km x 4 km) applied in the CALIOPE forecasting system correctly address the air pollution behaviour in (1) urban/industrial areas with a pervasive influence of anthropogenic emissions on a local scale and (2) areas with very complex terrains and meteorology like southern Europe. Therefore, the system has been implemented and evaluated operationally and air quality forecasts can be found in http://www.bsc.es/caliope.

6. Variability of concentration and speciation of particulate matter across Spain in the CALIOPE-IP system

6.1   Introduction

Particulate matter (PM) is of major scientific interest due to its demonstrated impact on human heath (WHO, 2006), ecosystems (Lovett et al., 2000), Earth's climate (Jacobson, 2001; Ramanathan et al., 2001; IPCC, 2007) and visibility (Hyslop and White, 2008). Although air quality in Europe has improved substantially over the past decades, air pollution by PM is a major threat to human health (EEA, 2010a). Not only do concentrations determine the effects of particles on human health, but also (1) their size, conditioning the degree of penetration into the respiratory system, (2) their composition, since the toxicity of the particles depends on the occurrence of specific hazardous PM compounds (Brauer et al., 1995) and (3) time of exposure. Although the effects of long-term exposure are much more uncertain than the effects of short-term exposure, they are believed to have a greater effect on health (Dockery et al., 1993; Pope et al., 2002). Recent studies carried out in Spain demonstrate that the levels of the finest PM fractions are important risk factors for daily cardiovascular mortality (Pérez et al., 2009; Maté et al., 2010) increasing the number of hospital admissions due to pollution caused by fine particles (Linares and Díaz, 2010a, b). Current European standards on air quality, driven by the directive 2008/50/EC (European Commission, 2008), set an annual limit value for PM10 (particles below 10 μm in diameter) of 40 μg m^{-3}; and a daily mean value of 50 μg m^{-3} should not be exceeded 35 times per year. For the first time, a European directive introduces a limit value for PM2.5 (particles below 2.5 μm in diameter) in the air quality standards to be accomplished in two stages: Stage I, a mean maximum annual limit value of 25 μg m^{-3} (deadline: 2015); and Stage II, a mean maximum annual limit value of 20 μg m^{-3} (deadline: 2020).

A number of studies (e.g. Sanz et al., 2000; Dueñas et al., 2002; Millán et al., 2002; Querol et al., 2004a, 2008b; Ribas and Peñuelas, 2004; Escudero et al., 2007a) show that the Iberian Peninsula (IP) exceeds some of the thresholds of air quality established in the legislation. Exceedances of the PM10 limit values were not only caused by anthropogenic emissions but also the long range transport of atmospheric mineral dust from deserts. The Sahara desert is one of the most important dust sources on the Planet, with northern Africa being responsible for half of the global emissions of mineral dust (Middleton and Goudie, 2001; Prospero et al., 2002). In the IP, the mineral fraction of PM comes mainly from local re-suspension and external contributions such as the

Saharan/Sahelian dust (Querol et al., 1998, 2001; Artíñano et al., 2001; Rodríguez et al., 2001, 2002).

Urban to regional air quality models play a key roles in assessing and understanding the dynamics of air pollution, forecasting the air quality and developing emissions abatement plans and alerting the population when health–related issues occur (European Commission, 2008). Examples of air quality forecasting systems currently operating in Europe are compiled in Menut and Bessagnet (2010) and in Balk et al. (2010), the latter in the framework of the COST ES0602 action (www.chemicalweather.eu), which also complement other air quality European initiatives such as the Global Monitoring for Environment and Security (GEMS , http://www.gmes.info/), PROtocol MOniToring for the GMES Service Element (PROMOTE , http://www.gse-promote.org/) and Monitoring Atmospheric Composition and Climate (MACC, htpp://www.gmes-atmosphere.eu/). Regional air quality models are useful tools to describe the continental transport of air pollutants. However, a higher spatial resolution is required to evaluate the exposure of the population to PM pollution in urban areas, especially over complex topography such as over the IP (Jiménez et al., 2006c). Up to now, there are several evaluation studies demonstrating the difficulty for models to simulate PM10 and PM2.5 concentration over Europe (Pay et al., 2010a and references therein). Most of them deal with regional background stations, mainly from EMEP network, and quantify the model performance to reproduce regional background aerosols. Overall these show a large gap between simulated and observed PM10 concentration (broadly a factor of 2) due to deficiencies in the physical and chemical understanding of the processes which lead to the formation of secondary aerosol and to the lack of accurate particulate matter emission inventories. It is worth noting that only a few published works (Hodzic et al., 2005; Flaounas et al., 2009; Chemel et al., 2010) report on performance characteristics of long-term aerosol simulations over urban domains hampered by the lack of measured PM compounds.

The CALIOPE modelling system is a state-of-the-art modelling system, specially developed with high spatial (4 km x 4 km) and temporal resolution (1 h) to forecast air quality across Spain. The modelling system was first evaluated in Pay et al. (2010a) for Europe, and Baldasano et al. (2011) for Spain, including gas and particulate pollutants over the full year 2004. The purpose of the present paper is to complement these results by (1) providing a detailed quantitative analysis of the capabilities of the CALIOPE modelling system to simulate daily aerosol distribution over Spain in terms of concentration, size and chemical composition, and (2) estimating and assessing the spatial and seasonal distribution of the different aerosols over Spain based on comparing model outputs and observations. The study is carried out for the full year 2004 for two main reasons: (1) the HERMES emission database was compiled for this year and (2) a number of data sets on levels of PM compounds are available for this year. An important novel approach of this work is the evaluation of the BSC-DREAM8b model using an experimental data set of African PM10-dust obtained with the methodology described in Escudero et al. (2007b). In addition, measurements of chemically speciated aerosol are available in a long time series for 2004 for different environments, which allow evaluating the skill of CALIOPE to reproduce PM in urban/suburban/rural areas.

The outline of the paper is as follows. Section 6.2 describes the CALIOPE system and the observational datasets used for the evaluation. In Section 6.3, measurements of aerosol size and

composition from IDAEA-CSIC/EMEP are used to identify the origin of the discrepancies in modelled aerosol and to quantify the deviation from observations. It also estimates and assesses the spatial and seasonal distribution of aerosols over Spain, for both size and composition, taking into account the discrepancies outlined in the previous section. Finally, conclusions and suggestions for further work are given in Section 6.4.

6.2 Methods

6.2.1 Modelling system formulation

The CALIOPE project has established an air quality forecasting system for Spain (Baldasano et al., 2008b). Current forecasts and near real-time evaluation are available through http://www.bsc.es/caliope/. CALIOPE encompasses a high-resolution air quality forecasting system being applied to Europe as a mother domain (12 km x 12 km, 1 hr) (Pay et al., 2010a) and Spain as the nested domain (4 km x 4 km, 1 hr) (Baldasano et al., 2011).

Meteorological input data for the chemistry transport model are calculated using the Advanced Research Weather Research and Forecasting (WRF-ARW) model v3.0.1.1 (Michalakes et al., 2004; Skamarock and Klemp, 2008). For the Spanish domain WRF-ARW is configured with a grid of 397 x 397 points corresponding to a 4 km x 4 km horizontal resolution and 38 σ vertical levels with 11 characterizing the planetary boundary layer (PBL). The model top is defined at 50 hPa to resolve the troposphere-stratosphere exchanges properly.

The Models-3 Community Multiscale Air Quality Modeling System (Models-3/CMAQ, Byun and Schere, 2006), is a three-dimensional Eulerian photochemical transport model that uses state-of-the-science routines to model the behavior of air pollutants from regional to local scales, due to its generalized coordinate system and its advanced nesting grid capability. CMAQ version 4.5, used in this study, has been extensively evaluated under various conditions and locations in the US (Appel et al., 2007, 2008; Roy et al., 2007), European continent (Matthias, 2008; Pay et al., 2010a), and Spain (Jiménez et al., 2006c; Baldasano et al., 2011). It includes gas, aerosol and heterogeneous chemistry. According to the work by Jiménez et al. (2003) the photochemical mechanism used in this study is the Carbon Bond IV mechanism (CBM-IV, Gery et al., 1989).

The aerosols are modelled using the AERO4 module (Binkowski and Roselle, 2003). This module comprises the following aerosol compounds: nitrate, sulphate, ammonium, elemental and organic carbon (with three subcomponents: primary, secondary anthropogenic and secondary biogenic), soil, sodium, and chlorine. Unspecified anthropogenic aerosols and aerosol water are additionally kept as separate components. Aerosols are represented by three size modes (Aitken, accumulation and coarse mode) each of them assumed to have a lognormal distribution. The coarse particles mode is treated as dry and chemically inert with a fixed geometric standard deviation of 2.2 (Kelly et al., 2010), thus there is no dynamic interaction between the fine and coarse mode. Secondary inorganic aerosols (SIA) are generated by nucleation processes from their precursors to form nitrate ammonium and non-marine sulphate aerosols. The thermodynamic equilibrium between gas and

inorganic fine aerosols is determined by the ISORROPIA model (Nenes et al., 1998). Secondary organic aerosol (SOA) can be formed from aromatics (anthropogenic organic aerosols) and terpenes (biogenic organic aerosols) (Schell et al., 2001). The production of sea-salt aerosol (SS) is implemented as a function of wind speed and relative humidity (Gong, 2003; Zhang et al., 2005) through the AERO4 aerosol module. Aerosol deposition is treated by a second-generation deposition velocity scheme (Binkowski and Shankar, 1995; Venkatram and Pleim, 1999). In this study simulated PM concentrations do not include the water mass and Stokes diameter are used for characterizing aerosol geometry.

Emissions are processed using the HERMES model (Baldasano et al., 2008a) specifically developed for Spain. Anthropogenic emissions are calculated by sector-specific sources or by individual installations and stacks following a bottom-up approach. Emissions are derived from the aggregation in space from 1 km x 1 km to 4 km x 4 km. According to natural biogenic emissions, HERMES calculates volatile organic compounds from vegetation as a function of temperature and photosynthetically active radiation (Guenther et al., 1995; Parra et al., 2004, 2006). Land-use categories for each grid cell are obtained from CORINE Land Cover 2000 map starting with a resolution of 100 m. In this study HERMES provides a comprehensive description of the gas-phase primary emissions speciated to the CBM-IV chemical speciation profile. The CBM-IV mechanism in CMAQv4.5 is modified from the original in Gery et al. (1989) in order to include gaseous species that are necessary to link gas-phase chemistry to aerosol formation (sulfuric acid, toluene, xylene, cresol, and monoterpenes). On the other hand, HERMES estimates PM10 and PM2.5 primary emission from anthropogenic origin, and after that it especiates fine particles in (1) organic aerosol, (2) elemental carbon, (3) sulphate, (4) nitrate; and (5) other fine PM based on profiles in SPECIATE 3.2 (http://www.epa.gov/ttn/chief/emch/speciation/cbiv-profiles_mar_4_2002.xls), which is sector dependent. Note that HERMES quantifies PM emissions resulting from paved road resuspension (Pay et al., 2010b) which is an important feature for PM10 studies in urban air pollution (Querol et al., 2008b; Amato et al., 2010).

Due to the importance of trans-boundary air pollution, HERMES also estimates emissions from Portugal and southern France using a top-down approach from the EMEP emission inventory (50 km x 50 km horizontal resolution) spatially disaggregated to 4 km x 4 km horizontal resolution.

The CMAQ horizontal grid resolution corresponds to that of WRF. Its vertical structure was obtained by a collapse from the 38 WRF layers to a total of 15 layers steadily increasing from the surface up to 50 hPa with a stronger density within the PBL. The mean altitude of the lowest layer of CMAQ in CALIOPE system is of 19.5 ±0.5 m above ground level. Boundary and initial conditions are derived from CALIOPE-EU simulation (12 km x 12 km grid for Europe and 1 hour in time) (Pay et al., 2010a).

The long-range transport of mineral dust from Sahara desert is modelled by BSC-DREAM8b (Pérez et al., 2006a,b) over the domains of study. In this framework, the model results for PM in both domains are achieved by adding the Saharan dust contribution from BSC-DREAM8bin to the CMAQ anthropogenic species over the accumulation- and coarse modes following the work by Jiménez-Guerrero et al. (2008a).

As CALIOPE is a fundamental model system, the authors wish to stress that apart from the discussion of Figure 6-4, Figure 6-7, Figure 6-10, and Figure 6-11 neither correction factors nor any adjusting model parameterization were applied to the model output or the original model codes.

6.2.2 Particulate matter observations in Spain: levels and chemical speciation

The levels and chemical speciated aerosol simulated by CALIOPE are compared against observations provided by the IDAEA-CSIC (Institute of Environmental Assessment and Water Research, Spanish Research Council). They provided measurements from selected Spanish stations for the whole year 2004. Figure 6-1 shows the location of the 25 stations which accomplish the objectives of spatial cover for representing most of the geographical areas in Spain and also anthropogenic activities. Thus, the selected stations are representative of the rural background, sub-urban background, urban background and urban-industrial background. Table 6-1 provides detailed characteristics of the aforementioned stations.
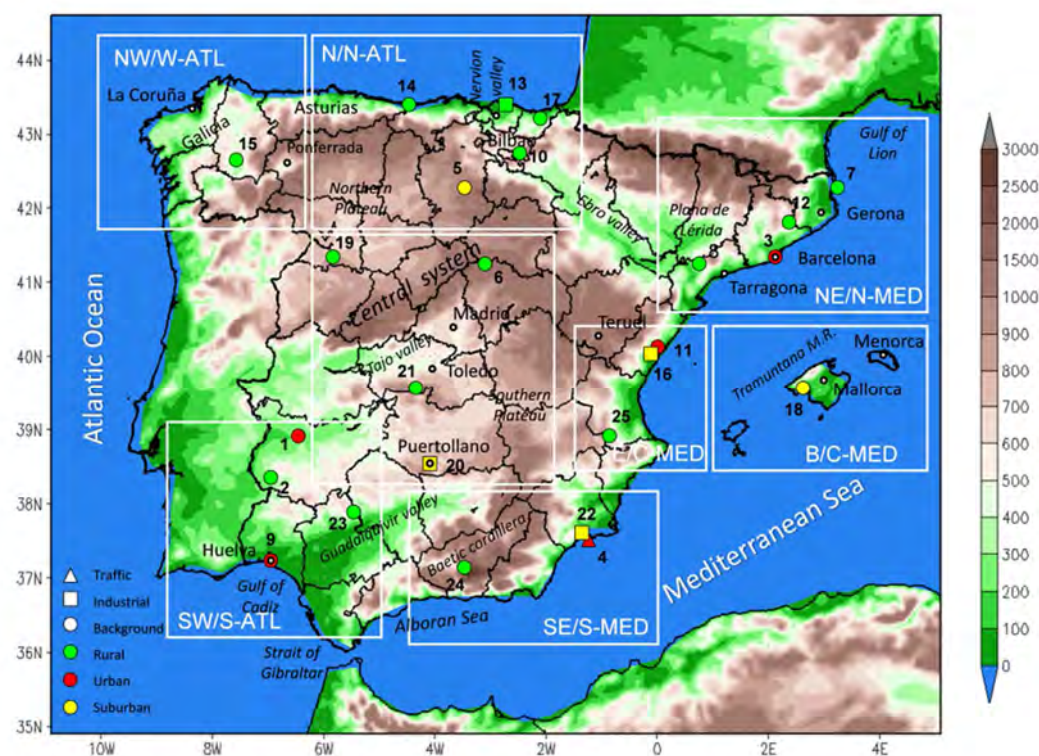
Figure 6-1. Location and type of the IDAEA-CSIC and EMEP stations over Spain with data available on a daily basis in 2004. Different types of stations are represented by symbols and color codes. The various symbols represent the major emissions types affecting each station (Traffic: triangle; Industrial: square; and Background: circle) while the colors reflect the environment of each station (Urban: red; Suburban: green; and Rural: orange). The map is split in eight zones in accordance with the geographical area. Table 6-1 lists the main characteristics and numbers of each station. Color chart represents terrain elevation in meters. Black circles indicate place names. Names in italic show geographical systems.

Besides PM10 and PM2.5 concentrations, six aerosol components are considered: total carbon (TC), sea salt (as sum of marine sulphate, chloride and sodium), non-marine sulphate (nm-SO$_4^{2-}$), nitrate (NO$_3^-$), ammonium (NH$_4^+$) and desert dust.

Table 6-1. Location and characteristics of the stations for 2004.

	Lat.[a]	Lon.[a]	Alt (m)	Source	Station Name	Code Name	Costal[b]	Geo.[c]	Type[d]	PM10	PM2.5	Speciated[e] PM2.5	SS[f]	DD[g]
1	+38.908	-6.359	188	IDAEA-CSIC	Badajoz	BAD	-	SW	UB	363	363	58	52	-
2	+38.476	-6.923	393	EMEP	Barcarrota	BAR	-	SW	RB	343	343	-	-	106
3	+41.385	+2.119	68	IDAEA-CSIC	Barcelona	BARC	N-MED	NE	UB	344	344	84	53	-
4	+37.604	-0.978	20	IDAEA-CSIC	Basterreche	BAS	S-MED	SE	UT	366	-	-	78	-
5	+42.335	-3.638	889	IDAEA-CSIC	Burgos	BUR	-	N	SB	350	366	85	87	-
6	+41.281	-3.143	1360	EMEP	Campisábalos	CAM	-	C	RB	323	304	-	-	70
7	+42.319	+3.316	23	EMEP	Cap de Creus	CAP	N-MED	NE	RB	326	317	-	-	57
8	+41.395	+0.721	470	EMEP	Els Torms	ELS	-	NE	RB	341	336	-	-	65
9	+37.270	-6.924	10	IDAEA-CSIC	Huelva	HUL	S-ATL	SW	UB	362	312	43	44	-
10	+42.653	-2.501	810	RedESP	Izki	IZK	-	N	RB	159	-	-	-	39
11	+40.074	-0.213	175	IDAEA-CSIC	L'Acora	LAC	C-MED	E	UB	283	31	-	88	-
12	+41.780	+2.378	730	IDAEA-CSIC	Montseny	MON	-	NE	RB	320	320	37	113	59
13	+43.406	-2.704	116	RedESP	Mundaka	MUN	N-ATL	N	RI	283	-	-	-	35
14	+43.439	-4.850	134	EMEP	Niembro	NIE	N-ATL	N	RB	228	228	-	-	20
15	+42.634	-7.703	506	EMEP	O Saviñao	OSA	W-ATL	NW	RB	333	306	-	-	28
16	+39.963	-0.250	163	IDAEA-CSIC	Onda	OND	C-MED	E	SI	191	26	-	58	-
17	+43.250	-2.155	215	RedESP	Pagoeta	PAG	N-ATL	N	RB	283	-	-	-	38
18	+39.564	+2.623	117	IDAEA-CSIC	Palma	PAL	C-MED	B	SB	315	-	75	71	81
19	+41.288	-5.867	985	EMEP	Peñausende	PEÑ	-	C	RB	348	339	-	-	65
20	+38.683	-4.089	670	IDAEA-CSIC	Puertollano	PUE	-	C	SI	302	-	98	97	-
21	+39.522	-4.353	1241	EMEP	Risco Llano	RIS	-	C	RB	327	326	-	-	69
22	+37.652	-1.018	15	IDAEA-CSIC	Santa Ana	SAN	S-MED	SE	SI	-	323	83	-	-
23	+37.996	-5.666	569	RedESP	Sierra Norte	SIE	-	SW	RB	292	-	-	-	96
24	+37.237	-3.534	1230	EMEP	Viznar	VIZ	-	SE	RB	351	344	-	-	118
25	+39.086	-1.102	885	EMEP	Zarra	ZAR	-	E	RB	353	355	-	-	84

[a] "+" is used to indicate North latitude and East longitude; "-" is used to indicate South latitude and West longitude.
[b] Classification of the coastal stations according to their location: northern Mediterranean (N-MED), central Mediterranean (C-MED), southern Mediterranean (S-MED), southern Atlantic (S-ATL), northern Atlantic (N-ATL), western Atlantic (W-ATL)
[c] Classification of the stations according to the geographical area: southeastern Spain (SE), southwestern Spain (SW), Balearic Islands (B), eastern Spain (E), central Spain (C), northeaster Spain (NE), northern Spain (N), northwestern Spain (NW).
[d] Classification of the stations according to the area type where they are located (first code: urban (U), suburban (S), and rural (R)), and according to what type of sources dominates the air pollution levels at the station (second code: traffic (T), industrial (I), and background (B)) following the specifications described in the Council Decision 97/101/EC dated January 27, 1997 (OJ L 35, 5.2.1997, p.14) and amended by Commission Decision 2001/752/EC (OJ L 282, 26.10.2001, p.69).
[e] Speciated aerosol measurements corresponding to nitrate (NO$_3^-$), ammonium (NH$_4^+$), nm-sulfate (nm-SO$_4^{2-}$), total carbon (TC).
[f] Sea-salt aerosol (SS) indicates the speciated aerosol corresponding to the sum of sodium (Na$^+$), chlorine (Cl$^-$) and marine sulfate in the PM10 fraction.
[g] Desert dust (DD) indicates the dust load from the Sahara desert in the PM10 fraction.

Measured PM10 and PM2.5 concentrations are estimated by means of the standard gravimetric method according with the Directive 1999/30/EC. Bulk acid digestion and water extraction were applied to sub-samples, as described by Querol et al. (2001). Non-mineral carbon concentrations are quantified indirectly by a CHNS elemental analyzer after subtraction of Carbon from $CaCO_3$, as deduced stoichiometrically from experimental Ca levels. The soluble anions (SO_4^{2-}, NO_3^- and Cl^-) in the water extracts were quantified by ion chromatography. NH_4^+ analyses were performed by FIA colorimetry or ion specific electrode. Marine aerosol is determined as the sum of the Na^+ (ICP-AES) and Cl^- (ion chromatography).

Desert dust from Sahara is estimated by a new methodology developed by the IDAEA-CSIC (Escudero et al., 2007b) which estimates daily African PM load during dust outbreaks in southern Europe. The daily net dust load in PM10 attributable to an African episode in a given region can be obtained by subtracting the daily regional background level (RB) from the PM10 concentration value for the day with African dust outbreak at the rural station. The RB is obtained from the monthly moving 40th percentile from the PM10 time series after a prior extraction of the data of the days with African dust transport.

6.2.3 Evaluation methods

Modelled raw outputs are post-processed in order to be compared with quantified measured aerosols. A list of CMAQ aerosol module variables can be found in Binkowski and Roselle (2003) and the sea-salt species have been updated in CMAQv4.5 as described by Shankar et al. (2005). From these variables, fine-particles [nm-SO_4^{2-}], [NO_3^-], [NH_4^+], [TC] are approximated by summing the appropriate Aitken- and accumulation-mode concentrations. TC is estimated by summing the modelled concentrations of primary organic aerosol, anthropogenic and biogenic secondary organic aerosol (SOA) and elemental carbon. To compare with measured PM10 sea-salt aerosol (SS), modelled sodium and chlorine (both in accumulation and coarse mode) and sulphate (coarse mode) are counted in the variable SS (SS = $[SS]_{fine}$ + $[SS]_{coarse}$). Modelled PM10 desert dust (DD) is estimated from BSC-DREAM8b corresponding bins $\leq 10\ \mu m$ (DD = $[DD]_{fine}$ + $[DD]_{coarse}$).

The BSC-DREAM8b is run offline and the outputs are then added to the CMAQ-calculated PM (Jiménez-Guerrero et al., 2008a). BSC-DREAM8b used a 50 km x 50 km horizontal resolution for integrations; its outputs are interpolated to the CMAQ's Lambert conformal conic grid with a 4 km x 4 km horizontal resolution in order to add the corresponding aerosol compounds. After the interpolation, fine-particle mass is approximated by summing the modelled concentrations of all Aitken- and accumulation-mode species from CMAQ (PM_{i+j}) and the corresponding BSC-DREAM8b bins with diameter $\leq 2.5\ \mu m$ ($[DD]_{fine}$) (Eq. 6-1):

$$PM2.5 = [nm\text{-}SO_4^{2-}] + [NO_3^-] + [NH_4^+] + [TC] + [SS]_{fine} + [DD]_{fine} + \text{Unspeciated Mass}_{fine} \qquad (6\text{-}1)$$

Analogously, modelled PM10 is the sum of the Aitken, accumulation- and coarse-mode (2.5-10µm) species from CMAQ (PM_{i+j+k}) and the corresponding BSC-DREAM8b bins with diameter $\leq 10\ \mu m$ (Eq. 6-2):

$$PM10 = PM2.5 + [SS]_{coarse} + [DD]_{coarse} + \text{Unspeciated Mass}_{coarse} \qquad (6\text{-}2)$$

Note that PM_{i+j} and PM_{i+j+k} are used as an approximation of PM2.5 and PM10, respectively, since measurements (PM2.5 and PM10) are based on aerodynamic diameters and model only considers the Stokes diameter to characterize the aerosol geometry. For more detail on this issue, see Jiang et al. (2006).

It is worth mentioning that CMAQv4.5(AERO4) only estimates $nm\text{-}SO_4^{2-}$, NO_3^-, and NH_4^+ in the fine fraction. Meanwhile, calcium and sodium salts with SO_4^{2-} and NO_3^- are not taken into account, since coarse mode is modelled as chemically inert.

Representativeness challenges continue to be present whenever gridded simulations are compared to observed data at a point in time and space as chemistry transport models simulations represent a volumetric average over an entire grid cell, meanwhile the stochastic compound embedded in the observations is not accounted for. Measurements have their own uncertainty due to biases and artifacts related to sampling and laboratory analysis methods. The European legislation (2008/50/EC) requires that the uncertainty of PM10 and PM2.5 measurements meet the quality objective of 25%. However, legislation does not establish uncertainty criteria for chemical species yet. According to Putaud et al. (2004), inorganic species may be accurately measured with an uncertainty of about ±10% for major species. Consideration of uncertainties and spatial scale should be given when comparing model simulation and ambient measurements for model performance evaluation because neither one represents the absolute truth.

Hence, a variety of statistical metrics and graphic methods are used to compare the observed and modelled concentrations (Dennis et al., 2010). Besides mean and standard deviation of modelled and measured values we calculate Mean Bias (MB), Root Mean Square Error (RMSE), correlation coefficient (r) and the fraction of modelled concentrations that are within a factor of two and five of the measured values. We also calculate the Mean Fractional Bias (MFB) and the Mean Fractional Error (MFE) following the recommendation of Boylan and Russell (2006). They proposed that the model performance goal is met when both the MFE and MFB are less than or equal to 50% and ±30%, respectively. The model performance criterion is met when both MFE $\leq 75\%$ and MFB ±60%. These criteria and goals are selected to provide metrics for the CALIOPE performances. Since measurements are on a daily basis, aerosols are compared in terms of daily averages from the modelling system.

6.3　Results and discussions

The annual and seasonal statistics averaged over all studied stations based on a daily values are indicated in Table 6-2. Scatter plots of the observed and modelled annual average concentration of each aerosol compound by station are shown in Figure 6-2, where points represent the annual mean and lines indicate the 75th and 25th percentile distribution of observed (horizontal lines) and modelled (vertical lines) concentrations.

6.3.1 Evaluation of PM2.5 and PM10

A total of 18 and 24 stations are used to evaluate the simulated PM2.5 and PM10 concentrations, respectively (Table 6-1 and Figure 6-1). For PM2.5 (PM10), 11 (15) stations are located in rural areas, 3 (4) in suburban areas, and 4 (5) in urban areas. In both cases rural background stations account for more than 50% of the number of sites (61% for PM2.5 and 58% for PM10).

Table 6-2. Annual and seasonal statistics for modeled aerosol calculated at IDAEA-CSIC stations in 2004. The calculated statistics are: Observed Mean (OM, µg m^{-3}), Modelled Mean (MM, µg m^{-3}), Mean Bias (MB, in µg m^{-3}), correlation coefficient (r), Root Mean Square Error (RMSE, in µg m^{-3}), normalized ratio of standard deviations of the modeled mean (σ(Mod./Obs.)). Data indicates the number of pairs model-observation used to calculate the statistics.

		Data	OM	MM	MB	R	RMSE	σ(Mod./Obs.)	% within factor 2
PM10	Annual	7,889	23.5	8.0	-15.5	0.59	22.3	0.45	21
	Winter	1,949	20.4	5.4	-15.0	0.52	23.7	0.24	18
	Spring	1,964	21.2	6.7	-14.5	0.60	19.4	0.46	16
	Summer	2,002	27.8	11.1	-16.7	0.59	24.6	0.51	27
	Fall	1,953	24.2	8.6	-15.6	0.64	21.1	0.50	24
PM2.5	Annual	5,253	14.2	5.6	-8.7	0.46	12.6	0.64	24
	Winter	1,255	14.0	3.6	-10.4	0.55	15.2	0.29	16
	Spring	1,246	13.4	4.6	-8.8	0.48	12.0	0.58	18
	Summer	1,387	15.7	7.9	-7.8	0.48	11.6	0.75	33
	Fall	1,350	13.8	6.0	-7.7	0.51	11.3	0.71	29
nm-SO$_4^{2-}$	Annual	563	3.5	1.4	-2.1	0.62	2.9	0.46	30
	Winter	127	2.9	0.7	-2.2	0.46	3.4	0.18	10
	Spring	147	3.3	1.2	-2.0	0.65	2.5	0.47	28
	Summer	149	4.3	2.2	-2.1	0.68	2.7	0.54	44
	Fall	140	3.5	1.4	-2.1	0.73	2.8	0.38	34
NO$_3^-$	Annual	563	1.7	0.7	-1.0	0.36	2.3	0.39	31
	Winter	127	2.6	0.7	-1.9	0.34	3.5	0.23	25
	Spring	147	1.9	0.8	-1.1	0.28	2.4	0.43	28
	Summer	149	0.7	0.5	-0.2	0.22	0.9	0.75	40
	Fall	140	1.6	0.8	-0.8	0.49	2.0	0.05	32
NH$_4^+$	Annual	563	1.9	0.6	-1.3	0.34	2.1	0.47	21
	Winter	127	1.9	0.6	-1.3	0.42	2.4	0.27	21
	Spring	147	2.1	0.6	-1.5	0.32	2.2	0.44	21
	Summer	149	1.8	0.3	-1.4	0.15	2.1	0.40	12
	Fall	140	1.7	0.7	-1.0	0.48	1.6	0.71	29
TC	Annual	563	5.1	1.4	-3.7	0.45	4.9	0.42	20
	Winter	127	5.8	1.3	-4.5	0.53	6.0	0.31	11
	Spring	147	4.3	1.2	-3.0	0.51	3.9	0.50	17
	Summer	149	4.6	1.4	-3.2	0.31	4.2	0.50	25
	Fall	140	5.7	1.7	-4.0	0.43	5.4	0.41	26
SS	Annual	738	1.2	0.9	-0.3	0.65	1.2	1.17	41
	Winter	153	1.3	0.9	-0.4	0.70	1.2	1.14	34
	Spring	210	1.3	1.0	-0.3	0.71	1.2	1.07	37
	Summer	193	1.2	1.1	-0.1	0.52	1.1	1.44	47
	Fall	182	1.2	0.7	-0.4	0.62	1.1	1.09	44
DD	Annual	1,030	19.4	13.5	-5.9	0.47	21.9	0.68	37
	Winter	88	14.4	5.3	-9.1	0.18	30.5	4.45	16
	Spring	228	17.0	8.3	-8.7	0.44	17.9	0.73	19
	Summer	409	22.0	16.9	-5.0	0.45	26.5	0.61	43
	Fall	305	19.2	15.1	-4.1	0.68	12.9	1.08	48

Figure 6-2a and b show that modelled PM2.5 and PM10 daily values are in good agreement with observations (r is 0.46 for PM2.5 and 0.59 for PM10) although modelled concentrations present a systematic negative bias. Differences in model performance for PM2.5 and PM10 are related to the major compounds in both fractions. CALIOPE's results indicate that over Spanish rural background areas carbonaceous and secondary inorganic aerosol are the major compounds in PM2.5, these account for 50-90% (30-70%) to PM2.5 (PM10), meanwhile mineral dust is the second contributor in PM10, it contributes 5-30% (10-50%) to PM2.5 (PM10). Based on correlation coefficients (Table 6-2), the model presents more accurate skills to reproduce the temporal evolution for PM10 than for PM2.5, which gives an indication that the main transport pattern are correctly represented by CALIOPE. In terms of normalized standard deviations, the amplitude of the daily variation is better reproduced for PM2.5 than for PM10 (0.64 versus 0.45, respectively), especially in summer, which suggests that modelled coarse particles daily variation seem to be too low. One source of underestimation in coarse particles is related to the fact that CMAQv4.5(AERO4) does not consider the formation of $Ca(NO_3)_2$ and $NaNO_3$ salts in the coarse fraction which are significant in Spain from mid-spring to mid-autumn (Rodríguez et al., 2002; Querol et al., 2008b).

Figure 6-2a and b show that the model skills are different at each site. Since all stations of the same category display similar features, the results are discussed in terms of the mean values, averaged over all rural (Figure 6-3a and b), suburban (Figure 6-3c and d) and urban (Figure 6-3e and f) stations. For more details, time series for representative stations are shown in Figure AIII – 2, Annex III.

Time series for PM2.5 and PM10 at rural sites show that model reproduces observations with correlation coefficients reaching 0.47 (PM2.5) and 0.65 (PM10), and with mean bias of -5.4 $\mu gPM2.5$ m^{-3} and -10.1 $\mu gPM10$ m^{-3}. Modelled PM at urban and suburban stations presents similar performance, the correlation coefficients reach r of 0.49-0.52 (PM2.5) and 0.47-0.51 (PM10) and annual MB are around -16 $\mu gPM2.5$ m^{-3} and -25 $\mu gPM10$ m^{-3}, in both environments. Therefore, it can be deduced that 35% (40%) of the PM2.5 (PM10) bias at urban and suburban stations is due to the underestimation of the regional background levels.

Overall, CALIOPE reproduces the observed PM daily variability along the year, with spring-summer maxima and the minimum levels in April, November and December. Modelled PM presents the best skills in summer (Table 6-2), when high PM levels are related to the low wet deposition (related to low humidity), low air mass renovation capacity due to the stable anticyclonic situation which generate recirculation episodes and accumulation in coastal areas (Baldasano et al., 1994; Millán et al., 1997), high natural resuspension of soil particles, enhanced frequency of African dust episodes and a high formation capacity of secondary aerosols by photochemical activity (Viana et al., 2002; Escudero et al., 2005). During this season the model is able to capture the amplitude of the daily variation for PM2.5 and PM10 ($\sigma(Mod./Obs.) = 0.75$ and $\sigma(Mod./Obs.) = 0.51$, respectively). Also high performances of CALIOPE are found during April, beginning November and December (Figure 6-3a and b), where PM variability is attributed to the higher frequency of advection of Atlantic air masses, associated with a high rainfall rate.
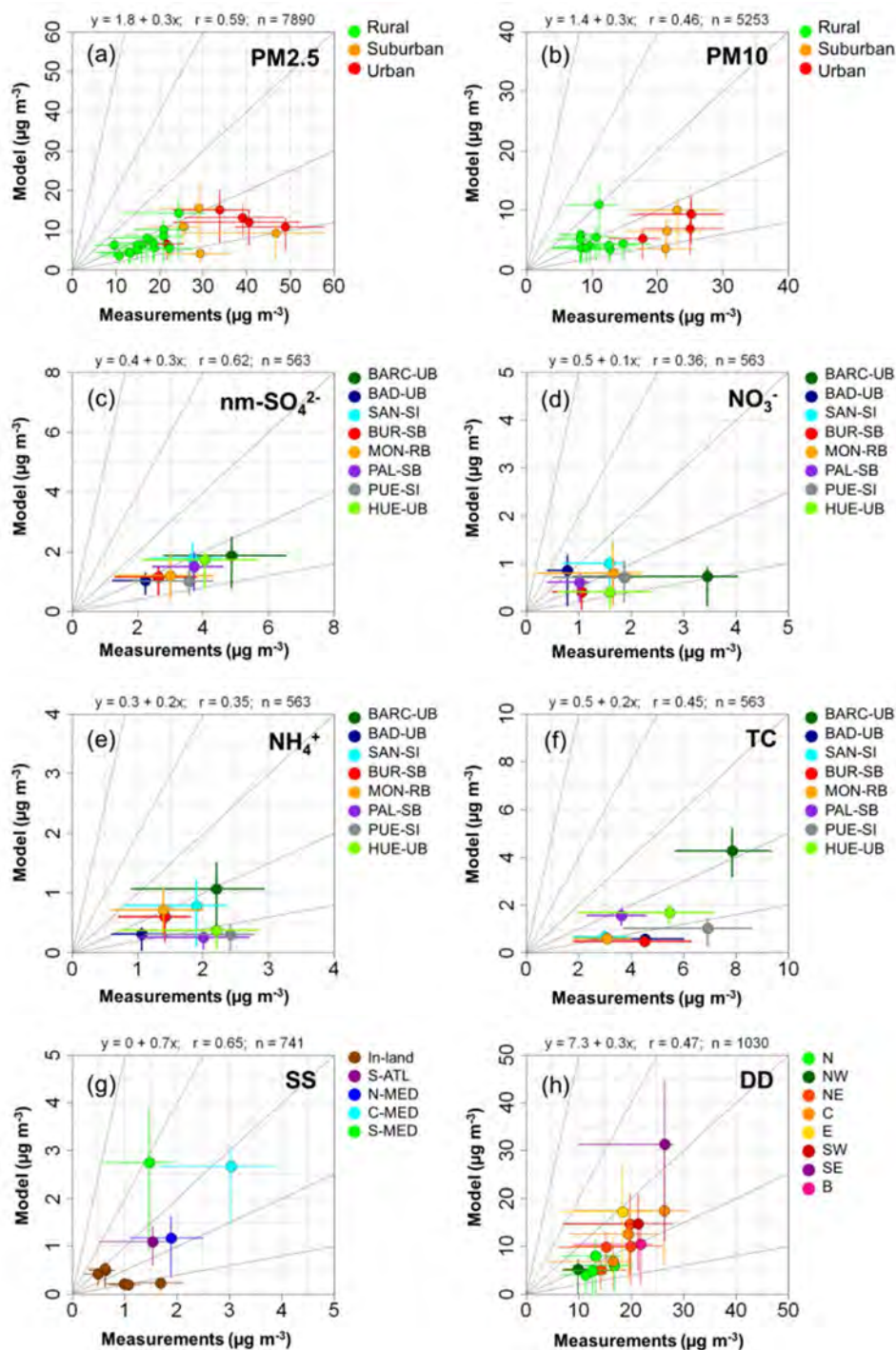
Figure 6-2. Modelled versus measured daily particulate matter (PM2.5 and PM10) and chemically speciated aerosols (nm-SO_4^{2-}, NO_3^-, NH_4^+, TC, SS and DD) concentrations (in $\mu g\ m^{-3}$) by station for the year 2004. Dots represent annual average concentration in the station. Horizontal and vertical lines indicate the 25p and 75p, respectively. PM10 (a) and PM2.5 (b) classifies stations as rural (green), suburban (orange) and urban (red). In c, d, e, and f each color represents a station (Figure 6-1). SS (g) classifies coastal stations according to the ocean where they are located. DD (h) classifies stations according to geographic area. The expression located on the top indicates the adjust equation, the correlation coefficient (r), and the number of data points (n).

However, in winter (February and ending November) the modelling system presents low skills to reproduce observation, underestimating the amplitude of the daily variation in PM2.5 and PM10 $(0.24 < \sigma \text{ (Mod./Obs.)} < 0.29)$. Local anthropogenic emissions dominated high PM levels at urban and industrial sites in February 2004 (or winter 2004) when strong anticyclonic atmospheric condition (17 days) took place in the western Mediterranean Basin leading to the accumulation of PM (Pey et al., 2010). Under low dispersive conditions in February and ending November the modelling system presents the major problems.
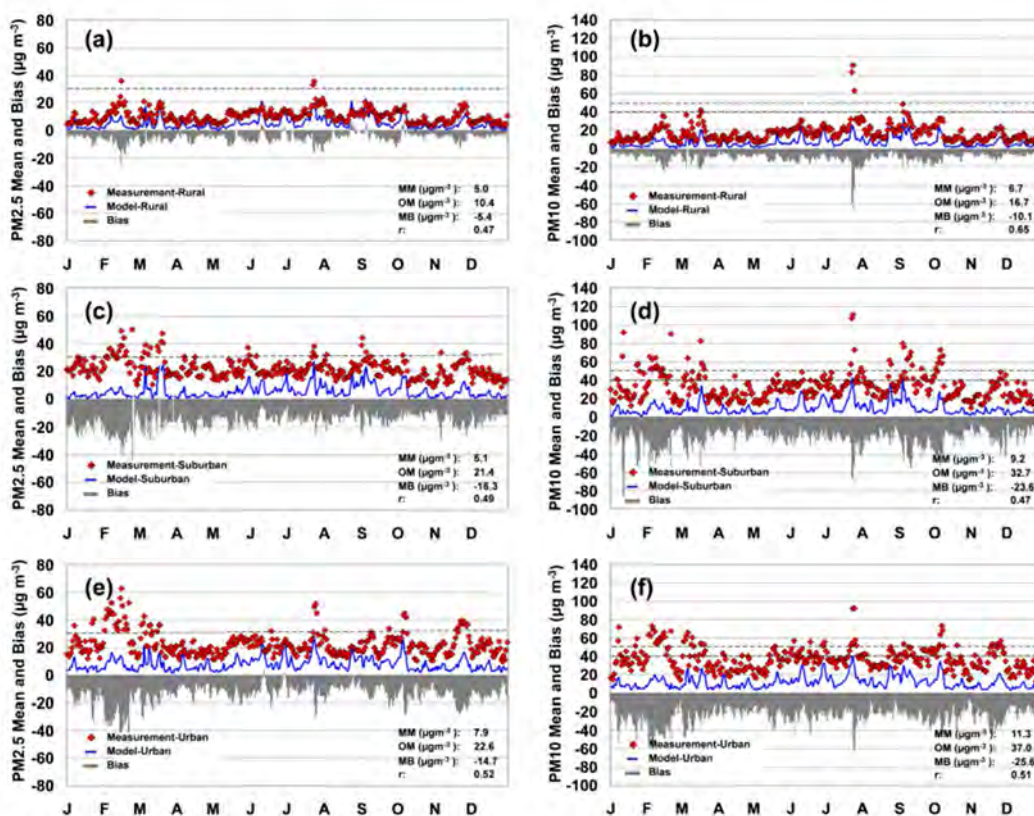
Figure 6-3. Time series of observed (red diamond) and simulated (blue continuous line) daily PM2.5 (left column) and PM10 (right column) for the year 2004 averaged over each type of site: (a, b) rural, (c, d) suburban, and (e, f) urban (Figure 6-1 and Table 6-1 for the sites). The dashed lines represent the current limit values in Europe (European Commission, 2008) for PM10 (annual and daily limit values of $40\ \mu\text{g m}^{-3}$ and $50\ \mu\text{g m}^{-3}$ not to be exceeded 35 times per year, respectively) and for PM2.5 (annual limit value of $25\ \mu\text{g m}^{-3}$). Statistics for each type of site are showed in the figure (bottom right): Modeled Mean (MM), Observed Mean (OM), Mean Bias (MB) and correlation coefficient (r).

6.3.2 Evaluation and assessment of PM speciation

The previous section analyzed the total concentration of PM2.5 and PM10. Although the modelling system reproduces quite well the temporal variability, systematic underestimations have been detected. It is important for these reasons to assess the modelling system ability to simulate the chemical composition of PM, not just the PM concentrations.

In the present section, we characterize the CALIOPE performance to reproduce the daily variability of the observed PM compounds (nm-SO_4^{2-}, NO_3^-, NH_4^+, TC, SS and DD) over Spain and we also estimate a multiplicative adjustment ratio for each compound. Several studies have demonstrated the benefit of adjusting site-specific air quality models using observational data to reduce systematic model error (e.g. Hogrefe et al., 2006; Djalalova et al., 2010). Bias-adjustment strategies range from the relatively simple mean bias and multiplicative ratio adjustments used by McKeen et al. (2005) to the more complex Kalman filter techniques (Delle Monache et al., 2006; Kang et al., 2010). In this study we estimate a spatial homogenous correction factor based on the ratio of annual modelled mean over measured mean. Figure 6-4 displays the annual time series of the raw and corrected daily modelled concentrations for PM chemical compounds for which the estimated adjusting ratio is different to 1.

A total of 8 stations are used to evaluate the simulated nm-SO_4^{2-}, NO_3^-, NH_4^+ and TC concentrations in the PM2.5 fraction: 1 station is located in rural areas, 4 in suburban areas and 3 in urban areas (Table 6-1 and Figure 6-1). 75% of these stations are background stations and the other 25% are industrial. SS is evaluated over 10 stations, 3 of them are inland stations (BAD, BUR and PUE), 3 are located over < 30 km away from the coastal line (LAC, MON and OND) areas, and 4 over the coastal line (BARC, BAS, HUL and PAL). DD is available over 16 rural background stations geographically distributed over Spain.

Furthermore, the present section provides a general description of the raw CALIOPE seasonal mean spatial distribution of the aerosol compounds across Spain (Figure 6-6 and Figure 6-8).

6.3.2.1 Non-marine sulphate (nm-SO_4^{2-})

On average modelled and measured nm-SO_4^{2-} concentrations present high correlation for daily concentrations (r = 0.62) (Figure 6-2c). The modelling system reproduces 30% of the observed daily nm-SO_4^{2-} concentrations indicating that modelled nm-SO_4^{2-} is about 70% lower than observations along the trend line. At most stations, simulated annual means are underestimated by a factor of 3, with low absolute bias (MB = -2.1 $\mu g\ m^{-3}$). In order to examine the annual variability, Figure 6-4a displays the annual time series of modelled and observed nm-SO_4^{2-} concentrations (black and red lines, respectively) on a daily basis averaged over all the stations. Modelled nm-SO_4^{2-} concentrations agree with the daily observations, especially during summer and fall (r = 0.68 and r = 0.73, respectively). In this period nm-SO_4^{2-} exhibited a maximum (Observed Mean, OM = 4.3 $\mu g\ m^{-3}$) because of the higher SO_2 oxidation velocity under high insolation conditions (Querol et al., 2008b). Nevertheless, the modelling system tends to underestimate the peaks during February, decreasing the correlation in winter (r = 0.46). SO_2 presents minimum concentration in winter (OM = 2.9 $\mu g\ m^{-3}$) and the modelled nm-SO_4^{2-} shows the largest underestimation (-2.2 $\mu g\ m^{-3}$) (Table 6-2). Winter underestimation of nm-SO_4^{2-} is a common issue in most models in Europe, representing a direct couplet of sulfur chemistry with photochemistry, even detected with CMAQ over Europe (Matthias, 2008; Chemel et al., 2010). This feature can be explained by the lack of model calculated oxidants or missing reactions (Kasibhatla et al., 1997; Tarrasón and Iversen, 1998; Schaap et al., 2004b). After multiplying the model results by the estimated adjusting ratio (factor of 3) the corrected modelled nm-SO_4^{2-} concentrations (blue line in Figure 6-4a) agree with the daily observations, especially during summer and fall.

Figure 6-6a and b shows the seasonal mean distribution of nm-SO$_4^{2-}$ concentration over Spain for winter and summer, respectively. nm-SO$_4^{2-}$ concentration has lower spatial variability than other PM2.5 species, with significant relationship with the distribution of emission sources, mainly downwind shipping and power plants, refineries and transformation industries that are the main responsible of high concentration of SO$_2$; nm-SO$_4^{2-}$ is mostly formed either from the gas-to-particle conversion of SO$_2$ in the atmosphere or from reactions in the aqueous phase. Because of the relatively slow rates of formation and removal, nm-SO$_4^{2-}$ becomes relatively well mixed (Park et al., 2006).
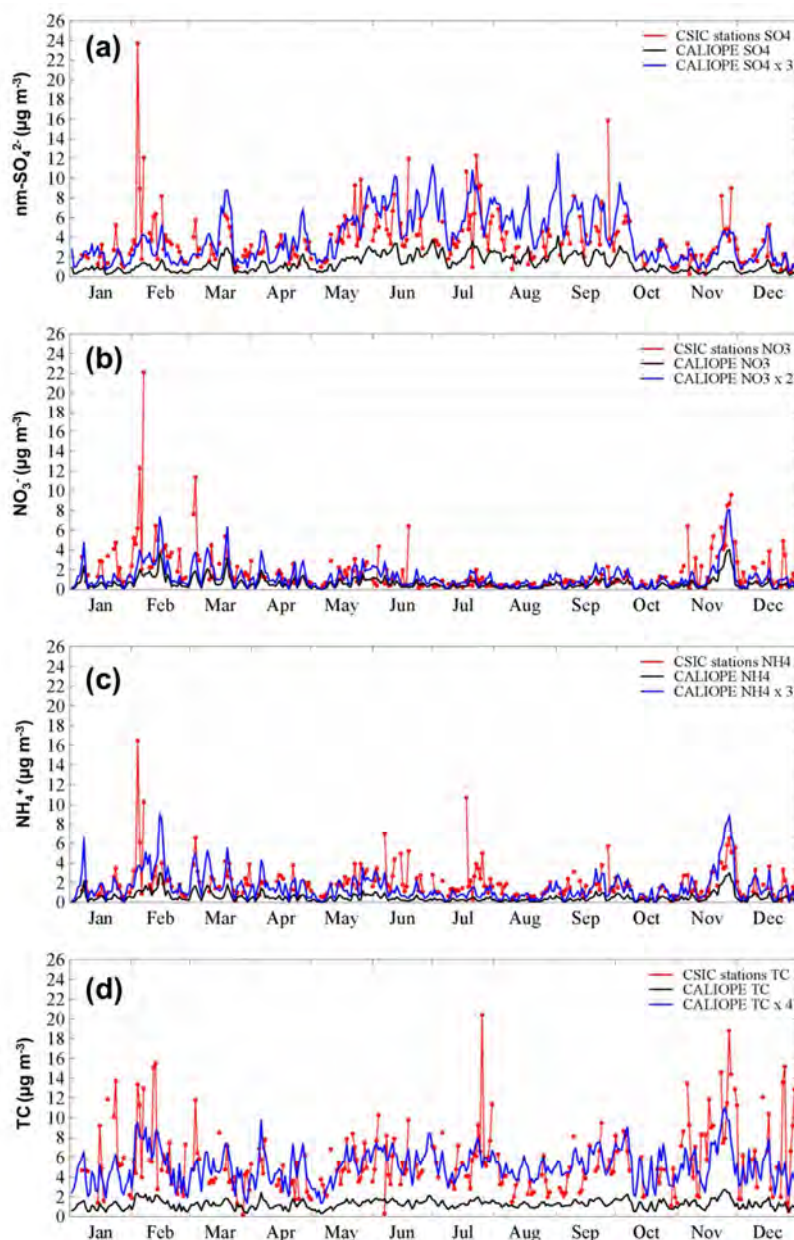
Figure 6-4. Time series of observed (red lines), simulated (black line) and simulated corrected (blue line) concentration for daily nm-SO$_4^{2-}$ (a), NO$_3^-$ (b), NH$_4^+$ (c) and TC (d) as an average of all the stations for the year 2004.

Over Spain, $(NH_4)_2SO_4$ presents minimum levels in winter (Figure 6-6a) and reaches maximum concentrations in summer (Figure 6-6b). This seasonal pattern is related to the stronger insolation favouring the higher oxidation of SO_2 to $nm-SO_4^{2-}$, low air renovation at regional scale, and the increment of the summer mixing layer depth favouring the regional mixing of polluted air masses. Overall, $nm-SO_4^{2-}$ concentrations decrease from the coast to the continent related to the fact that high density of refineries and power plant are located near the coastal line, and also because shipping is also an important source of SO_2.

During winter lowest concentrations (< 0.5 μg m^{-3}) are detected over the main Iberian mountain ranges meanwhile winter maximum concentrations around emission sources are ~ 1 μg m^{-3}. During summer the highest concentrations are found in the Atlantic regions (northwestern Spain) (~ 3.5 μg m^{-3}) due to the presence of geographically-close power plants, and refineries in the area of Galicia, Ponferrada, Asturias and Bilbao where SO_2 modelled level is ~ 10 μg m^{-3}, or even 50 μg m^{-3} around the La Coruña refinery. The dispersion pattern in northwestern Spain is significantly dominated by the northern and northeastern winds oxidizing SO_2 during the transport inland. High $nm-SO_4^{2-}$ concentrations are present along the Mediterranean coast, ~ 2.5 μg m^{-3}. Northeastern Spain is mostly affected by the Andorra power plant from Teruel (Aragón region) where $nm-SO_4^{2-}$ is secondarily formed during the canalization of the Ebro valley towards the Mediterranean Sea. Furthermore, shipping across the Mediterranean Sea may be a cause of high $nm-SO_4^{2-}$ along the coast. Summer $nm-SO_4^{2-}$ is low (~ 1-1.5 μg m^{-3}) in northern and southern plateaus corresponding with areas with low precursors emissions. The central Spanish plateau displays low levels of $nm-SO_4^{2-}$ despite presenting one of the most important refinery and power plants around Puertollano (Castilla-La Mancha region).
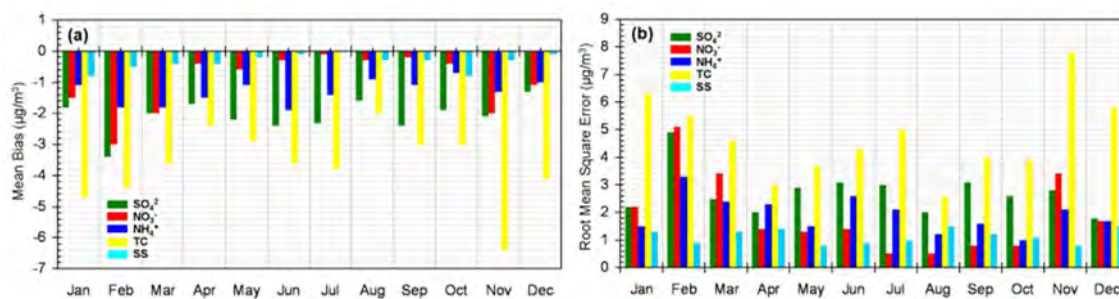
Figure 6-5. Mean Bias (a, in μg m^{-3}) and Root Mean Squared Error (b, in μg m^{-3}) for $nm-SO_4^{2-}$ (green), NO_3^- (red), NH_4^+ (dark blue), TC (yellow) and SS (cyan) averaged over the IDAEA-CSIC stations for each month of the year 2004.

Qualitative comparisons between the simulated pattern of seasonal $nm-SO_4^{2-}$ and description based on measurements provided by Querol et al. (2008b) reveals a good agreement. Such finding demonstrates the accuracy in the spatial description of the source regions and various industrial hot-spots.
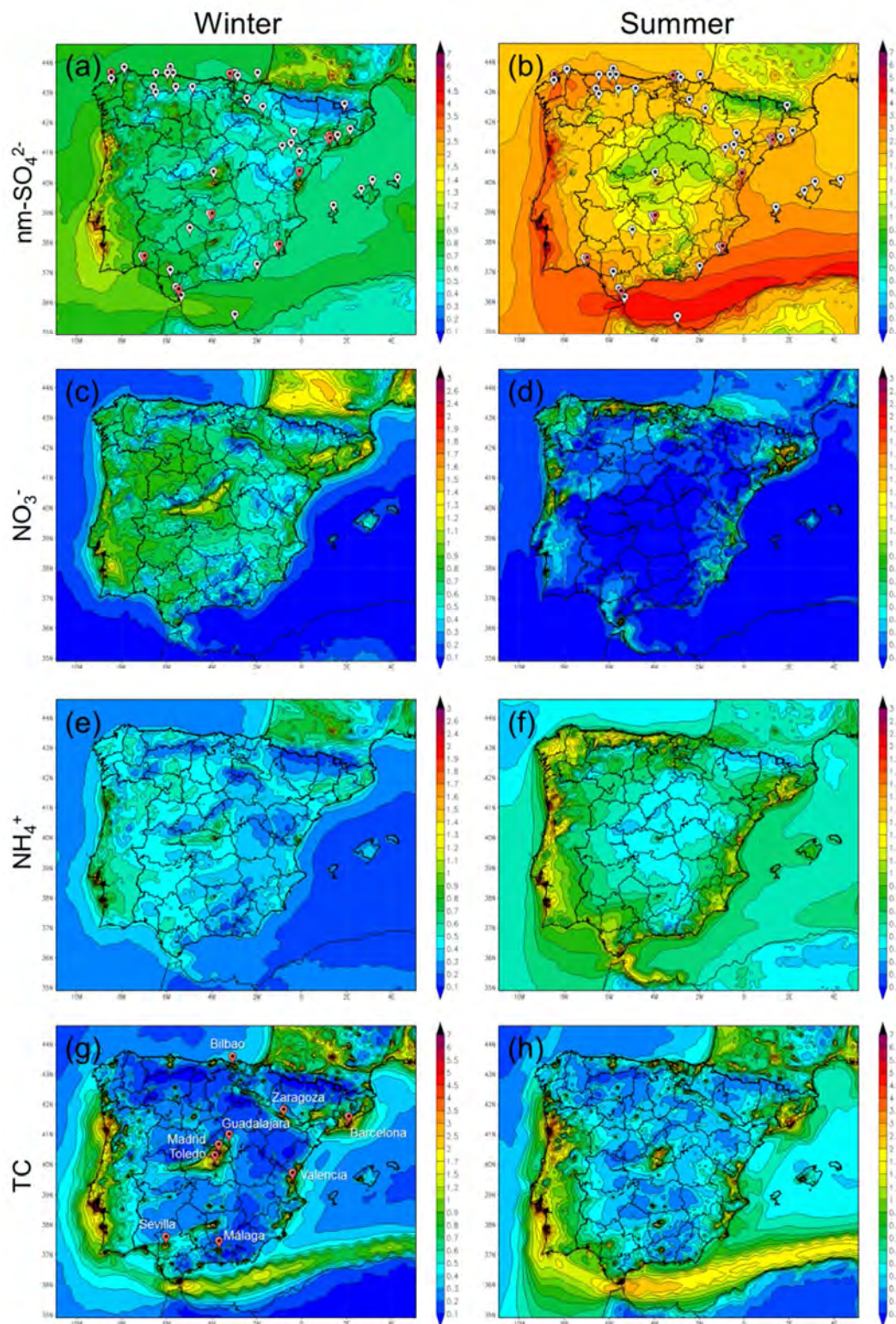
Figure 6-6. Annual average concentration (in μg m⁻³) for nm-SO₄²⁻ (a, b), NO₃⁻ (c, d), NH₄⁺ (e, f) and TC (g, h) in winter (right) and in summer (left) at lower-most level simulated by CALIOPE over Spain at a 4 km x 4 km spatial resolution. Winter corresponds to January, February and March. Summer corresponds to June, July and August. Red icons in a and b represent the Spanish refineries meanwhile white icons represent power plants.

Over the ocean high nm-SO_4^{2-} concentrations (~4 $\mu g\ m^{-3}$) are located in the shipping route from the Atlantic Ocean through the Strait of Gibraltar towards the Mediterranean Sea. As indicated in Baldasano et al. (2011), ship emissions are large contributors of the total SO_2 concentrations along the ship tracks, and the subsequent formation of nm-SO_4^{2-} downwind. Maximum nm-SO_4^{2-} concentrations are in the narrow Gibraltar regions with a dispersion pattern dominated by western winds. The high nm-SO_4^{2-} in this area is a combination of high emissions from shipping, industry, power generation and oil refinery processes in the Gibraltar bay and Algeciras industrial area (Pandolfi et al., 2011).

6.3.2.2 Nitrate (NO_3^-)

Fine ammonium nitrate (NH_4NO_3) is produced by the oxidation of NO_x to nitric acid (HNO_3) during night and day (e.g. Meng et al. 1997; Nguyen and Dabdub, 2002). HNO_3 dissolves in the aqueous particles along with the ammonia (NH_3) and produces NO_3^- determined by the composition of the particle. Therefore, the behavior of nitrate is one of the most intriguing issues of inorganic atmospheric aerosols because its concentration depends not only on the amount of gas-phase HNO_3, but also on the availability of NH_3 and nm-SO_4^{2-}, together with temperature and relative humidity (Mozurkewich, 1993; Nenes et al., 1998; Bassett and Seinfeld, 1983; Zhang et al., 2000; Schaap et al., 2004b).

On average the CALIOPE system underestimates measured fine NO_3^- concentrations (Figure 6-2d) by a factor 2 with very low bias (MB = -1.0 $\mu g\ m^{-3}$). The cause of this underestimation is related to errors in the simulation of NH_x (NH_4^+ + NH_3), SO_4^{2-}, and, to a lesser extent, TNO_3 (NO_3^- + HNO_3) (Yu et al., 2005). However, the temporal variability and therefore the transport patterns of NO_3^- are captured (Figure 6-4b) especially during fall (r = 0.49), although the modelling system hardly reproduces the amplitude of the events. Modelled NO_3^- concentrations present a good agreement with the observation when a factor of 2 is applied to the results (blue line). As for nm-SO_4^{2-}, the adapted results for NO_3^- match consistently with the observations except for February.

The seasonal mean concentration pattern of fine NO_3^- over Spain (Figure 6-6c and d) shows a marked seasonal evolution characterized by a summer minimum. The oxidation rate of NO_x ranges from 5% till 50% per hour (Spicer et al., 1981) faster than that of SO_2. Also, HNO_3 deposits rapidly and NH_4^+ presents a low thermal stability in warm season (Harrison and Pio, 1983; Querol et al., 2008b). Thus, NO_3^- is spatially less homogeneously distributed than nm-SO_4^{2-} in summer as shown seasonal distribution in Figure 6-6d. Levels decrease from the coastal areas to inland, with the lowest regional background levels over central and southern plateaus (~0.3 $\mu g\ m^{-3}$).

In contrast, high NO_3^- concentration and homogeneous distributions are found in winter (Figure 6-6c) favoured by the higher stability of NH_4NO_3 in cool conditions, which causes a higher portion of NO_3^- to partition to the aerosol, which has a longer lifetime than HNO_3 against deposition (Schaap et al., 2004b) and favoured by less dispersive conditions in the boundary layer. Overall, rural background NO_3^- concentrations remain ~ 1 $\mu g\ m^{-3}$, reaching the lowest values in the higher mountains ranges (< 0.5 $\mu g\ m^{-3}$). High levels (~ 1.2 $\mu g\ m^{-3}$) are found over the intensive agricultural areas of Plana de Lérida and Gerona and along the urban plume from Madrid metropolitan area which transports precursors from the agriculture and road traffic (see NH_3 and NO_2 patterns,

Figure AIII – 3, Annex III) following a south-western direction conditioned by the barrier of the Central System (2500 m height) and the canalization of Tajo Valley in the southern part ($\sim$ 1.2 μg m^{-3}).

Furthermore, humidity plays a key role stabilizing NH_4NO_3 in the coasts, even at relatively high temperatures. In northeastern Spain (Galicia) there is no a significant seasonal trend of NO_3^-. Levels remain $\sim$ 0.9 μg m^{-3} due to the frequent Atlantic advection and the high-density industry located there. At Nervion valley, the seasonal trend of NO_3^- is smooth probably as a consequence of the significant summer breeze transport of atmospheric pollutants from the coastal industrial zones along the valley and the high humidity conditions.

Along the Mediterranean coast, the seasonal trend of NO_3^- presents low variability compared with central Spain as reported by Querol et al. (2008b). The spatial difference is related to (1) the relative low disperse atmospheric condition prevailing in the Mediterranean Basin (Millán et al., 1997) compared with those in the Atlantic regions; (2) the high ammonia emission along the Mediterranean coast, above all in the northeast of Spain, caused by emission from intensive cultivation and farming (Figure AIII – 3, Annex III); and (3) the high humidity conditions which stabilize NH_4NO_3 even during the summer. Furthermore, traffic NH_3 emissions in urban areas with high humidity (coastal areas) may also provoke high NH_4NO_3 levels (Athanasopoulou et al., 2008).

Thus, in contrast to nm-SO_4^{2-}, NO_3^- levels are independent of the relevance of the regional/local emission of NO_3^- precursors. This spatial distribution shows no relationship either with road traffic flows (given that cities such as Madrid and Barcelona with similar inhabitants present different NO_3^- concentrations) or with industrial density so sites with similar industrial development (Huelva and Tarragona) have very different NO_3^- levels as shown by Querol et al. (2008b).

6.3.2.3 Ammonium (NH_4^+)

Along the year the overall variability of the modelled NH_4^+ concentrations compares favourably with observations (Figure 6-2e and Figure 6-4c) with r = 0.34 . As for nm-SO_4^{2-}, modelled annual mean of NH_4^+ is underestimated by a factor of 3 with very low bias (MB = -1.3 μg m^{-3}). As for NO_3^-, NH_4^+ presents the worst performance during warmer seasons (0.15 < r < 0.32) while is better simulated during the colder seasons (0.42 < r < 0.48), especially during fall season (σ(Mod./Obs.) = 0.71, r = 0.48). When a factor of 3 is applied the magnitude of most of the single events is captured (Figure 6-4c). Similar CMAQ model results were found in Matthias (2008) and Chemel et al. (2010) where NH_4^+ concentration is underestimated in summer and the agreement with the observations is much better in winter and fall. The explanation is likely related to the uncertainties in the seasonal distribution of NH_3 emissions (Gilliland et al., 2006). There is not, to the author's knowledge, a large dataset of NH_3 measurement available in Spain thus not so many conclusions can be taken over the equilibrium NO_3^-/NH_4^+. However, through the degree of nm-SO_4^{2-} neutralization (DON) indicator, described in the supplementary material, it is possible to provide indirectly information about how well the modelling system estimates NH_3 concentrations. PM2.5 nm-SO_4^{2-} is almost always completely neutralized by NH_3 in the modelling system (Figure AIII – 4, Annex III). Observations suggest that PM2.5 nm-SO_4^{2-} is fully neutralized in warm

seasons and exists in the form of NH_4^+ bisulphate in the colder months. This finding suggests that there should be more free ammonia in the gas phase or less NH_4^+ in the photochemical model. The representation of NH_3 emissions can have a large effect on air quality model simulations of aerosol NO_3^- and NH_4^+ concentrations.

The bias performance of NH_4^+ is strongly correlated with that of nm-SO_4^{2-} (r = 0.69) and NO_3^- (r = 0.62), because both anions are neutralized by NH_4^+. Therefore, the performance of NH_4^+ at single stations is mostly in between that of nm-SO_4^{2-} and NO_3^-. At locations where nm-SO_4^{2-} dominates over NO_3^- the performance is close to that of nm-SO_4^{2-}, whereas in regions with high modelled NH_4NO_3 the performance is closer to NO_3^-. CALIOPE performance for SIA is better for nm-SO_4^{2-} than for the other compounds based on high correlation coefficient (0.62 vs. 0.36-0.34) and normalized RMSE (0.82 vs. 1.3-1.1).

NH_4^+ is secondarily formed as NH_3 neutralizes H_2SO_4 and HNO_3. The amount of NH_4^+ is highly dependent on the relative amounts of H_2SO_4 and NH_3, and indirectly of HNO_3. The seasonal distribution pattern of NH_4^+ is shown in Figure 6-6e and f for winter and summer, respectively. As for NO_3^-, the less dispersive conditions in the boundary layer favoured a relative small spatial variability for NH_4^+ during winter. Average levels are ~ 0.6 µg m^{-3}, meanwhile over high mountain ranges the levels are low (< 0.2 µg m^{-3}). In summer NH_4^+ concentrations present a more complex pattern. Concentrations over the coastal areas increase (~ 1.2 µg m^{-3}) determined by its association with nm-SO_4^{2-}. Over the Atlantic coast, northern winds determined the generation of NH_4^+ inland.

6.3.2.4 Total carbon (TC)

The annual temporal evolution of the modelled TC concentrations compares reasonably well with the observations (r = 0.45), albeit the CALIOPE system underestimates the amplitude of daily concentrations, σ (Mod./Obs.) = 0.42 (Figure 6-2f and Table 6-2). Most measured annual mean concentrations at individual stations are underestimated by a factor of 4. These results agree with a large number of studies showing that air quality models generally underestimate organic aerosol concentrations, especially in urban air masses (Carlton et al., 2008; Murphy and Pandis, 2009; Smyth et al., 2009 among others).

The urban background station at Barcelona presents the lowest underestimation (factor of 2). In cities, a large proportion of TC is emitted by road traffic. In large conurbations (>500,000 inhabitants), like Barcelona, the road traffic emission module is specifically described in HERMES, including the definition of the road network, divided in stretches (inside the 1 km x 1 km cells), with specific temporary disaggregating profiles (distinguishing day-type: weekday-holiday, and month), average speed circulation, annual average daily traffic (number of vehicles per day), stretch length, route type (highway, road or urban) and circulation zones. Because of this complexity, the emissions at large cities are correctly described (Baldasano et al., 2008a) and hence the model tends to perform better with respect to areas with a larger uncertainty in emissions.

The TC temporal series averaged over all stations is shown in Figure 6-5. The highest measured TC concentrations are found during winter (5.8 µg m^{-3}). Although the modelled TC reproduces temporal variability with high correlation (r = 0.53), absolute MB and RMSE are relatively weak (MB = -4.5 µg m^{-3}, RMSE = 6 µg m^{-3}). On the other hand, during summer TC is modelled with the

lowest correlation (r = 0.31), partly due to lack of SOA yield paths. The SOA model adopted in CMAQv4.5 does not include biogenic SOA formation from isoprene and sesquiterpenes (Appel et al., 2008). The predominant vegetation types in the Spanish domain favour isoprene as the main biogenic volatile organic compound (bVOC) (Keenan et al., 2009). The absence of the isoprene-SOA route on SOA modelling in the domain of study may impact significantly air quality during summer, when elevated bVOC emissions combine with an enhanced photochemistry.

The model underestimations of TC are mainly related to (1) the state-of-the-science concerning to SOA formation pathways, as commented before (Eder and Yu, 2006; Edney et al., 2007; Appel et al., 2008) and (2) probable underestimation of primary carbonaceous emission (Cooke and Wilson, 1996; Bond et al., 2004; Tsyro et al., 2007).

Figure 6-6 shows the winter (g) and summer (h) mean concentration of TC over Spain in 2004. Elemental carbon is a primary pollutant so its spatial variability is relatively high. Major sources of elemental carbon include diesel engines, particulate heavy-duty trucks, and combustion process (including biomass and fossil fuel), thus high levels are associated with urban areas. In contrast, organic carbon is emitted directly or, in a large proportion, formed from the condensation of low-volatility organic compounds. Thus, the spatial variability of organic carbon is between that of purely primary and secondary pollutants. Major primary sources of organic carbon include diesel and gasoline-burning engines, biomass burning and some industrial processes, so organic carbon will be found in urban and rural background environments.

Due to the high disaggregation and the specifically detailed emissions implemented in the HERMES model, the impact of principal highways is noticeable, (e.g., Madrid-Sevilla, Barcelona-Bilbao, the A-7 Mediterranean highway) where annual mean values range from 0.5 to 2 µg m^{-3}.

In urban environment (e g. Zaragoza, Valencia, Málaga, Sevilla, Madrid and Barcelona) the seasonal trend of TC is characterized by a winter maximum (Rodríguez et al., 2002 at Barcelona site and Querol et al., 2008b at many sites), indicating a major local anthropogenic origin. Reduced dispersion conditions in the boundary layer together with enhanced condensation due to the low temperature explain the seasonal evolution of carbon in the urban environment. The urban plumes from the two largest Spanish cities (Madrid and Barcelona) reach the highest TC concentrations (~5 µg m^{-3}). In both regions, on-road traffic constitutes the main source of primary pollutants in the region (Gonçalves et al., 2009b) and TC follows the same pattern as NO$_2$, as shown in Baldasano el al. (2011) and in Figure AIII – 3, Annex III.

In Madrid during winter the TC dispersion follows a south-western direction conditioned by the barrier of Central System and the canalization of Tajo valley dominated by the predominant Atlantic advection episodes. The urban plume reaches the highest concentration at the urban nuclei (~7 µg m^{-3}), moving towards Toledo (south) and reaching Guadalajara (east) to a lesser extent (~1.5 µg m^{-3}). In contrast in summer, the urban plumes is less disperse, determined by the developed of the IP Thermal Low over the central plateau which couple with several deep convective cells that inject aged pollutant aloft for the Madrid area.

A different TC pattern is observed in Barcelona. The TC dispersion shows a perpendicular flow to the coast dominated by the northwestern winds. The dispersion pattern is intensified in summer

due to the frequent regional recirculation events characterized by sea breeze over the Mediterranean (Baldasano et al., 1994; Millán et al., 1997). The very complex coastal terrain induces mesoscale phenomena which control the superficial wind flows. Sea-breezes and mountain valley winds contribute to the accumulation and recirculation of air masses. The littoral mountain chain (1000–1500 m height) acts as a barrier, recirculating TC flow towards the Mediterranean Sea channeled by the river valleys. Also the high isolation favours the formation of SOA.

The industrialized area of Tarragona and Castellón and the urban area of Valencia, all located along the Mediterranean coast, present significant levels of TC also affected by mesoscale phenomena dominated by sea-breezes which determine TC flow perpendicular to the coast. In northern Spain, the urban and industrial areas of Bilbao show significant TC levels dispersed along an estuary that runs almost 16 km from the center of the city to the sea and is aligned in an SE–NW direction.

In contrast, background levels of carbonaceous aerosols exhibited a light spatial variability, but a seasonal trend characterized by a summer maxima ~0.5 μg m^{-3}. An important fraction of SOA could arise from bVOC emissions given their increase in the warm season due to enhanced plant transpiration (Rodríguez et al., 2002; Keenan et al., 2009) and also from biomass burning from agricultural and domestic sources.

Similarly to nm-sulphate, the major shipping route originating from the northern Atlantic, toward northern Africa is shown to have a notable impact on TC concentrations, which is intensified in summer due to the increase of maritime traffic and the favoured photochemistry. Concentrations of TC range from ~1.5 μg m^{-3} near the coastlines of Portugal and Gulf of Cadiz to ~2 μg m^{-3} over the Alboran Sea. Background concentration of TC over the sea ranges between ~0.7 μg m^{-3} and < 0.2 μg m^{-3} over the Mediterranean and Atlantic Sea, respectively, owing to distinct Atlantic-Mediterranean regimes of Spain.

6.3.2.5 PM10 sea-salt aerosol (SS)

For SS, the modelling system reproduces correctly 70% of the observed values with a correctly temporal variability (r = 0.65) (Figure 6-2g). 40% of modelled concentrations are within a factor of 2 with observations (Table 6-2). The modelling system presents a good skill to reproduce the amplitude of the daily variation of SS with σ (Mod./Obs.) = 1.17. Highest correlations are obtained during spring and winter when high wind velocities take place and the flux of SS is high. However, under stagnant situations, like summer over Mediterranean, the modelled sea salt is reproduced with lower correlation and higher daily variability, r = 0.52 and σ (Mod./Obs.) = 1.44, respectively. As shown in Figure 6-2g, at coastal stations the CALIOPE system tends to slightly overestimates SS, meanwhile at continental areas salts concentrations tends to be underestimated. Over the southern Atlantic and central Mediterranean the CALIOPE system performance agrees better with the observations. Part of the underestimation and the excessive variability modelled is because AERO4 considers coarse-mode aerosols as dry and inert. This approach does not allow important aerosol processes, such as the replacement of chloride by NO$_3^-$ in mixed marine/urban air masses (Kelly et al., 2010) especially intense in summer when HNO$_3$ is released by the thermal instability of NH$_4$NO$_3$ (Querol et al., 2004a). Moreover, degassing of Cl$^-$ is not implemented in the model, and heterogeneous reactions are not taken into account. Transfer from PM10 to PM2.5 is also not

considered in AERO4. Furthermore, only sea-salt emissions from open-ocean are included so the detected underestimation over coastal areas is in part due to the fact that surf-zone mechanism is not implemented (Athanasopoulou et al., 2008). The results subscribe the modelled SS calculation performed over Mediterranean Basin in Jiménez-Guerrero et al. (2011).
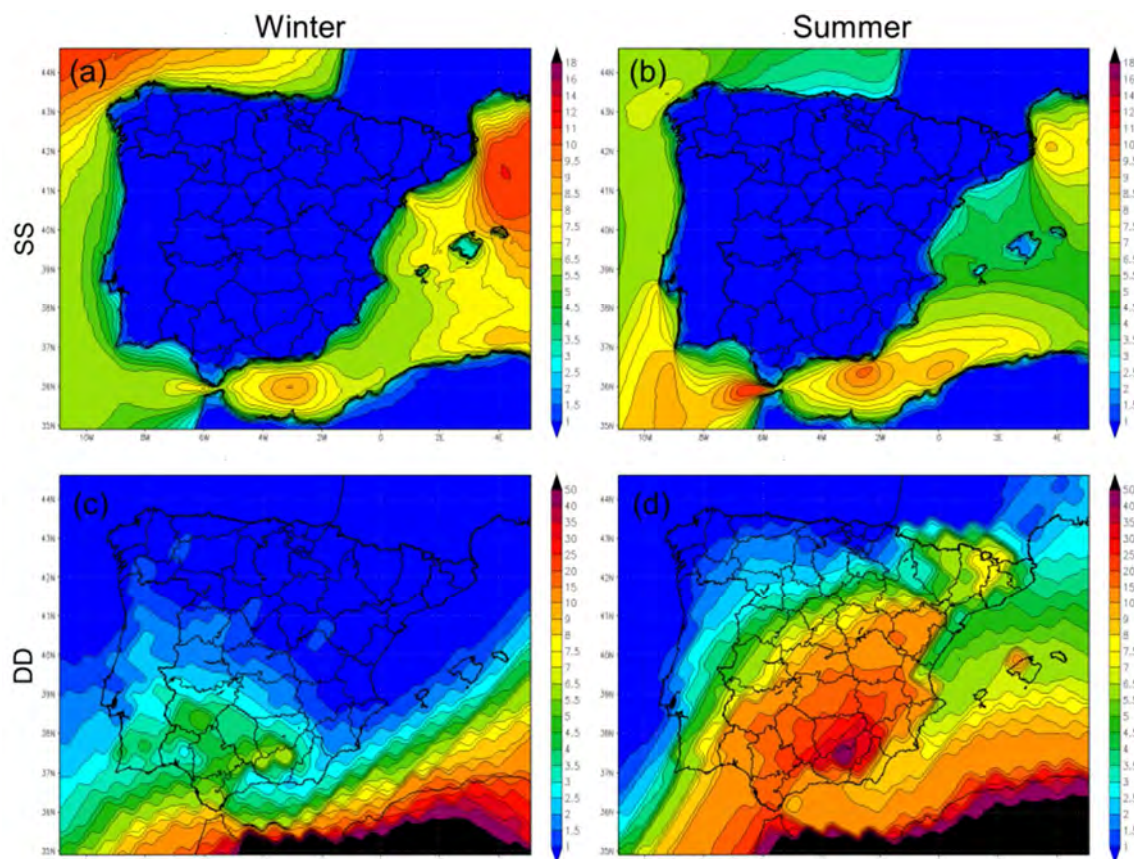
Figure 6-7. Annual average concentration (in μg m⁻³) for PM10 sea-salt aerosol (SS) (a, b), and PM10 desert dust (DD) (c, d), in winter (right) and in summer (left) at lower-most level simulated by CALIOPE over Spain at a 4 km x 4 km spatial resolution. Winter corresponds to January, February and March. Summer corresponds to June, July and August.

Figure 6-7a and b shows the non-uniform behavior of SS in the surrounding Spanish oceans, showing a strong seasonality and dependence on the wind speed variation. Over the ocean, the maximum concentrations are simulated during winter. A winter maxima of ~ 12 μg m⁻³ is detected in the northern Atlantic Ocean and Gulf of Lion, the first related to the occurrence of intense frontal systems and strong winds events that peak during this season (Alpert and Ganor, 1993; Saaroni et al., 1998). Zakey et al. (2008) state that the Gulf of Lion is a region of strong Mediterranean cyclogenesis, with maximum activity taking place in the winter and fall months (Camuffo et al., 2000; Cavaleri, 2005). Under this condition maximum SS concentrations over the continents are found along the Atlantic coastal area of Galicia (~3 μg m⁻³) and over the whole Mallorca (~ 3 μg m⁻³) and Menorca (~ 9 μg m⁻³) islands affected by the dynamics in the Gulf of Lion. A different SS pattern is observed in summertime accentuated by the Atlantic-Mediterranean

regimes. Maximum concentrations are simulated over the eastern Strait of Gibraltar ($\sim$ 10 µg m^{-3}). The Azores high-pressure system is displaced westward and it develops high western winds which are intensified when they reach the strait due to its complex topography inducing SS dispersion aligned in a west to east direction (Millán et al., 2002). On the other hand, along the Mediterranean coast SS presents the maximum concentration in summer ($\sim$2 µg m^{-3}) when the intensive thermal inversions, the lower convective dynamics and the low dispersive local circulations intensifies sea breeze circulation over the coast and transport SS inland.

6.3.2.6 PM10 desert dust (DD)

Figure 6-2h presents the comparisons of the modelled DD surface concentration from BSC-DREAM8b with the DD estimated according the methodology reported by Escudero et al. (2007b). Despite the episodic character of Saharan dust outbreaks and their dependency on the synoptic scale, when BSC-DREAM8b is compared with measurements it presents a rather high correlation coefficient (r = 0.47) and captures the amplitude of the daily variations of desert dust episodes with high confidence, σ(Mod./Obs.) = 0.68.
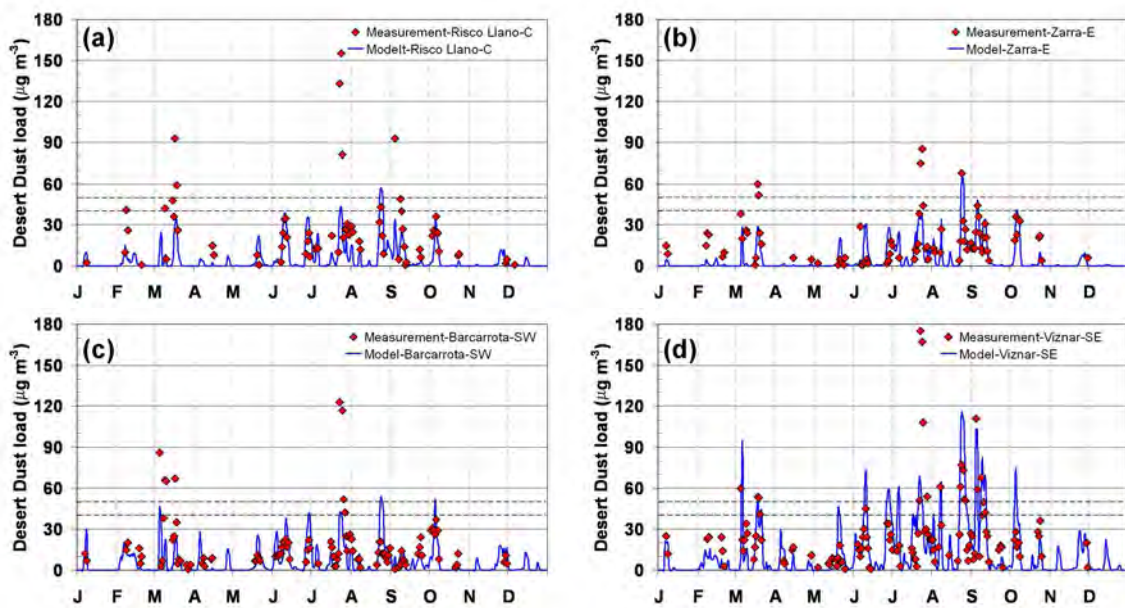
Figure 6-8. Time series of observed (red diamond) and simulated (blue continuous line) daily PM10 desert dust load for the year 2004: at (a) Risco Llano, (b) Zarra, (c) Barcarrota, and (d) Víznar (Figure 6-1 and Table 6-1 for the location of the sites). The continuous red lines represent the current limit values for PM10: the annual limit value of 40 µg m^{-3} and the daily mean value of 50 µg m^{-3} not to be exceeded 35 times in a year (European Commission, 2008).

Figure 6-8 shows the time series at four stations considered to be representative of the different geographical areas where Saharan dust presents a significant contribution: central (a), eastern (b), southwestern (c) and southeastern (d) Spain. BSC-DREAM8b is able to reproduce most of the Saharan dust outbreaks along the year 2004, both in time and value. Highest correlations were obtained for southeastern stations, like Víznar (r= 0.57), which are directly affected due to the

proximity to the African continent and at high altitude. However, BSC-DREAM8b underestimates some dust events associated with meteorological situations when emissions come directly from the Atlas region. The complex orography of this region produces a mesoscale phenomenon that hampers the simulation of meteorological parameters at surface level (like winds and precipitation) and consequently, the dust emissions. The observed episode in middle March is difficult to reproduce by BSC-DREAM8b over central and southern Spain. During the 18th and 19th March, Saharan mineral dust followed an Atlantic trajectory from North Africa achieving the western part of the IP. The low Saharan dust observed before the aforementioned episode was caused by the arrival of Atlantic air masses preceding the northward high particulate flow. Another important dust event is underestimated by the BSC-DREAM8b during late July.

As shown in Figure 6-7 modelled DD concentration shows a high spatial variability marked by a south-to-north gradient with minimum levels in the north (< 2 µg m^{-3} as annual average) and maxima in the southeastern Spain (~ 7-9µg m^{-3} as annual average) linked to frequent African dust plumes affecting IP (Rodríguez et al., 2001; Escudero et al., 2007b; Basart et al., 2009). These results agree with findings presented in Querol et al. (2009b). In addition, the DD contribution presents significant different patterns between winter (Figure 6-7c) and summer (Figure 6-7d) governed by synoptic situations as described Escudero et al. (2005). In winter African dust outbreaks were less frequent in 2004 (Figure 6-8) and mainly affecting the southwestern Spain (~ 6 µg m^{-3}) since a typical winter African transport scenario consists on the location of an anticyclone over the IP at surface levels. This creates a curved plume affecting the IP firstly on its western flank. Thus, high DD contribution during winter is found there (~ 5 µg m^{-3}). On the other hand, in summer large amounts of DD are transported along southern and eastern Spain linked to frequent African dust outbreaks (Rodríguez et al., 2001; Escudero et al., 2005; Sicard et al., 2011; among others). Saharan dust reaches southern Spain when the north Atlantic anticyclone (Azores high) is displaced westward and the North African high is centered over Algeria (Rodríguez et al., 2001). In these episodes, DD is transported at high altitudes, between 1500 and 4000 m a.s.l (Talbot et al., 1986; Escudero et al., 2005; Pérez et al., 2004, 2006b; Olmo et al., 2008; Córdoba-Jabonero et al., 2011). The largest summer mean contribution of DD coincides with the Sierra Nevada mountain range with values reaching up to 40 µg m^{-3}. Such concentrations are the consequences of (1) the mountain range location within the main zone of dust (Middleton and Goudie, 2001) and (2) the existence of several peaks within the mountain range 3000 m a.s.l. which corresponds to the altitude range for Saharan dust transport (Córdoba-Jabonero et al., 2011). In a lesser extent, summer concentration of PM10 DD load reaches concentration between 9 and 15 µg m^{-3} over southern, central and eastern Spain, including the Tramontane Mountain Range (Balearic Islands).
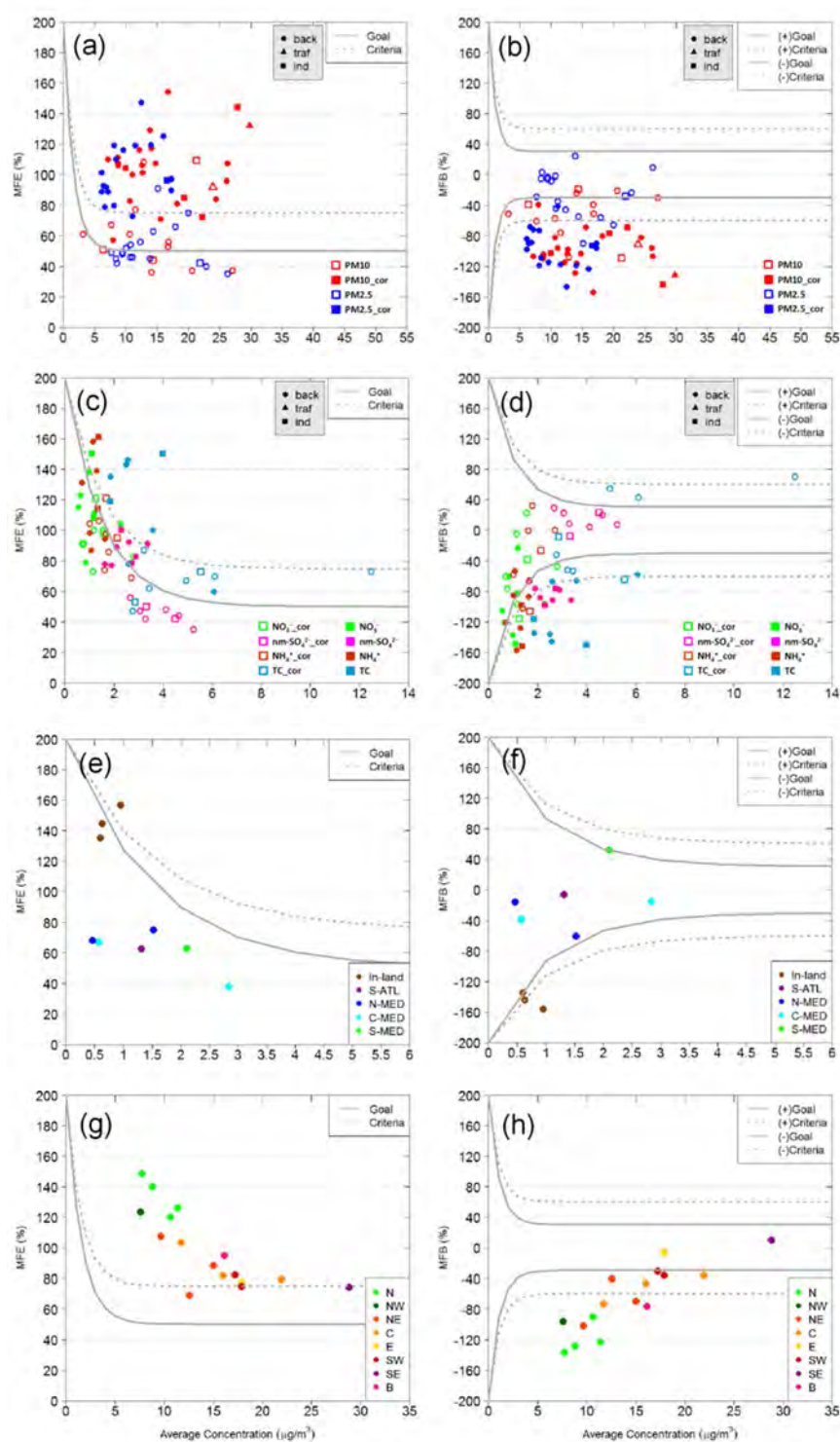
Figure 6-9. Mean fractional error (MFE, left) and bias (MFB, right) by station as annual average compared to proposed performance goals and criteria by Boylan and Russell (2006). Plots are carried out for different species: PM2.5 and PM10 (a and b), nm-SO_4^{2-}, NO_3^-, NH_4^+ and TC (c and d), SS (e and f) and DD (g and h). Solid symbols represent statistics for the raw modeled outputs. Empty symbols indicate corrected values calculated from the statistics evaluation. The corrected factors are 3 for nm-SO_4^{2-}, 2 for NO_3^-, 3 for NH_4^+ and 4 for TC. Corrected PM2.5 and PM10 are calculated from the corrected chemical species.

6.3.3 Modelled aerosol performance goals and criteria

Figure 6-9 shows the annual MFE and MFB at each of the studied stations for PM10, PM2.5, nm-SO_4^{2-}, NO_3^-, NH_4^+, TC, SS and DD. The Boylan and Russell (2006) criteria for MFB and MFE are not met for most of the stations for PM10 and PM2.5. Figure 6-9 also shows the MFE and MFB for the aforementioned species when the multiplicative correction factors from the statistical evaluation are applied over individual species. When applied, most of the stations largely meet the model performance goals for all the species. For background stations the correction factors are effective to meet the goals although they result less effective at traffic and industrial stations.

For nm-SO_4^{2-}, NO_3^-, NH_4^+ and TC (Figure 6-9c and d) the model performance criteria for MFE is met at 21 stations out of 32. Nevertheless for MFE only 50% of the stations meet the model performance criteria. Better results are obtained for nm-SO_4^{2-} (-100% < MFB < -90%, MFE < 100%) than for NO_3^-, NH_4^+ and TC. The stations of Barcelona meet the criteria for MFB and MFE for TC. When bias-correction factors are applied all the stations meet the criteria for MFE and MFB, and most of them meet the goals.

For SS only 8 stations out of 9 accomplished the criteria proposed by Boylan and Russell (2006). Most of the largest errors (MFE > 130%) and biases (MFB < -120%) correspond to inland stations (Figure 6-9e and f). For DD (Figure 6-9g and h) the central eastern and southern stations meet or nearly meet the Boylan and Russell criteria, 9 stations out of 16 corresponding to desert dust concentrations of ~ 16 µg m^{-3}. The highest MFE and MFB are found in northern and northeastern stations associated to low DD concentrations (~ 9 µg m^{-3}).

6.3.4 Spatial and seasonal pattern of PM2.5 and PM10

The present section provides a general description of the seasonal mean spatial distribution of PM size fractions (PM2.5 and PM10) across Spain. Note that the discussion performed over PM2.5 and PM10 takes into account the model-observations discrepancies highlighted in Section 6.3.2 for each compound by means the adjusting ratios estimated.

Figure 6-10, left column, presents the seasonal mean concentration simulated with CALIOPE for PM2.5. From the statistical evaluation of the chemical compounds, multiplicative bias-correction factors where estimated for nm-SO_4^{2-}, NO_3^-, NH_4^+, and TC with the objective to reduce the annual mean bias. Figure 6-10, right column, shows the modelled PM2.5 when the aforementioned factors are applied for each species over the whole domain. Furthermore, seasonal mean observations are also represented in both cases. In order to quantify the CALIOPE performance to reproduce the observed spatial and seasonal variability of PM2.5, the spatial correlation (r) is shown bottom-left. PM10 seasonal and spatial variability is discussed analogously in Figure 6-11.

When the factors are applied individually to PM2.5 compounds, spatial correlations improve during all the seasons. The largest improvements are found in summer (from 0.48 to 0.70) associated with the increased formation of secondary aerosols, mainly nm-SO_4^{2-} and TC as shown in Section 6.3.2.4. According to PM10, modelled corrected concentrations only improve correlation coefficients during winter (from 0.60 to 0.66) and spring (from 0.59 to 0.68). There is an increase in

the observed PM2.5 and PM10 levels during summertime, which is more pronounced in the coarse fraction than in the finer fraction due to the contribution of coarser size of the re-suspended dust and summer-nitrate particles (Querol et al., 2009a). The applied factors do not correct these compounds, given that coarse NO_3^- is not implemented in the current version of CMAQv4.5 and only re-suspended material from road traffic is included. Overall, corrected-PM10 and PM2.5 from CALIOPE increase correlation spatially and seasonally when multiplicative correction factors for SIA and TC are applied. However, further analyses should be carried out on the coarse fraction.

Note that when the model is corrected, systematic high PM2.5 values (~10 μgPM2.5 m^{-3}) are found along the Mediterranean coast, Guadalquivir and Tajo valleys, where the impact of principal highways (Barcelona-Bilbao, the A-7 Mediterranean highway) and industrial sources (Huelva, Valencia, Tarragona) are noticeable. The highest PM2.5 concentrations are located around the biggest Spanish cities of Madrid and Barcelona (> 15 μgPM2.5 m^{-3}). During summer PM2.5 background level increase, and the concentration pattern presents a low spatial variability (~10 μgPM2.5 m^{-3}). Similar patterns are found for corrected modelled PM10, although concentrations are dominated by the DD contribution in the southern and eastern IP.

6.4 Conclusions

The CALIOPE system has been evaluated in terms of PM levels (PM2.5 and PM10) and chemical compounds (nm-SO_4^{2-}, NO_3^-, NH_4^+, TC, SS and DD) at ground level. Even more, CALIOPE annual results over the full year 2004 has been used to describe the seasonal pattern of PM and their chemical composition in Spain, increasing the knowledge on aerosol distribution.

The model performance presents wide variations among the different geographical areas in Spain. These variations also depend on the type of environment. The evaluation depicts that CALIOPE can reproduce the variability of PM2.5 and PM10 and their main aerosols compounds over Spain (0.45 < r < 0.64). However, concentrations are underestimated. At urban and suburban stations PM2.5 and PM10 levels present bias of -15 μgPM2.5 m^{-3} and -25 μgPM10 m^{-3}, where 40% and 30% of these biases are due to the underestimation in the regional background concentrations.

For the first time, the BSC-DREAM8b model coupled within CALIOPE system has been evaluated in terms of DD surface concentration in the PM10 fraction. The BSC-DREAM8b reproduces most of the Saharan dust outbreaks in 2004, in time and value, in areas of central, southwestern and southeastern Spain. However the BSC-DREAM8b presents difficulties to reproduce episodes where Saharan mineral dust followed an Atlantic trajectory from North Africa achieving the western IP. These later episodes are less intense than the summer ones. Concerning SS in PM10, CALIOPE reproduces correctly 70% of the daily observed concentration with a correctly temporal variability. At coastal stations the modelling system tends to simulate slightly higher SS than that measured meanwhile at continental areas SS tends to be underestimated. For both natural aerosol, DD and SS, CALIOPE accomplishes the model performance criteria proposed by Boylan and Russell (2006).
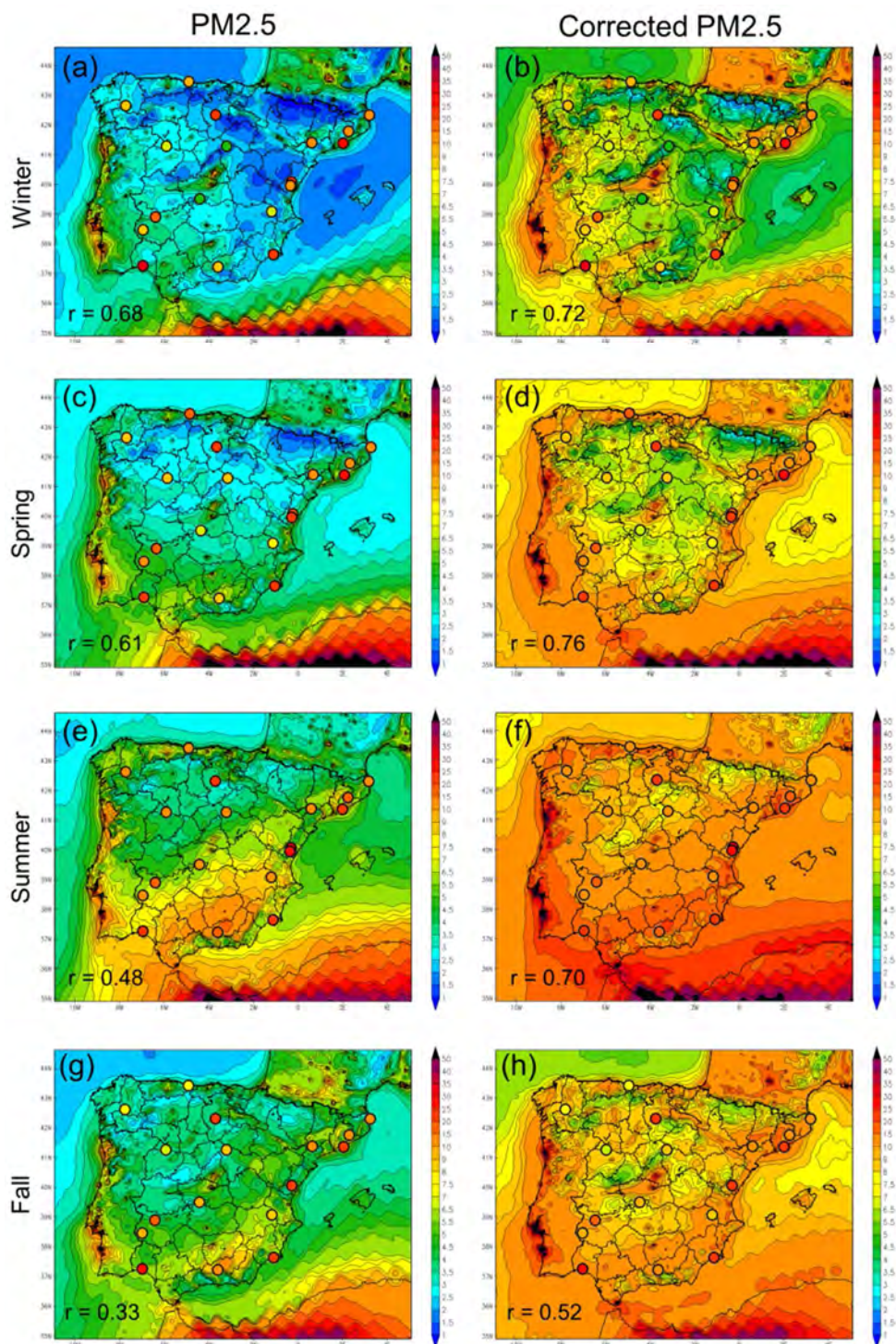
Figure 6-10. Seasonal average concentrations at lower-most level (μg m^{-3}) of (left) raw modeled PM2.5 and (right) corrected PM2.5 when multiplicative correction factors are applied to nm-SO$_4^{2-}$, NO$_3^-$, NH$_4^+$, and TC in the PM2.5 fraction. Seasons correspond to winter (a and b), spring (c and d), summer (e and f) and fall (g and h). Points represent measured seasonal averaged concentrations at the IDAEA-CSIC stations. The number of data points used to compute measured seasonal averaged concentrations is indicated in Table 2 in the column named Data. The number at bottom-left in each figure indicates the spatial correlation between model and observations
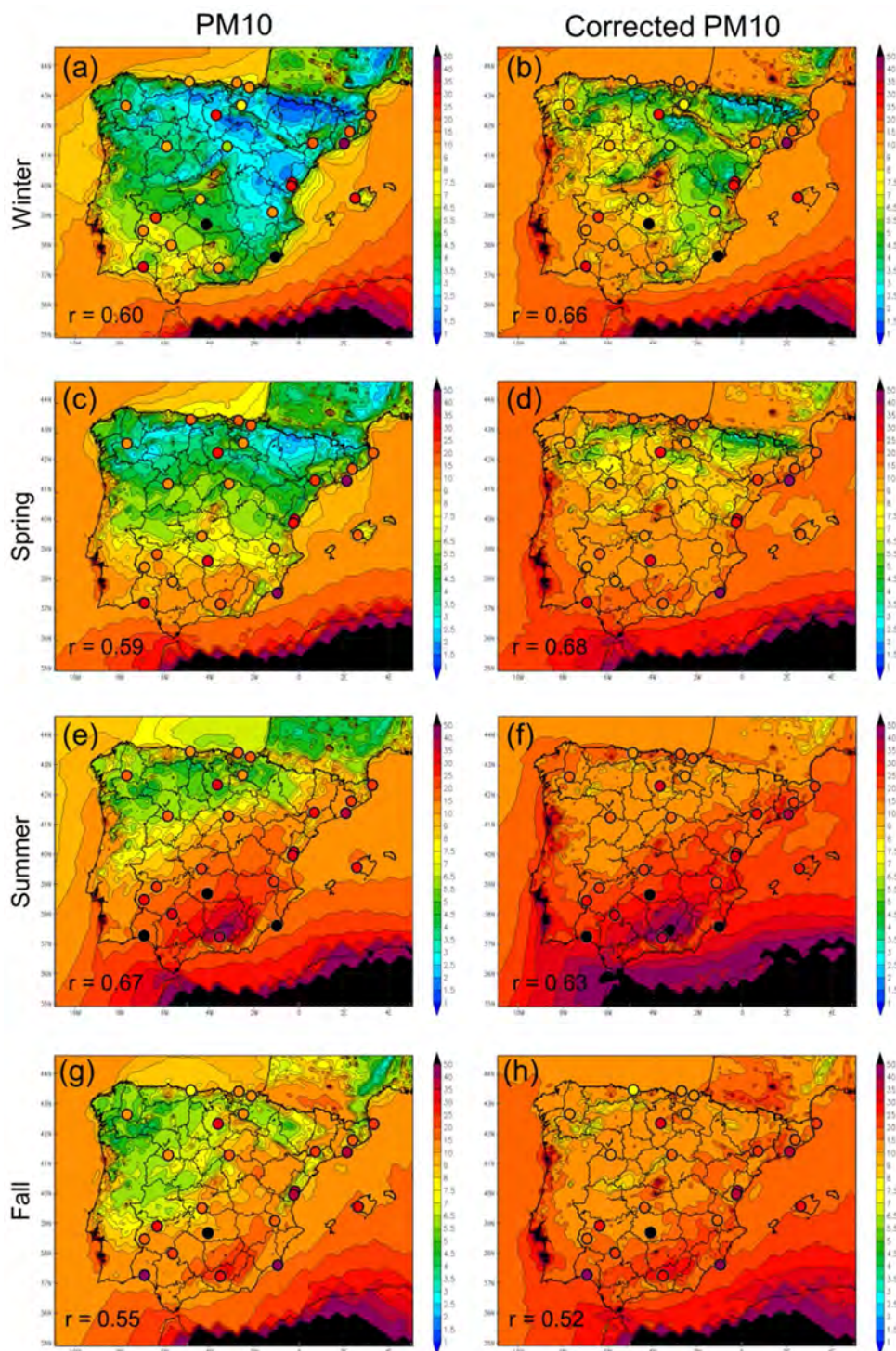
Figure 6-11. Seasonal average concentrations at lower-most level (μg m^{-3}) of (left) raw modeled PM10 and (right) corrected PM10 (right) when multiplicative correction factors are applied to nm-SO$_4^{2-}$, NO$_3^-$, NH$_4^+$, and TC in the PM2.5 fraction. Seasons correspond to winter (a and b), spring (c and d), summer (e and f) and fall (g and h). Points represent measured seasonal averaged concentrations at the IDAEA-CSIC stations. The number of data points used to compute measured seasonal averaged concentrations is indicated in Table 2 in the column named Data. The number at bottom-left in each figure indicates the spatial correlation between model and observations

The most important underestimations are linked to nm-SO_4^{2-}, fine NO_3^-, NH_4^+ and TC. nm-SO_4^{2-} and NH_4^+ are underestimated in a factor of 3, which is resembled in the model performance for NO_3^- which is underestimated in a factor of 2. Most uncertainties in the equilibrium nm-SO_4^{2-}/NH_4^+/NO_3^- are related to the treatment of NH_3 emission as it exhibits large spatial and temporal gradients. Annual mean concentration of TC at individual stations correlates by a factor of 4. These results agree with a large number of studies showing that air quality models generally underestimate organic aerosol concentrations, especially in urban air masses associate with uncertainties in secondary organic aerosol formation and bVOC emissions. Both temporal and spatial evaluations indicate that modelled skills for the aforementioned species improve when bias multiplicative bias correction factors are applied over each compound. Temporally, corrected model results accomplish model performance criteria for MFB and MFE established by Boylan and Russell (2006) for each compound and total levels (PM2.5 and PM10) at each station. Spatially, maximum improvements are found in summer for PM2.5 where global correlation increases from 0.48 to 0.70.

Concerning the CALIOPE results across the whole Spanish domain, PM chemical compounds exhibit geographical variations as well as marked seasonal patterns which are in agreement with the literature findings nm-SO_4^{2-} is found to be dependent mostly on the degree of industrialization of the regions. Fine NO_3^- concentration exhibits a winter maxima with no significant relationship with the distribution of emission sources, but highly dependent to the temperature and humidity. NH_4^+ spatial variability is relatively small in winter, usually being dominated by its association with nm-SO_4^{2-}. TC presents a clear winter maximum over urban environments that show its high correlation with anthropogenic emissions. SS shows a strong seasonality and dependence on the wind speed variation. Saharan air masses reach Spain when the synoptic situation is governed by depressions located to the west or southwest of the IP (winter) or when the North African anticyclone shifts to the East or Southeast of the IP (summer). DD contribution decreases from southeastern to northeastern Spain, with maximum contribution in summer (7–30 $\mu g \, m^{-3}$) affecting more than 50% of the Spanish country.

PM2.5 and PM10 seasonal patterns registered maximum concentration in summer, associated with the higher frequency of African dust outbreaks, lower precipitation, higher resuspension due to soil dryness, increased formation of secondary aerosols and recirculation of air masses that prevent air renovation. Our conclusion agrees with Flaounas et al. (2009) who showed that in Mediterranean areas the use of large-scale dust emissions and transport models, such as the BSC-DREAM8b, provide more reliable PM10 simulations. Furthermore, modelled annual DD contribution in Spain subscribes the measurements which estimated that the mean annual net dust contribution to the annual PM10 mean recorded at rural background sites reached < 2 $\mu g \, m^{-3}$ in the northern Spain and 6 $\mu g \, m^{-3}$ in the southeastern Spain (Querol et al., 2009b). On the other hand, PM10 and PM2.5 patterns present the highest variability during winter when intense pollution episodes of either anthropogenic (winter anticyclonic scenarios) or natural (African dust) origins take place. Local pollution episodes occur mainly in these periods: the anthropogenic emission increase and the atmospheric condition favours the accumulation of pollutants around the emission sources (development of intensive thermal inversion, lower convective dynamics and low dispersive local circulations).

The results of this study suggest an increase of the spatial coverage and temporal resolution of data sets on organic and inorganic aerosols. Furthermore, measurements of gas precursor like HNO_3, NH_3 and VOC are currently needed to test model results and identify sources of uncertainty in aerosol modelling.

The present analysis demonstrates that CALIOPE high-resolution modelling system (4 km × 4 km, 1 h) is a useful tool which complements measurements for increasing our knowledge about PM in terms of levels and composition in (1) urban/industrial areas with a pervasive influence of anthropogenic emissions on a local scale and (2) areas with very complex terrains and meteorology like Spain. However, there are a number of possible improvements to be done in chemical transport models. Within CALIOPE, and because of the results presented here, future work should be devoted to the improvements of secondary organic aerosol formation and dynamic interactions of fine and coarse fractions by the implementation of the updated version of CMAQ (v4.7.1, aerosol module AERO5) and revision of ammonia and bVOC emission implemented in HERMES model.

7. Conclusions

Although detail discussions of the results and conclusions have been included in the corresponding Chapter (from 2 to 6), the present Section summarizes the most important aspects of those discussions and theirs implication.

7.1 General conclusions

The present Ph.D. thesis has shown the evaluation experience with the **CALIOPE air quality modelling system**. The work has contributed to the assessment of the capability of the state-of-the-art regional and urban AQM systems to reproduce air pollution in Europe and Spain. Furthermore, it has set up the basis for modelling air quality, since it has identified strengths and necessities of improvement that should take into account in order to simulate air pollution over the target domains.

The CALIOPE system, WRF-ARW/HERMES-EMEP/CMAQ/BSC-DREAM8b, involves a set of models. The WRF-ARW meteorological model together with HERMES emission model, CMAQ chemical transport model and BSC-DREAM8b mineral dust model represent the state-of-the-art in AQM at regional and urban scales and they are highly supported and developed. The application of these models coupled in an AQM system involves a novel approach to reproduce the atmospheric dynamics across Europe and Spain for several reasons. First, it is applied with high-resolution on a computational grid necessary to resolve complex physico-chemical processes in complex terrains, as southern Europe. Second, it calculates high-resolution emissions using up-to-date information and the state-of-the-art methodologies for emission estimations. Third, it includes the state-of-the-art of physical and chemical processes involving the modelling of gaseous and particulate matter pollutants. Fourth, it takes into account the influence of Saharan dust on an hourly basis through the coupling to a desert dust model. Furthermore, the availability of the MareNostrum supercomputer, held in the BSC-CNS, together with the advances in the parallelization of air quality model codes for their implementation in these infrastructures, have allowed high-resolution simulations over a full year.

The most important conclusion from the research is that in order to reproduce air pollution in major anthropogenic emission hotspots, a high-resolution and high-disaggregated emission model becomes necessary. At regional scale, the HERMES-EMEP emission model (within CALIOPE-EU), which used the 2004 annual EMEP emission inventory, has allowed reproducing high NO_2, SO_2 and PM concentrations directly related to anthropogenic and biogenic emissions over Europe. The reproduction of the high variability of these patterns is possible thanks to the spatial top-down disaggregation methodology. Such methodology remaps emission data (50 km x 50 km) to the finer grid (12 km x 12 km) applying sector-dependent criteria through three main data sets: high-resolution land use map, coordinates of industrial sites and road cartography. The major air pollution problems are found over highly populated areas and industrialized areas in Europe such

as The Netherland, Belgium, central and eastern England, the Ruhr region and main cities (e.g. Milan, Paris, London, Barcelona, Madrid). Furthermore, northwestern Spain and eastern Europe (Poland, Serbia, Rumania, Bulgaria and Greece) are highly polluted areas linked to SO_2 emissions from power plants and transformation industries. Emissions from shipping largely contribute to high concentrations of SO_2 and NO_2 over the ocean along shipping routes (originating from the North Sea, passing by the English Channel, through Portugal, Strait of Gibraltar towards the Suez Canal) and near these coastal areas.

Furthermore, such high resolution in emission disaggregation, together with the accurate biogenic emission estimations, the high resolution meteorological patterns and the detailed boundary condition from LMDz-INCA2 model have provided a realistic tropospheric O_3 modelling in Europe (1) over regions chemically driven by a high-NO_x regimes, such as populated cities or within the shipping routes where minimum O_3 levels are found (annual mean concentration 50-55 $\mu g\ m^{-3}$); and (2) over the Mediterranean Basin (90-105 $\mu g\ m^{-3}$)

At urban scale, the results obtained using the CALIOPE-IP system have demonstrated that high-resolution and specific description of emissions are key points to simulate AQ levels at a local scale in urban/suburban areas affected by traffic or industrial emissions. Such results are possible due to the high-disaggregation and the detailed emissions of biogenic and anthropogenic sources implemented in the HERMES model, specifically developed for Spain with high spatial and temporal resolution (1 km x 1km, and 1h). On the one hand, the CALIOPE-IP system has allowed reproducing the high concentrations of NO_2, PM2.5 and PM10 (especially TC) from principal highways (e.g, Madrid-Sevilla, Barcelona-Bilbao, the A-7 Mediterranean highway) and from largest Spanish metropolitan areas (e.g., Madrid, Barcelona, Valencia, Sevilla, Málaga). The NO_2 urban plumes from Madrid and Barcelona reach the highest concentrations (~25-40 $\mu g\ m^{-3}$). The on-road traffic emission module, implemented in HERMES, takes into account the specific vehicle fleet composition and has a detailed definition of the road network and the traffic volumes.

On the other hand, the large plumes of high-SO_2 content (> 15 $\mu g\ m^{-3}$), and subsequently SO_4^{-2} (~2.5 $\mu g\ m^{-3}$), are allocated close to power plants and refineries over northern Spain (Galicia, Ponferrada, Asturias and Bilbao), eastern Spain (power plant of Teruel), and southern Spanish plateau (Puertoallano). SO_2 annual mean concentration reaches maximum levels (~50 $\mu g\ m^{-3}$) near the two refineries in Bilbao and La Coruña and over the narrow Gibraltar region (~12-18 $\mu g\ m^{-3}$) where the influence of shipping is combined with the contributions from one large refinery, industrial processes and electric generation carried out in the Gibraltar bay. HERMES calculates emissions by individual installations and stacks following a bottom-up approach. Evaluation results of CALIOPE-IP have been accurately reproduced since those sources are correctly allocated and characterized.

The high resolution of the HERMES model together with accurate meteorological patterns simulated by WRF-ARW have allowed reproducing spatial and temporal variability of O_3 concentrations. The lowest annual mean O_3 concentrations (~40-60 $\mu g\ m^{-3}$) are presented over areas affected by high-NO_x emissions which act as sinks of O_3 such as (1) the two largest Spanish metropolitan areas (Madrid and Barcelona), and (2) the Strait of Gibraltar region affected by frequent shipping and high density of industry. In contrast, the highest O_3 concentrations are found during summertime (from April to September), specifically 8-h maximum O_3 concentrations

exceeded the value of 120 μg m^{-3} by more than 30 days downwind the main NO$_x$ emission sources from Madrid and Barcelona cites and from industrial areas along the eastern Spanish Mediterranean coast. Dynamics of pollutants during summer and primary emission sources along the eastern coast and the central plateau of the IP determinate the location of those exceedances.

To be able to simulate PM at a regional scale over Europe, some key points have been identified. On the one hand, a state-of-the-art chemical mechanism that includes heterogeneous chemistry, a coupled gas-phase/aerosol chemistry and the description of the corresponding thermodynamic processes is needed. On the other hand, introducing desert dust (DD) aerosol contribution on an hourly basis with the BSC-DEAM8b model is essential for simulating hourly PM10 peaks during desert dust outbreaks, especially in southern Europe (Spain). Furthermore, over coastal areas the implementation of sea-salt (SS) emissions can help to accurately reproduce PM10 concentration, contributing ~3 and ~5 μg m^{-3} to the annual mean PM10 concentration over the Mediterranean and Atlantic coasts, respectively. Modelled SS concentrations within the CALIOPE system only take into account emissions from open-ocean.

On the other hand, reproducing both regional background concentrations is essential to simulate PM at urban scales over urban/suburban location in Spain. The latter aspect, the local contribution to PM, has been remarkable improved by means of the implementation of resuspension emissions from paved roads (RPR) on an hourly basis in the HERMES model. This approach is accurate and effective in order to reproduce PM10 concentrations near road traffic. The RPR contributes to increase PM10 concentrations up to 7 μg m^{-3} as annual mean in or near the largest urban zones.

Despite the aforementioned improvements, PM2.5 and PM10 concentrations remain underestimated, e.g. around 50% at regional scale. In the global context, CALIOPE system does not include global PM contributions, since boundary conditions from LMDz-INCA2 in the present configuration do not include aerosols mass. Biomass burning emissions, which are an important source of PM in the Iberian Peninsula, are not currently calculated by HERMES. This fact could be responsible for PM underestimations in episodes during dry seasons, especially in summertime. Furthermore, underestimation of urban PM sources may be related to underestimation of PM sources like the local natural erosion emissions resulting from saltation processes, especially important due to the Spanish climate.

Evaluation of aerosol chemical composition indicates that fine carbonaceous aerosols present the highest underestimations partly related to (1) the state-of-the-art concerning the SOA formation pathways, and (2) probable underestimation of primary carbonaceous emissions. The SOA model implemented in CMAQv4.5 does not include biogenic SOA formation from isoprene and sesquiterpenes. The predominant vegetation types in the Spanish domain favour isoprene as the main bVOC. The absence of the isoprene-SOA route on SOA modelling in the domain of study may impact significantly AQ during summer, when elevated bVOC emissions combine with an enhanced photochemistry. On the other hand, SIA are also underestimated. The uncertainty in the equilibrium nm-SO$_4^{2-}$/NH$_4^+$/NO$_3^-$ is related to the treatment of NH$_3$ emissions as it exhibits large spatial and temporal gradients.

Another source of underestimation in modelled PM2.5 and PM10 concentrations when compared with filter-based gravimetric measurement is due to the fact that PM measurements include water

content, but it is not quantified. The Reference Method recommended by the European Committee for Standardization (used in EMEP and EU for determining PM2.5 and PM10 concentrations at monitoring sites) establishes that dust-loaded filters should be equilibrated at about 50% relative humidity and 20°C temperature before they are weighted. Therefore, gravimetrically measured PM concentrations do not necessarily represent dry PM10 and PM2.5 concentrations. The CALIOPE system estimates aerosol water content, but its contributions has been neither evaluated nor taken into account.

Due to the complex topography and climatic particularities of Europe and the Iberian Peninsula, it becomes necessary to make the simulations with high spatial and temporal resolutions. In the case of the CALIOPE-IP, the resolution of 4 km x 4 km has allowed reproducing the transport patterns for pollutants in coastal (Atlantic and Mediterranean) and continental areas.

A comparison of the performance of the CALIOPE system with other European models has been done in terms of statistical parameters for air quality levels: gases (O_3, NO_2, SO_2), PM (PM2.5 and PM10), PM chemical composition (SO_4^{2-}, NO_3^-, and NH_4^+) and gas-phase precursors of aerosols (SO_2, NH_3/TNH_3 and HNO_3/TNO_3). The comparison has been done at regional scale over the European domain. No comparison is done at urban scale over Spain since up to this Ph.D. thesis the availability of published works on the topic is scarce. Despite the comparison is not a proper inter-comparison study, since the studies were performed under different conditions, it provides a good basis for assessing the reliability of the results obtained in the context of the European evaluation models. The selected European evaluation studies have several characteristics in common: (1) European domain; (2) regional scale; (3) simulated period, mainly annual; and (4) the use of EMEP monitoring network.

The results of this comparison suggested that the modelling system based on CMAQ, like CALIOPE-EU, performs better for NO_2 and SO_2 daily means than for O_3 daily mean and daily peaks. While most European models obtain correlation coefficients for O_3 annual daily peaks between 0.70 and 0.80, modelling systems based on CMAQ (e.g. CALIOPE-EU) reach a maximum of 0.69. However, the annual correlation coefficient obtained with CALIOPE-EU is higher than values reported by other studies using CMAQ, even than studies performed over US domain.

On the other hand, annual SO_2 and NO_2 performances are more accurate for CALIOPE-EU than for other European studies. Concerning the correlation coefficient, the annual daily mean variability reproduced with CALIOPE-EU is higher than the calculated in other European studies, $r = 0.67$ versus $r = 0.03$-0.47 in the case of NO_2; and $r = 0.60$ versus $r = 0.24$-0.49 for SO_2. Most models are based on the same emissions inventory, the EMEP database (50 km x 50 km spatial resolution), but the disaggregation techniques or additional integrated modules may differ. In this sense, the higher horizontal resolution of the CALIOPE-EU system (12 km x 12 km) compared to the other European studies (in the range of 25-55 km) and the disaggregation criteria may be responsible for the better scores obtained in NO_2 and SO_2.

Overall, the performance of PM concentrations and variability (PM2.5 and PM10) is relatively poor, but this comparison shows that the underestimated mean concentrations are a general feature affecting most models. According to the temporal variability, the annual daily mean correlation coefficient obtained with CALIOPE-EU is in the upper range of other European studies, $r = 0.47$

versus r = 0.44-0.54 for PM2.5; and r = 0.57 versus r = 0.38-0.57 for PM10. Substantial efforts should be made in the chemical description of PM formation and the accuracy of PM sources in all the studies European systems.

The evaluation performed on aerosol chemical compounds and gas-phase precursors has shown that HNO_3 and NH_3 (precursors) and fine-particle NH_4NO_3 are relatively poor, but the model evaluation comparison detailed in this work shows that the uncertainties and the lack of understanding around N-compounds is a general feature affecting most models.

The CALIOPE model evaluation against ground-based measurements suggests several points that must be taken with care. On the one hand, representativeness challenges are still present whenever gridded simulations are compared to observed data at point in time and space. The CALIOPE system simulations represent a volumetric average over an entire grid cell, meanwhile the stochastic compounds embedded in the observations is not accounted for. On the other hand, measurements have their own uncertainty due to biases and artefacts related to sampling and laboratory analysis methods. Consideration of measured uncertainty and spatial scale should be given when comparing model simulation and ambient measurements for model performance evaluation because none of them represent the absolute truth.

It is noteworthy that either correction factors or adjusting parameterizations have not been applied to the output of CALIOPE system during the evaluation process in order to identify the origin of the discrepancies and to determine the sources of uncertainty.

It may be stated that the objectives proposed for the present Ph.D. thesis (highlighted in Section 1.5) have been achieved, since the CALIOPE system has demonstrated a potential capability as a tool for assessing environmental issues related to AQ in Europe and Spain through a complex modelling system of nesting domains. First of all, at the regional scale, CALIOPE-EU (mother domain) provides an accurate representation of the background AQ levels over Europe, which is valuable to provide accurate chemical boundary conditions to simulate AQ levels in Spain by means of a nested-domain simulation (CALIOPE-IP). Second, the urban scale resolution simulation, CALIOPE-IP (one-way nested over the mother domain) correctly addresses the air pollution behaviour in urban environments with a pervasive influence of anthropogenic emissions and areas with very complex terrains thanks to (1) the high levels of temporal (1 h) and spatial disaggregation (1 km x 1 km) of the HERMES model which uses a bottom-up approach for the emission inventory specifically developed for Spain; and (2) the high horizontal and vertical resolution (4 km x 4 km and 15 layers, respectively) of the modelling system.

Furthermore, the present full year evaluation has warranted the use of CALIOPE system for forecasting the AQ in Spain, studying future scenarios, and for regulatory modelling applications, such as the modification of urban management strategies or requirements of the legislations.

7.2   Implications of the CALIOPE system

In the present Ph.D. thesis the **CALIOPE air quality modelling system** has been widely evaluated and assessed for the European and Spanish domains over an annual cycle (2004). First of all, the evaluation study has been focused on the regional scale over Europe (CALIOPE-EU). **Chapter 2** discusses the modelled results in terms of air quality levels: O_3, NO_2, SO_2, PM2.5 and PM10. CALIOPE-EU has been evaluated against remote rural background measurements from the EMEP monitoring network. Relevant conclusions are listed as follows:

- O_3 statistical indicators achieve satisfactory performances for both daily mean and daily maximum concentrations, especially in summer, with annual mean correlation of $r = 0.66$ and $r = 0.69$, respectively. MNBE and MNGE for O_3 are comprised within the recommendations proposed by the US EPA. The model skills improve notably from winter to summer as a result of the increasing importance of the photochemical production of O_3.

- The boundary conditions of the simulated domain were shown to strongly affect the evolution of O_3 background concentrations throughout the year, especially at the stations near the boundaries (such as Ireland and the countries along the North and Baltic Seas). The use of the LMDz-INCA2 global climate model as monthly mean to force the chemical boundary condition (interpolated in the horizontal and vertical dimensions of CALIOPE-EU) resulted an accurate option to simulate the contribution of O_3 by global transport with the CMAQ chemical transport model.

- The annual trends and daily variation of primary pollutants NO_2 and SO_2 are accurately modelled. On the one hand, daily mean concentrations of NO_2 agree with observations presenting correlations of $r = 0.67$, but tend to be underestimated ($MB = -4.0 \ \mu g \ m^{-3}$). Highest underestimations are found around Great Britain where high pollution events are caused by emissions from road traffic and combustion processes. Such underestimation may arise in unaccounted emissions and also in the spatial and temporal distribution of the sources. On the other hand, modelled SO_2 concentrations accurately reproduce annual and daily variability of measurements ($MB = 0.5 \ \mu g \ m^{-3}$) with relatively high annual temporal correlation between model-observation ($r = 0.60$), although peaks are generally overestimated. As for NO_2, the top-down spatial disaggregation, horizontally from 50 to 12 km; and vertically in the altitude-distribution of emissions, is a source of uncertainties.

- Temporal variability of model-observation for particulate matter, PM2.5 and PM10, are reproduced with high temporal correlation coefficients, $0.49 < r < 0.62$. However, mean concentrations remain systematically underestimated. It was found that CALIOPE-EU underestimates measured regional background concentrations by ~50 %. The spatial distribution of correlation coefficient and mean bias for winter and summer points out that CALIOPE-EU reproduces PM10 concentrations better in southern than in northern Europe. The implementation of both natural aerosol contributions, the Saharan desert dust throughout the BSC-DREAM8b model, and the sea salt aerosol emissions, largely contributes to the improvement of the PM10 concentrations in southern Europe and along coastal areas.

AQ assessments of annual spatial patterns are examined for each pollutant and compared with other modelled and experimental studies.

- O_3 annual mean pattern over Europe shows an increasing gradient from the northern and western boundaries to the more continental and Mediterranean areas, resulting from large variations in the climate pattern as it is shown in other modelling and experimental studies. The highest O_3 annual mean concentrations are found across the Mediterranean Basin (90-105 μg m^{-3}) affected by an intense photochemical production of O_3 and local coastal recirculations forced by a complex topography. Northwestern areas show rather low O_3 concentrations (60-67 μg m^{-3}) due to reduced solar radiation and the influence of the clean marine air.

- High modelled NO_2 concentrations at the regional scale (20-30 μg m^{-3}) are reported in the Netherlands and Belgium, central and eastern England, the Ruhr region and the industrial Po Valley. The highest NO_2 annual concentrations (30-40 μg m^{-3}) are estimated in populated cities (such as Milan, London, Paris). The largest contributors to NO_2 concentrations are the emissions from on-road transport (40% of NO_x total emissions) followed by power plants and other fuel converters (22% of NO_2 total emissions).

- Modelled SO_2 annual mean levels present high concentrations (20-40 μg m^{-3}) over eastern Europe, UK, Belgium, and southwestern Netherlands. The highest annual concentrations (70-90 μg m^{-3}) are found in northern Spain. Combustion emissions from power plants and transformation industries are the main responsible for such high SO_2 concentrations over Europe (64% of SO_x total emissions).

- Modelled PM2.5 spatial pattern shows average background concentrations around 3-10 μg m^{-3} in northwestern, central and eastern Europe. The highest PM2.5 levels are found in the Po Valley (14-22 μg m^{-3}) followed by the Benelux region (8-12 μg m^{-3}). Such concentration is mainly associated with primary anthropogenic emissions from on-road traffic and secondary aerosols. Concerning PM10, the highest annual mean concentrations are found in southern Europe (15-25 μg m^{-3}) and are linked to the transport of coarse particles from the Sahara desert. In this sense, the contribution of the desert dust throughout the BSC-DREAM8b model is essential to reproduce the high PM10 concentrations in southern Europe, whose estimations indicate annual contribution up to 40% to the PM10 (2-10 μg m^{-3} annual mean over southern Europe; 16-20 μg m^{-3} annual mean in southern Spain).

In order to identify the origin of discrepancies in the underestimation of PM and to determine the sources of uncertainty, an evaluation of the PM chemical components and their gas precursors against rural background measurements results essential. In this sense, **Chapter 3** presents a diagnostic evaluation which assesses how well the CALIOPE-EU modelling system reproduces the spatial and temporal variability of inorganic aerosol chemical components (SO_4^{2-}, NO_3^-, NH_4^+) and their important gas precursor species (SO_2, HNO_3 and NH_3). Model evaluation is performed using measurements from the EMEP network at remote rural background stations. Main conclusions are summarized as follows:

- The positive bias for SO_2 (as indicated before) suggests that non-marine SO_4^{2-} formation (MB = -0.3 $\mu g\ m^{-3}$) is often limited by oxidant availability and not always by SO_2 availability.

- Modelled NO_3^- concentrations are underestimated (MB = -1.0 $\mu g\ m^{-3}$). The uncertainty of NO_3^- and HNO_3 measurements hampers to discern if the model overestimation of HNO_3 results from a deficiency in model-process descriptions. The summer overestimation of HNO_3 and underestimation of NO_3^- should have minimal impact on regulatory applications since the warm temperatures do no favour the NH_4NO_3 formation.

- Simulated NH_4^+ concentrations were generally underestimated (MB = -0.4 $\mu g\ m^{-3}$). Two factors that most strongly influence simulated NH_4^+ concentration in Europe are NH_3 emissions and SO_4^{2-} concentrations. Modelled NH_3 does not compare as well with observation as NH_4^+ does. The modelled NH_3 concentrations are underestimated by ~100% during summer.

- SO_2/SO_4^{2-} and TNH_3/NH_4^+ monthly concentrations accomplish the criteria for bias and errors established by Boylan and Russell (2006) who suggested that MFB $\leq \pm\ 60\%$ and MFE $\leq 75\%$. Larger errors and biases are found for HNO_3 and NO_3^-.

- A strong relationship is depicted between model-observation biases for SO_4^{2-} and NH_4^+ (r = 0.59) and also between NO_3^- and NH_4^+ (r = 0.75). Nevertheless, there is no significant relationship between secondary inorganic aerosols (SIA) evaluation and performance for gas-phase precursors. These weak relationships indicate that the CALIOPE-EU performance for precursor gases does not directly translate into model biases for PM species in the same ambient sample. This likely reflects the different time scales of particulate formation and the influence of the regional transport.

Furthermore, the CALIOPE-EU system and EMEP measurements are used to assess sensitivity regimes of SIA formation in Europe:

- Fresh sulphur dominates eastern Europe, western Iberian Peninsula, and the major shipping routes, where oxidants are limiting the formation of sulphate. On the other hand, central Europe and the Mediterranean Basin are regions affected by the secondary SO_4^{2-} transported from the aforementioned sources.

- Fine-nitrate formation is mainly limited by the availability of HNO_3 over continental regions in Europe. Formation of SIA in Europe tends to be limited by SO_2 and HNO_3 gas precursors due to the relatively high NH_3 emissions, mainly from agriculture, especially in northwestern Europe. Regulatory strategies in this part of Europe should focus on the reduction of NO_x and SO_2, rather than on NH_3, to control NH_4NO_3 and $(NH_4)_2SO_4$, respectively.

Evaluation results in Chapter 2 and Chapter 3 indicate that the CALIOPE-EU system reproduces reasonably well the AQ background levels in Europe. The results are in the range of other

European models. These results assure the use of the CALIOPE-EU system for further nested calculations on the smaller domain of the Iberian Peninsula (CALIOPE-IP).

Once we have made sure that the CALIOPE-EU system is able to provide accurate chemical boundary conditions with high temporal and spatial resolution (12 km x 12 km, 1 h) to nested domains, the modelling system has been run at a higher spatial resolution at the urban scale across Spain (4 km x 4 km, 1h). Model evaluation over Spain suggested some necessities of improvement in the HERMES emission model. Therefore, HERMES was updated with the following: inclusion of agriculture and livestock emissions (SNAP10 sector), improvements in the spatial distribution of biogenic emission and population density via the use of the CORINE Land Cover information at a 100-m resolution, and introduction of emissions from the road traffic sector in small cities (SNAP10 sector). In addition, PM emissions resulting from paved road resuspension (RPR) is implemented in the last version of the on-road traffic emission module of the HERMES model, as described in detail in **Chapter 4**.

The implementation of the newly developed emission module considering resuspended PM from paved road by on-road traffic highly improved the PM10 concentration estimations over a domain covering Spain for a whole year of simulation (2004). This study suggests several relevant points:

- The implementation of RPR emissions indicates a remarkable improvement of the modelled PM10 concentration, reducing the biases and errors around 15-18% and 2.6 μg m^{-3} for the mean bias in all Spain.

- The RPR emissions have a strong local effect on the modelled particle concentrations in or near the largest urban zones (up to 17 μg m^{-3} as the annual average), albeit those positive effects are more limited in background areas, since the deposition mechanism was found to be a significant sink of RPR in the CMAQ model.

- Under precipitation conditions, RPR emissions decrease proportionally to the frequency of measurable precipitation. The precipitation effect is included in the calculation of the RPR emission.

- Therefore, RPR emission approach is accurate and effective in order to improve the simulation of PM10 and becomes essential to achieve the standards set in the regulations for modelling applications.

The last version of the HERMES model has been implemented in the CALIOPE system for the Iberian Peninsula domain (CALIOPE-IP) and evaluated in terms of air quality: O$_3$, NO$_2$, SO$_2$ and PM10 in **Chapter 5.** The evaluation of CALIOPE-IP is performed over measurement stations from the Spanish monitoring network on an hourly basis. The model performance showed a strong dependency on the type of environment (urban, suburban, and rural) and the dominant emissions sources (traffic, industrial, and background), which led the model to reproduce the high spatial and temporal disaggregation of the anthropogenic emissions. The main conclusions of the evaluation show:

- The modelled O_3 annual trends agree with measurements presenting high temporal correlations for hourly concentrations and daily maximum (r = 0.57, r = 0.64, respectively). In the high photolytical season (summer), the mean variability and high peaks are generally well reproduced. However, the modelled variability in winter months is characterized by difficulties to capture the mean trend due to inaccurate description of cross-tropopause exchanges in CMAQ. Statistics for annual O_3 concentrations (hourly and peaks) at each station category meet the recommendations proposed by the US EPA and the European regulations. Modelled O_3 shows accurate results in urban stations, especially those affected by direct on-road traffic emissions in large cities, especially at Madrid and Barcelona, since stations influence by traffic emissions (high-NO_x environments) are better characterized with a more pronounced daily variability. NO_x/O_3 chemistry is better represented under non-limited-NO_2 regimes.

- Generally, the modelled NO_2 annual trend is well captured with a clear signal of the main winter pollution events. However, mean NO_2 concentrations are persistently underestimated (MB = -12.3 μg m^{-3}). The best model behaviour reported corresponds to both rural stations influenced by background emissions and urban stations located in very large cities such as Madrid and Barcelona. In general, measurements at suburban or urban stations from small- to medium-sized cities were simulated with less accuracy due to an incomplete characterization of emissions from small cities and to the influence of the model resolution on sub-grid emission sources.

- Despite episodic extreme SO_2 concentrations are underestimated in general, the CALIOPE-IP system is capable to reproduce the annual trend. Annual MB is low, ranging from -3.1 μg m^{-3} for urban to 0.6 μg m^{-3} for suburban stations. Due to the frequent episodic character of high SO_2 events and their dependency on meteorology and emissions, hourly correlation coefficients are rather low (r = 0.14 for urban/suburban stations; 0.28 for rural stations). Meteorological patterns, spatial resolution (horizontal and vertical) and distribution of emission sources are crucial in the model performance of SO_2. Furthermore, sub-grid scale must be considered when comparing modelled results with measurements.

- Annual PM10 concentrations are persistently underestimated by CALIOPE-IP at rural, suburban and urban stations (MB = -21.8 μg m^{-3}). However, the hourly variability is accurately modelled, with the major events correctly reproduced and synchronized with measured concentrations. The mean correlation coefficient for all stations is 0.38 with higher correlations at rural stations (r = 0.43, ranging from 0.28 to 0.58 by station). The implementation of the Sahara desert dust contribution throughout the BSC-DREAM8b model is responsible for the satisfactory representation of such concentration peaks. The evaluation highlighted less accurate modelled concentrations at suburban and urban locations mostly influenced by industrial and traffic emissions.

Furthermore, AQ annual spatial patterns simulated with CALIOPE-IP are analysed. They are found to be consistent with other experimental studies. The assessment of CALIOPE-IP annual mean AQ patterns across Spain led to conclude:

- The highest O_3 mean concentrations are located in the open Mediterranean Sea (up to 90 $\mu g\ m^{-3}$) and the Spanish Mediterranean coast (~80 $\mu g\ m^{-3}$). Such concentrations are favoured by the prevailing intense photochemistry in the region, the local formation and transport, the persistent subsidence over the region and the low O_3 dry deposition over the sea. The lowest O_3 mean concentrations (~40-60 $\mu g\ m^{-3}$) are found in both regions of low precursor emissions (northern and southern plateaus) or in areas affected by large NO-to-NO_2 concentration ratios, corresponding to major Spanish metropolitan cities, highways of high traffic flow and the major shipping routes in the Mediterranean Sea.

- One of the main air quality-related problems in Spain is the high levels of O_3 concentrations at groun level. A quarter of the Iberian Peninsula shows more than 30 days exceeding the value 120 $\mu g\ m^{-3}$ for the maximum 8-h O_3 concentration as a consequence of the transport of O_3 precursors downwind to/from the Madrid and Barcelona metropolitan area, and industrial areas in cities in the Mediterranean coast.

- Annual spatial pattern of SO_2 concentration is mainly produced from stacks injected at elevated layers, from combustion in energy and transformation industries (83% of SO_2 total emission), which generate large plumes of high SO_2 concentrations affecting the air quality from a local (above 15 $\mu g\ m^{-3}$) to regional scale (~3 $\mu g\ m^{-3}$). SO_2 reaches maximum annual mean concentrations (~50 $\mu g\ m^{-3}$) near two refineries in Bilbao and La Coruña. On the other hand, shipping from the Atlantic, through the Strait of Gibraltar, toward the major Mediterranean harbours present high SO_2 annual concentrations (~8 $\mu g\ m^{-3}$).

- Spatial distribution of NO_2 concentrations at ground level is dominated by emission of combustion in energy and transformation industries (41% of NO_x total emission) followed by road transport (37% of NO_x total emission), which are subjected to a much stronger temporal variation than the SO_2 emissions. The urban plumes of Madrid and Barcelona reach the highest annual mean NO_2 concentrations (~25-40 $\mu g\ m^{-3}$). In north-western Spain the NO_2 contribution from power plants emissions is larger than the urban contribution, where NO_2 annual mean concentration reaches ~7-15 $\mu g\ m^{-3}$.

- PM10 annual mean concentrations increase from south (~25 $\mu g\ m^{-3}$) to north (~5 $\mu g\ m^{-3}$). In the southern Iberian Peninsula, African dust outbreaks contribute significantly to the aerosol loadings (~16-20 $\mu g\ m^{-3}$). PM10 annual mean concentrations present high values (~15 $\mu g\ m^{-3}$) over large cities (such as Madrid, Barcelona, Valencia, and Bilbao). Industrial areas in the eastern coast of Spain dominated by ceramic industry, present high levels of PM10 (~10 $\mu g\ m^{-3}$).

Hourly evaluation performed in Chapter 4 in terms of PM10 concentration has not been enough to identify necessities of improvements in aerosol modelling within CALIOPE-IP across Spain. In this sense, **Chapter 6** complemented such analysis providing a detailed qualitative analysis in terms of aerosol size (PM2.5 and PM10) and chemical composition (SO_4^{2-}, NO_3^{-}, NH_4^{+}, TC, SS and DD) against measurement at different types of stations in Spain from the IDAEA-CSIC monitoring network. The evaluation results indicate the following:

- Bias performances of the SIA in the PM2.5 fraction (nm-SO_4^{2-}/NO_3^-/NH_4^+) are highly correlated with each other. The nm-SO_4^{2-} and NH_4^+ modelling results underestimate annual mean observations by a factor of 3. An underestimation of fine NO_3^- was also evidenced (factor 2). Fine nm-SO_4^{2-} is almost always completely neutralized by NH_3 in CALIOPE-IP as $(NH_4)_2SO_4$. However, observations suggest that nm-SO_4^{2-} is present as bisulphate in most cases. The representation of NH_3 emissions can have a large effect on the equilibrium nm-SO_4^{2-}/NO_3^-/NH_4^+.

- Daily concentration of TC modelled with CALIOPE-IP is underestimated by a factor of 4 at individual stations. However, general annual trends are accurately reproduced (r = 0.45). During summer, TC is modelled with the lowest correlation coefficient (r = 0.31), partly due to lack of SOA yield paths. Accurate performance of CALIOPE-IP is found at the suburban station of Barcelona, mainly affected by road traffic emissions.

- Modelled PM10 sea salt (SS) is highly dependent on wind speed and presents high correlation with experimental data in coastal areas (r = 0.65). Higher performances are found during winter than in summer (r = 0.70 and r = 0.52, respectively). At coastal stations CALIOPE-IP tends to simulate slightly higher SS than that measured meanwhile at continental areas SS tends to be underestimated.

- The new experimental data set of Saharan dust PM10 concentration developed by the IDAEA-CSIC is a useful tool to evaluate modelled desert dust (DD) contribution from the BSC-DREAM-8b model over Spain. Such evaluation shows that the BSC-DREAM8b model slightly underestimates annual mean measurements (-5.9 $\mu g\ m^{-3}$) although it is able to reproduce most of the outbreaks affecting southern Spain. The highest temporal correlation coefficients were obtained for southern stations, such as Víznar (r = 0.57). The BSC-DREAM8b model underestimates some dust events associated with meteorological situations when emissions come directly from the Atlas region.

- Modelled natural aerosol, both sea salt and desert dust, accomplishes the model performance criteria establish by Boylan and Russell (2006).

Concerning the CALIOPE-IP results across Spain, PM chemical components exhibit geographical variations as well as marked seasonal patterns which are in agreement with the literature. Furthermore, the simulated patterns at ground level increase the knowledge in areas where measurements are not available until now.

- Spatial pattern of nm-SO_4^{2-} concentration is found to be dependent mostly on the degree of industrialization. Over Spain, nm-SO_4^{2-} presents minimum levels in winter and reaches maximum concentrations in summer. Maximum levels in summer are found mainly downwind power plants, refineries and transformation industries (~2.5-3.5 $\mu g\ m^{-3}$); and shipping routes (~4 $\mu g\ m^{-3}$), which are the main responsible for high SO_2 concentrations (as shown in Chapter 5).

- Conversely to nm-SO_4^{2-}, seasonal spatial pattern of NO_3^- concentration exhibits a winter maxima with no significant relationship with the distribution of emission sources. The

Spanish Mediterranean coast presents high fine-NO$_3^-$ levels related to the relative low dispersive atmospheric condition prevailing in the Mediterranean Basin and the high NH$_3$ caused by emission from intensive cultivation and farming.

- NH$_4^+$ spatial variability is relatively small in winter, usually being dominated by its association with nm-SO$_4^{2-}$.

- TC presents a clear winter maximum over urban environments showing high correlation with anthropogenic emissions. The urban plumes from Madrid and Barcelona metropolitan areas reach the highest TC concentration. In both regions, on-road traffic constitutes the main source of primary pollutants in the region and TC follows the same spatial pattern as NO$_2$ as shown in Chapter 5. Similar to nm-SO$_4^{2-}$/SO$_2$ and NO$_2$, the major shipping route from the northern Atlantic toward northern Africa and Suez Canal presents high TC concentrations.

- SS shows a strong seasonality and dependence on the wind speed variation. Maximum concentrations are simulated during winter, especially during northern Atlantic Ocean and the Gulf of Lion ($\sim$12 μg m^{-3}). In summer, maximum concentration of SS are found along the Strait of Gibraltar ($\sim$12 μg m^{-3}), meanwhile over the Mediterranean coast concentrations are around $\sim$2 μg m^{-3}.

- DD contribution decreases from southeastern to notheastern Spain, with maximum contributions between spring and summer (7-30 μg m^{-3}) affecting more than 50% of Spain, when the North African anticyclone shifts to the east or southeast of the Iberian Peninsula.

Evaluation results in Chapter 4, Chapter 5 and Chapter 6 demonstrate that the configuration of the CALIOPE-IP system over 2004 reproduces temporal and spatial patterns of AQ in urban/suburban areas affected by traffic and industrial emissions.

7.3   Emerging areas and future challenges

Despite the accurate performance of the **CALIOPE modelling system** potential applications and improvements are currently under further research. From the work compiled in the present Ph.D. thesis, future lines of research could focus on the following issues.

- **Evaluation study of the CALIOPE system in forecasting mode**. Nowadays, the CALIOPE system -with the same configurations as those presented in CALIOPE-EU and CALIOPE-IP for Europe and Spain, respectively- is routinely forecasting AQ in both domains. Operational AQ forecasts (O$_3$, NO$_2$, SO$_2$, PM2.5 and PM10) for 48h are available at www.bsc.es/caliope. Indeed, the CALIOPE forecasting system is currently included in the European Open Access Chemical Weather Forecasting Portal.

CALIOPE forecasts are evaluated in nearly real-time on an hourly basis. For the Spanish domain, non-validated near real time air quality measurements from more than 273 surface stations from the Spanish monitoring network are compared to ground-concentration forecast.

- **Research challenge on emission inventory and modelling**. Emission inventories are continuously being improved, not only in the framework of this work, but also due to the developments that the Earth Science Department of the BSC-CNS is performing nowadays. On the one hand, emissions inventory databases are currently being updated for the years 2008/2010. On the other hand, disaggregation methodologies are being improved using a more realistic spatial disaggregation (over the boundaries of countries and over the interface land-sea) and taking into account NACE codes (Classification of Economic Activities in the European Community) to disaggregate emissions over industrial sources. Furthermore, datasets used as criteria for desegregation are being updated, such as the CORINE Land Cover database (updated to 2006) which increases its coverage (e.g. Turkey, Norway, Serbia, Montenegro); and the E-PRTR database (European Pollutant Release and Transfer Register) (updated to 2008) which replaces and improves the previous EPER database (European Pollutant Emission Register) with more than 69.190 industrial sources (against 11.505 in 2004).

  Concerning the on-road traffic emission estimations in the bottom-up inventory approach, the methodology and emission factors are being updated to the new COPER IV-CORINAIR methodology.

  Also, future research in emission modelling should be focused on: (1) a review of temporal characterization of temporal NH_3 emissions from agricultural and livestock, and on (2) the implementation of biomass burning emissions (mainly NO_x, VOC and PM) and NO_x production from soils and lightning. Biogenic emissions estimated with HERMES emission model are being revised.

- **Increasing the vertical and horizontal resolution in the CALIOPE system**. The next stage of application of the CALIOPE system may be increase the vertical and horizontal resolution. The developments in this aspect are conditioned by the computational resources. An increase of the supercomputing capability of MareNostrum is currently planned.

- **Chemical boundary conditions from global models to CALIOPE-EU**. Using chemical boundary conditions from the LMDz-INCA2 model has improved the simulation skills at regional scale by providing more realistic temporal variation and spatial distribution, especially for O_3 concentrations. However, under some episodes, the outputs from the global model produced excessive transport of O_3 aloft in the boundary conditions leading to unrealistically high O_3 concentrations at the surface layer during the regional simulation. CMAQ does not have a stratospheric component or stratosphere-troposphere exchange mechanism.

  Research must be focused on resolving the inconsistency of vertical structures between LMDz-INCA2 model (containing both the tropospheric and stratospheric components) and CMAQ (containing only the tropospheric component) to yield better surface O_3 simulation. To resolve that vertical incompatibility, tropopause information should be incorporated into any coupled global and regional model excluding any stratospheric O_3 from being included in the regional

air quality model since CMAQ is only designed for tropospheric application and any stratospheric O_3 or stratospheric intrusion should be considered inapplicable in CMAQ.

- **Improved understanding and parameterization of physical and chemical processes**. A new version of CMAQ is being tested in the CMAS community, namely CMAQv5.0. It includes a new aerosol module, AERO5, which contains substantial scientific improvements over the AERO4 released in version 4.5, especially devoted to improve SOA formation and dynamic interactions of fine and coarse aerosol. Some new features in CMAQv5.0 against version 4.5 are listed as follows:

  - CMAQv5.0 allows semi-volatile aerosol components to condense and evaporate from the coarse mode and non-volatile sulphate to condense on the coarse mode. Dynamic mass transfer is simulated for the coarse mode, whereas the fine modes are equilibrated instantaneously with the gas phase.

  - The unspeciated PM was improved by adding 9 new PM2.5 species, including primary non-carbon organic matter (NCOM), and particulate Fe, Al, Si, Ti, Ca, Mg, K and Mn. Anthropogenic emissions of 4 existing PM2.5 species (NH_4^+, Na^+, Cl^- and H_2O) are now included.

  - Modelled Fe and Mn concentrations are now explicitly used to catalyse aqueous oxidation of SO_2 to SO_4^{2-}.

  - An oxidative aging reaction was added for primary organic aerosol. There were some minor updates to the SOA yield parameterization.

  - The updated version ISORROPIA aerosol thermodynamics module (ISORROPIAv2) is included in CMAQ5.0. In contrast to CMAQv4.5, the "reverse" mode of ISORROPIA is used in CMAQv5.0.

Concerning the natural emissions, an optional algorithm for windblown dust was added to the CMAQv5.0 model. Furthermore, on coastal regions, CMAQv5.0 allows significant emissions of sea salt from wave-breaking in the surf zone. CMAQv4.5 only accounts sea-salt emissions from open ocean.

CMAQv5.0 includes several improvements for gas-phase chemistry. The Carbon Bond chemical mechanism version 05 (CB05) now includes updated toluene chemistry, revised rate constants for N_2O_5 hydrolysis based on the latest recommendation of IUPAC, and additional reactions of toluene and xylene with chlorine radical.

- **Experimental data availability to evaluate the CALIOPE system.** The performance of the CALIOPE system has been evaluated against ground-based measurements sufficiently large in time and spatial coverage for O_3, SO_2, NO_2 and PM10; which are measured routinely at most monitoring networks. Data availability of PM2.5 and size- and chemically-resolved PM data is scarce. However, the evaluation of modelling system in Europe should focus on PM2.5 instead

of PM10, as it is more relevant form a health perspective and also recently regulated by a new European directive (2008/50/EC).

For PM, the model evaluation should not be restricted to only PM10 and PM2.5. Furthermore, the understanding and evaluation of the chemical components of PM and their gas precursors is needed to make sure that the model predictions are right for the right reason, and to close the gap between modelled and measured concentrations of PM. For instance, the evaluation of only the PM10 concentrations may not reveal serious shortcomings in a model with respect to the treatments of the PM components. Moreover, size-resolved PM data are crucial in order to reduce uncertainties in our understanding of the modelling of emissions, dispersion and transformation of PM.

The spatial and temporal coverage of measurements for diagnostic pollutants (such as HNO_3, NH_3, NH_4^+, organic aerosol, especially separate OC and EC) is scarce. The increase of spatial coverage and temporal resolution of data sets is necessary for a complete evaluation of photochemical model results.

Modelling of organic aerosols has suffered for a long time from the limited availability of ambient organic aerosol measurements (including speciation and tracers) due to the high cost, low sensitivity, and low time and size resolution of most organic aerosol measurement methods until recently. Experimental field campaigns such as MILAGRO, CalNex, GVAX, BEACHON, DAURE, etc) provide in that perspective a unique dataset to study the formation and evolution of aerosols and their precursors which is valuable to investigate the efficiency of formation pathways represented in the model.

The recent DAURE field campaign performed over the western Mediterranean provides intensive measurements of aerosols (with particular attention to carbonaceous aerosols) and gas precursors; and could be a useful framework to evaluate the CALIOPE system and indirectly the HERMES emission model.

- **Model inter-comparison.** Besides the comparison of CALIOPE results to ground-based measurements, several other steps should be considered to ensure model quality, such as model inter-comparisons performs under the same conditions (simulated year, meteorological data, boundary condition, emissions data, etc.). The Earth Science Department of the BSC-CNS is currently working on that topic, performing an inter-comparison of the result from two chemical transport model CMAQ (version 4.5) and CHIMERE (version 2008c) in the framework of the CALIOPE project. The differences between CMAQ and CHIMERE results reveal the strengths and weaknesses of particular models and parameterizations schemes and could help to characterize conceptual uncertainties arising from the choice and implementation of the physical models applied.

The present Ph.D. thesis demonstrates by means of evaluation methods that the high temporal and spatial resolution modelling system CALIOPE correctly addresses the air pollution behaviour in Europe (configuration CALIOPE-EU; 12 km x 12 km, 1 h), and Spain (configuration CALIOPE-IP; 4 km x 4 km, 1 h) over (1) background levels across Europe, (2) urban/industrial areas with a pervasive influence of anthropogenic emissions on a local scale, (3) areas with very complex terrains

and meteorology like southern Europe; and (4) Iberian Peninsula and South Europe highly affected by frequent Saharan dust outbreaks. Therefore, the present modelling system has been implemented and evaluated to operationally forecast air quality in both European and Spanish domains (currently available at http://www.bsc.es/caliope).

8. References

Abu-Allaban, M., Gillies, J.A., Gertler, A.W., Clayton, R., Proffitt, D., 2003. Tailpipe, resuspended road dust, and brake-wear emission factors from on-road vehicles. *Atmos. Environ.*, **37**, 5283-5293.

Adams, L.I., Davis, J., Japar, S.M., Finley, D.R., 1990. Real-time, in situ measurements of atmospheric optical absorption in the visible via photoacoustic spectroscopy e IV. Visibility degradation and aerosol optical properties in Los Angeles. *Atmos. Environ.*, **24**A, 605-610.

Adams, P.J., Seinfeld, J.H., Koch, D.M., 1999. Global concentrations of tropospheric sulfate, nitrate, and ammonium aerosol simulated in a general circulation model. *J. Geophys. Res.*, **104**, 13791-13823.

Alpert, P., Ganor, E., 1993. A jet stream associated heavy dust storm in the western Mediterranean. *J. Geophys. Res.*, **98**, 7339-7349. doi: 10.1029/92JD01642.

Altshüller, A.P., 1984. Atmospheric particle sulfur and sulfur dioxide relationships at urban and nonurban locations. *Atmos. Environ.*, **18**, 1421-1431.

Amann, M., Bertok, I., Cofala, J., Gyarfas, F., Heyes, C., Klimont, Z., Schöpp, W., Winiwater, W., 2004. Baseline Scenarios for the Clean Air for Europe (CAFE) programme. Technical Report. European Commission, DG Environment, Dir. C Environment and Health.

Amato, F., Pandolfi, M., Escrig, A., Querol, X., Alastuey, A., Pey, J., Perez, N., Hopke, P.K., 2009a. Quantifying road dust resuspension in urban environment by multilinear engine: a comparison with PMF2. *Atmos. Environ.*, **43**, 2770-2780.

Amato, F., Pandolfi, M., Viana, M., Querol, X., Alastuey, A., Moreno, T., 2009b. Spatial and chemical patterns of PM10 in road dust deposited in urban environment. *Atmos. Environ.*, **43**, 1650-1659.

Amato, F., Nava, S., Lucarelli, F., Querol, X., Alastuey, A., Baldasano, J.M., Pandolfi, M., 2010. A comprehensive assessment of PM emissions from paved roads: real-world emission factors and intense street cleaning trials. *Sci. Total Environ.*, **408**, 4309-4318.

Ansari, A.S., Pandis, S., 1998. Response of inorganic PM to precursor concentrations. *Environ. Sci. Technol.*, **32**, 2706-2714

Appel, W.K., Gilliland, A., Sarwar, G., Gilliam, R.C., 2007. Evaluation of the Community Multiscale Air Quality (CMAQ) model version 4.5: uncertainties and sensitivities impacting model performance: Part I - ozone. *Atmos. Environ.*, **41** (40), 9603-9613.

Appel, W.K., Bhave, P.V., Gilliland, A.B., Sarwar, G., Roselle, S.J., 2008. Evaluation of the Community Multiscale Air Quality (CMAQ) model version 4.5: sensitivities impacting model performance; Part II - particulate matter. *Atmos. Environ.*, **42** (24), 6057-6066.

Arévalo, G., Salvador, R., Gassó, S., Millán, M., Baldasano, J.M., 2004. Application of a high-resolution emission model in Valencia Community (Spain). Air Pollution 2004. Rhodes, Greece: WIT Press. pp. 31-40.

Artíñano, B., Querol, X., Salvador, P., Rodríguez, S. and Alastuey, A., 2001. Assessment of airborne particulate matter in Spain in response to the new EU-directive. *Atmos. Environ.*, 35, 43-53.

Asman, W.A.H., 2001. Modelling the atmospheric transport and deposition of ammonia and ammonium: an overview with special reference to Denmark. *Atmos. Environ.*, **35**, 1969-1983.

Athanasopoulou, E., Tombrou, M., Pandis, S.N., Russell, A.G., 2008. The role of sea-salt emissions and heterogeneous chemistry in the air quality of polluted coastal areas. *Atmos. Chem. Phys.*, **8**, 5755-5769.

Atkinson, R., 2000. Atmospheric chemistry of VOCs and NO_x. *Atmos. Environ.*, **34**, 2063-2101.

Atkinson, R., Arey, J., 2003. Gas-phase tropospheric chemistry of biogenic volatile organic compounds: a review. *Atmos. Environ.*, **37**, S197-S219.

Atkinson, R., 2007. Gas-phase tropospheric chemistry or organic compounds: a review. *Atmos. Environ.*, **41**, S200-S240.

Bakeas, E.B., Argyris, D.I., Siskos, P.A., 2003. Carbonyl compounds in the urban environment of Athens, Greece. *Chemosphere*, **52**, 805-813.

Baker, K., Scheff, P., 2007. Photochemical model performance for PM2.5 sulfate, nitrate, ammonium, and precursor species SO_2, HNO_3, and NH_3 at background monitor locations in the central and eastern United States. *Atmos. Environ.*, **41**, 6185-6195.

Baldasano, J.M., Cremades, L., Soriano, C., 1994. Circulation of air pollutants over the Barcelona geographical area in summer. Proceedings of Sixth European Symposium Physic-Chemical Behaviour of Atmospheric Pollutants. Varese, Italy, 18-22 October. Report EUR 15609/1 EN: 474-479.

Baldasano, J.M., Calbó, J., Costa, M., 1995. Importance of atmospheric transport processes in the urban air quality: the case of Barcelona. In: Urban Air Pollution II, Chapter 2, Ed. N. Moussiopoulos et al., Computational Mechanics Publications, Southampton, UK, 41-68.

Baldasano, J.M., 1998. Guidelines and formulation of an upgrade source emission model for atmospheric pollutants. In: Air Pollution Emissions Inventory, Volume 3. Power, H., Baldasano, J.M. (Eds). Computational Mechanics publications, Southampton (UK), 238 pp.

Baldasano, J.M., 1999. Conaminación Atmosférica I: Historia y Elementos Básicos. *TecnoAMBIENTE*, IX, 89, 19-22.

Baldasano, J. M. and Millán, M. M., 2000. Guía para la Aplicación de Modelos de Calidad del Aire (Guide for the application of Air Quality Models). IV Seminario sobre la Calidad del Aire en España. Sitges, Spain. 38 pp.

Baldasano, J.M., Valera, E., Jiménez, P., 2003. Air quality data form large cities. *Sci. Total Environ.*, **307**(1-3), 141-165.

Baldasano, J.M., Güereca, L.P., López, E., Gassó, S., Jimenez-Guerrero, P., 2008a. Development of a high-resolution (1 km x 1 km, 1 h) emission model for Spain: the high-elective resolution modelling emission system (HERMES). *Atmos. Environ.*, **42**, 7215-7233.

Baldasano, J.M., Jiménez-Guerrero, P., Jorba, O., Pérez, C., López, E., Güereca, P., Martín, F., Vivanco, M.G., Palomino, I., Querol, X., Pandolfi, M., Sanz, M.J., Diéguez, J.J., 2008b. Caliope: an operational air quality forecasting system for the Iberian Peninsula, Balearic Islands and Canary Islands-first annual evaluation and ongoing developments. *Adv. Sci. Res.*, **2**, 89-98.

Baldasano, J.M., Pay, M.T., Jorba, O., Gassó, S., Jiménez-Guerrero, P., 2011. An annual assessment of air quality with the CALIOPE modeling system over Spain. *Sci. Total Environ.*, **409**, 2163-2178.

Balk, T., Kukkonen, J., Karatzas, K., Bassoukos, T., Epitropou, V., 2010. An European open access chemical weather forecasting portal. *Atmos. Environ.* doi: 10.1016/j.atmosenv.2010.09.058.

Baklanov, A., Fay, B., Kaminski, J., Sokhi, R., Pechinger, U., De Ridder, K., Delcloo, A., Korsholm, U.S., Gross, A., Männik, A., Kaasik, M., Sofiev, M., Reimer, E., Schlüzen, H., Tombrou, M., Bossioli, E., Finardi, S., Maurizi, A., Castelli, T.S., Finzi, G., Carnevale, C., Pisoni, E., Volta, M., Struzewska, J., Kaszowski, W., Godlowska, J., Rozwoda, W., Miranda, A.I., San José, R., Persson, C., Foltescu, V., Clappier, A., Athanassiadou, M., Hort, M.C., Jones, A., Vogel, H., Suppan, P., Knoth, O., Yu, Y., Chemel, C., Hu, R.M., Grell, G., Schere, K., Manins, P., Flemming, J., 2008. Overview of existing integrated (off-line and on-line)

mesoscale meteorological and chemical transport modelling systems in Europe, WMO TD No. 1427, WMO, Geneva, Switzerland.

Barros, N., Toll, I., Soriano, C., Jiménez, P., Borrego, C., Baldasano, J.M., 2003. Urban Photochemical Pollution in the Iberian Peninsula: the Lisbon and Barcelona Airsheds. *J. Air Waste Manage.*, **53**, 347-359.

Basart, S., Pérez, C., Cuevas, E., Baldasano, J.M., Gobbi, G.P., 2009. Aerosol characterization in Northern Africa, Northeastern Atlantic, Mediterranean Basin and Middle East from direct-sun AERONET observations. *Atmos. Chem. Phys.*, 9, 8265-8282.

Bassett, M., Seinfeld, J.H., 1983. Atmospheric equilibrium model of sulphate and nitrate aerosols. *Atmos. Environ.*, **17**, 2237-2252.

Beck, J., Grennfeld, P., 1993. Distribution of ozone over Europe. In: The Proceedings of the EUROTRAC Symposium, 43-58 pp.

Beirle, S., Platt, U., Wenig, M., Wagner, T., 2004. Highly resolved global distribution of tropospheric NO_2 using GOME narrow swath mode data. *Atmos. Chem. Phys.*, **4**, 1913-1924.

Bessagnet, B., Hodzic, A., Vautard, R., Beekmann, M., Cheinet, S., Honoré, C., Liousse, C., Rouïl, L., 2004. Aerosol modeling with CHIMERE-preliminary evaluation at the continental scale. *Atmos. Environ.*, **38**, 2803-2817.

Binkowski, F.S., Shankar, U., 1995. The regional particulate model 1. Model description and preliminary results. *J. Geophys. Res.*, **100** (D12), 26191-26209.

Binkowski, F.S., 1999. Aerosols in models-3 CMAQ. In: Byun, D.W., Ching, J.K.S. (Eds.), Science Algorithms of the EPA Models-3 Community Multiscale Air Quality (CMAQ) Modeling System. EPA, 600, 99-30.

Binkowski, F.S., Roselle, S.J., 2003. Models-3 Community Multiscale Air Quality (CMAQ) model aerosol component. 1. Model description. *J. Geophys. Res.*, **108**(D6), 4183.

BOE, 2011. Real Decreto 102/2011, de 28 de enero, relativo a la mejora de la calidad del aire. Ministerio de la Presidencia. BOE número 25. BOE-A-2011-1645. 53 pp.

Boersma, K.F., Eskes, H.J., Veefkind, J.P., Brinksma, E.J., van der A, R.J., Sneep, M., van der Oord, G.H.J., Levelt, P.F., Stammes, P., Gleason, J.F., Bucsela, E.J., 2007. Near real time retrieval of tropospheric NO_2 from OMI. *Atmos. Chem. Phys.*, **7**, 2103-2118.

Bond, T.C., Streets, D.G. Yarber, K.F., Nelson, S.M., Woo, J.H. and Klimont, Z., 2004. A technology-based global inventory of black and organic carbon emissions from combustion. *J. Geophys. Res.*, **109**, D14203, doi: 10.1029/2003JD003697.

Boylan, J., Russell, A., 2006. PM and light extinction model performance metrics, goals, and criteria for three-dimensional air quality models. *Atmos. Environ.*, **40**, 4946-4959.

Britter, R., Schatzmann, M., 2007. Model evaluation guidance and protocol document, COST Action 732. Quality assurance and improvement of micro-scale meteorological models, 27 pp.

Borrego, C., Schatzmann, M., Galmarini, S., 2003. Quality assurance of air pollution models. In: EUROTRAC, 2003. Air quality in cities. SATURN EUROTRAC-2 Subproject. Final Report, Springer Publisher. Chapter 7, 156-183.

Borrego, C., Miranda, A.I., Costa, A.M., Monteiro, A., Ferreira, J., Martins, H., Tchepel, O., Carvalho, A.C., 2006. Uncertainties of models and monitoring. Air4EU Milestone Report 6.5. Available at: http://www.air4eu.nl/PDF/Reports_products/D5.2.pdf.

Borrego, C., Gauss, M., 2007. Aspects of Scale Interactions in Atmospheric Modelling. In: Proceedings of the ACCENT Workshop on Model Benchmarking and Quality Assurance 29/30 May 2006, Thessaloniki, Greece. Eds. Moissiopoulos and Isaksen.

Borrego, C., Monteiro, A., Ferreira, J., Miranda, A.I., Costa, A.M., Carvalho, A.C., Lopes, M., 2008. Procedures for estimation of modelling uncertainty in air quality assessment. *Environ. Inter.*, **34**, 613-620.

Boylan, J., Russell, A., 2006. Pm and light extinction model performance metrics, goals, and criteria for three-dimensional air quality models. *Atmos. Environ.*, **40**, 4946-4959.

Brauer M., Dumyahn T.S., Spengler J.D., Gutschmidt K., Heinrich J., Wichmann H.E., 1995. Measurement of acidic aerosol species in eastern Europe: implications for air pollution epidemiology. *Environ. Health Persp.*, **103**, 482–488.

Brunekreef, B., Holgate, S.T., 2002. Air pollution and health. *Lancet*, **360** (9341), 1233-1242. doi:10.1016/S0140-6736(02)11274-8.

Bytnerowicz, A., Omasa, K., Paoletti, E., 2007. Integrated effects of air pollution and climate change on forests: A northern hemisphere perspective. *Environ. Poll.*, **147**, 438-445.

Byun, D.W., Ching, J.K.S., 1999. Science Algorithms of the EPA Models-3 Community Multiscale Air Quality (CMAQ) Modeling System. Atmospheric Modeling Division, National Exposure Research Laboratory, US Environmental Protection Agency, Research Triangle Park, NC 27711.

Byun, D., Schere, K.L., 2006. Review of the governing equations, computational algorithms, and other components of the Models-3 Community Multiscale Air Quality (CMAQ) modeling system. *Appl. Mech. Rev.*, **59** (2), 51-77.

CAFE, 2005. Communication from the Commission to the Council and the European parliament: Thematic Strategy on air pollution SEC(2005)1132 and SEC(2005)1133, European Commission, Brussels. 13 pp.

Calbó, J., Baldasano, J.M., 1995. PROMETEO: an hydrostatic mesoscale model applied to the simulation of land-sea breeze in the Barcelona area. *Environ. Soft.*, **10**, 139-155.

Camuffo, D., Secco, C., Brimblecombe, P., Martin-Vide, J., 2000. Sea storms in the Adriatic Sea and the western Mediterranean during the last millennium. *Climatic Change*, **46**, 209-223. doi: 10.1023/A:1005607103766.

Carlton, A. G., Turpin, B. J., Altieri, K. E., Seitzinger, S. P., Mathur, R., Roselle, S. J., and Weber, R. J., 2008. CMAQ model performance enhanced when in-cloud secondary organic aerosol is included: Comparisons of organic carbon predictions with measurements. *Environ. Sci. Technol.*, **42**(23), 8798–8802.

Carter, W.P.L., 2000. Implementation of the SAPRC-99 Chemical Mechanism into the Models-3 Framework. Report to the United States Environmental Protection Agency, January 29. Available at: http://www.cert.ucr.edu/~carter/absts.htm#s99mod3.

Carter, W.P.L., 2010. Development of the SAPRC-07 chemical mechanism and updated ozone reactivity scales, report to the California Air Resources Board. Available at: http://www.engr.ucr.edu/~carter/SAPRC/saprc07.pdf.

Cavaleri, L., 2005. The wind and wave atlas of the Mediterranean Sea-The calibration phase. *Adv. Geosci.*, **2**, 255-257.

Chang, J.C., Hanna, S.R., 2004. Air quality model performance evaluation. Meteorol. *Atmos. Phys.*, **87**, 167-196.

Chemel, C., Sokhi, R.S., Yu, Y. Hayman, G.D., Vincent, K.J., Dore, A.J., Tang, Y.S., Prain, H.D., Fisher, B.E.A., 2010. Evaluation of a CMAQ simulation at high resolution over the UK for the calendar year 2003. *Atmos. Environ.*, **44**, 2927-2939.

Ching, J., Herwehe, J., Swall, J., 2006. On joint deterministic grid modeling and subgrid variability conceptual framework for model evaluation. *Atmos. Environ.*, **40**, 4935-4945.

Chylek, P., Wong, J., 1995. Effect of absorbing aerosols on global radiation budget. *Geophys. Res. Lett.*, **22** (8), 929-931. doi:10.1029/95GL00800.

Cohen, A.J., Anderson, H.R., Ostro, B., Pandey, K.D., Krzyzanowski, M., Künzli, N., Gutschmidt, K., Pope, C.A.I., Romieu, I., Samet, J.M., Smith, K.R., 2004. Urban air pollution. In: LA Ezzati, M., Rodgers, A., Murray, C.J.L. (eds) Comparative quantification of health risks: global and regional burden of disease attributable to selected major risk factors, vol 2. World Health Organization, Geneva, pp. 1153–1433.

Cooke, W.F. and Wilson, J.J.N., 1996. A global black carbon aerosol model. *J. Geophys. Res.*, 101, 19395-19409.

Corbett, J.J., Fischbeck, P., 1997. Emissions from ships. *Science*, **278**(5339), 823-824. doi:10.1126/science.278.5339.823.

Corbett, J.J., Koehler, H.W., 2003. Updated emissions from ocean shipping. *J. Geophys. Res.*, **108**(D20), 4650. doi:10.1029/2003JD003751.

Córdoba-Jabonero, C., Sorribas, M., Guerrero-Rascado, J.L., Adame, J.A., Hernández, Y. Lyamani, H., Cachorro, V., Gil, M., Alados-Arboledas, L., Cuevas, E., de la Morena, B., 2011. Synergetic monitoring of Saharan dust plumes and potential impact on surface: a case study of dust transport from Canary Islands to Iberian Peninsula. *Atmos. Chem. Phys.*, **11**, 3067-3091.

COST, 2009. Towards a European Network on Chemical Weather Forecasting and Information Systems (ENCWF). Technical Report. COST Action ES0602, Monitoring Progress Report.

Costa, M., Baldasano, J.M., 1996. Development of a source emission model for atmospheric pollutants in the Barcelona area. *Atmos. Environ.*, **30**, 309-318.

Cowell, D., Apsimon, H., 1996. Estimating the cost of damage to buildings by acidifying atmospheric pollution in Europe. *Atmos. Environ.*, **30**, 2959-2968.

Cox, W.M., Tikvart, J.A., 1990. Statistical procedure for determining the best performing air quality simulation model. *Atmos. Environ.*, **24**, 2387-2395.

Cristofanelli, P., Bonasoni, P., 2009. Background ozone in the southern Europe and Mediterranean area: influence of the transport processes. *Environ. Pollut.*, **157**, 1399-1406.

Cuvelier, C., Thunis, P., Vautard, R., Amann, M., Bessagnet, B., Bodogni, M., Berkowicz, R., Brandt, J., Brocheton, F., Builtjes, P., Carnavale, C., Coppalle, A., Denby, B., Douros, J., Graf, A., Hellmuth, O., Hodzic, A., Honoré, C., Jonson, J., Kerschbaumer, A., de Leeuw, F., Minguzzi, E., Moussiopoulos, N., Pertot, C., Peuch, V.H., Pirovano, G., Rouil, L., Sauter, F., Schaap, M., Stern, R., Tarrasón, L., Vignati, E., Volta, M., White, L., Wind, P., Zuber, A., 2007. City Delta: a model intercomparison study to explore the impact of emission reductions in European cities in 2010. *Atmos. Environ.*, **41**, 189-207.

Delle Monache, L., Nipen, T., Deng, X., Zhou, Y., Stull, R., 2006. Ozone ensemble forecasts: 2. A Kalman filter predictor bias correction. *J. Geophys. Res.*, **110**, D05308.

Delgado, R., Toll, I., Soriano, C., Baldasano, J.M., 2000. Vehicle emission model of air pollutants from road traffic. Application to Catalonia (Spain) for 1994. In: Air Pollution VIII, section 4. Edited by J.W.S. Longhurst, C.A., Brebbia and H. Power. Wit Press, UK, 379-388.

Denby, B., Larssen, S., Guerreiro, C., Li, L., Douros, J., Moussiopoulos, N., et al., 2010. Guidance on the use of models for the European Air Quality Directive. A working document of the Forum for Air Quality Modelling in Europe. FAIRMODE. In: Denby, B., editor. Technical Report Version 4.2ETC/ACC.

Dennis, R., Fox, T., Fuentes, M., Gilliland, A., Hanna, S., Hogrofe, C., Irwin, J., Trivikrama, R., Scheffe, R., Schere, K., Steyn, D., Venkatram, A., 2010. A framework for evaluating regional-scale numerical photochemical modeling systems. *Environ. Fluid Mech.* doi: 10.1007/s10652-009-9163-2.

van Dingenen, R., Raes, F., Putaud, J.P., Baltensperger, U., Charron, A., Facchini, M.C., Decesari, S., Fuzzi, S., Gehrig, R., Hansson, H.C., Harrison, R.M., Hüglin, C., Jones, A.M., Laj, P., Lorbeer, G., Maenhaut, W., Palmgren, F., Querol, X., Rodríguez, S., Schneider, J., Brink, H., Tunved, P., Torseth, K., Wehner, B., Wingartner, E., Wiedensohler, A., Wahlin, P.,

2004. A European aerosol phenomenology – 1: physical characteristics of particulate matter at kerbside, urban, rural and background sites in Europe. *Atmos. Environ.*, **38**, 2561-2577.

Djalalova, I., Wilczak, J., McKeen, S., Grell, G., Peckham, S., Pagowski, M., Delle Monache L., McQueen, J., Tang, Y., Lee, P., McHenry, J., Gong, W., Bouchet, V., Mathru, R., 2010. Ensemble and bias-corretion thechniques for air quality model forecast of surface O_3 and PM2.5 during the TEXAQS-II experiment of 2006. *Atmos. Environ.*, **44**, 455-467.

Dockery, D.W., Pope III, C.A., Xu, X., Spengler, J.D., Ware, J.H., Fay, M.E., Ferris Jr., B.G., Speizer, F.E., 1993. An association between air pollution and mortality in six U.S. cities. *New Engl. J. of Med.*, **329**, 1753-1759.

Dodge, M.C., 2000. Chemical oxidant mechanisms for air quality modeling: critical review. *Atmos. Environ.*, **34**, 2103-2130.

Dudhia, J., 1989. Numerical study of convection observed during the winter monsoon experiment using a mesoscale two-dimensional model. *J. Atmos. Sci.*, **46**(20), 3077-3107. doi:10.1175/1520-0469.

Dueñas, C., Fernández, M.C., Cañete, S., Carretero, J., Liger, E., 2002. Assessment of ozone variations and meteorological effects in an urban area in the Mediterranean coast. *Sci. Total Environ.*, **299**, 97-113.

Düring, I., Jacob, J., Lohmeyer, A., Lutz, M., Reichenbacher, W., 2002. Estimation of the "non-exhaust pipe" PM10 emissions of streets for practical traffic air pollution modelling, in: 11th Intl. Symposium on Transport and Air Pollution, Graz University of Technology, Institute for Internal Combustión Engines and Thermodynamics, vol 1., pp. 309-316.

Düring, I., Wolfgang, B., Bsinger, R., Wolfgang, J., Lohmeyer, A., 2004. Experiences when modelling roadside PM10 concentration, in: JRC-EI (Ed.), Proceedings of the 9th International conference on Harmonisations within Atmospheric Dispersion Modelling for Regulatory Purposes, Garmisch Partenkirchen. pp. 208-212.

Dyer, A.J., Hicks, B.B., 1970. Flux-gradient relationships in the constant flux layer. *Q. J. R. Meteorol. Soc.*, **96**(410), 715-721. doi:10.1002/qj.49709641012.

Eder, B., Yu, S., 2006. A performance evaluation of the 2004 release of models-3 CMAQ. *Atmos. Environ.*, **40**, 4811-4824. doi:10.1016/j.atmosenv.2005.08.045.

Edney, E.O., Kleindienst, T.E., Lewandowski, M. and Offenberg, J.H., 2007. Updated SOA chemical mechanism for the community multi-scale air quality model, EPA 600/X-07/025, US Environmental Protection Agency, Research Triangle park, North Carolina.

EEA, 2000. CORINE Land Cover, 2000. Technical Report. European Environmental Agency. Available at: http://sia.eionet.europa.eu/CLC2000.

EEA, 2005. Air Pollution by Ozone in Europe in Summer 2004. Technical Report 3/2005. European Environmental Agency.

EEA, 2006. EMEP-CORINAIR Emission Inventory Guidebook 2006. Technical Report 30. European Environmental Agency.

EEA, 2007. Air Pollution in Europe 1990-2004. Technical Report 2/2007. European Environmental Agency.

EEA, 2009a. Air pollution by ozone across Europe during summer 2008. Technical Report 2/2009. European Environmental Agency.

EEA, 2009b. Spatial assessment of PM10 and ozone concentrations in Europe (2005). Technical Report 1/2009. European Environmental Agency.

EEA, 2010a. The European Environment. State and outlook 2010. Air pollution. European Environmental Agency. Luxembourg, Publication Office of the European Union. ISBN 978-92-9213-152-4. doi:10.2800/57792.

EEA, 2010b. Air pollution by ozone across Europe during summer 2009. Overview of exceedances of EC ozone threshold values for April-September 2009. Technical Report 2/2010. European Environmental Agency.

Eisele, H., Scheel, H.E., Sladkovic, R., Trickl, T., 1999. High-resolution lidar measurements of stratosphere-troposphere exchange. *J. Atmos. Sci.*, **56**, 319-330.

Elleman, R.A., Covert, D. S., 2009. Aerosol size distribution modeling with the Community Multiscale Air Quality modeling system (CMAQ) in the Pacific Northwest: 1. Model comparison to observations. *J. Geophys. Res.*, **114**, D11206. doi:10.1029/2008JD010791.

EMEP, 2004. EMEP Assessment Part I. In: Lövblad, G., Tarrasón, L., Torseth, K., Dutchak, S. (Eds.), European Perspective. Available at: http://www.emep.int.

EMEP, 2007. National Emissions Reported to the Convention on Long-range Transboundary Air Pollution (LRTAP Convention). Air Emission Annual Data Reporting (EMEP/MSC-W). Technical Report. European Environmental Agency, The Norwegian Meteorological Institute, Oslo, Norway.

EMEP, 2009. EMEP/EEA air pollutant emission inventory guidebook – 2009. Technical report 9/2009.

Emmerson, K.M., Evans, M.J., 2009. Comparison of tropospheric gas-phase chemistry schemes for use within global models. *Atmos. Chem. Phys.*, **9**, 1831-1845.

Escudero, M., Castillo, S., Querol, X., Avila, A., Alarcón, M., Viana, M.M., Alastuey, A., Cuevas, E., Rodríguez, S., 2005. Wet and dry African dust episodes over Eastern Spain. *J. Geophys. Res.*, **110**, 4731-4746.

Escudero, M., Querol, X., Avila, A., Cuevas, E., 2007a. Origin of the exceedances of the European daily PM limit value in regional background areas in Spain. *Atmos. Environ.,* **41**, 730-744.

Escudero, M., Querol, X., Pey, J., Alastuey, A., Pérez, N., Ferreira, F., Alanso, S., Rodríguez, S., Cuevas, E., 2007b. A methodology for the quantification of the net African dust load in air quality monitoring networks. *Atmos. Environ.*, **41**, 5516-5524.

ESRI, 2003. Europe Highways Cartography 2003. Technical Report. GIS de ESRI (ESRI) España Geosistemas S.A: http://www.esri-es.com.

European Commission, 1991. Council Directive 91/676/EEC of 12 December 1991 concerning the protection of waters against pollution caused by nitrates from agricultural sources as amended by Regulation 1882/2003/EC and 1137/2008/EC.

European Commission, 1996. Council Directive 96/62/EC of 27 September 1996 on Ambient Air Quality Assessment and Management Laid the Foundations for a Common Strategy to Define and Establish Objectives for Ambient Air Quality. Technical Report 1996/62/EC, L296. Off. J. Eur. Comm.

European Commission, 1999. Council Directive 1999/30/EC of 22 April 1999 Relating to Limit Values for Sulphur Dioxide, Nitrogen Dioxide and Oxides of Nitrogen, Particulate Matter and Lead in Ambient Air. Technical Report 1999/30/EC, L 163. Off. J. Eur. Comm.

European Commission, 2001. Commission Decision of 17 October 2001 Amending Annex V to Council Directive 1999/30/EC Relating to Limit Values for Sulphur Dioxide, Nitrogen Dioxide and Oxides of Nitrogen, Particulate Matter and Lead in Ambient Air (Text with EEA Relevance) (Notified Under Document Number C (2001) 3091). Technical Report 2001/744/EC, 278. Off. J. Eur. Comm.

European Commission, 2002. Directive 2002/3/EC of the European Parliament and of the Council of 12 February 2002 Relating to Ozone in Ambient Air. Technical Report 2002/3/EC, L67. Off. J. Eur. Comm.

European Commission, 2005. Forest fires in Europe 2004. Report 5. Official Publication of the European Commission. http://www.fire.uni-freiburg.de/programmes/eu-comission/EU-Forest-Fires-in-Europe-2004.pdf. S.P.I.05.147 EN.

European Commission, 2008. Directive 2008/50/EC of the European Parliament and of the Council of 21 May 2008 on Ambient Air Quality and Cleaner Air for Europe. Technical Report 2008/50/EC, L152. Off. J. Eur. Comm.

Fagerli, H., Aas, W., 2008. Trends of nitrogen in air and precipitation: Model results and observations at EMEP sites in Europe, 1980-2003. *Environ. Pol.*, **154**, 448-461.

Finlayson-Pitts, B.J., Pitts, J.N., 2000. Chemistry of the upper and lower atmosphere-Theory, experiments and applications. Academic, San Diego, 969 pp.

Finlayson-Pitts, B.J., 2010. Atmospheric chemistry. Proceedings of the National Academy of Science of the United States of America, 107, 6566-6567.

Fishman, J., Crutzen, P., 1978. The origin of ozone in the troposphere. *Nature*, **274**, 855-858.

Flaounas, E., Coll, I., Armengaud, A., Schmechtig, C., 2009. The representation of dust transport and missing urban sources as major issues for the simulation of PM episodes in a Mediterranean area. *Atmos. Chem. Phys.*, **9**, 8091-8101.

Folberth, G., Hauglustaine, D.A., Lathière, J., Brocheton, J., 2006. Interactive chemistry in the Laboratoire de Météorologie Dynamique general circulation model: model description and impact analysis of biogenic hydrocarbons on tropospheric chemistry. *Atmos. Chem. Phys.*, **6**, 2273-2319.

Foster, C., Wandinger, U., Wotawa, G., James, P, Mattis, I., Althausen, D., Simmonds, P., O'Doherty, S., Jennings, S.G., Kleefeld, C., Schneider, J., Trickl, T., Kreipl, S., Jäger, H., Stohl, A., 2001. Transport of boreal forest fire emissions from Canada to Europe. *J. Geophys. Res.*, **106**, 22887-22906.

Fountoukis, C., Nenes, A., 2007. ISORROPIA II: a computationally efficient thermodynamic equilibrium model for K^+-Ca_2^+-Mg_2^+-NH_4^+-Na^+-SO_4^{2-}-NO_3^--Cl^--H_2O aerosols. *Atmos. Chem. Phys.*, **7**, 4639-4659.

Gangoiti, G., Millán, M.M., Salvador, R., Mantilla, E., 2001. Long-range transport and re-circulation of pollutants in the western Mediterranean during the project Regional Cycles of Air Pollutions in the West-Central Mediterranean Area. *Atmos. Environ.*, **35**, 6267-6276.

Galmarini, S., Bianconi, R., Klug, W., Kikkelsen, T., Addis, R., Andronopoulos, S., Astrup, P., 2004a. Ensemble dispersion forecasting, Part I: concept, approach and indicators. *Atmos. Environ.*, **38**, 4607-4617.

Galmarini, S., Bianconi, R., Addis, R., Andronopoulos, S., Astrup, P., Bartzis, J.C., Bellasio, R., Buckley, R., Champion, H., Chino, M., D'Amours, R., Davakis, E., Eleveld, H., Glaab, H., Manning, A., Mikkelsen, T., Pechinger, U., Polreich, E., Prodanova, M., Slaper, H., Syrakov, D., Terada, H., van der Auwera, L., 2004b. Ensemble dispersion forecasting, Part II: application and evaluation. *Atmos. Environ.*, **38**, 28, 4619-4632.

Garber, W., Closio, J., Grittner, S., Larssen, S., Rasse, D., Schneider, J., Housiau, M., 2002. Guidance on the Annexes to Decission 97/101/EC on Exchange of Information as revised by Decision 2001/752/EC. Technical Report. European Commission, DG Envrionment.

Gehrig, R. Hill, M., Buchmann, B., Imhof, D., Weingartner, E., Baltensperger, U., 2004. Separate determination of PM10 emission factors of road traffic for tailpipe emissions and emissions from abrasion and resuspensions processes. *Int. J. Environ. Pollut.*, **22**, 312-25.

Gerasopoulos, E., Kouvarakis, G., Vrekoussis, M., Kanakidou, M., Mihalopoulos, N., 2005. Ozone variability in the marine boundary layer of the eastern Mediterranean based on 7-year observations. *J. Geophys. Res.*, **110**(D15309).

Gery, M.W., Whitten, G.Z., Killus, J.P., Dodge, M.C., 1989. A photochemical kinetics mechanism for urban and regional scale computer modeling. *J. Geophys. Res.*, **94**(D10), 12925-12956.

Gilliland, A.B., Dennis, R.L., Roselle, S.J., Pierce, T.E., 2003. Seasonal NH_3 emission estimates for the eastern United States based on ammonium wet concentrations and an inverse modeling method. *J. Geophys. Res.*, **108**(D15), 4477. doi:10.1029/2002JD003063.

Gilliland, A. B., Appel, W.K., Pinder, R.W., Dennis, R.L., 2006. Seasonal NH_3 emissions for the continental united states: Inverse model estimation and evaluation. *Atmos. Environ.*, **40**, 4986-4998.

Goliff, W.S., Stockwell, W.R., 2008. The Regional Atmospheric chemistry Mechanism, version 2, an update, International conference on Atmospheric Chemical Mechanisms, University of California, Davis.

Gonçalves, M., Jiménez-Guerrero, P., López, E., Baldasano, J.M., 2008. Air quality models sensitivity to on-road traffic speed representations: Effects on air quality of 80 km h^{-1} speed limit in the Barcelona Metropolitan area. *Atmos. Environ.*, **42**, 8389-8402.

Gonçalves, M., Jiménez-Guerrero, P., Baldasano, J.M., 2009a. High-resolution modeling of the effects of alternative fuels use on urban air quality: Introduction of natural gas vehicles in Barcelona and Madrid Greater Areas (Spain). *Sci. Total Environ.*, **407**, 776-790.

Gonçalves, M., Jiménez-Guerrero, P., Baldasano, J.M., 2009b. Contribution of atmospheric processes affecting the dynamics of air pollutions in South-Western Europe during a typical summertime photochemical episode. *Atmos. Chem. Phys.*, **9**, 849-864.

Gong, S.L., 2003. A parameterization of sea-salt aerosol source function for sub- and super-micron particles. *J. Geophys. Res.*, **17**, 1097. doi:10.1029/2003GB002079.

Grell, G.A., Peckham, S.E., Schimtz, R., McKeen, S.A., Frost, G., Skamarock, W.C., Eder,B., 2005. Fully coupled online chemistry within the WRF model. *Atmos. Environ.*, **39**, 6957-6975.

Gross, A., Stockwell, W.R., 2003. Comparison of the EMEP, RADM2, and RACM mechanism. *J. Atmos. Chem.*, **44**, 151-170.

Gryparis, A., Forsberg, B., Katsouyanni, K., Analitis, A., Touloumi, G., Schwartz, J., Samoli, E., Medina, S., Anderson. H.R., Niciu, E.M., Wichmann, H.-E., Bohumir, K., Kosnik, M., Skorkovsky, J., Vonk J.M., Dörtbudak, Z., 2004. Acute effects of ozone on mortality from the air pollution and health: a European approach project. *Am. J. Respir. Crit. Care Med.*, **170**(10), 1080-1087.

Guenther, A.B., Hewitt, C.N., Erickson, D., Fall, R., Geron, C., Graedel, T., Harley, P., Klinger, L., Lerdau, M., Mckay, W.A., Pierce, T., Scholes, B., Steinbrecher, R., Tallamraju, R., Taylor, J., Zimmerman, P., 1995. A global model of natural volatile organic compound emissions. *J. Geophys. Res.*, **100**, 8873-8892.

Guerova, G., Bey, I., Attié, J.L., Martin, R.V., Cui, J., Sprenger, M., 2006. Impact of transatlantic transport episodes on summertime ozone in Europe. *Atmos. Chem. Phys.*, **6**, 2057-2072.

Gurjar, B.R., Jain, A., Sharma, A., Agarwal, A., Gupta, P., Nagpure, A.S., Lelieveld, J., 2010. Human health risks in megacities due to air pollution. *Atmos. Environ.*, **44**, 4606-4613.

Haagen-Smit, A.J., Darley, E.F., Zaitlin, M., Hull, H., Nobel, W., 1951. Investigation on injury to plants from air pollution in the Los Angeles area. *Plant Physiology*, **27**, 18.

Halmilton, J.F., Webb, P.J., Lewis, A.C., Hopkins, J.R., Smith, S., Davy, P., 2004. Partially oxidised organic components in urban aerosol using GCXGC-TOF/MS. *Atmos. Chem. Phys.*, **4**, 1279-1290.

Hamed, A., Birmili, W., Joutsensaari, J., Mikkonen, S., Asmi, A., Wehner, B., Spindler, G., Jaatinen, A., Wiedensohler, A., Korhonen, H., Lehtinen, K.E., Laaksonen, A., 2010. Changes in the production rate of secondary aerosol particles in Central Europe in view of decreasing SO_2 emissions between 1996 and 2006. *Atmos. Chem. Phys.*, **10**, 1071-1091.

Harrison, R. M., Pio, C., 1983. Sized differentiated composition of inorganic aerosol of both marine and continental polluted origin, *Atmos. Environ.*, **17**, 1733-1738.

Hass, H., van Loon, M., Kessler, C., Stern, R., Matthijsen, J., Sauter, F., Zlatev, Z., Langner, J., Foltescu, V., Schaap, M., 2003. Aerosol modeling: results and intercomparison from European regional scale modeling systems. Special Report. EUROTRAC-2 ISS, Garmisch Partenkirschen.

Harrison, R.M., van Grieken, R.E., 1998. Atmospheric Particles. IUPAC series on analytical and physical chemistry of environmental sytems. J. Buffle and H.P. van Leeuwen. John Wiley & Sons, 610 pp.

Hauglustaine, D.A., Hourdin, F., Jourdain, L., Filiberti, M.A.,Walters, S., Lamarque, J.F., Holland, E.A., 2004. Interactive chemistry in the Laboratoire de Meteorologie Dynamique general circulation model: description and background tropospheric chemistry evaluation. *J. Geophys. Res.*, **109**, D04314. doi:10.1029/2003JD003957.

Heald, C.L., Jacob, D.J., Park, R.J., Alexander, B., Fairlie, T.D., Yantosca, R.M., Chu, D.A., 2006. Transpacific transport of Asian anthropogenic aerosols and its impact on surface air quality in the United States. *J. Geophys. Res.*, **111**, D14310.

Hewitt, C.D., Griggs, D.J., 2004. Ensembles-based Predictions of Climate Changes and their Impacts. Technical Report. 1, Eos, 85.

Hodzic, A., Vautard, R., Bessagnet, B., Lattuati, M., Moreto, F., 2005. Long-term urban aerosol simulation versus routine particulate matter observations. *Atmos. Environ.*, **39**, 5851-5864.

Hogrefe, C., Hao, W., Civerolo, K., Ku, J.Y., Sistla, G., 2006. Exploring approaches to integrate observations and CMAQ simulations for improved air quality forecast. Presented at the 5th annual CMAQ User's Conference, Chapel Hill, NC. Available at: http://www.cmascenter.org/conference/2006/abstracts/hogrefe_session3.pdf.

Hong, S.Y., Dudhia, J., Chen, S.H., 2004. A revised approach to ice microphysical processes for the bulk parameterization of clouds and precipitation. *Mon. Weather Rev.*, **132** (1), 103-120. doi:10.1175/1520-0493.

Hyslop, N.P., White, W.H., 2008. An evaluation of interagency monitoring of protected visual, environments (IMPROVE) collocated precision, and uncertainty estimates. *Atmos. Environ.*, **42**, 2691-2705.

Internacional Maritime Organization and Marine Environment Protection Committee, 2001. Prevention of air pollution from ships—sulfur monitoring 2000. Technical Report; 2001. London.

IPCC, 2007. Climate Change 2007: the Physical Science Basis. Contribution of Working Group I to the Fourth Assessment Report of the IPCC (ISBN: 978 0521 88009-1 Hardback: 978 0521 70596-7 Paperback).

Jacob, D.J., 2000. Heterogeneous chemistry and tropospheric ozone. *Atmos. Environ.*, **34**, 2131-2159.

Jacob, D.J., Field, B.D., Jin, E.M., Bey, I., Li, Q.B., Logan, J.A., Yantosca, R.M., Singh, H.B., 2002. Atmospheric budget of acetone. *J. Geophys. Res.*, **107**(D10). doi: 10.1029/2001JD000694.

Jacob, D.J., Winner, D.A., 2009. Effect of climate change on air quality. *Atmos. Environ.*, **43**, 51-63.

Jacobson, M.Z., 1999. Fundamentals of atmospheric modeling. Cambridge University Press, UK, 656 pp.

Jacobson, M.Z., 2001. Global direct radiative forcing due to multicomponent anthropogenic and natural aerosols. *J. Geophys. Res.*, **106**(D2), 1551-1568. doi:10.1029/2000JD900514.

Jacobson, M.Z., 2002. Atmospheric Pollution: History, Science and Regulation. Cambridge University Press.

Jaenicke, R., Schütz, L., 1978. Comprehensive study of physical and chemical properties of the surface aerosols in the Cape Verde islands region. *J. Geophys. Res.*, **83**(C7), 3585-3599.

Janjic, Z.I., 1977. Pressure gradient force and advection scheme used for forecasting with steep and small scale topography. *Contrib. Atmos. Phys.*, **50**, 186-199.

Janjic, Z.I., 1979. Forward-backward scheme modified to prevent two grid-interval noise and its application in sigma coordinate models. *Contrib. Atmos. Phys.*, **52**, 69-84.

Janjic, Z.I., 1984. Non-linear advection schemes and energy cascade on semi-staggered grids. *Mon. Weather Rev.*, **112**, 1234-1245.

Janjic, Z.I., 1990. The step-mountain coordinate: physical package. *Mon. Weather Rev.,* **118**, 1429-1443.

Janjic, Z.I., 1994. The step-mountain eta coordinate model: further developments of the convection, viscous sublayer and turbulence closure schemes. *Mon. Weather Rev.,* **122**, 927-945.

Japar, S.M., Brachaczek, W.W., Gorse Jr., R.A., Norbeck, J.M., Pierson, W.R., 1986. The contribution of elemental carbon to the optical properties of rural atmospheric aerosols. *Atmos. Environ.,* **20**, 1281-1289.

Jenkin, M.E., 2008. Trends in ozone concentration distributions in the UK since 1990: Local, regional and global influences. *Atmos. Environ.,* **42**, 5434-5445.

Jiang, W., Smyth, S., Giroux, E., Roth, H., Yin, D., 2006. Differences between CMAQ fine mode particle and PM2.5 concentrations and their impact on model performance evaluation in the lower Fraser Valley. *Atmos. Environ.,* **40**, 4973-4985.

Jiménez, P., Baldasano, J.M., Dabdub, D., 2003. Comparison of photochemical mechanisms for air quality modeling. *Atmos. Environ.,* **374**, 4179-4194.

Jiménez, P., Baldasano, J.M., 2004. Ozone response to precursor controls in very complex terrains: Use of photochemical indicators to assess O_3-NO_x-VOC sensitivity in the northeastern Iberian Peninsula. *J. Geophys. Res.,* **109**, D20309. doi: 10.1029/2004JD004985.

Jiménez, P., Parra, R., Gassó, R., Baldasano, J.M., 2005a. Modeling the ozone weekend effect in very complex terrains: a case study in the northeastern Iberian Peninsula. *Atmos. Environ.,* **39**, 429-444.

Jiménez, P., Jorba, O., Parra, R., Baldasano, J.M., 2005b. Influence of high-model gird resolution on photochemical modelling in very complex terrains. *Int. J. Environ. Pollut.,* **24**, 180-200.

Jiménez, P., Jorba, O., Parra, R, Baldasano, J.M., 2006a. Evaluation of MM5-EMICAT2000-CMAQ performance and sensitivity in complex terrain: High-resolution application to the northeastern Iberian Peninsula. *Atmos. Environ.,* **40**, 5056-5072.

Jiménez, P., Jorba, O., Baldasano, J.M., 2006b. Modeling the dynamics of air pollutants over the Iberian Peninsula under typical meteorological siturations. 28th NATO/CCMS International Technical Meeting on Air Pollution Modeling and its application. Leipzing, Germany May 15-19.

Jiménez, P., Lelieveld, J., Baldasano, J.M., 2006c. Multi-scale modeling of air pollutants dynamics in the northwestern Mediterranean basin during a typical summertime episode. *J. Geophys. Res.,* **111**(D18306), 1-21. doi:10.1029/2005JD006516.

Jiménez, P., Parra, R., Baldasano, J.M., 2007. Influence of initial and boundary conditions for ozone modeling in very complex terrains: A case study in the northeastern Iberian Peninsula. *Environ. Modell. Softw.,* **22**, 1294-1306.

Jiménez-Guerrero, P., Pérez, C., Jorba, O., Baldasano, J.M., 2008a. Contribution of Saharan dust in an integrated air quality system and its on-line assessment. *Geophys. Res. Lett.,* **35** (L03814). doi:10.1029/2007GL031580.

Jiménez-Guerrero, P., Jorba, O., Baldasano, J.M., Gassó, S., 2008b. The use of a modelling system as a tool for air quality management: annual high resolution simulations and evaluation. *Sci. Total Environ.,* **390**, 323-340.

Jiménez-Guerrero, P., Jorba, O., Pay, M.T., Montávez, J.P., Jerez, S., Gómez-Navarro, J.J., Baldasano, J.M., 2011. Comparison of two different sea-salt aerosol schemes as implemented in air quality models applied to the Mediterranean Basin. *Atmos. Chem. Phys.,* **11**, 4833-4850. doi: 10.5194/acp-11-4833-2011.

Jorba, O., Gassó, S., Baldasano, J.M., 2003. Regional circulations within the Iberian Peninsula east coast. In: 26th NATO/CCMS International Technical Meeting on Air Pollution Modelling and Its Application. Kluwer Academic/Plenum Publishers, 388-395.

Jorba, O., Pérez, C., Rocadenbosch, F. and Baldasano, J. M., 2004. Cluster Analysis of 4-Day Back Trajectories Arriving in the Barcelona Area, Spain, from 1997 to 2002. *J. Appl. Meteorol.,* **43**(6), 887-901.

Kang, D., Mathur, R., and Rao, S.T., 2010. Real-time bias-adjusted O_3 and PM2.5 air quality index forecast and their performance evaluations over the continental United States. *Atmos. Environ.,* **44**, 2203-2212.

Kain, J.S., Fritsch, J.M., 1990. A one-dimensional entraining/detraining plume model and its application in convective parameterization. *J. Atmos. Sci.,* **47**(23), 2784-2802. doi:10.1175/1520-0469.

Kain, J.S., Fritsch, J.M., 1993. Convective parameterization for mesoscale models: the Kaine Fritsch scheme, the representation of cumulus convection in numerical models. In: Emanuel, K.A., Raymond, D.J. (Eds.), Amer. Meteor. Soc., 165-170 pp.

Kasibhatla, P., Chameides, W. L., Jonn, J.S., 1997. A three dimensional global model investigation of seasonal variations in the atmospheric burden of anthropogenic sulphate aerosols. *J. Geophys. Res.,* **102**, 3737-3759.

Keenan, T., Niinemets, U., Sabate, S., Gracia, C., Peñuelas, P., 2009. Process based inventory of isoprenoid emissions from European forests: model comparisons, current knowledge and uncertainties. *Atmos. Chem. Phys.,* **9**, 4053-4076.

Kelly, J.T., Bhave, P.V., Nolte, C.G., Shankar, U., Foley, K.M., 2010. Simulating emission and chemical evolution of coarse sea-salt particles in the Community Multiscale Air Quality (CMAQ) model. *Geosci. Model Dev.,* **3**, 257-273.

Ketzel, M., Omstedt, G., Johansson, C., Düring, I., Pohjola, M., Oettl, D., Gidhagen, L., Wåhlin, P., Lohmeyer, A., Haakana, M., Berkowicz, R., 2007. Estimation and validation of PM2.5/PM10 exhaust and non-exhaust emission factors for practical street pollution modeling. *Atmos. Environ.,* **41**, 9370-9385.

Kim, Y., Sartelet, K., Seigneur, C., 2009. Comparison of two gas-phase chemical kinetic mechanisms of ozone formation over Europe. *J. Atmos. Chem.,* **62**, 89-119.

Kim, Y., Sartelet, K., Seigneur, C., 2011. Formation of secondary aerosols over Europe: comparison of two gas-phase chemical mechanisms. *Atmos. Chem. Phys.,* **11**, 583-598.

Kormann, R., Fischer, H., de Reus, M., Lawrence, M., Brühl, Ch., von Kuhlmann, R., Holzinger, R., Williams, J., Lelieved, J., Warneke, C., de Gouw, J., Heland, J., Ziereis, H., Schlanger, H., 2003. Formaldehyde over the Eastern Mediterranean during MINOS: Comparison of airborne in-situ measurements with 3D-model results. *Atmos. Chem. Phys.,* **3**, 851-861.

Kuhn, M., Builtjes, P.J.H., Poppe, D., Simpson, d., Stockwell, W.R., Andersson-Sköld, Y., Baart, A., Das, M., Fiedler, F., Hov., O., Kirchner, F., Makar, P.A., Milford, J.B., Roemer, M.G.M., Ruhnke, R., Strand, A., Vogel, B., Vogel, H., 1998. Intercomparison o fthe gas-phase chemistry in serveral chemistry and transport models. *Atmos. Environ.,* **32**, 693-709.

Kupiainen, K.J., Tervahattu, H., Räisänen, M., Mäkelä, T., Aurela, M., Hillamo, R., 2005. Size and composition of airborne particles from pavement wear, tires, and traction sanding. *Environ. Sci. Technol.,* **39**, 699-706.

Laj, P., Klausen, J., Bilde, M., Plaß-Duelmer, C., Pappalardo, G., Clerbaux, C., Baltensperger, U., Hjorth, J., Simpson, D., Reimann, S., Coheur, P.-F., Richter, A., DeMazière, M., Rudich, Y., McFiggans, G., Torseth, K., Wiedensohler, A., Morin, S., Schulz, M., Allan, J., Attié, J.-L., Barnes, I., Birmilli, W., Cammas, P., Dommen, J., Dorn, H.-P., Fowler, D., Fuzzi, J.-S., Glasius, M., Granier, C., Hermann, M., Isaksen, I., Kinne, S., Koren, I., Madonna, F., Maione, M., Massling, A., Moehler, O., Mona, L., Monks, P.S., Müller, T., Orphal, J., Peuch, V.-H., Sratmann, F., Tanré, D., Tyndall, G., Riziq, A.A., van Roozendael, M., Villani, P., Wehner, B., Wex, H., Zardini, A.A., 2009. Measuring atmospheric composition change. *Atmos. Environ.,* **43**, 5345-5406.

Lam, Y.F., Fu, J.S., 2009. A novel downscaling technique for the linkage of global and regional air quality modeling. *Atmos. Chem. Phys.,* **9**, 9169-9185.

Larssen, S., Sluyter, R., Helmis, C., 1999. Criteria for EUROAIRNET, the EEA Air Quality Monitoring and Information Network. Technical Report 12. European Environment Agency. Available at: http://reports.eea.eu.int/TEC12/en.

Lave, L., Seskin, E.P., 1970. Air pollution and human health. *Science,* **169**(3947), 723-733. doi:10.1126/science.169.3947.723.

de Leeuw, F., Vixseboxse, E., 2010. Reporting on ambient air quality assessment-preliminary results for 2008. Technical Report. The European Topic Centre on Air and Climate Change (ETC/ACC) Technical Paper 2009/10.

Legreid, G., Reimann, S., Folini, D., Staehelin, J., Balzani, J., Steinbacher, M., Vollmer, K.M., 2008. Measurements of organic trace gases including OVOCs at the high alpine site Jungfraujoch (Switzerland): seasonal variation and source allocations. *J. Geophys. Res.,* **113**, D05307.

Lelieveld, J., Berresheim, H., Borrmann, S., Crutzen, P.J., Dentener, F.J., Fischer, H., Feichter, J., Flatau, P.J., Heland, J., Holzinger, R., Korrmann, R., Lawrence, M. G., Levin, Z., Markowicz, K.M., Mihalopoulos, N., Minikin, A., Ramanathan, V., de Reus, M., Roelofs, G.J., Scheeren, H.A., Sciare, J., Schlager, H., Schultz, M., Siegmund, P., Steil, B., Stephanou, E.G., Stier, P., Traub, M., Warneke, C., Williams, J., Ziereis, H., 2002. Global air pollution crossroads over the Mediterranean. *Science,* **298**, 794-799.

Lenschow, P., Abraham, H.J., Kutzner, K., Lutz, M., Preu, J.D., Reichenbcher, W., 2001. Some ideas about the sources of PM10. *Atmos. Environ.,* **35**, S23-S33.

Li, Q., Jacob, D.J., Bey, I., Palmier, P., Duncan, B.N., Field, B.D., Martin, R.V., Fiore, A.M., Yantosca, R.M., Parrish D.D., Simmonds, P.G., Oltmans, S.J., 2002. Transatlantic transport of pollution and its effects on surface ozone in Europe and North America. *J. Geophys. Res.,* **107**(D13), 4166. doi:10.1029/2001JD001422.

Lipfert, F.W., 1994. Air Pollution and Community Health e a Critical Review and Data Source Book. Van Nostrand Reinhold, New York, ISBN 0-442-01444-9, 576 pp.

Li, S., Matthews, J., Sinha, A., 2008. Atmospheric hydroxyl radical production from electronically excited NO_2 and H_2O. *Science,* **319**, 1657-166.

Liao, H., Seinfeld, J.H., 2005. Global impacts of gas-phase chemistry-aerosol interactions on direct radiative forcing by anthropogenic aerosols and ozone. *J. Geophys. Res.,* **110**, 18208.

Linares, P., Romero, C., 2000. A multiple criteria decision making approach for electricity planning in Spain: economic versus environmental objectives. *J. Oper. Res. Soc.,* **51**(6), 736-743.

Linares, C., Díaz, J., 2010a. Short-term effect of PM2.5 on daily hospital admissions in Madrid (2003–2005). *Int. J. Environ. Health Res.,* **20**, 129–40.

Linares, C., Díaz, J., 2010b. Short-term effect of concentrations of fine particulate matter on hospital admissions due to cardiovascular and respiratory causes among the over-75 age group in Madrid, Spain. *Public Health,* **124**, 28–36.

van Loon, M., Roemer, M.GM., Builtjes, P.J.H., Bessagnet, B., Rouil, L., et al., 2004. Model inter-comparision in the framework of the review of the Unified EMEP model. TNO-Report R2004/282, 53 pp.

van Loon, M., Vautard, R., Schaap, M., Bergstrom, R., Bessagnet, B., Brandt, J., Builtjes, P.J.H., Christensen, J.H., Cuvelier, C., Graff, A., Jonson, J.E., Krol, M., Langner J., Roberts, P., Rouil, L., Stern, R., Tarrasón, L., Thunis, P., Vignati, E., White, L., Wind, P., 2007. Evaluation of long-term ozone simulations from seven regional air quality models and their ensemble. *Atmos. Environ.,* **41**, 2083-2097. doi:10.1016/j.atmosenv.2006.10.073.

Lovett, G.M., Traynor, M.M., Pouyat, R.V., Carreiro, M.M., Zhu, W.X., Baxter, J.W., 2000. Atmospheric deposition to oak forests along an urban-rural gradient. *Environ. Sci. Technol.,* **34**(20), 4294-4300.

LUA, 2000. Vorgehensweise bei der Schwebstaubimmissionsberechnung nach Richtlinie 1999/30/EG. Technical Report. Landesumweltamt Brandenburg, Entwurf des Referats I3 vom 21.12.2000.

Luecken, D.J., Phillipsa, S., Sarwara, G., Janga, C., 2008. Effects of using the CB05 vs. SARPC99 vs. CB4 chemical mechanism on model predictions: ozone and gas-phase photochemical precursor concentrations. *Atmos. Environ.*, **42**, 5805-5820.

Lyons, W.A., Pielke, R.A., Tremback, C.J., Walko, R.L., Moon, D.A., Keen, C.S., 1995. Modeling the impacts of mesoscale vertical motions upon coastal zone air pollution dispersion. *Atmos. Environ.*, **29**, 283-301.

Manders, A.M.M., Schaap, M., Querol, X., Albert, M.F.M.A., Vercauteren, J., Kuhlbusch, T.A.J., Hoogerbrugge, R., 2010. Sea salt concentrations across the European continent. *Atmos. Environ.*, **44**, 2434-2442.

Marenco, A., Gouget, H., Nedelec, P., Pages, J.-P., 1994. Evidence of a long term increase in tropospheric ozone from Pic du Midi data series: Consequences: positive radiative forcing. *J. Geophys. Res.*, **99**, 16617-16632.

Marmer, E., Dentener, F., Aardenne, J., Cavalli, F., Vignati, E., Velchev, K., Hjorth, J., Boersma, F., Vinken, G., Mihalopoulos, N., Raes, F., 2009. What can we learn about ship emission inventories from measurements of air pollutants over the Mediterranean Sea? *Atmos. Chem. Phys.*, **9**, 6815-6831. doi: 10.5194/acp-9-6815-2009.

Martín-Vide, J., Olcina, J., 2001. Climas y tiempos de España. Ed. Alianza, Madrid, 258 pp.

Maté, T., Guaita, R., Pichiule, M., Linares, C., Díaz, J., 2010. Short-term effect of fine particulate matter (PM$_{2.5}$) on daily mortality due to diseases of the circulatory system in Madrid (Spain). *Atmos. Environ.*, **408**, 5750-5757.

Matthias, V., 2008. The aerosol distribution in Europe derived with the community multiscale air quality (CMAQ) model: comparison to near surface in situ and sunphotometer measurements. *Atmos. Chem. Phys.*, **8**, 5077-5097.

McKeen, S., Wilczak, J., Grell, G., Djalalova, I., Peckham, S., Hsie, E.Y., Gong, W., Bouchet, V., Menard, S., Moffett, R., McHenry, J., McQueen, J., Tang, Y., Carmichael, G., Pagowski, M., Chan, A.C., Dye, T.S., Frost, G., Lee, P., Mathur, R., 2005. Assessment of an ensemble of seven real-time ozone forecast over eastern North America during the summer of 2004. *J. Geophys. Res.*, **110** (D21307).

McQeen, J.T., Draxter, R.R., Rolph, G.D., 1995. Influence of grid size and terrain resolution on wind field predictions from an operational mesoscale model. *J. Appl. Meteorol.*, **34**(10), 2166-2181.

De Meij, A., Krol, M., Dentener, F., Vignati, E., Cuvelier, C., Thunis, P., 2006. The sensitivity of aerosol in Europe to two different emission inventories and temporal distribution of emissions. *Atmos. Chem. Phys.*, **6**, 4287-4309.

Melios, G., Van Aalst, R., Samaras, Z., 2006. Validation of road traffic urban emission inventories by jeans of concentration data measured at air quality monitoring stations in Europe. *Atmos. Environ.*, **40**, 7362-7377.

Menut, L., Bessagnet, B., 2010. Atmospheric composition forecasting in Europe. *Ann. Geophys.*, **28**, 61-74.

Meng, Z., Dabdub, D., Seinfeld, J.H., 1997. Chemical coupling between atmospheric ozone and particulate matter. *Science*, **277**, 116-117.

Metzger, S.M., Dentener, F.J., Lelieveld, J., Pandis, S.N., 2002. Gas/aerosol partitioning I: a computationally efficient model. *J. Geophys. Res.*, **107**, 109-132.

Michalakes, J., Dudhia, J., Gill, D., Henderson, T., Klemp, J., Skamarock,W.,Wang,W., 2004. The weather research and forecast model: software architecture and performance. In: Mozdzynski, E.G. (Ed.), To Appear in Proceeding of the Eleventh ECMWF Workshop on

the Use of High Performance Computing in Meteorology, 25-29 October 2004, Reading, U.K, 117-124.

Middleton, N. J., Goudie, A.S., 2001. Saharan dust: sources and trajectories. *Trans. Inst. Br. Geogr.,* **26**, 165.

Millán, M.M., Salvador, R., Mantilla, E., 1997. Photooxidant dyanmics in the Mediterranean basin in summer: Results from European research projects. *J. Geophys. Res.,* **102**(D7), 8811-8823.

Millán, M.M., 2002. Ozone dynamics in the Mediterranean basin, a collection of scientific papers resulting from the MECAPIP, RECAPMA and SECAP Projects. Technical Report. European Commission and CEAM.

Millán, M.M., Sanz, M.J., Salvador, R., Mantilla, E., 2002. Atmospheric dynamics and ozone cycles related to nitrogen deposition in the western Mediterranean. *Energy Policy,* **118**, 167-186.

Mlawer, E.J., Taubman, S.J., Brown, P.D., Iacono, M.J., Clough, S.A., 1997. Radiative transfer for inhomogeneous atmosphere: RRTM, a validated correlated-k model for the longwave. *J. Geophys. Res.,* **102**(D14), 16663-16682.

Molina, L.T., Kolb, C.E., de Foy, B., Lamb, B.K., Brune, W.H., Jimenez, J.L., Molina, M.J., 2007. Air quality in North America's most populous city – overview of the MCMA-2003 campaign. *Atmos. Chem. Phys.,* **7**, 2447-2473.

Monks, P.S., 2005. Gas-phase radical chemistry in the troposphere. *Chem. Soc. Rev.,* **34**, 376-395.

Monks, P.S., Granier, C., Fuzzi, S., Stohl, A., Williams, M.L., Akimoto, H., Amann, M., Baklanov, A., Baltensperger, U., Bey, I., Blake, N., Blake, R.S., Carslaw, K., Cooper, O.R., Dentener, F., Fowler, D., Fragkou, E., Frost, G.J., Generoso, S., Ginoux, P., Grewe, V., Guenther, A., Hansson, H.C., Henne, S., Hjorth, J., Hofzumahous, A., Huntrieser, H., Isaksen, I.S.A., Jenkin, M.E., Kaiser, J., Kanakidou, M., Klimont, Z., Kulmala, M., Laj, P., Lawrence, M.G., Lee, J.D., Liousse, C., Maione, M., McFiggans, G., Metzger, A., Mieville, A., Moussiopoulos, N., Orlando, J.J., O'Dowd, C.D., Palmer, P.I., Parrish, D.D., Petzold, A., Platt, U., Pöschl, U., Prévôt, A.S.H., Reeves, C.E., Reimann, S., Rudich, Y., Sellegri, K., Steinbrecher, R., Simpson, D., ten Brink, H., Theloke, J., van der Werf, G.R., Vautard, R., Vestreng, V., Vlachokostas, Ch., von Glasow, R., 2009. Atmospheric composition change – global and regional air quality. *Atmos. Environ.,* **43**, 5268-5350.

Moulin, C., Lambert, E., Dayan, U., Masson, V., Ramonet, M., Bousquet, P., Legrand, M., Balkanski, Y.J., Guelle, W., Marticorena, B., Bergametti, G., Dulac, F., 1998. Satellite climatology of African dust transport in the Mediterranean atmosphere. *J. Geophys. Res.,* **103**, 13137-13144.

Moussiopoulos, N., 1994. MARS-Model for the Atmospheric dispersion of Reactive Species. In: The EUMAC Zooming Model. Model Structure and applications. Edited by N. Moussiopoulos, EUROTRAC, Garmisch-Partenkirchen, Germany.

Moussiopoulos, N., 2003. Air quality in cities. SATURN EUROTRAC-2 Subproject. Final Report, Springer Publisher, 292 pp.

Mozurkewich, M., 1993. The dissociation constant of ammonium nitrate and its dependence on temperature, relative humidity and particle size. *Atmos. Environ.,* **27**, 261-270.

Murphy, B. N., Pandis, S. N., 2009. Simulating the formation of semivolatile primary and secondary aerosol in a regional chemical transport model. *Environ. Sci. Technol.,* **43**, 4722– 4728.

NEI, 2009. National emission inventory for Spain in 2008. Ministerio de medioambiente y medio rural y marino. Available at: http://www.marm.es/es/calidad-y-evaluacion-ambiental/temas/sistema-espanol-de-inventario-sei-/.

Nenes, A., Pilinis, C., Pandis, S.N., 1998. ISORROPIA: a new thermodynamic equilibrium model for multiphase multicomponent inorganic aerosols. *Aquat. Geochem.,* **4**(1), 123-152. doi:10.1023/A:1009604003981.

Nguyen, K., and Dabdub, D., 2002. NO_x and VOC control and its effects on the formation of aerosols. *Aerosol Science and Tech.,* **36**, 560-572.

Nickovic, S., Kallos, G., Papadopoulos, A., Kakaliagou, O., 2001. A model for prediction of desert dust cycle in the atmosphere. *J. Geophys. Res.*, **106**(D16), 18113-18129. doi:10.1029/2000JD900794.

Niyogi, D., Chang, H.I., Saxena, V.K., Holt, T., Alapaty, K., Booker, F., Chen, F., Davis, K.F., Holben, B., Matsui, T., Meyers, T., Oechel, W.C., Pielke, R.A., Wells, R., Wilson, K., Xue, Y., 2004. Directs obervations of the effects of aerosol loading on net ecosystem CO_2 exhanges over different landscapes. *Geo. Res. Lett.*, **31**. doi: 10.1029/2004GL020915.

Noh, Y., Cheon, W.G., Hong, S.Y., Raasch, S., 2003. Improvement of the k-profile model for the planetary boundary layer based on large eddy simulation data. *Boundary Layer Meteorol.*, **107**(2), 401-427. doi:10.1023/A:1022146015946.

Ntziachristos, L., Samaras Z., 2000. COPERT III. Computer programme to calculate emissions from road transport. Methodology and emission factors (Version 2.1). Technical Report 49. European Environmental Agency. 86 pp.

Olmo, F.J., Quitantes, A., Lara, V., Lyamani, H., Alados-Arboledas, L., 2008. Aerosol optical properties assessed by an inversion method using the solar principal plane for non-spherical particles. *J. Quant. Spectrosc. Radiat. Transfer.*, **109**, 1504-1516.

Ortiz de Zárate, I., Ezcurra, A., Lacaux, J.P., Dinh, P.V., de Argandoña, J.D., 2005. Pollution by cereal waste burning in Spain. *Atmos. Res.*, **73**(1–2), 161-170. doi:10.1016/j.atmosres.2004.07.006.

Oxley, T, Valiantis, M., Elshkaki, A., ApSimon, H.M., 2009. Background, Road and Urban Transport modelling of Air quality Limit values (The BRUTAL model). *Environ. Modell. Softw.*, **24**, 1036–1050. doi:10.1016/j.envsoft.2009.02.011.

Pan, Y., Zhang, Y., Sarwar, G., 2008. Impact of gas-phase chemistry on WRF/CHEM predictions of O_3 and $PM_{2.5}$: mechanism implementation and comparative evaluation, 7th annual CMAS conference, Chapel Hill, North Carolina.

Pandis, S.N., Harley, R.A., Cass, G.R., Seinfeld, J.H., 1992. Secondary organic aerosol formation and transport. *Atmos. Environ.*, **26**, 2269-2282.

Pandolfi, M., Gonzalez-Castanedo, Y., Alastuey, A., de la Rosa, J.D., Mantilla, E., de la Campa, A.S., Querol, X., Pey, J., Amato, F., Moreno, T., 2011. Source apportionment of PM10 and PM2.5 at multiple sites in the strait of Gibraltar by PMF: impact of shipping emissions. *Environ. Sci. Pollut. Res.*, **18**, 260-269.

Parra, R., Baldasano, J.M., 2004. Modelling the on-road traffic emissions from Catalonia (Spain) for photochemical air pollution research. Weekday-weekend differences. In: 12th International Conference on Air Pollution, Rhodes, Greece.

Parra, R., Gassó, S., Baldasano, J.M., 2004. Estimating the biogenic emissions of non-methane volatile organic compounds from the North western Mediterranean vegetation of Catalonia, Spain. *Sci. Total Environ.*, **329**, 241-259.

Parra, R., Jiménez, P., Baldasano, J.M., 2006. Development of the high-spatial resolution EMICAT2000 emission model for air pollutants from the north-eastern Iberian Peninsula (Catalonia, Spain). *Environ. Poll.*, **140**, 200-219.

Parrish, D.D., Millet, D.B., Goldstein, A.H., 2009. Increasing ozone concentration in marine boundary layer air inflow at the west coasts of North America and Europe. *Atmos. Chem. Phys.*, **9**, 1303-1323.

Paulson, C.A., 1970. The mathematical representation of wind speed and temperature profiles in the unstable atmospheric surface layer. *J. Appl. Meteorol.*, **9**(6), 857-861. doi:10.1175/1520-0450.

Park, S.K., Cobb, C.E., Wade, K., Mulholland, J., Hu, Y., Russell, A.G., 2006. Uncertainty in air quality model evaluation for particulate matter due to spatial variations in pollutant concentrations. *Atmos. Environ.*, **40**, S563-S573.

Pay, M.T., Piot, M., Jorba, O., Basart, S., Gassó, S., Jiménez-Guerrero, P., Gonçalves, M., Dabdub, D., Baldasano, J.M., 2010a. A full year evaluation of the CALIOPE-EU air quality system in Europe for 2004: a model study. *Atmos. Environ.*, **44**, 3322-3342. doi:10.1016/j.atmosenv.2010.050140.

Pay, M.T., Jiménez-Guerrero, P., Baldasano, J.M., 2010b. Implementation of resuspension from paved roads for the improvement of CALIOPE air quality system in Spain. *Atmos. Environ.*, **45**, 802-807. doi:10.1016/j.atmosenv.2010.10.032.

Pénard-Morand, C., Charpi, D., Raherison, C., Kopferschmitt, C., Caillaud, D., Lavaud, F., Annesi-Maesano, I., 2005. Long-term exposure to background air pollution related to respiratory and allergic health in schoolchildren. *Clin. Exp. Allergy*, **35**(10), 1279-1287. doi:10.1111/j.1365-2222.2005.02336.

Pérez, C., Sicard, M., Jorba, O., Comerón, A., Baldasano, J.M., 2004. Summertime re-circulations of air pollutants over the north-eastern Iberian coast observed from systematic EARLINET lidar measurements in Barcelona. *Atmos. Environ.*, **38**, 3983-4000.

Pérez, C., Nickovic, S., Baldasano, J.M., Sicard, M., Rocadenbosch, F., Cachorro, V.E., 2006a. A long Saharan dust event over the western Mediterranean: Lidar, sun photometer observations, and regional dust modeling. *J. Geophys. Res.*, **111**(D15214), 1-16. doi:10.1029/2005JD006579.

Pérez, C., Nickovic, S., Pejanovic, G., Baldasano, J.M., Ozsoy, E., 2006b. Interactive dust-radiation modeling: a step to improve weather forecasts. *J. Geophys. Res.*, **111**(D16206), 1-17. doi:10.1029/2005JD006717.

Pérez, C., Haustein, K., Janjic, Z., Jorba, O., Huneeus, N., Baldasano, J.M., Black, T., Basart, S., Nickovic, S., Miller, R.L., Perlwitz, J.P., Schulz, M., Thomson, M., 2011. Atmospheric dust modelling from meso to global scales with the online NMMB/BSC-Dust model – Part 1: Model description, annual simulation and evaluation. *Atmos. Chem. Phys. Diss.*, **11**, 17551-17620.

Pérez, L., Medina-Ramón, M., Künzli, N., Alastuey, A., Pey, J., Pérez, N., Garcia, R., Tobias, A., Querol, X., Sunyer, J., 2009. Size fractionate particulate matter, vehicle traffic, and case-specific daily mortality in Barcelona, Spain. *Environ. Sci. Technol.*, **43**, 4707-4714.

Pey, J., Pérez, N., Querol, X., Alastuey, A., Cusack, M., Reche, C., 2010. Intense winter atmospheric pollution episodes affecting the Western Mediterranean. *Sci. Total Environ.*, **408**, 1951-1959.

Pinder, R.W., Dennis, R.L., Bhave, P.V., 2008. Observable indicators of the sensitivity of PM2.5 nitrate to emission reductions-Part I: Derivation of the adjusted gas ratio and applicability at regulatory-relevant time scales. *Atmos. Environ.*, **42**, 1275-1286.

Pio, C.A., Legrand, M., Oliveira, T., Afonso, J., Santos, C., Caseiro, A., Fialho, P., Barata, F., Puxbaum, H., Sanchez-Ochoa, A., Kasper-Giebl, A., Gelencsér, A., Preunkert, S., Schock, M., 2007. Climatology of aerosol composition (organic versus inorganic) at non-urban areas on a West-East transect across Europe. *J. Geophys. Res.*, **112**, D23S02. doi:10.1029/2006JD008038.

Piot, M., Jorba, O., Jimenez, P., Baldasano, J.M., 2008. The Role of Lateral Boundary Conditions and Boundary Layer in Air Quality Modelling System. Eos Trans. AGU 8, H212+, Abstract A41H-0212.

Pope III, C.A., Burnett, R.T., Thun, M.J., Calle, E.E., Krewski, D., Ito, K., Thurston, G.D., 2002. Lung cancer, cardiopulmonary mortality, and long-term exposure to fine particulate air pollution. *J. Am. Med. Inform. Assn.*, **287**, 1132-1141.

Pope, C.A., Dockery, D.W., 2006. Health effects of fine particulate air pollution: lines that connect. *J. Air Waste Manage.*, **56**(6), 709-742.

Pope, C.A.I., Ezzati, M., Dockery, D.W., 2009. Fine-particulate air pollution and life expectancy in the United States. N. Engl. J. Med. 360, 376-386. Pregger, T., Friedrich, R., 2009. Effective

pollutant emission heights for atmospheric transport modelling based on real-world information. *Environ. Pollut.*, **157**(2), 552-560.

Prospero, J.M., 1999. Long-term measurements of the transport of African mineral dust to the southeastern United States: implication for regional air quality. *J. Geophys. Res.*, **104**, 15917-15927.

Prospero, J.M., Ginoux, P., Torres, O., Nicholson, S.E., Gill, T.E., 2002. Environmental characterization of global sources of atmospheric soil dust identified with the nimbus 7 total ozone mapping spectrometer (TOMS) absorbing aerosol product. *Rev. Geophys.*, **40**, 1002. doi:10.1029/2000RF000095.

Pöschl, U., 2005. Atmospheric aerosols: composition, transformation, climate and health effects. Angew. *Chem. Int. Ed.*, **44**, 7520-7540.

Pulles, T., Kuenen, J., Pesik, J., Cadman, J., Wagner, A., 2006. EPER e the European Pollutant Emission Register. Technical Report. Available at: http://eper.eea.eu.int/eper.

Putaud, J-P., Raes, F., van Dingenen, R., Brüggemann, E., Facchini, M.C., Decesari, S., Fuzzi, S., Gehrig, R., Hüglin, C., Laj, P., Lorbeer, G., Maenhaut, W., Mihalopoulos, N., Müller, K., Querol, X., Rodríguez, S., Schneider, J., Spindler, G., ten Brink, H., Torseth, K., Wiedensohler, A., 2004. A European aerosol phenomenology-2: chemical characteristics of particulate matter at kerbside, urban, rural and background sites in Europe. *Atmos. Environ.*, **38**, 2579-2595.

Putaud, J.-P., van Dingenen, R., Alastuey, A., Bauer, H., Birmili, W., Cyrys, J., Flentje, H., Fuzzi, S., Gehrig, R., Hansson, H., Harrison, R., Herrmann, H., Hitzenberger, R., H¨uglin, C., Jones, A., Kasper-Giebl, A., Kiss, G., Kousa, A., Kuhlbusch, T., Löschau, G., Maenhaut, W., Molnar, A., Moreno, T., Pekkanen, J., Perrino, C., Pitz, M., Puxbaum, H., Querol, X., Rodriguez, S., Salma, I., Schwarz, J., Smolik, J., Schneider, J., Spindler, G., ten Brink, H., Tursic, J., Viana, M., Wiedensohler, A., and Raes, F., 2010. A European aerosol phenomenology - 3: Physical and chemical characteristics of particulate matter from 60 rural, urban, and kerbside sites across Europe. *Atmos. Environ.*, **44**, 1308–1320, doi:10.1016/j.atmosenv.2009.12.011.

Querol, X., Alastuey, A., Puicercus, J.A., Mantilla, E., Miro, J.V., Lopez-Soler, A., Plana, F., Artiñano, B., 1998. Seasonal evolution of suspended particles around a large coal-fired power station: particulate levels and sources. *Atmos. Environ.*, **32**, 1963-1978.

Querol, X., Alastuey, A., Rodríguez, S., Plana, F., Ruiz, C.R., Cots, N., Massagué, G., Puig, O., 2001. PM10 and PM2:5 source apportionment in the Barcelona metropolitan area, Catalonia, Spain. *Atmos. Environ.*, **35**(36), 6407-6719.

Querol, X., Alastuey, A., Rodríguez, S., Viana, M.M., Artiñano, B.A., Salvador, P., et al., 2003. Estudio y evaluación de la contaminación atmosférica por material particulado en España: Informes finales. Technical Report. IJA CSIC, ISCIII, CIEMAT. Universidad de Huelva, Universidad del País Vasco.

Querol, X. Alastuey, A., Viana, M.M., Rodriguez, S., Artiñano, B., Salvador, P., Garcia do Santos, S., Fernandez Patier, R., Ruiz, C.R., de la Rosa, J., Sanchez de la Campa, A., Menendez, M., Gil, J.I., 2004a. Speciation and origin of PM10 and PM2.5 in Spain. *J. Aerosol Sci.*, **35**, 1151-1172.

Querol, X., Alastuey, A., Ruiz, C.R., Artiñano, B., Hansson, H.C., Harrison, R.M., Buringh, E., ten Brink, H.M., Lutz, M., Bruckmann, P., Straehl, P., Schneider, J., 2004b. Speciation and origin of PM10 and PM2:5 in selected European cities. *Atmos. Environ.*, **38**, 6547-6555.

Querol, X., Alastuey, A., Moreno, T., Viana, M., 2008a. New Directions: Legislative considerations for controlling exposure to atmospheric aerosols in rural areas. *Atmos. Environ.*, **42**, 8979-8984.

Querol, X., Alastuey, A., Moreno, T., Viana, M.M., Castillo, S., Pey, J., Rodríguez, S., Artiñano, B., Salvador, P., Sánchez, M., Garcia Dos Santos, S., Herce Garraleta, M.D., Fernandez-Patier, R., Moreno-Grau, S., Negral, L., Minguillón, M.C., Monfort, E., Sanz, M.J., Palomo-Marín,

R., Pinilla-Gil, E., Cuevas, E., de la Rosa, J., Sánchez de la Campa, A., 2008b. Spatial and temporal variations in airborne particulate matter (PM10 and PM2:5) across Spain 1999–2005. *Atmos. Environ.*, **42**(17), 3964-3979. doi:10.1016/j.atmosenv.2006.10.071.

Querol, X, Alastuey, A., Pey, J., Cusack, M., Pérez, N., Mihalopoulos, N., Theodosi, C., Gerasopoulos, E., Kubilay, N., Koçak, M., 2009a. Variability in regional background aerosols within the Mediterranean. *Atmos. Chem. Phys.*, **9**, 4575-4591.

Querol, X, Pey, J., Pandolfi, M., Alastuey, A., Cusack, M., Pérez, N., Moreno, T., Viana, M., Mihalopoulos, N., Kallos, G., Kleanthous, S., 2009a. African dust contributions to mean ambient PM10 mass-levels across the Mediterranean Basin. *Atmos. Environ.*, **43**, 4266-4277.

Ramanathan, V., Crutzen, P.J., Kiehl, J.T., Rosenfeld, D., 2001. Aerosols, climate, and the hydrological cycle. *Science*, **294**(5549), 2119-2124. doi:10.1126/science.1064034.

Rauterberg-Wulff, 2000. Untersuchung ber 313 die Bedeutung der Staubaufwirbelung fr die PM10-Immission an einer Hauptverkehrsstrae. Technical Report. Techn. Univ. Berlin, Fachgebiet Luftreinhaltung.

Reidmiller, D.R., Fiore, A.M., Jaffe, D.A., Bergmann, D., Cuvelier, C., Dentener, F.J., Duncan, B.N., Folberth, G., Gauss, M., Gong, S., Hess, Jonson, J.E., Keating, T., Lupu, A., Marmer, E., Park, R., Schultz, M.G., Shindell, D.T., Szopa, S., Vivanco, M. G., Wild, O., Zuber, A., 2009. The influence of foreign vs. North American emissions on surface ozone in the US. *Atmos. Chem. Phys.*, **9**, 5027-5042.

Renner, E., Wolke, R., 2010. Modelling the formation and atmospheric transport of secondary inorganic aerosols with special attention to regions with high ammonia emissions. *Atmos. Environ.*, **44**, 1904-1912.

Ribas, A., Peñuelas, J., 2004. Temporal patterns of surface ozone levels in different habitats of the North Western Mediterranean basin. *Atmos. Environ.*, **38**, 985-992.

Rodríguez, S., Querol, X., Alastuey, A., Kallos, G. and Kakaliagou, O., 2001. Saharan dust contribution to PM10 and TSP levels in Southern and Eastern Spain. *Atmos. Environ.*, **35**, 14, 2433-2447.

Rodríguez, S., Querol, X., Alastuey, A., Plana, F., 2002. Sources and processes affecting levels and composition of atmospheric aerosol in the western Mediterranean. *J. Geophys. Res.*, **107**(D24), 4777.

Rodwell, M.J., Hoskins, B.J., 2001. Subtropical anticyclones and summer monsoons. *J. Climate*, **14**, 3192-3211.

Roemer, M., Beekmann, M., Bergström, R., Boersen, G., Feldmann, H., Flatoy, F., et al., 2003. Ozone trends according to ten dispersion models. Special Report. EUTROTRAC-2 ISS, Garmisch Partenkirschen.

Roy, B., Mathur, R., Gilliland, A.B., Howard, S.C., 2007. A comparison of CMAQ-based aerosol properties with IMPROVE, MODIS, and AERONET data. *J. Geophys. Res.*, **112** (D14301). doi:10.1029/2006JD008085.

Russell, A., Dennis, R., 2000. NARSTO critical review of photochemical models and modeling. *Atmos. Environ.*, **34**, 2283-2324.

Saaroni, H., Ziv, B., Bitan, A., Alpert, P., 1998. Easterly wind storms over Israel. *Theor. Appl. Climatol.*, **59**, 61-77. doi: 10.1007/s007040050013

Saltelli, A., Ratto, M., Tarantola, S., Campolongo, F., 2005. Sensitivity analysis for chemical models. *Chem. Rev.*, **105**(7), 2811-2828.

Salisbury, G., Williams, J., Holzinger, R., Gros, V., Mihalopoulos, N., Vrekoussis, M., Sarda-Estève, R., Berresheim, H., von Kuhlmann, R., Lawrence, M., Lelieveld, J., 2003. Ground-based PTR-MS measurements of reactive organic compounds during the MINOS campaign in Crete, July-August 2001. *Atmos. Chem. Phys.*, **3**, 925-940.

San José, R., Rodriguez, M.A., Cortés, E., González, R.M., 1999. EMMA model: an advanced operational mesoscale air quality model for urban and regional environments. *Environ. Manage. Health*, **10**(4), 258-266.

Sander, R., Crutzen, P.J., 1996. Model study indicating halogen activation and ozone destruction in polluted air masses transported to the sea. *J. Geophys. Res.*, **101**, 9121-9138.

Sanz, M.J., Calatayud, V., Calvo, E., 2000. Spatial pattern of ozone injury in Aleppo pine related to air pollution dynamics in a coastal-mountain region of eastern Spain. *Environ. Pollut.*, **108**, 239-247.

Sartelet, K.N., Debry, E., Fahey, K., Roustan, Y., Tombette, M., Sportisse, B., 2007. Simulation of aerosols and gas-phase species over Europe with the Polyphemus system: part I. Model-to-data comparison for 2001. *Atmos. Environ.*, **41**, 6116-6131.

Sarwar, G., Luecken, D., Yarwood, G., Whitten, G.Z., Carter, W.P.L., 2008. Impact of an updated carbon bond mechanism on predictions from the CMAQ modeling system: Preliminary assessment. *J. Appl. Meteor. Climatol.*, **47**, 3-14.

Schaap, M., Gon, H.V.D., Dentener, F.J., Visschedijk, A.J.H., van Loon, M., ten Brink, H. M., Putaud, J.P., Guillaume, B., Liousse, C., Builtjes, P.J.H., 2004a. Anthropogenic black carbon and fine aerosol distribution over Europe. *J. Geophys. Res.*, **109**(D18207). doi:10.1029/2003JD004330.

Schaap, M., van Loon, M., ten Brink, H.M., Dentener, F.J., Builtjes, P.J.H, 2004b. Secondary inorganic aerosol simulations for Europe with special attention to nitrate. *Atmos. Chem, Phys.*, **4**, 857-874.

Schaap, M., Spindler, G., Schulz, M., Acker, K., Maenhaut, W., Berner, A., Wieprecht, W., Streit, N., Müller, K., Brüggemann, E., Putaud, J.-P., Puxbaum, H., Baltensperger, U., ten Brink, H.M., 2004c. Artefacts in the sampling of nitrate studied in the "INTERCOMP" campaigns of EUROTRAC-AEROSOL. *Atmos. Environ.*, **38**, 6487-6496.

Schaap, M., Timmermans, R.M.A., Roemer, M., Boersen, G.A.C., Builtjes, P., Sauter, F., Velders, G., Beck, J., 2008. The LOTOS-EUROS model: description, validation and latest developments. *Int. J. Environ. Pollut.*, **32**, 270-290.

Schaap, M., Manders, A.M.M., Hendriks, E.C.J., Cnossen, J.M., Segers, A.J.S., Denier van der Gon, H.A.C., Jozwicka, M., Sauter, F., Velders, G., Matthijsen, J., Builtjes, P.J.H, 2009. Regional modelling of particulate matter for the Netherlands. Available at: www.pbl.nl.

Schell, B., Ackermann, I.J., Hass, H., Binkowski, F.S., Ebel, A., 2001. Modeling the formation of secondary organic aerosol within a comprehensive air quality model system. *J. Geophys. Res.*, **106**(D22), 28275-28293. doi:10.1029/ 2001JD000384.

Schlesinger, S., Crosbie, R.E., Gagné, R.E., Innis, G.S., Lalwani, C.S., Loch, J., Sylvester, R.J., Wright, R.D., Kheir, N., Bartos, D., 1979. Terminology for model credibility. *Simulation*, **32**(3), 103-104.

Schluenzen, K.H., Sokhi, R.S., 2008. Overview of tools and methods for meteorological and air pollution meso-scale model evaluation and user training. Joint Report of COST Action 728 and GURME, WMO/TD-N0 147, ISBN 978-1-905313-59-4.

Schmidt, H., Derognat, C., Vautard, R., Beekmann, M., 2001. A comparison of simulated and observed ozone mixing ratios for the summer of 1998 in Western Europe. *Atmos. Environ.*, **6**, 6227-6297.

Seinfeld, J.H., 1988. Ozone air quality models: a critical review. *JAPCA J. Air Waste Ma.*, **38**(5), 616-645.

Seinfeld, J.H., Pandis, S.N., 1998. Atmospheric chemistry and physics: from air pollution to climate change. John Wiley & Sons, Inc., 1326 pp.

Shankar, U., Bhave, P.V., Vukovich, J.M., Roselle, S.J., 2005. Initial application of sea salt emissions and chemistry algorithms in the CMAQv4.5-AERO4 module. In the 2005 Models-3 Users Workshop, Chapel Hill, North Carolina, September 26-28.

Sicard, M., Rocadenbosch, F., Reba, M.N.M., Comerón, A., Tomás, S., García-Vízcaino, D., Batet, O., Barrios, R., Kumar, D., Baldasano, J.M., 2011. Seasonal variability of aerosol optical properties observed by means of a Raman lidar at an EARLINET site over Northeastern Spain. *Atmos. Chem. Phys.*, **11**, 175-190.

Simpson, D., Fagerli, H., Jonson, J., Tsyro, S., Wind, P., Tuovinen, J., 2003. Transboundary acidification and eutrophication and ground level ozone in Europe. Technical Report. EMEP Status Report 1/03, Part I: Unified EMEP Model Description. The Norwegian Meteorological Institute, Oslo, Norway.

Simpson, D.W., Yttri, K.E., Klimont, Z., Kupiainen, K., Caseiro, A., Gelencsér, A., Pio, C., Puxbaum, H., Legrand, M.R., 2007. Modeling carbonaceous aerosol over Europe: analysis of the CARBASOL and EMEP EC/OC campaigns. *J. Geophys. Res.*, **112**(D23S14). doi:10.1029/2006JD008158.

Skamarock, W.C., Klemp, J.B., 2008. A time-split nonhydrostatic atmospheric model for weather research and forecasting applications. *J. Comput. Phys.*, **227**(7), 3465-3485. doi:10.1016/j.jcp.2007.01.037.

Smith, S.N., Mueller, S.F., 2010. Modeling natural emissions in the community multiscale air quality (CMAQ) model—part 1: building an emissions data base. *Atmos. Chem. Phys.*, **10**, 4931-4952.

Smyth, S.C., Jiang, W., Roth, H., Moran, M.D., Makar, P.A., Yang, f., Bouchert, W.S., Landry, H., 2009. A comparative performance evaluation of the AURAMS and CMAQ air quality modeling systems. *Atmos. Environ.*, **43**, 1059-1070.

Solberg, S., 2006. VOC measurements 2004. EMEP/CCC Report 8/2006. Available at: http://www.nilu.no/projects/ccc/reports/cccr8-2006.doc.

Song, C.K., Byun, D.W., Pierce, R.B., Alsaadi, J.A., Schaack, T.K., Vukovich, F., 2008. Downscale linkage of global model output for regional chemical transport modeling: method and general performance. *J. Geophys. Res.*, **113**(D08308). doi:10.1029/2007JD008951.

Soret, A., Jiménez-Guerrero, P., Baldasano, J.M., 2011. Comprehensive air quality planning for the Barcelona Metropolitan Area through traffic management. *Atmos. Poll. Res.*, **2**, 255-266.

Soriano, C., Baldasano, J.M., Buttler, W.T., Moore, K., 2001. Circulatory patterns of air pollutants within the Barcelona air basin in a summertime situation: liar and numerical approaches. *Bound.-Lay. Meteorol.*, **98**, 33-55.

Spicer, C.W., Koetz, J.R., Keigley, G.W., Sverdrup, G.M., Ward, G.F., 1981. A study of nitrogen oxides reactions within urban plumes transported over the ocean. US-EPA, Research Triangle Park, NC.

Staudt, M., Bertin, N., Frenzel, B., Seufert, G., 2000. Seasonal variations in amount and composition of monoterpenes emitted by young Pinus pinea trees—implications for emission modeling. *J. Atmos. Chem.*, **35**, 77-99.

Stein, A., Mantilla, E., Millán, M., 2005. Using measured and modeled indicators to assess ozone-NO_x-VOC sensitivity in a western Mediterranean coastal environment. *Atmos. Environ.*, **39**, 7167-7180.

Steinbrecher, R., Smiatek, G., Köble, R., Seufert, G., Thelokec, J., Hauff, K., Ciccioli, P., Vautard, R., Curci, G., 2009. Intra-and interannual variability of VOC emissions from natural and semi-natural vegetation in Europe and neighbouring countries. *Atmos. Environ.*, **43**, 1380-1391.

Stern, R., Builtjes, P., Schaap, M., Timmermans, R., Vautard, R., Hodzic, A., Memmesheimer, M., Feldmann, H., Renner, E., Wolke, R., Kerschbaumer, A., 2008. A model inter-comparison study focussing on episodes with elevated PM10 concentrations. *Atmos. Environ.*, **42**, 4567-4588. doi:10.1016/j. atmosenv.2008.01.068.

Stockwell, W.R., Kirchner, F., Kuhn, M., Seefeld, S., 1997. A new mechanism for regional atmospheric chemistry modeling. *J. Geophys. Res.*, **102**, 25847-25879.

Swall, J.L., Foley, K.M., 2009. The impact of spatial correlation and incommensurability on model evaluation. *Atmos. Environ.*, **43**, 1204-1217.

Szopa, S., Foret, G., Menut, L., Cozic, A., 2009. Impact of large scale circulation on European summer surface ozone and consequences for modelling forecast. *Atmos. Environ.*, **43**, 1189-1195.

Talbot, R.W., Harriss, R.C., Browell, E.V., Gregory, G.L., Sebacher, D.I., Beck, S.M., 1986. Distribution and geochemistry of aerosols in the tropical north Atlantic troposphere: relationship to Saharan dust. *J. Geophys. Res.*, **91** (D4), 5173-5182.

Tang, Y., Carmichael, G.R., Thongboonchoo, N., Chai, T., Horowitz, L.W., Pierce, R.B., Al-Saadi, J.A., Pfister, G., Vukovich, J.M., Avery, M.A., Sachse, G.W., Ryerson, T.B., Holloway, J.S., Atlas, E.L., Flocke, F.M.,Weber, R.J., Huey, L.G., Dibb, J.E., Streets, D. G., Brune, W.H., 2007. Influence of lateral and top boundary conditions on regional air quality prediction:a multiscale study coupling regional and global chemical transport models. *J. Geophys. Res.*, **112**(D10S18), 2083-2097. doi:10.1029/2006JD007515.

Tang, Y., Lee, P., Tsidulko, M., Huang, H.C., McQueen, J.T., Di Mego, G.J., Emmons, L.K., Pierce, R.B., Lin, H.M., Kang, D., Tong, D., Yu, S.C., Mathur, R., Pleim, J.E., Otte, T.L., Pouliot, G., Young, J.O., Schere, K.L., Davidson, P.M., 2008. The impact of chemical lateral boundary conditions on CMAQ predictions of tropospheric. Ozone over the continental United States. *Environ. Fluid Mech.*, **9**(1), 43-58. doi:10.1007/s10652-008-9092-5.

Tarrasón, L., Iversen, T., 1998. Modelling intercontinental transport of atmospheric sulphur in the northern hemisphere, *Telus B*, **50**, 4331-4352.

Tarrasón, L., Benedictow, A., Fagerli, H., Jonson, J., Klein, H., van Loon, M., Simpson, D., Tsyro, S., Vestreng, V., Wind, P., 2005. Transboundary acidification, eutrophication and ground level ozone in Europe in 2003. Technical Report 1/05. The Norwegian Meteorological Institute, Oslo, Norway.

Tarrasón, L., Fagerli, H., Klein, H., Simpson, D., Benedictow, A., Vestreng, V., Rigler, E., Emberson, L., Posch, M., Spranger, T., 2006. Transboundary acidification, eutrophication and ground level ozone in Europe from 1990 to 2004. Technical Report 1/06: to Support the Review of the Gothenburg Protocol. The Norwegian Meteorological Institute, Oslo, Norway.

Tarrasón, L., Fagerli, H., Jonson, J.E., Simpson, D., Benedictow, A., Klein, H., Vestreng, V., 2007. Transboundary acidification, eutrophication and ground level ozone in Europe in 2005. Technical Report 1/07. The Norwegian Meteorological Institute, Oslo, Norway.

Tesche, T.W., Morris, R., Tonnesen, G., McNally, D., Boylan, J., Brewer, P., 2006. CMAQ/CAMx annual 2002 performance evaluation over the eastern US. *Atmos. Environ.*, **40**, 4906-4919.

Thibodeau, L.A., Reed, R.B., Bishop, Y.M.M., Kammerman, L.A., 1980. Air pollution and human health: a review and reanalysis. *Environ. Health Perspect.*, **34**, 165-183.

Thorpe, A., Harrison, R.M., Boulter, P.G., McCrae I.S., 2007. Estimation of particle resuspension source strength on a major London Road. *Atmos. Environ.*, **41**, 8007-8020.

Thorpe, A., Harrison, R.M., 2008. Sources and properties of non-exhaust particulate matter from road traffic: a review. *Sci. Total Environ.*, **400**, 279-282.

Toll, I., Baldasano, J.M., 2000. Modeling of photochemical air pollution in the Barcelona area with highly disaggregated anthropogenic and biogenic emissions. *Atmos. Environ.*, **34**, 3060-3084.

Torseth, K., Hov, O., 2003. The EMEP monitoring strategy 2004-2009. Technical Report 9/2003. EMEP/CCC.

Tsyro, S.G., 2005. To what extent can aerosol water explain the discrepancy between model calculated and gravimetric PM10 and PM2.5. *Atmos. Chem. Phys.*, **5**, 515-532.

Tsyro, S., Simpson, D., Tarrasón, L., Klimont, Z., Kupiainen, K., Pio, C., Yttri, K.E., 2007. Modeling of elemental carbon over Europe. *J. Geophys. Res.*, **112** (D23S19).

UNECE, 1999. The 1999 Gothenburg Protocol to Abate Acidification, Eutrophication and Ground-level Ozone UNCE, Gothenburg, Report.

UNECE, 2007. Hemispheric transport of air pollution 2007. Air Pollution Studies No. 16. United Nations, New York and Geneva.

US EPA, 1984. Interim procedures for evaluating air quality models (Revised). Technical Report. EPA-450/4-91-013. U.S. Environmental Protection Agency, Office of Air Quality Planning and Standards, Research Triangle Park, NC. U.S. EPA, 1991. Guideline for Regulatory Application of the Urban Airshed Model. Technical Report. EPA-450/4-91-013. U.S. Environmental Protection Agency, Office of Air Quality Planning and Standards, Research Triangle Park, NC.

US EPA, 1991. Guideline for regulatory application of the urban airshed model. Technical Report. EPA-450/4-91-013. U.S. Environmental Protection Agency. Office of Air Quality Planning and Standards. Research Triangle Park, NC.

US EPA, 1997. AP-42, 5. Edition, Volume 1, Chapter 13, Section 13.2.1. Miscellaneous sources. Technical Report. U.S. Environmental Protection Agency. Office of Air Quality Planning and Standards. Research Triangle Park, NC.

US EPA, 2006. AP-42. 5th Edition, Volume VI, Chapter 13, Section 13.2.1. Paved roads. Technical Report. U.S.-Environmental Protection Agency. US EPA, 2007. Guidance on the use of models and other analyses for demonstrating attainment of air quality goals for ozone, PM2.5, and regional haze. Technical Report. EPA-454/B-07-002. U.S. Environmental Protection Agency. Office of Air Quality Planning and Standards. Research Triangle Park, NC.

US EPA, 2007. Guidance on the use of models and other analyses for demonstrating attainment of air quality goals for ozone, PM2.5, and regional haze. Technical Report. EPA-454/B-07-002. U.S. Environmental Protection Agency, Office of Air Quality Planning and Standards, Research Triangle Park, NC.

US EPA, 2009. Guidance on the development, evaluation, and application of environmental models. Council for regulatory environmental modelling. United States Environmental Protection Agency. Report EPA/100/K-09/003. Available at: http://www.epa.gov/crem/library/cred_guidance_0309.pdf.

Valari, M., Menut, L., 2008. Does an increase in air quality models' resolution bring surface ozone concentrations closer to reality?. *J. Atmos. Oceanic Technol.*, **25**, 1955-1968.

Vautard, R., Builtjes, P.H.J., Thunis, P., Cuvelier, C., Bedogni, M., Bessagnet, B., Honoré, c., Moussiopoulos, N., Pirovano, G., Schaap, M., Sern, R., Tarrasón, L., Wind, P., 2007. Evaluation and intercomparison of Ozone and PM10 simulations by several chemistry transport models over four European cities within the CityDelta project. *Atmos. Environ.*, **41**, 173-188.

Vautard, R., Bessagnet, B., Chin, M., Menut, L., 2005a. On the contribution of natural eolian sources to particulate matter concentrations in Europe: testing hypotheses with a modelling approach. *Atmos. Environ.*, **39**(18), 3291-3303.

Vautard, R., Honoré, C., Beekmann, M., Rouïl, L., 2005b. Simulation of ozone during the august 2003 heat wave and emission control scenarios. *Atmos. Environ.*, **39**(16), 2957-2967. doi:10.1016/j.atmosenv.2005.01.039.

Vautard, R., Schaap, M., Bergström, R., Bessagnet, B., Brandt, J., Builtjes, P.J.H., Christensen, J.H., Cuvelier, C., Foltescu, V., Graff, A., Kerschbaumer, A., Krol, M., Roberts, P., Rouïl, L., Stern, R., Tarrason, L., Thunis, P., Vignati, E., Wind, P., 2009. Skill and uncertainty of a regional air quality model ensemble. *Atmos. Environ.*, **43**, 4822-4832. doi:10.1016/j.atmosenv.2008.09.083.

Vayenas, D.V., Takahama, S., Davidson, C.I., Pandis, S.N., 2005. Simulation of the thermodynamics and removal processes in the sulfate-ammonia-nitric acid system during

winter: Implication for PM2.5 control strategies. *J. Geophys. Res.,* **110** (D07S14), doi:10.1029/2004JD005038.

Venkatram, A., Pleim, J., 1999. The electrical analogy does not apply to modeling dry deposition of particles. *Atmos. Environ.,* 33(18), 3075-3076. doi:10.1016/S1352-2310(99)00094-1.

Venkatram, A., 2000. A critique of empirical emission factor models: a case study of the AP-42 model for estimating PM10 emissions from paved roads. *Atmos. Environ.,* **34**, 1-11.

Viana, M., Querol, X., Alastuey, A., Cuevas, E., Rodríguez, S., 2002. Influence of African dust on the levels of atmospheric particulates in the Canary Islands air quality network. *Atmos. Environ.,* **36**, 5751-5875.

Viana, M., Pérez, C., Querol, X., Alastuey, A., Nickovic, S., Baldasano, J.M., 2005. Spatial and temporal variability of PM levels and composition in a complex summer atmospheric scenario in Barcelona (NE Spain). *Atmos. Environ.,* **39**, 5343-5361.

Vingarzan, R., 2004. A review of surface ozone background levels and trends. *Atmos. Environ.,* **38**, 3431-3442.

Visser, H., Buringh, E., van Breugel, P.B., 2001. Composition and origin of airborne particulate matter in the Netherlands. National Institute for Public Health and the Environment, RIVM, The Netherlands, Report 650010029. 104 pp.

Vivanco, M.G., Correa, M., Azula, O., Palomino, I., Martin, F., 2008. Influence of model resolution on ozone predictions over Madrid area (Spain). Computational science and its applications-ICCSA 2008, 165–178.

Vivanco, M.G., Palomino, I., Vautard, R., Bessagnet, B., Martín, F., Menut, L., Jiménez, S., 2009. Multi-year assessment of photochemical air quality simulation over Spain. *Environ. Modell. Softw.,* **24**, 63-73.

Volkamer, R., Sheehy, P.M., Molina, L.T., Molina, M.J., 2010. Oxidative capacity of the Mexico City atmosphere – part 1: a radical source perspective. *Atmos. Chem. Phys.,* **10**, 6969-6991.

Volz, A., Kley, D., 1998. Evaluation of the Montsouris series of ozone measurements made in the 19th-Century. *Nature,* **332**, 240-242.

Warneck, P., 1988. Chemistry of the natural atmosphere. International Geophysics Series. Wiley & Sons, 41. Academy Press, 757 pp.

Wayne, R.P., 2000. Chemistry of atmospheres. 3nd Edition. Oxford University Press, 775 pp.

Webb, E.K., 1970. Profile relationships: the log-linear range, and extension to strong stability. *Q. J. R. Meteorol. Soc.,* **96**(407), 67-90. doi:10.1002/qj.49709640708.

Weil, J.C., Sykes, R.I., Venkatram, A., 1992. Evaluating air-quality models: review and outlook. *J. Appl. Meteorol.,* **31**, 1121-1145.

Wennberg, P.O., Dabdub, D., 2008. Rethinking ozone production. *Science,* **319**, 1624-1625.

Wesely, M.L., Hicks, B., 2000. A review of the current status of knowledge on dry deposition. *Atmos. Environ.,* **34**, 2261-2282.

WHO, 2003. Health aspects of air pollution with particulate matter, ozone and nitrogen fioxide. Report on a WHO working group. Bonn, Germany. January, 13-15.

WHO, 2005. Global update 2005. Report on a working group meeting, Bonn, Germany. 99 pp.

WHO, 2006: WHO Europe air quality guidelines for particulate matter, ozone, nitrogen dioxide and sulfur dioxide. Global update 2005. World Health Organization, 2005. Available at: http://www.euro.who.int/__data/assets/pdf_file/0005/78638/E90038.pdf.

Wilkins, E.T., 1954. Air pollution and the London fog of December 1952. *J. R. Sanit. Inst.,* **74**, 1-21.

Wu, S.-Y., Hu, J.-L., Zhang, Y., Aneja, V.P., 2008. Modeling atmospheric transport and fate of ammonia in North Carolina – Part II: effect of ammonia emissions of fine particulate matter formation. *Atmos. Environ.,* **42**, 3437-3451.

Yarwood, G., Rao, S., Yocke, M., Whitten, G., 2005. Updates to the carbon bond chemical mechanism: CB05 Final Report to the US EPA, RT-0400675. Available at: http://www.camx.com/publ/pdfs/CB05_Fiinal_Report_120805.pdf.

Yttri, K.E., Hanssen, J.E., Tsyro, S., Lazaridis, M., Facchini, M.C., Jennings, S.G., 2005. Transboundary particulate matter in Europe. Technical Report. EMEP Status Report 4/05. The Norwegian Meteorological Institute, Oslo, Norway.

Yttri, K.E., Aas, W., Forster, C., Torseth, K., Tsyro, S., Tarrasón, L., Simpson, D., Vestreng, V., Lazaridis, M., Kopanakis, I., Aleksandropoulou, V., Gehrig, R., Adams, M., Woodfield, M., Putaud, J., Schultz, M., 2006. Transboundary particulate matter in Europe. Technical Report 4/06. The Norwegian Meteorological Institute, Oslo, Norway.

Yu, S., Dennis, R., Roselle, S., Nenes, A., Walker, J., Eder, B., Schere, K., Swall, J., Malm, W., Robarge, W., 2005. An assessment of the ability of three-dimensional air quality models with current thermodynamic equilibrium models to predict aerosol NO_3^-. *J. Geophys. Res.*, **110**, D07S13.

Yu, S., Eder, B., Dennis, R., Chu, S., Schwartz, S., 2006. New unbiased symmetric metrics for evaluation of air quality models. *Atmos. Sci. Lett.*, **7**, 26-34.

Yu, S., Mathur, R., Sarwar, G., Kang, D., Tong, D., Pouliot, G, Pleim, J., 2010. Eta-CMAQ air quality forecasts for O_3 and related species using three different photochemical mechanisms (CB4, CB05, SAPRC-99): comparisons with measurements during the 2004 ICARTT study. *Atmos. Chem. Phys.*, **10**, 3001-3025.

Zakey, A.S., Giorgi, F., Bi, X., 2008. Modeling of sea salt in a regional climate model: Fluxes and radiative forcing. *J. Geophys. Res.*, **113**, D14221. doi: 10.1029/2007JD009209.

Zhang, Y., Seigneur, C., Seinfeld, J.H., Jacobson, M., Clegg, S.L., Binkowski, F.S., 2000. A comparative review of inorganic aerosol thermodynamic equilibrium modules: differences, and their likely causes. *Atmos. Environ.*, **34**, 117-137.

Zhang, K., Knipping, E., Wexler, A., Bhave, P., Tonnesen, G., 2005. Size distribution of sea-salt emissions as a function of relative humidity. *Atmos. Environ.*, **39**, 3373-3379.

Zhang, Y., Liu, P., Pun, B., Seigneur, C., 2006. A comprehensive performance evaluation of MM5-CMAQ for the summer 1999 southern oxidants study episode, part III: diagnostic and mechanistic evaluations. *Atmos. Environ.*, **40**, 4856-4873. doi:10.1016/j.atmosenv.2005.12.046.

Zhang, Y., 2008. Online-coupled meteorology and chemistry models: history, current status, and outlook. *Atmos. Chem. Phys.*, **8**, 2895-2932. doi:10.5194/acp-8-2895-2008.

Annex I: Evaluation of the meteorological model in the European and Spanish domains

1. Meteorological model evaluation in the CALIOPE-EU system

Model results from the WRF-ARW model implemented in the CALIOPE-EU system have been evaluated against 931 surface meteorological stations. The spatial distribution of the stations largely covers the Atlantic coast, the plain area of Europe, the Alps region and the Mediterranean coast. There is less coverage over southern European countries such as Spain, Italy and Greece as shown in Figure AI - 1. The observational dataset consist of hourly measurements from METAR, SYNOP, AWOS and ASOS networks.
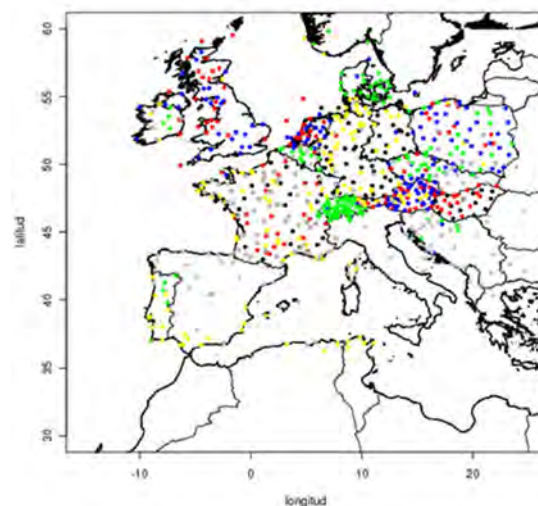
Figure AI - 1. Meteorological stations (METAR, SYNOP, AWOS and ASOS) with available measurements on an hourly basis located at ground-level.

Table AI - 1 shows a summary of the annual statistics of key meteorological variables evaluated against measurements: 2-m temperature, 2-m dew point temperature, 10-m wind speed, and 10-m wind direction. In general, the mean absolute error (MAE) for temperature variables remains below 2ºC. A slight cold bias in temperature is produced. Also, the wind shows a rather good performance with MAE below 2 m s^{-1} and 64.66º. The model tends to overestimate the wind speed.

The monthly mean evolution of the MAE and MB for these variables (Figure AI - 2 and Figure AI - 3) shows a cold bias at surface levels, observed during most parts of the year. The WRF-ARW model implemented in the CALIOPE-EU system tends to simulate colder and dryer atmospheres during most parts of the year (Figure AI - 2), as indicated by the larger underestimation of dew

point temperature compared with the sensible temperature. This bias difference between both temperatures is rather constant and the MAE remains between 1.7 ºC and 2.0ºC.

Table AI - 1. Summary of annual mean errors of the WRF-ARW meteorological model (in CALIOPE-EU) for 2-m temperature, 2-m dew point temperature, 10-m wind speed, and 10-m wind direction for 2004.

	RMSE	MAE	MBE
2-m temperature (ºC)	2.64	1.91	-0.67
2-m dew point temperature (ºC)	2.51	1.78	-0.44
10-m wind speed (m s^{-1})	2.64	1.88	0.87
10-m wind direction (º)	110.05	64.66	-12.33

The WRF-ARW model overestimates the surface wind speed (Figure AI - 3), although the error remains below 2.5 m s^{-1} during wintertime and below 1.6 m s^{-1} in summertime. Note that the direction error is quite stable, around 60º. These results indicate the reasonable good performance at surface level of the meteorological model over Europe for 2004.
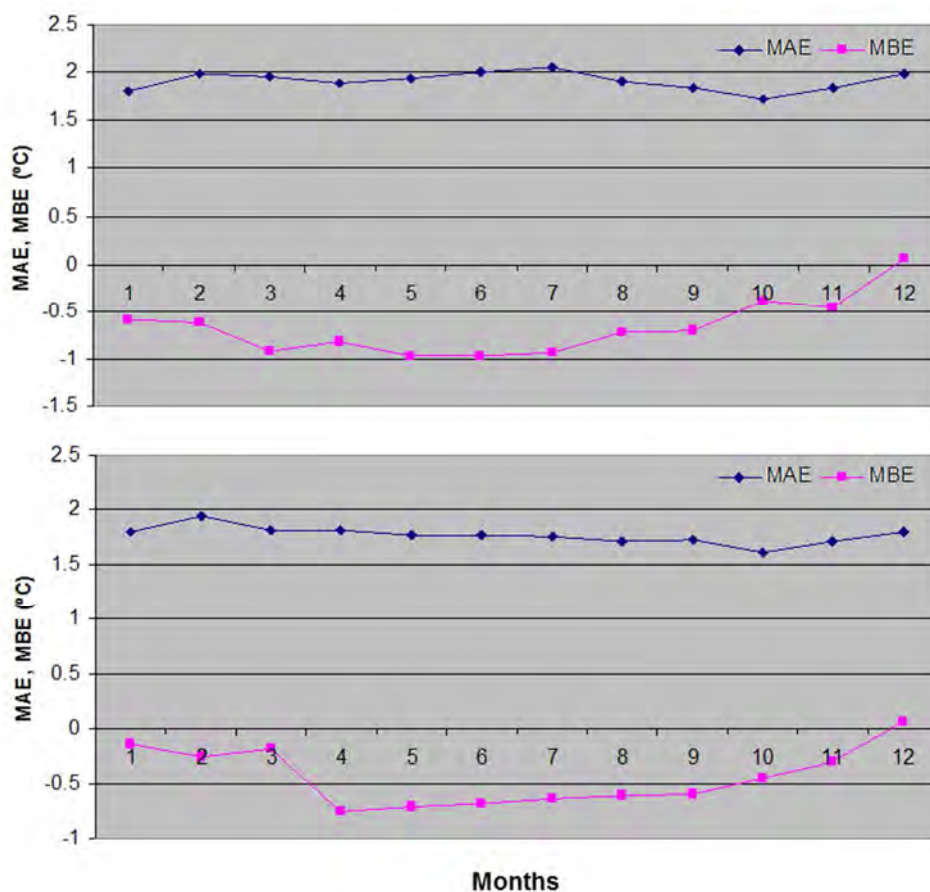
Figure AI - 2. Monthly evolution of the MAE (blue lines) and MBE (pink lines) for the 2-m temperature (top) and the 2-m dew point temperature (bottom) in ºC.
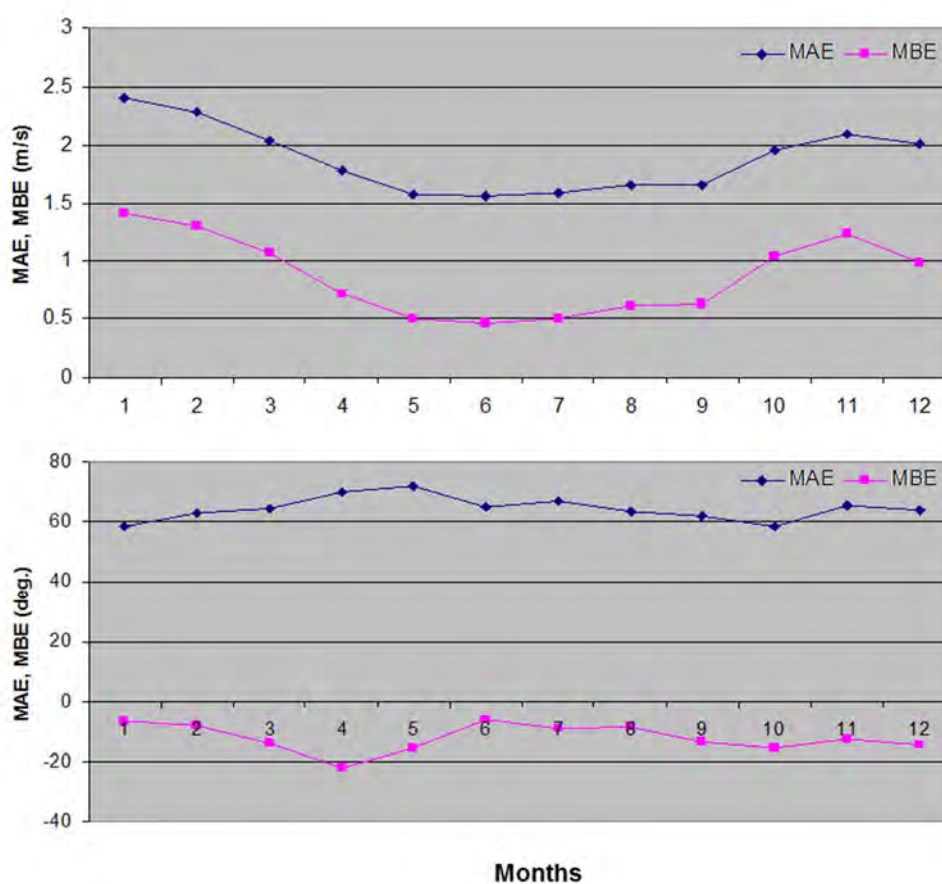
Figure AI - 3. Monthly evolution of the MAE (blue lines) and MBE (pink lines) for the 10-m wind speed (top) and the 10-m wind direction (bottom) in °.

2. Meteorological model evaluation in the CALIOPE-IP system

In the framework of the evaluation of the CALIOPE-IP modelling system to reproduce the temporal and spatial variability of air quality over Spain in 2004, we performed an evaluation of the WRF-ARW results over the same year in order to quantify the model skills to capture the seasonality of meteorological variables in Spain. Hence, the 2-m temperature, 2-m dew point temperature, 10-m wind speed and direction were evaluated against surface meteorological stations. 158 meteorological stations are used to evaluate the temperature and wind variables over all Spain. The observational datasets consist of hourly measurements from METAR, CEAM and AEMET (Spanish Meteorological Office).

The quantitative evaluation is performed using classical statistics for temperature and wind, like Root Mean Squared Error (RMSE), the Mean Absolute Error (MAE) and the Mean Bias Error (MBE). Table AI - 2 shows the annual statistics for 2-m temperature, 2-m dew point temperature, 10-wind speed and direction.

Table AI - 2. Summary of annual mean errors of the meteorological model WRF-ARW (in CALIOPE-IP) for 2-m temperature, 2-m dew point temperature, 10-m wind speed, and 10-m wind direction for 2004.

	RMSE	MAE	MBE
2-m temperature (ºC)	2.54	2.01	-1.15
2-m dew point temperature (ºC)	2.76	2.02	-0.77
10-m wind speed (m s^{-1})	2.21	1.63	0.76
10-m wind direction (º)	66.67	47.95	1.68

In general, temperatures present a mean absolute error around 2ºC. A slight cold bias in temperature is produced. The monthly mean evolution of the MAE and MBE for temperature shows a cold bias at surface level during most part of the year (Figure AI - 4). The model tends to simulate colder and dryer atmospheres as indicated by the larger underestimation of dew point temperature compared with the sensible temperature. The monthly MBE difference between both temperatures is rather constant and the MAE remains between 1.7ºC and 2.4ºC in both cases.
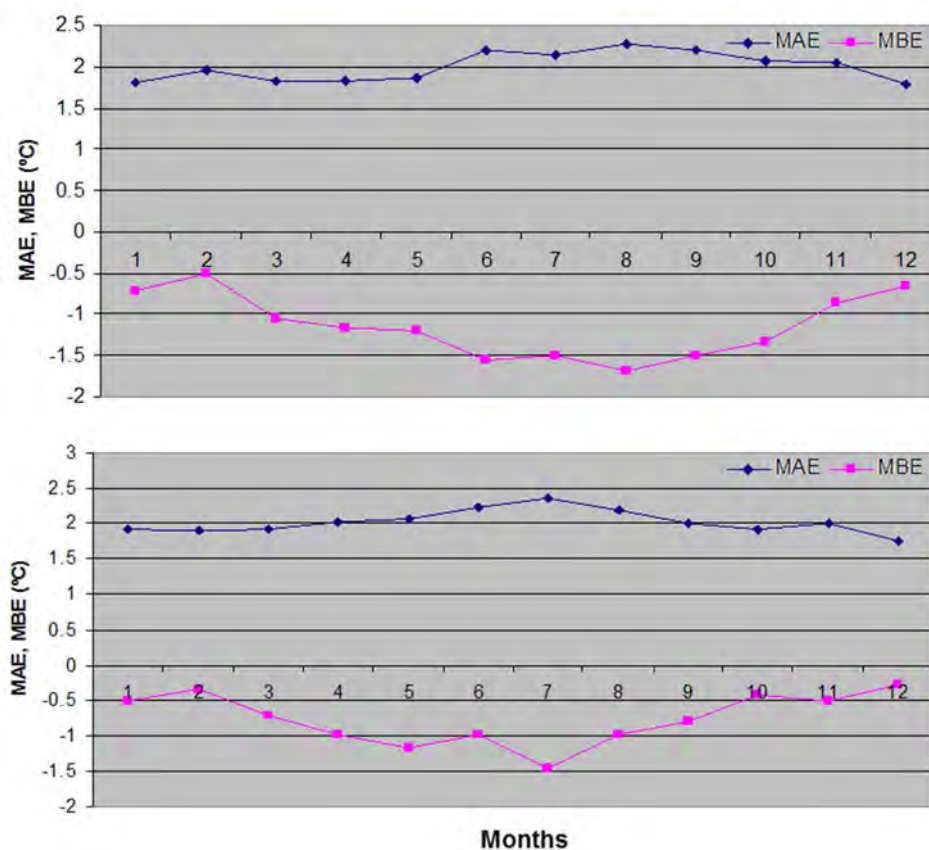

Figure AI - 4. Monthly evolution of the MAE (blue lines) and MBE (pink lines) for the 2-m temperature (top) and the 2-m, dew point temperature (bottom) in ºC.
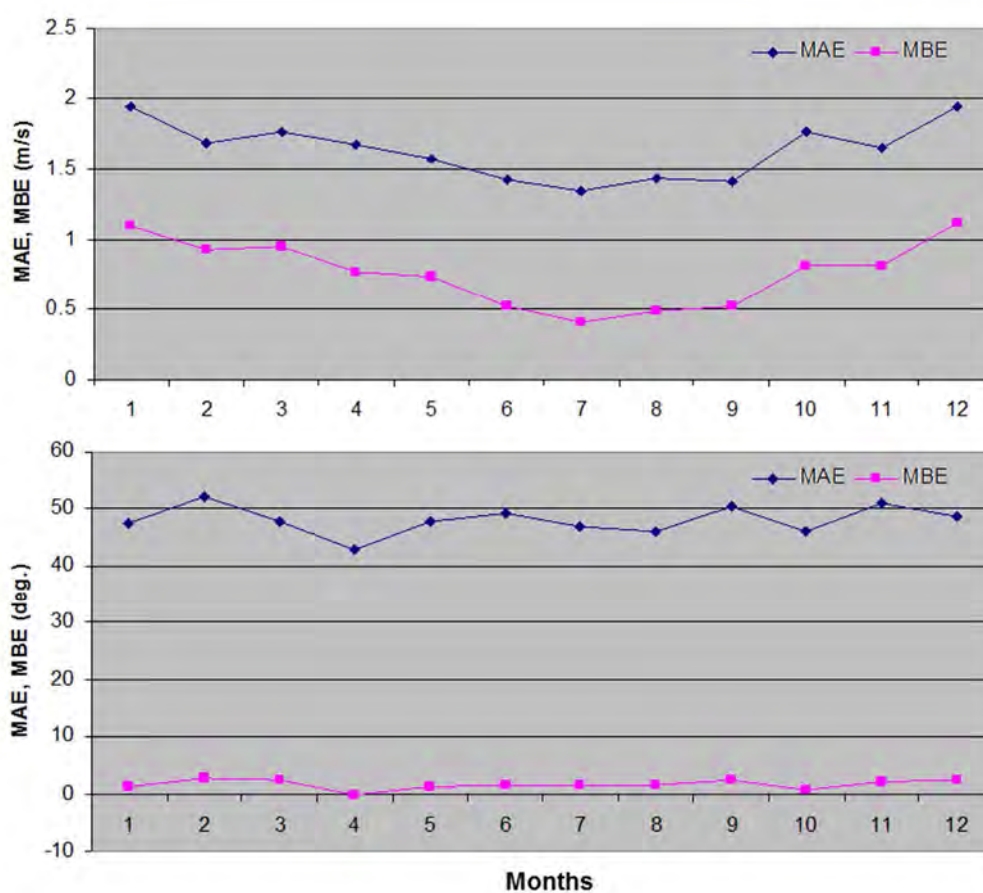
Figure AI - 5. Monthly evolution of the MAE (blue lines) and MBE (pink lines) for the 10-m wind speed (top) and the 10-m wind direction (bottom) in º.

The wind shows a rather good performance with MAE near 2 m s^{-1} and 48º (Table AI - 2). The model tends to overestimate wind, although the error remains below 0.8 m s^{-1} during summertime and around 0.9 m s^{-1} in winter (Figure AI - 5). Note that the bias direction error is quite stable, around 45º. These results indicate the reasonable good performance at surface level of the meteorological model over Spain in 2004.

Annex II. Chemical boundary condition from the LMDz-INCA2 global model

Sensitivity studies were performed in CALIOPE system in order to assess the impact of chemical boundary conditions (BC) and vertical model resolution on the quality of the simulations, using datasets from the LMDz-INCA2 chemical global model. The objective of such studies is to achieve a detailed analysis of the model behaviour over a tested month (May 2004), in view of improving the quality of the operational simulations.
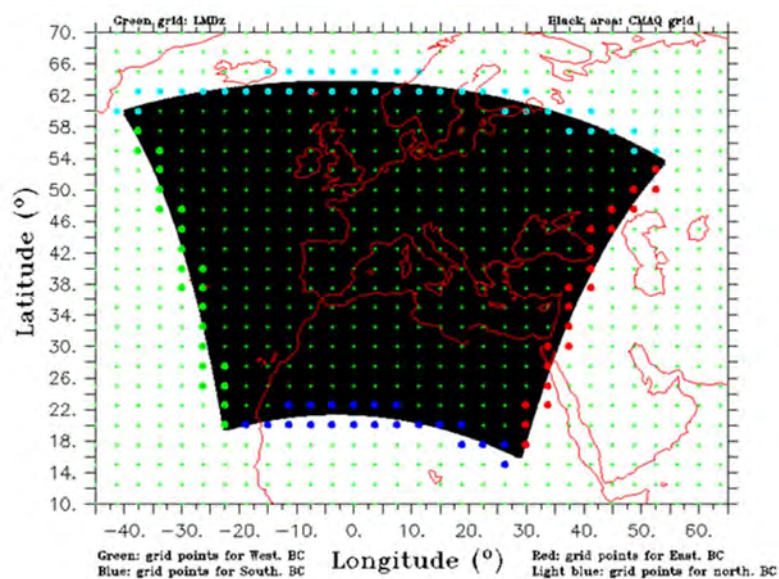

Figure AII - 1. CALIOPE-EU grid (black area) within LDMz-INCA2 grid (green +). Green points represent western boundary conditions. Blue points represent southern boundary condition. Red points represent eastern boundary conditions. Light-blue points represent northern boundary conditions

Several studies have shown the importance of chemical boundary conditions for regional chemical transport models (CTM) (Tang et al. 2007; Tang et al. 2008; Song et al. 2008; Szopa et al. 2008). Also, inter-continental transport of pollutants is known to have a substantial impact on their concentrations within the simulated domain (e.g., Derwent, et al., 2004; Guerova et al. 2006). To implement such variations in the concentration of pollutants, invariable synthetic profiles used to define the chemical conditions at the boundaries of a domain must be ruled out. The increasing availability of global chemical model (GCM) outputs has led us to reconsider the profiles used at the boundaries of the model. Among the European GCM running, the LMDz-INCA2 held by the French Laboratoire de Météorologie Dynamique (LMD) provides various datasets which may be used to constrain the chemistry at the boundaries of our model. Climatological data are freely available and provide mean concentrations of the period 1997-2001 (Szopa et al., 2007) for 14 species including O_3, NO_y, HO_x, PAN, CH_4, CO. The model outputs for the specific year of 2004 were provided by S. Szopa (personal communication). For 2004, the concentration of 49 species

were calculated on a 3.75 lon x 2.5 lat grid (96 x 72 grid points), over 19 sigma-p vertical layers reaching up to 3 hPa. We constrained the concentration of O_3, NO, NO_2, HNO_3, $HCHO$, H_2O_2, PAN and CO at the boundaries of our model domain using a horizontally and vertically weighted nearest- neighbor interpolation method, respectively (Figure AII - 1). The data at each grid point of the LMDz-INCA2 closest to the boundaries of WRF-CMAQ-DREAM are processed to generate the boundary condition profiles (Figure AII - 1: bold grid points in green, blue, red, light blue for west, south, east and north, respectively). This interpolation method allows an accurate horizontal as well as vertical resolution in the profiles used. In order to reduce uncertainties in vertical diffusion, the number of sigma-p vertical layers described in CMAQ was increased from 8 to 15 layers (Figure AII - 2).
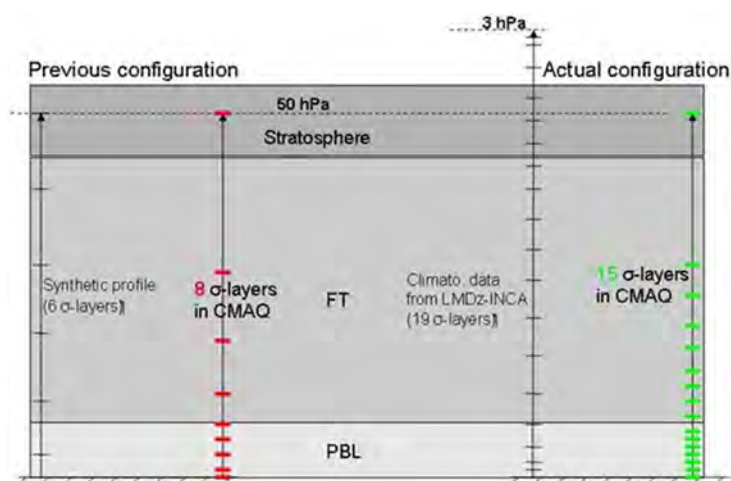

Figure AII - 2. Previous and current vertical configuration of the CALIOPE system FT indicates free troposphere. PBL indicates Planetary Boundary Layer.

In order to evaluate the performances of the model, model simulations were compared to 64 and 25 stations throughout Europe from the EMEP network for O_3 and NO_2, respectively (Figure AII - 3). To assess the impact of the different chemical boundary conditions, we performed tests on a specific month, May 2004 (Figure AII - 4).
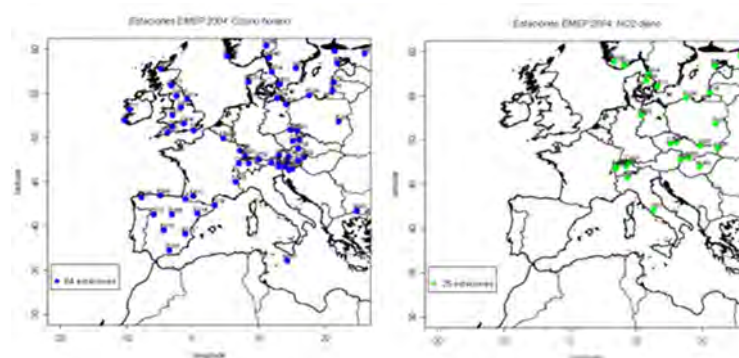

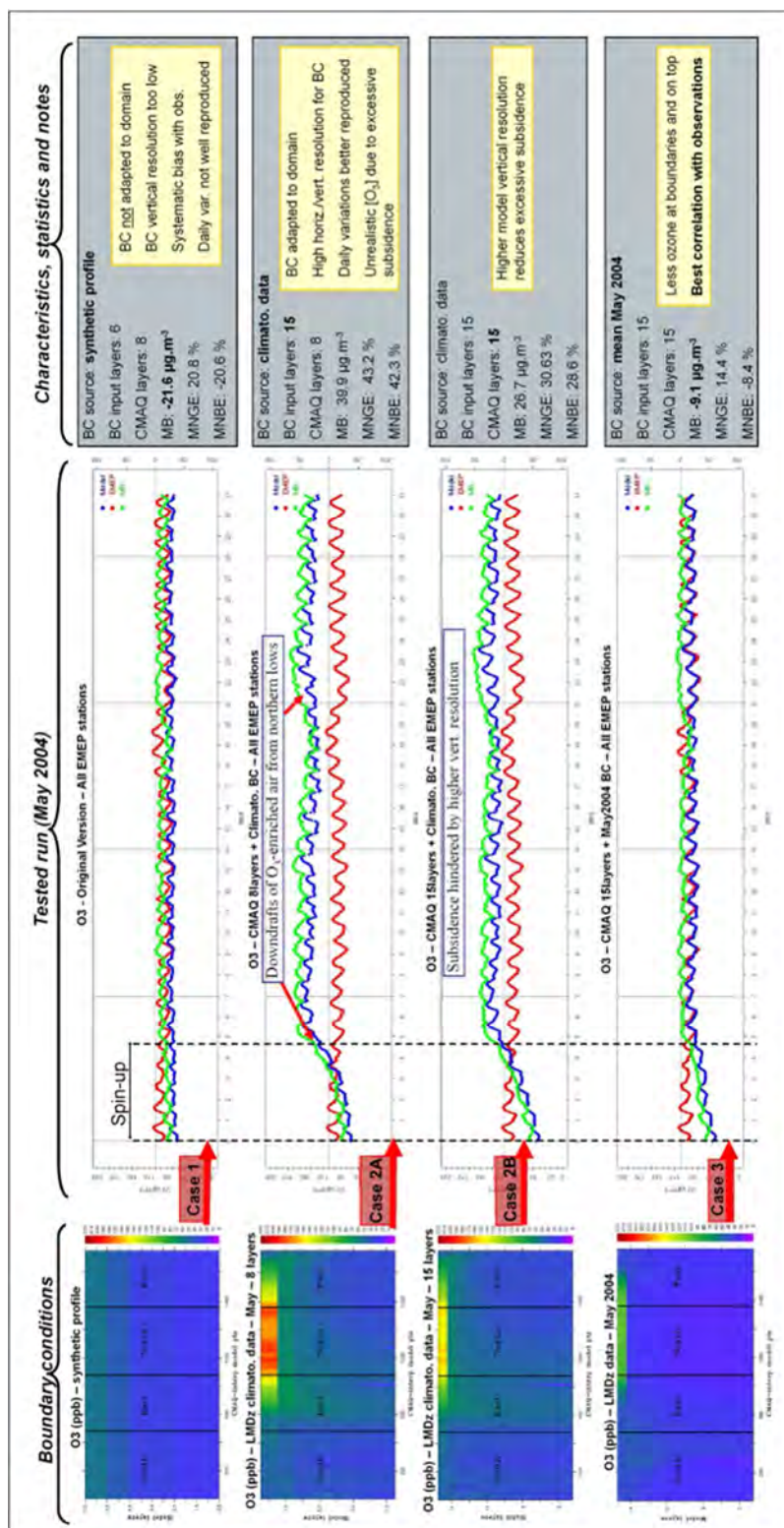Figure AII - 3. EMEP stations for O_3 (left) and NO_2 (right) concentrations.

Figure AII - 4. Synthetic boundary conditions over 6 vertical layers were used in preliminary simulations (Case 1). Then, climatological data (Szopa et al., 2007) provided by the global climate-chemistry model LMDz-INCA2 were tested to define more consistent lateral conditions (Cases 2A and 2B). In order to improve the conditions at the boundaries, a simulation was also performed using the May-2004 dataset from this model (Case 3).

The use of climatological data to force the boundary conditions provided more reliable conditions than the synthetic profile for the model boundaries but did not improve the quality of simulated O_3 ground-based concentration in the model domain. Higher vertical resolution notably improved the trend and daily variations of O_3 concentration and hindered unrealistic subsidence of O_3-enriched air caused by tropopause folding. BC constrained by the May-2004 dataset led to a satisfactory correlation with observations (MB: -9.1 $\mu g.m^{-3}$). The chemistry of NO_2 was found to be mostly governed by local emissions, with little influence of the boundary conditions. Data from the LMDz-INCA2 model will certainly be used for the operational system. Figure AII - 5 shows O_3 vertical profiles boundary condition from LMDz-INCA2 global model in monthly mean used in CALIOPE-EU for 2004.

References

Guerova, G., Bey, I., Attié, J.-L., Martin, R. V., Cui, J., Sprenger, M., 2006. Impact of transatlantic transport episodes on summertime ozone in Europe. *Atmos. Chem. Phys.*, **6**, 2057-2072

Derwent, R. G., Stevenson, D. S., Collins, W. J., Johnson, C. E., 2004. Intercontinental transport and the origins of the ozone observed at surface sites in Europe. *Atmos. Environ.*, **38**, 1891-1901

Song, C.-K., Byun, D. W., Pierce, R. B., Alsaadi, J. A., Schaack, T. K., Vukovich, F., 2008. Downscale linkage of global model output for regional chemical transport modeling: Method and general performance. *J. Geophys. Res.*, **113** (D08308). doi:10.1029/JD008951

Szopa, S., D. A. Hauglustaine and P. Ciais, 2007. Relative contributions of biomass burning emissions and atmospheric transport to carbon monoxide interannual variability, *J. Geophys. Res. Lett.*, **34**, L18810, doi:10.1029/2007GL030231.

Szopa, S., Foret, G., Menut, L., Cozic, A., 2008. Impact of large scale circulation on European summer surface ozone and consequences for modelling forecast. *Atmos. Environ.*, **1**, 1-16.

Tang, Y., Carmichael, G. R., Thongboonchoo, N., Chai, T., Horowitz, L. W., Pierce, R. B. Al-Saadi, J. A., Pfister, G., Vukovich, J. M., Avery, M. A., Sachse, G. W., Ryerson, T. B., Holloway, J. S., Atlas, E. L., Flocke, F. M., Weber, R. J., Huey, L. G., Dibb, J. E., Streets, D. G. Brune, W. H., 2007. Influence of lateral and top boundary conditions on regional air quality prediction: A multiscale study coupling regional and global chemical transport models. *J. Geophys. Res.*, **112**, 2083-2097, doi: 10.1029/2006JD007515.

Tang, Y., Lee, P., Tsidulko, M., Huang, H.-C., McQueen, J. T., DiMego, G. J., Emmons, L. K., Pierce, R. B., Lin, H.-M., Kang, D., Tong, D., Yu, S.-C., Mathur, R. Pleim, J. E., Otte, T. L., Pouliot, G., Young, J. O., Schere, K. L., Davidson, P. M., 2009. The Impact of Chemical Lateral Boundary Conditions on CMAQ Predictions of Tropospheric Ozone over the Continental United States. *Env. Fluid Mech.*, **9**, 43-58
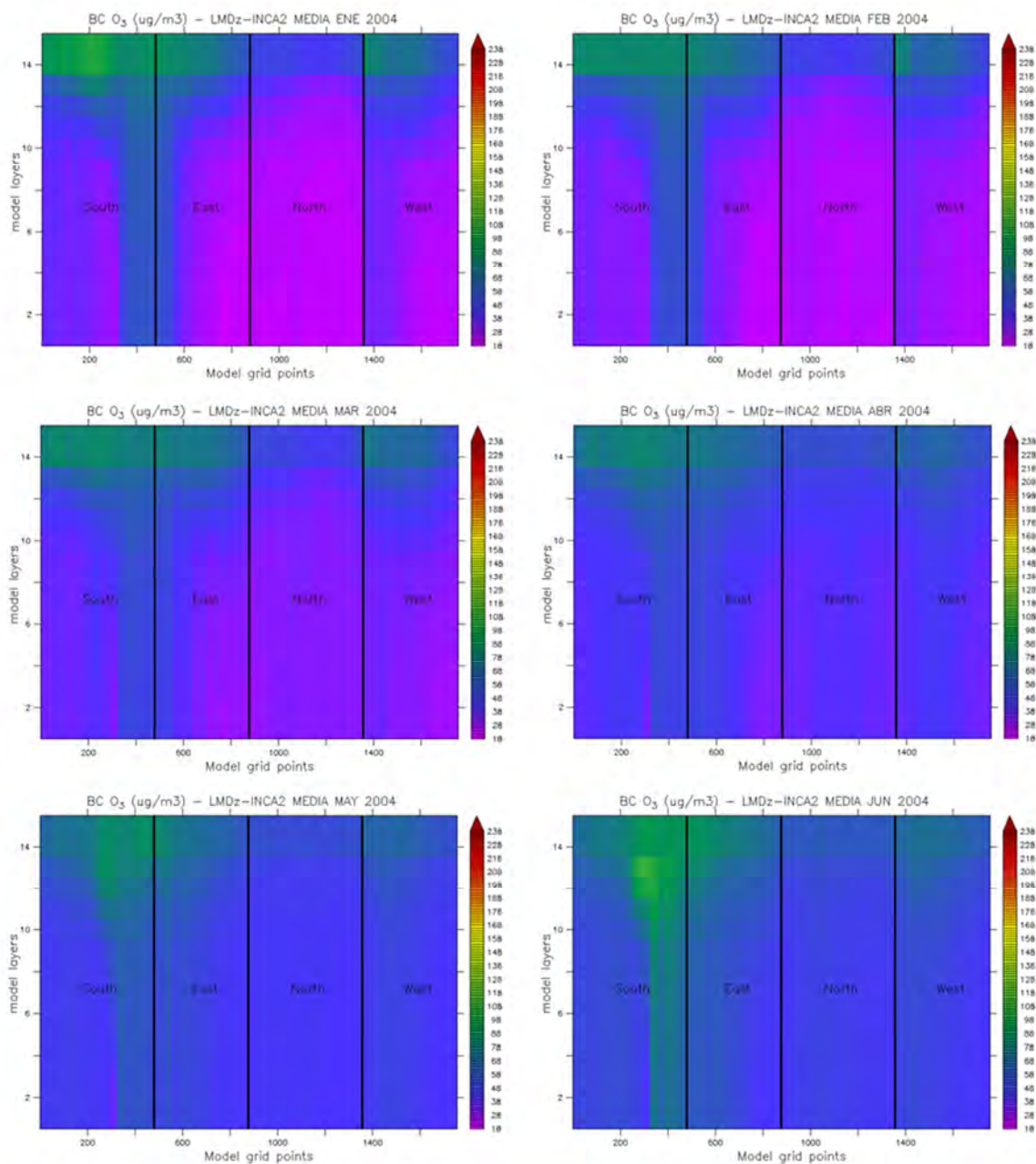
Figure AII - 5. O$_3$ Chemical boundary condition from LMDz-INCA2 global model in monthly mean used in CALIOPE-EU for 2004.
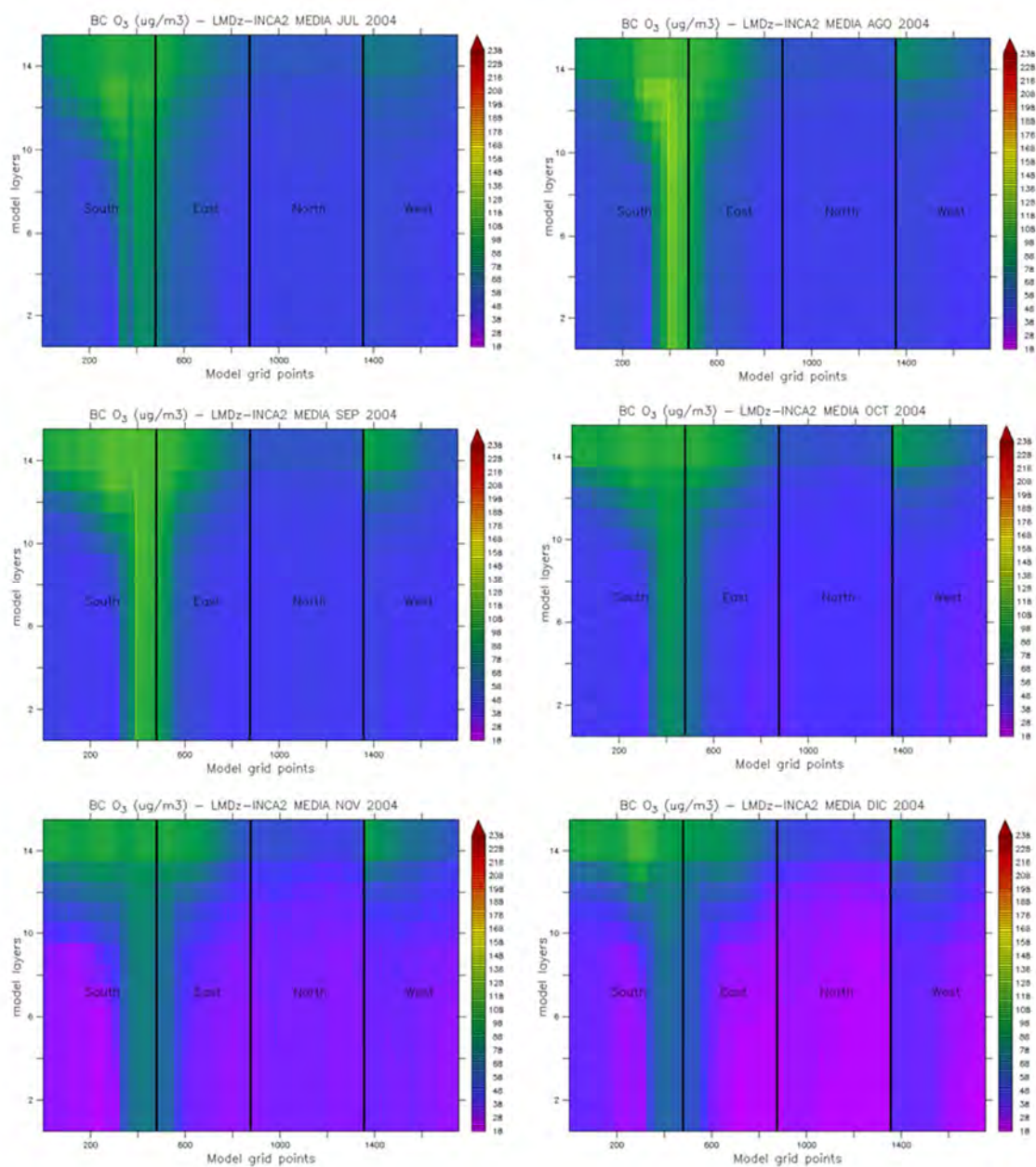
Figure AII - 5. (continued)

Annex III. Supplementary material

1. Annual pattern of NO$_2$ ground-based concentrations in Europe

Figure AIII - 1 shows the annual spatial pattern of NO$_2$ concentrations in Europe simulated with CALIOPE-EU system in 2004. High NO$_2$ annual mean concentrations are directly related to anthropogenic emissions. The Netherlands, Belgium, the Po Valley, England and western Germany present the highest NO$_2$ concentrations (20-30 μg m^{-3}). Note that shipping from the North Sea, passing by the English Channel, through Portugal, Spain and northern Africa towards the Suez Canal substantially affect the coastal NO$_2$ concentrations with a maximum 18 μg m^{-3} for the annual mean. Comparison with measurements shows a high spatial agreement between CALIOPE-EU and EMEP observations (r=0.75). Such analysis demonstrates the relative accuracy in the spatial description of the source regions and various European hot-spot.
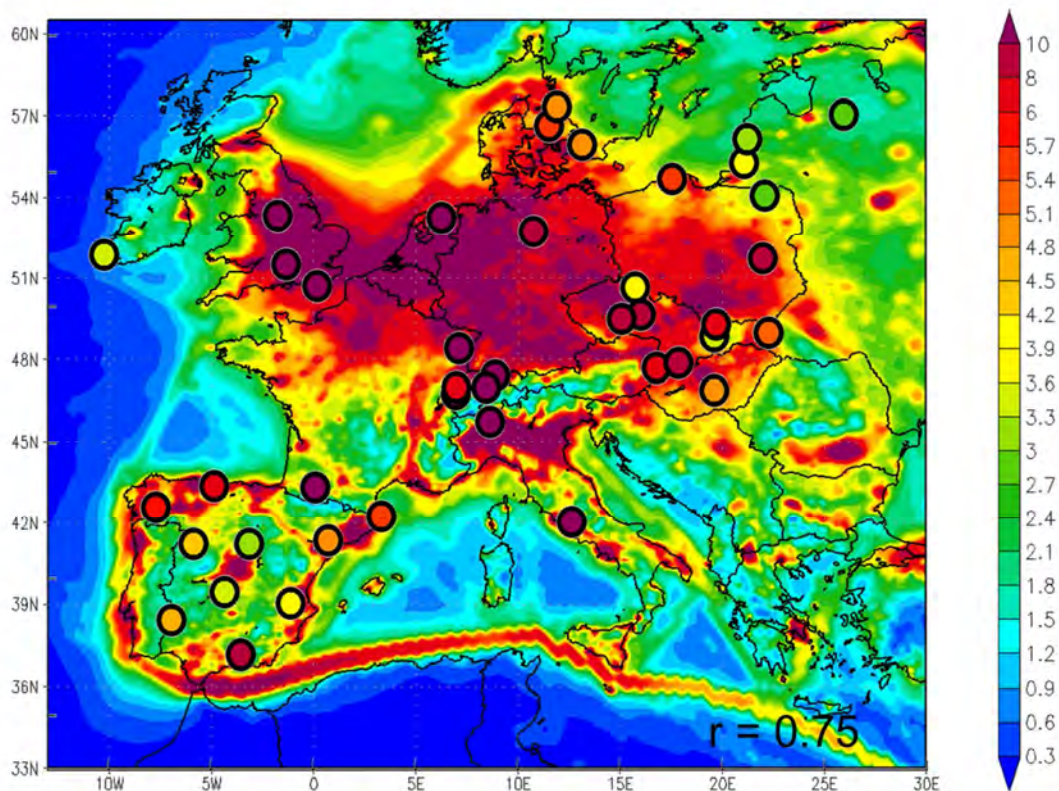

Figure AIII - 1. Annual mean concentrations (in μg m^{-3}) for NO$_2$ at lower-most level simulated by CALIOPE-EU system over Europe at a 12 km x 12 km spatial resolution in 2004. Points represent measured annual concentrations at the EMEP stations. Number at bottom-left in each figure is the spatial correlation between modeled and observed annual mean at each station.

2. Time series of PM2.5 and PM10 at the station of Víznar, O Saviñao, Barcelona and Huelva

Víznar is a representative station of the rural background in southern Spain. It is affected by an enhanced summer maximum and high frequent African air mass intrusion episodes, during summer and fall affecting southern Spain owing to the proximity to the North Africa.
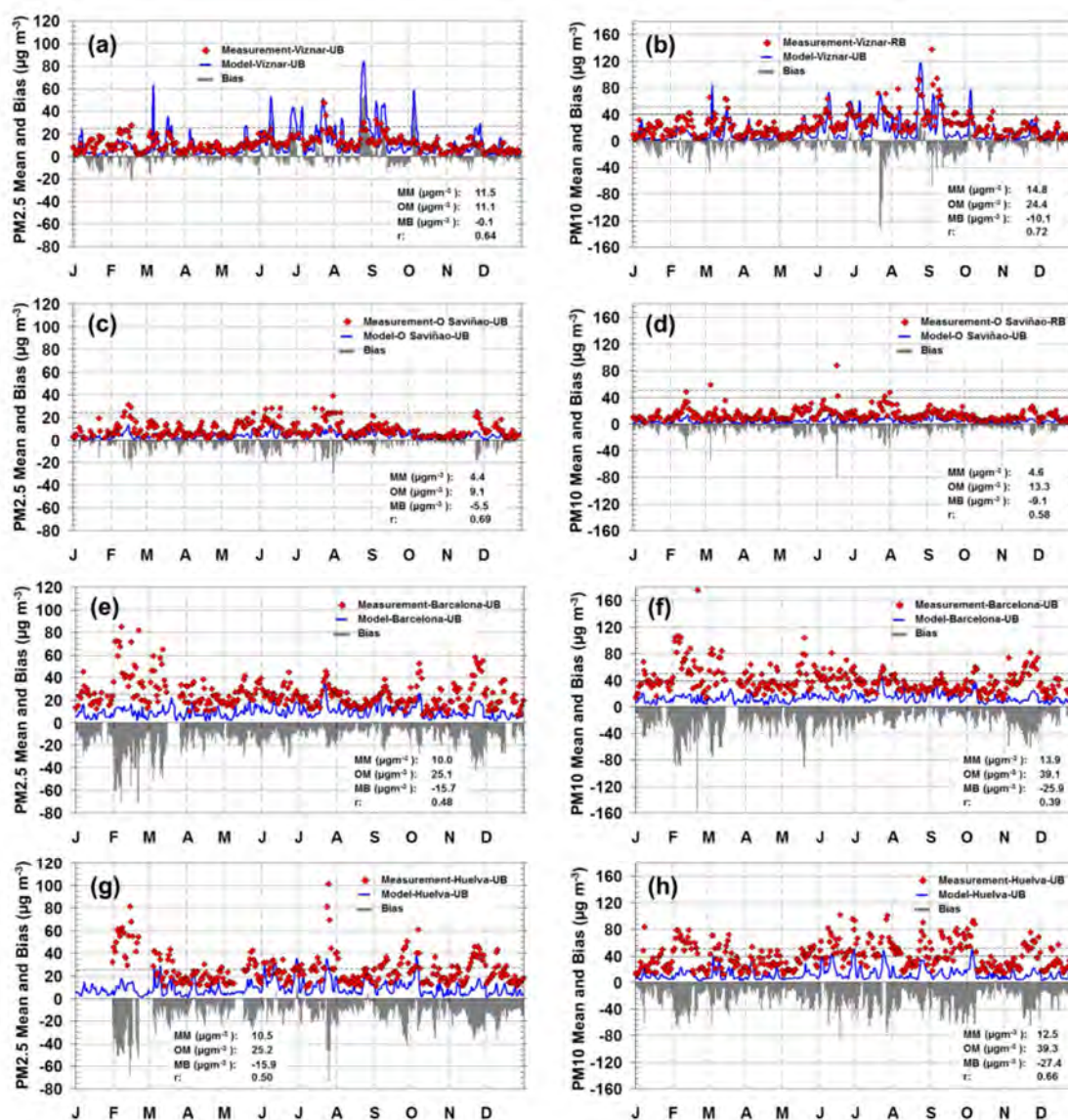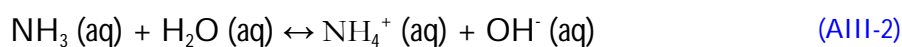

Figure AIII - 2. Time series of observed (red diamond) and simulated (blue continuous line) daily PM2.5 (left column) and PM10 (right column) for the year 2004: at (a, b) Víznar, (c, d) O Saviñao, (e, f) Barcelona, and (g, h) Huelva (see Fig. 1 and Table 1 for the location of the sites). UB and RB refer to urban background and rural background types of sites, respectively. The dashed lines represent the current limit values in Europe (European Commission, 2008) for PM10 (annual and daily limit values of 40 μg m⁻³ and 50 μg m⁻³ not to be exceeded 35 times in a year, respectively) and for PM2.5 (annual limit value of 25 μg m⁻³). Statistics for each station are shown in the figure (bottom right): modelled mean (MM), observed mean (OM), mean bias (MB) and correlation coefficient (r).

Time series (Figure AIII - 2a and b) show that CALIOPE reproduces daily variability along the year with high correlation of 0.62 (0.72) in PM2.5 (PM10) favoured by the hourly contribution of the Saharan dust modelled by the BSC-DREAM8b (Jiménez-Guerrero et al. 2008). On the other hand, CALIOPE system presents a good performance at rural background stations in Atlantic regions, like O Saviñao (r of 0.69 (0.58) in PM2.5 (PM10)) affected by frequent westerly winds and frontal system advection of Atlantic air masses (Figure AIII - 2c and d). Nevertheless CALIOPE present difficulties to reproduce PM levels in urban stations like Barcelona (Figure AIII - 2e and f) and Huelva (Figure AIII - 2g and h). Huelva is an urban background station under the influence of industrial and traffic sources and also affected by desert dust episodes. Maximum levels are found in summer. To understand the cause of underestimation is important to evaluate chemical composition of PM.

# 3. Seasonal pattern for gas precursors of PM

Figure AIII - 3 presents the seasonal spatial pattern of gas precursors of secondary inorganic aerosol modelled with CALIOPE-IP system in 2004. Although annual pattern of SO_2 is described in Baldasano et al. (2011), Figure AIII - 3c and d show the different in SO_2 distribution between summer and winter. The location of the main power plants and refineries in Spain let us know that combustion emission from these industries are the main responsible of high concentration of SO_2 over land in Spain. Over sea, the highest concentrations are found along the main shipping route, since fuels used have high sulphur content. SO_2 concentration over the sea are intensified during summer, may be due to the high frequent of maritime traffic.

Ammonia is the predominant basic gas in the atmosphere and neutralizes sulphuric acid and nitric acid to form aerosols, and small quantities can also be absorbed into liquid aerosols by quantities governed by considerations of vapour-liquid equilibrium (Eq. AIII-1 and Eq. AIII-2):

$$NH_3 \text{ (g)} \leftrightarrow NH_3 \text{ (aq)} \tag{AIII-1}$$

$$NH_3 \text{ (aq)} + H_2O \text{ (aq)} \leftrightarrow NH_4^+ \text{ (aq)} + OH^- \text{ (aq)} \tag{AIII-2}$$

Intensive agriculture is estimated to produce around 90% of NH_3 emissions in Europe (CORINAIR, 2007). From those, between 80 and 90% arise from the excreta produced by livestock. Figure AIII - 3 show the distribution patter of NH_3 during winter (Figure AIII - 3a) and summer (Figure AIII - 3b) from agriculture and livestock. In Spain, these areas are located in the northeastern.
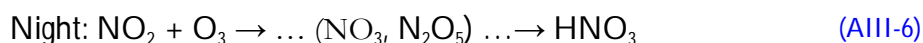
Non-marine sulfate is directed emitted, generated by nucleation and/or condensation from the gas phase oxidation of SO_2 and hydroxyl radical and by heterogeneous oxidation of SO_2 in clouds (aqueous-phase oxidation by H_2O_2, O_3, Fe^{3+} and Mn^{2+}, and peroxyacetic acid; see Binkowski and Roselle, 2003) (Eq. AIII-3):

$$SO_2 + OH + O_3 + H_2O \rightarrow \cdots \rightarrow H_2SO_2 + HO_2 \qquad \text{(AIII-3)}$$
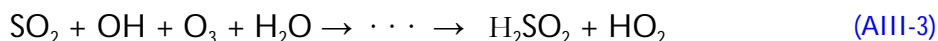
If ammonia is available, the sulphuric acid reacts with ammonia resulting in ammonium sulphate, ammonium bisulphate and letovicite on the particle surface (Eq. AIII-4).

$$HSO_4^- \ (aq) \leftrightarrow H^+ \ (aq) + SO_4^{2-} \ (aq) \qquad \text{(AIII-4)}$$
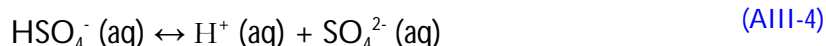
Sub-micron nitrate is predominantly present in the form of ammonium nitrate (NH_4NO_3), a semi-volatile compound. Atmospheric ammonia is first neutralized by sulphuric acid to form ammonium sulphate. Remaining ammonia may then combine with nitric acid to form ammonium nitrate (Dentener and Crutzen, 1993). The production of ammonium and nitrate follow 2 major production routes that occur in the daytime and night-time. The following reaction chains mainly yield the nitric acid in the gas phase and partly in the liquid phase (Nguyen and Dabdub, 2002; Meng et al. 1997) (Eq. AIII-5 and Eq. AIII-4):

$$\text{Day: } NO_2 + OH \rightarrow HNO_3 \qquad \text{(AIII-5)}$$

$$\text{Night: } NO_2 + O_3 \rightarrow \dots (NO_3, N_2O_5) \dots \rightarrow HNO_3 \qquad \text{(AIII-6)}$$

Then nitric acid will dissolve in the aqueous particles (or liquid aerosol) along with the ammonia and produce nitrate determined by the composition of the particle (Eq. AIII-7):

$$HNO_3 \ (g) \leftrightarrow H^+ \ (aq) + NO_3^- (aq) \qquad \text{(AIII-7)}$$
(HNO_3 dissolves when there is excess NH_3 to from nitrate ion)

When relative humidity is so low (aerosol liquid water content comprises less than 20% of the total aerosol mass) and there is excess NH_3, the heterogeneous reaction between HNO_3 and NH_3 in the particle-phase to form dry ammonium nitrate represents an important process to modulate the gaseous HNO_3 concentration (Eq. AIII-8).

$$NH_3 \ (g) + HNO_3 \ (g) \leftrightarrow NH_4NO_3 \ (s) \qquad \text{(AIII-8)}$$
(Low RH and excess NH_3 form dry NH_4NO_3)

The gas-aerosol partitioning of nitrate depends strongly on the availability of its precursor gases (NH_3 and HNO_3) and on the ambient conditions (Ansari and Pandis, 1998). Atmospheric ammonia is first neutralized by sulphuric acid to form ammonium sulphate. Remaining ammonia may then combine with nitric acid to form ammonium nitrate (Dentener and Crutzen, 1993).

In contrast to ammonium sulphate, the formation of which is fast and irreversible, ammonium nitrate is a semi-volatile compound which forms on the aerosol surface in equilibrium with its gaseous precursors.
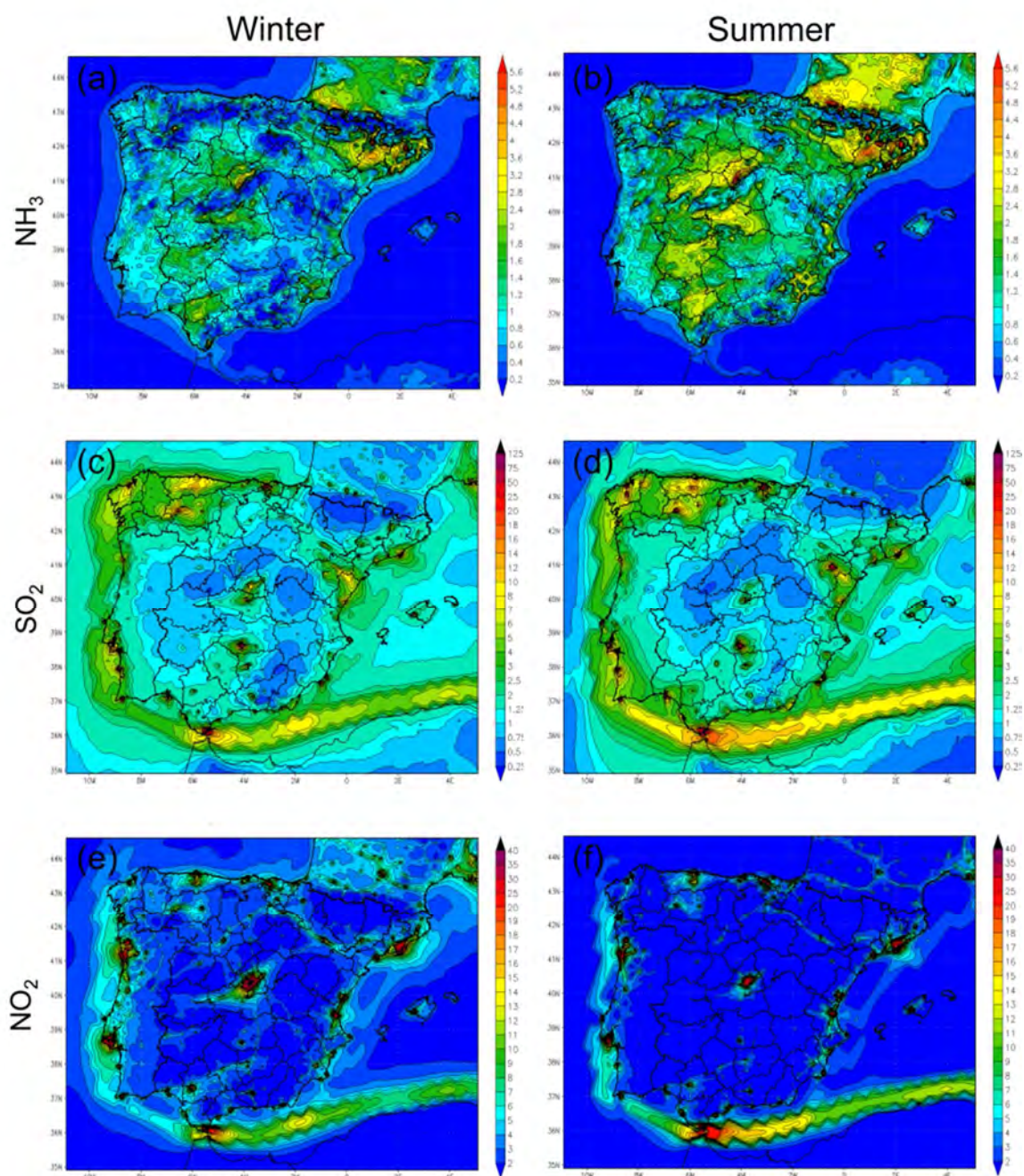

Figure AIII - 3. Summer (right) and winter (left) average concentrations (in $\mu g\ m^{-3}$) for ammonium (a, b), sulphur dioxide (c, d) and nitrogen dioxide (e, f) at lower-most level simulated by CALIOPE over Spain at a 4 km x 4 km spatial resolution in 2004. Winter correspond to January, February and March. Summer corresponds to June, July and August.

4. Degree of sulphate neutralization

To assess the chemical behaviour of aerosol chemical composition, we introduce the indicator degree of neutralization (DON) (Pinder et al., 2008) that is estimated to determine whether sulphate is completely acidic, fully neutralized by ammonia, or in between. Concentrations are expressed as µg m^{-3} in the DON equation (Eq. AIII-9).

$$DON = \frac{NH_4^+/18 - NO_3^-/62}{SO_4^{2-}/96}$$

(AIII-9)

There are 2 moles of ammonium for every mole of sulphate when sulphate is fully neutralized in the form of ammonium sulphate, giving a DON value of 2. If DON is 1, then sulphate would be ammonium bisulphate and particulate sulphuric acid when DON is 0. This equation assumes that nitrate is only neutralized by ammonia. This assumption may be too simplistic for other locations where nitrate is often neutralized by sodium or calcium.
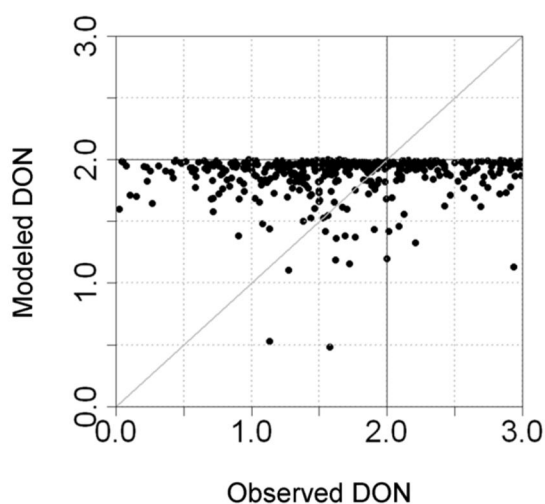

Figure AIII - 4. Degree of sulphate neutralization by ammonia (DON).

Sulphate acidity indirectly provides information about how well the modelling system estimates regional ammonia concentrations. This is useful when no ammonia measurements are available. The CALIOPE-IP system performance in predicting the DON by ammonia is show in Figure AIII - 4. Measured DON ranges outside the expected value of 0-2 because of reduced measurement precision at low concentrations and occasional samples where nitrate may be neutralized by an ion other than ammonium. PM2.5 sulphate is almost always completely neutralized by ammonia in the modelling system. Observations suggest that PM2.5 sulphate is fully neutralized in warm seasons and exists in the form of ammonium bisulphate in the colder months. This finding suggests there should be more free ammonia in the gas phase or less ammonium in the photochemical model.

5. References

Ansari, A.S., Pandis, S., 1998. Response of inorganic PM to precursor concentration. *Environ. Sci. Technol.* **32**, 2706-2714.

Baldasano, J.M., Pay, M.T., Jorba, O., Jiménez-Guerrero, P., 2011. An annual assessment of air quality with the CALIOPE modeling system over Spain. *Sci. Total Environ.,* **409**, 2163-2178. doi:10.1016/j.scitotenv.2011.01.041.

Binkowski, F. S., Roselle, S. J., 2003. Models-3 Community Multiscale Air Quality (CMAQ) model aerosol component: 1. Model description. *J. Geophys. Res.,* **108**(D16), 4183.

CORINAIR, 2007. http://reports.eea.europa.eu/EMEPCORINAIR5/en/B1090vs2.pdf.

Dentener, F.J., Crutzen, P.J., 1993. Reaction of N2O5 on tropospheric aerosols: Impact on the global distributions of NO_x, O_3, and OH. *J. Geophys. Res.,* **98**, 7149-7163.

Jiménez-Guerrero, P., Pérez, C., Jorba, O., Baldasano, J.M., 2008. Contribution of Saharan dust in an integrated air quality system and its on-line assessment. *Geophys. Res. Lett.,* **35** (L03814). doi:10.1029/2007GL031580.

Meng, Z., Dabdub, D., Seinfeld, J.H., 1997. Chemical coupling between atmospheric ozone and particulate matter. *Science,* **277**, 116-199.

Nguyen, K., Dabdub, D., 2002. NO_x and VOC control and its effects on the formation of aerosols. *Aerosol Sci. Tech.,* **36**, 560-572.

Pinder, R.W., Dennis, R.L., Bhave, P.V., 2008. Observable indicators of the sensitivity of $PM_{2.5}$ nitrate to emission reductions-Part I: Derivation of the adjusted gas ratio and applicability at regulatory relevant time scales. *Atmos. Environ.,* **42**, 1275-1286.